THE UNIVERSITY
of EDINBURGH

Mechanisms of mechanosensation in *Drosophila melanogaster* proprioceptors

Iain Hunter

A thesis submitted in support of the degree of PhD

The University of Edinburgh

2019

Declaration

I declare that the work in this thesis is entirely my own, unless stated otherwise (e.g. in the case of images from other publications or done in conjunction with colleagues). It has not been submitted in application for any other degree.

Signed: _____ (Iain Hunter)

Date: _____

Acknowledgements

I would like to thank my supervisor, Andrew Jarman, for his support. His guidance and patience were exemplary. I will take inspiration from Andy moving forward; I hope that I can demonstrate the same professional and personal values that he does.

I have been lucky enough to benefit from the help and/ or company of several Jarman lab members over the years. Those people were: Petra zur Lage, the Jarman lab legend who always made time for me despite a busy schedule (hope to see you on the hills); Lynn Powell, whose friendly face and kind words provided much-needed encouragement; Tom Suslak and Katarzyna Styczynska-soczka, the PhD students who were finishing as I joined the lab; Fay Newton, who humoured my questions on fly genetics. Finally, a special mention to Alex Ahl and Jenny Lennon. Thanks to Alex for the 4 (and hopefully many more) years of friendship, punctuated by deep-and-meaningful conversation diluted by Starbucks coffee, drunk from badly-decorated cups. Thanks to Jenny for bringing optimism and balance to our little group, and for collaborating with me to deliver some of the crawling and hearing experiments featured in this Thesis.

Barry Denholm has been essential to this work. Besides being a high-calibre human being who humoured my terrible conversation in the fly room, Barry let me use Denholm lab equipment to generate what are arguably the most interesting results in this Thesis. So, thank you to Barry and former Denholm lab technician Luigi Zechini, for use of the GCaMP microscope and camera.

Next, I'd like to extend my gratitude to my Thesis committee of Mike Shipston, Guy Bewick and Douglas Armstrong. Thanks to Mike for being helpful and friendly, and for letting me use the electrophysiology rig. I am grateful that Guy made a concerted effort to stay involved in my project despite being based in Aberdeen, and that Douglas supported my work despite having to balance it with so many other commitments.

I would like to thank the Biotechnology and Biological Sciences Research Council for funding my research, plus the University of Edinburgh for providing the infrastructure necessary to conduct it. It has been a privilege to be associated with such a prestigious institution. Similarly, thank you to the myriad members of University staff who input: Peter Duncan, Richard Ribchester, Nico Romano, Amit Nair and Stefan Pulver (University of St. Andrews) all made time to discuss my work.

I must thank my family: My parents, Len and Claire, for their understanding and for sacrificing their study so that I could finish writing without having to smuggle a 35kg wolfdog into the library. I would also like to thank my future in-laws, Kev and Ina, for the same understanding; they were exceptionally patient as I took up room in their home, getting this done. Finally, I would of course like to thank my fiancée, Amy Reid, who has been selfless in helping me to complete this work. Amy is a special little person, and one I try to learn from: I hope I can use the time we have together to return the kindness she extends to me.

Abstract

Proprioception is the ability to detect position in space. It is necessary for normal motor control and could share molecular mechanisms with other senses, such as hearing. These mechanisms are poorly understood and clarifying them may reveal novel targets for treatment of muscle spasticity, seizure and hardness of hearing. This research uses *Drosophila* models to clarify the behavioural role and molecular properties of proprioceptors; the dbd neuron and the chordotonal neurons. I hypothesise that the dbd neuron is both a pain and stretch receptor that requires DmPiezo to respond to both physiological and nociceptive stimuli. In contrast, evidence suggests that chordotonal neurons sense could sound and stretch stimuli through different mechanisms, which depend on nan/ iav/ NompC and DmPiezo respectively.

We employed optogenetics, crawling, nociceptive reflex ('pinch' response), GCaMP imaging and whole-cell patch-clamp electrophysiology to investigate the role and mechanisms of mechanosensation in the dbd neuron. Similarly, I used crawling, hearing and GCaMP experiments to assess the role and mechanisms of mechanosensation in the chordotonal neurons. I found the dbd neuron difficult to investigate; a 'nociceptive' phenotype originally attributed to dbd neuron stimulation disappeared when the related driver, Bd-Gal4, was expressed in the background of a mutant (*amos*^{1}) that lacks the dbd neuron. Moreover, while electrophysiology gave results like those published previously, my data were limited by issues including low seal values (~40MΩ, significantly lower than the desired 1GΩ) that were exacerbated by stretch.

Chordotonal (ch) neurons were easier to study. GCaMP imaging of the larval ventral nerve cord showed that ch neurons respond to both tonal (1024Hz) and muscle contraction stimulation (mean $\Delta F/ F_0$ (%) 11.47 ± 2.93 and 7.56 ± 4.38, respectively). I imaged the ch neurons (lch1-5, vch1 and vchAB) directly, and doing so revealed some interesting spatial and temporal differences in response to sound, which implies specific tuning of neurons within the chordotonal neuron population~~(s)~~(s). GCaMP imaging also showed that *CG17669*, a gene with a human orthologue (*DNAAF3*) associated with primary ciliary dyskinesia, is necessary for ch neuron response to 1024Hz and muscle contraction.

In conclusion, the behavioural role and mechanisms of the dbd neuron remain unclear and require further investigation. However, it appears that while the ch neurons can detect stretch (and so act as proprioceptors), this function is not required for normal movement in larvae. The ch neurons appear to be a sense organ with a single mechanism of mechanosensation, that is optimised for detection of tonal stimuli in the hearing range. Finally, this research is the first to: (1) image the response of vch1 and vchAB ch neurons response to sound; (2) provide

evidence that subsets of *Drosophila* ch neurons may be tuned to respond to specific amplitudes and/ or frequencies; (3) use real-time calcium imaging to demonstrate the effect of *CG17669* mutation on the function of ch neurons.

Lay summary

Proprioception is the ability to feel the body's position in space and is obvious in the party game: "pin the tail on the donkey"; players can sense where their hand is, without seeing it. This sense is facilitated by a special type of muscle fibre, called a muscle spindle, which relays characteristics of movement and position from the muscle to the central nervous system. This system can go wrong and when it does, is responsible for symptoms like spasticity and seizure, which are experienced by patients living with cerebral palsy. Another of the senses, hearing, depends on specialised cells in the inner that ear sense vibration and relay it to the central nervous system, where we perceive vibration as sound. Failures in these cells and the associated systems in the brain lead to hearing loss. Proprioception and hearing are therefore surprisingly similar, because they both involve turning a mechanical stimulus (movement or vibration) into an internal signal. Thus, they are both examples of "mechanosensation". Given that cerebral palsy occurs in 1 in 500 births and that hearing loss affects 1 in 6 people in the U.K., finding new ways of treating dysfunctional mechanosensation could improve quality of life for a lot of people.

While it is thought that the mechanisms responsible for proprioception and hearing are similar, scientists are still trying to find out exactly how they work. Specifically, researchers are trying to identify and characterise the protein molecules that facilitate sensitivity to stretch in proprioception, and vibration in hearing. In both cases, such proteins are thought to be the primary means by which the body senses mechanical disturbance and so they are called the primary mechanoelectrical transducers. However, both proprioception and hearing occur in cells deep in the human body, so are difficult to study.

The work described in this thesis uses the fruit fly, an organism with hearing and proprioception that works surprisingly like ours. Studying the relevant sensory cells in this organism may therefore help to identify the primary mechanoelectrical transducer proteins and how they work. But, technical limitations of current methods used to investigate proprioception prevented firm conclusions being made in the present thesis. My preliminary findings highlight the importance of technical care and reliability and this should guide future investigations. By contrast, I made significant progress in my research related to hearing. Specifically, I found evidence that type of cell, the chordotonal neuron, respond to sounds; something that was unclear before this work. I also showed that genes related to motor proteins (dyneins) and a debilitating disease call primary ciliary dyskinesia (PCD), are necessary for both hearing and proprioception in flies. Thus, my findings represent: (1) progress in understanding the fly as a model of mechanosensation; (2) an opportunity to continue research into the role of dyneins

in mechanosensation; (3) the potential that this knowledge could be applied to help treat patients with cerebral palsy, hearing loss, PCD and other disorders of mechanosensation.

Table of Figures

Contents

1 Introduction

Our senses are mediated by sensory neurons. For example, photoreceptors respond to light, chemoreceptors detect changes in CO_2, O_2 and pH; thermoreceptors respond to changes in temperature, and mechanoreceptors detect deformation. In humans, the information encoded in these neurons is interpreted as sight, smell, taste, hearing, touch, pressure, nociception, balance and proprioception. Many of these (hearing, touch, pressure, nociception, balance and proprioception) reflect activity in mechanosensory neurons. This research focuses on specific mechanisms of mechanosensation in *Drosophila*, in anticipation that understanding them better will lead to improved treatment of disease in humans.

1.1 Mechanosensation

Mechanosensation is the ability to sense a mechanical stimulus. Dysfunctional mechanosensation can lead to sensory neuropathy, hearing impairment and spasticity/ seizure, which are common. Bilateral deficit (associated with sensory neuropathy) occurs in ~54% of people aged 85 or older in the U.S. (Daousi *et al.*, 2004), hearing loss affects ~17% of people in the United Kingdom (Loss, 2011) and Cerebral Palsy, which is associated with spasticity and seizure, occurs in ~1 in 500 births worldwide (Odding, Roebroeck and Stam, 2006; Blair and Watson, 2006). Another disorder of mechanosensation, primary ciliary dyskinesia (PCD), is debilitating and has a prevalence that has been reported as high as 1: 2,265 (in a group of British Asians (O'Callaghan, Chetcuti and Moya, 2010)). Improving our understanding of mechanosensation would provide both insight into its fundamental physiological mechanism, and a better foundation for identifying and evaluating novel treatments for patients with dysfunctional mechanosensation. Consequently, two modes of mechanosensation, hearing and proprioception, are explored in the present research.

1.1.1 Hearing: From mammals to arthropods

The human ear channels sound waves along the outer-ear canal, to the tympanic membrane and ossicles of the middle ear. The ossicles vibrate and transmit the sound to the inner ear. The inner ear features the hearing end-organ, the cochlea - a coiled duct separated by partitions. The cochlea is highly specialised: The stiffness and resonant frequency of its basal membrane decreases from its base to its apex, so that discrete regions of the organ are tuned to specific frequencies (of sound/ vibration). Sensory regions of the cochlear partition express inner and outer hair cells (IHCs and OHCs, respectively). Both convert the mechanical stimulus of sound wave vibration into a change in cellular potential; hair cells are mechanotransducers ((Frolenkov *et al.*, 2004), see Figure 1.1). Arthropods hear using a similar system; they sense sound/ vibration by a tympanic membrane or antenna. Both are associated with specialised (chordotonal, ch) neurons that are like hair cells; ch neurons are ciliated, and mechanosensitive proteins expressed in the cilium facilitate mechanotransduction. The rest of this section explores human and dipteran arthropod hearing in detail.

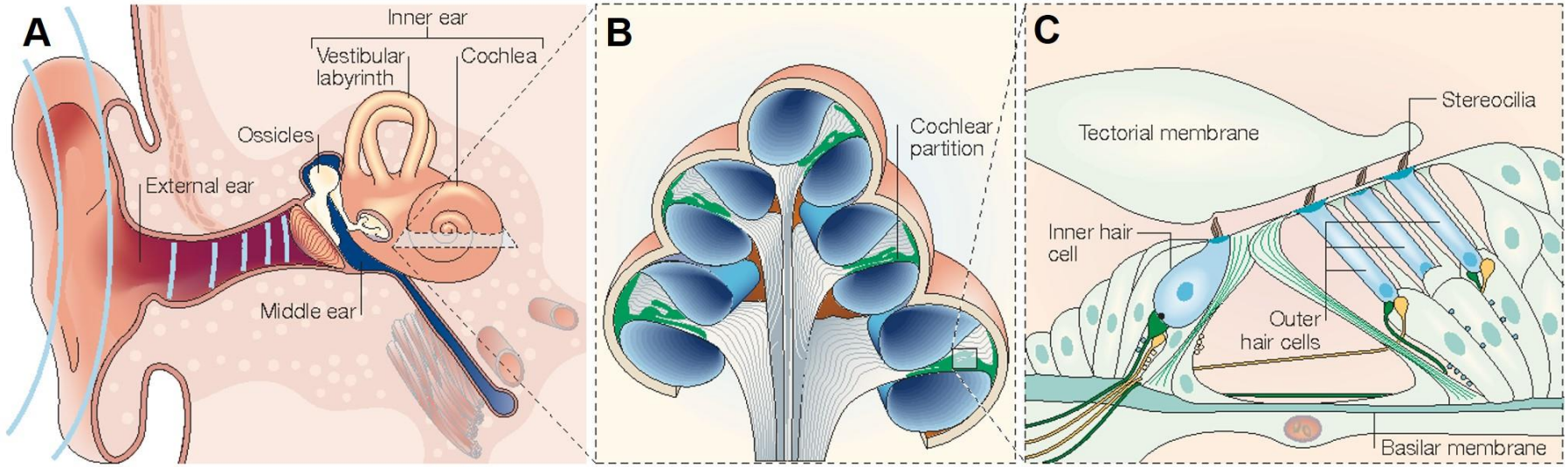

Figure 1.1: Anatomy of human hearing. *A: Overview of ear anatomy. Shows sound waves entering external ear and key anatomy of middle and inner ear. B: Cross-section of cochlea. Demonstrates cochlear structure, especially cochlear partitions and position of inner ear machinery. C: Zoomed-in view of sensory part of cochlear partition. Shows inner and outer hair cells, and their relationship with surrounding structures. Adapted from (Frolenkov et al., 2004).*

The apical side of a hair cell features hair bundles. Bundles are groups of actin-rich stereocilia and each stereocilium expresses a mechanoelectrical transducer channel (MET) at its tip (Figure 1.2). Stereocilia are arranged from shortest to tallest, with tips connected by tip-links comprised of protocadherin 15 (PCDH15) and cadherin 23 (CDH23) (Gillespie and Muller, 2009; Schwander, Kachar and Muller, 2010; Beurg *et al.*, 2008) (Figure 1.2). Hair cells express mechanosensitive channels besides the primary MET (reviewed in (Qiu and Muller, 2018), however, this research concerns the primary MET only. The identity of other channels is not explored here, and references to the MET made beyond this point refer to the channel pore of the MET localised to the tips of stereocilia, or the insect equivalent (e.g. *Drosophila* chordotonal (ch) neurons). Deflection of the hair bundle towards the tallest stereocilia increases MET open probability (Ohmori, 1985; Crawford, Evans and Fettiplace, 1989; Nicolson *et al.*, 1998), and this process depends on the tip links (Assad, Shepherd and Corey, 1991).

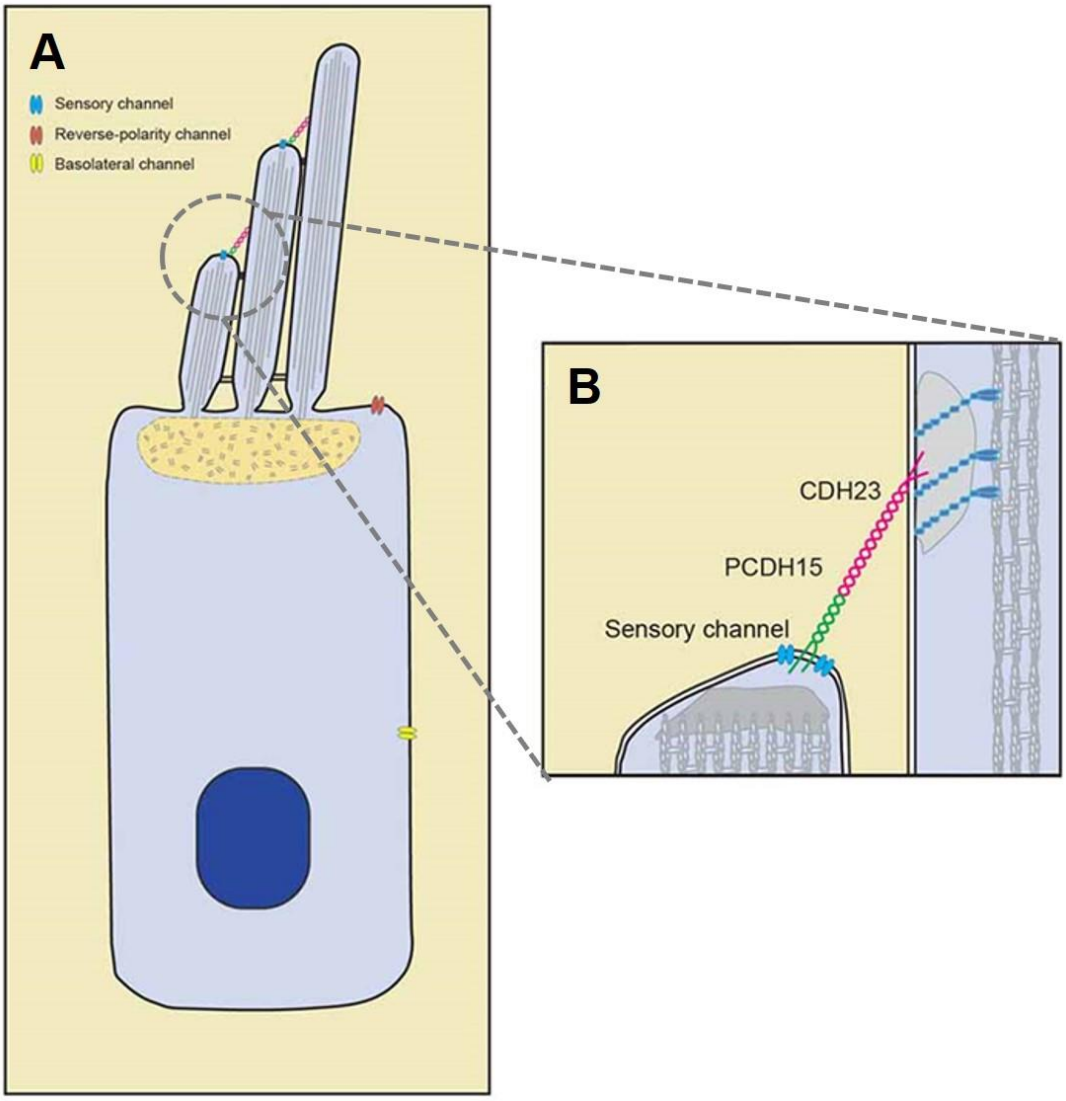

Figure 1.2: Hair cell with stereocilia. *A: Hair cell showing localisation of sensory channel (primary MET) at tip of stereocilia, reverse-polarity channel in the apical cell surface and basolateral channel in corresponding membrane. B: Zoomed-in view of position of sensory channel and tip-link proteins, PCDH15 and CD23. Adapted from Qui and Muller, 2018.*

The location of human hair cells makes them inaccessible for electrophysiology, however, IHCs, OHCs and related vestibular hair cells (VHCs) in other mammals have been used to investigate hair cell currents. Transducer currents generated in rat IHCs deflected by fluid jet, were defined by a large single channel conductance (260pS at -84mV), and characterised the MET as a fast-adapting, calcium-sensitive nonselective cation channel (Beurg *et al.*, 2006). Allowing for some (expected) variance in current size due to experimental design, these characteristics are consistent across a significant body of research: (Kros, Rusch and Richardson, 1992; Geleoc *et al.*, 1997; Kennedy *et al.*, 2003; He, Jia and Dallos, 2004; Jia, Dallos and He, 2007). Given that the biophysical properties of the IHC MET are well characterized, it should be straightforward to identify the channel. However, the (biophysical)

properties do not match those of known mechanosensory pore-forming proteins (reviewed in (Peng and Wu, 2007) and (Qiu and Muller, 2018)). Similarly, MET pharmacology is different to known mechanosensory channels (Farris *et al.*, 2004) and its single channel properties suggest that it is a heteromer (Ricci, Crawford and Fettiplace, 2003). Indeed, there is significant evidence to support a channel complex that includes transmembrane channel-like proteins 1 and 2 (TMC1/2), tetraspan membrane protein in hair cell cilia (TMHS) and transmembrane inner ear expressed gene (TMIE) (Qiu and Muller, 2018).

TMC1/2 bind PCDH15 (Maeda *et al.*, 2014) and are necessary for MET function: TMC1 mutation causes hearing loss in humans and mice (Kurima *et al.*, 2002; Vreugde *et al.*, 2002) and overexpression of either TMC1 or TMC2 rescues MET function on TMC1/2-deficient hair cells (Kawashima *et al.*, 2011; Pan *et al.*, 2013; Askew *et al.*, 2015). Moreover, TMC1/2 expression changes single-channel conductance, Ca^{2+} selectivity and adaptation time in hair cells (Kim and Fettiplace, 2013; Pan *et al.*, 2013; Corns *et al.*, 2017); TMC1 mutation reduces the tonotopic gradient of single-channel conductance in OHCs and the Ca^{2+} permeability and single-channel conductance in IHCs (Pan *et al.*, 2013).

TMHS is localised to the lower end of tip links, near the MET (Xiong *et al.*, 2012; Beurg *et al.*, 2015; Mahendrasingam *et al.*, 2017). Specifically, TMHS binds to the C-terminus of PCDH15 (Beurg *et al.*, 2015) and contributes to transport of PCDH15 and TMC1 into the stereocilia, affecting assembly of the tip link~~(s)~~(s) and transduction machinery (Xiong *et al.*, 2012). As expected, given its role in MET complex assembly, THMS mutation causes deafness and a reduction of MET currents and adaptation in OHCs in mice (Xiong *et al.*, 2012). Interestingly, despite evidence of contributing to the process, TMHS is not essential for tip link complex assembly; ~30% of stereocilia assemble tip link complexes in the absence of TMHS (Xiong *et al.*, 2012). This, in addition to residual currents measured in hair cells lacking TMHS, has led to the suggestion that TMHS is an auxiliary subunit of the pore-forming protein of the MET, where it could regulate the channel in a similar way that TARP proteins regulate AMPA receptors (Xiong *et al.*, 2012; Beurg *et al.*, 2015).

Like THMS, TMIE is localised to the tips of stereocilia and binds PCDH15; TMIE binds to PCDH15-CD2, a splice variant of PCDH15 that regulates the MET (Zhao *et al.*, 2014). Disturbing this interaction by either: (1) overexpression on the C-terminal fragment of TMIE which binds PCDH15 inhibits MET transduction; (2) expression of a fragment of PCDH15, inhibits the MET (Zhao *et al.*, 2014). This suggests that PCDH15, TMIE (and THMS) could form a complex necessary for MET function. TMIE may be particularly critical, as TMIE-deficient hair cells do not demonstrate MET currents, even though all known components of the MET/ MET complex are intact (Zhao *et al.*, 2014). Thus, TMIE is a candidate that could contribute the MET channel pore. Finally, though not thought to be part of the MET complex,

Piezo2 is expressed near the base of stereocilia (Wu *et al.*, 2017) and could form the pore of the reverse-polarity channel (Figure 2A); Piezo2 channels facilitate rapidly-activating, fast-adapting currents like those recorded for the reverse-polarity channel (Coste *et al.*, 2012; Beurg, Kim and Fettiplace, 2014) and reverse-polarity currents are abolished in Piezo2 mutant hair cells (Wu *et al.*, 2017). Piezo2 may also play a role in repair of hair cells, as it does in bone (Ivanusic, 2017).

It is possible that work in arthropods could help identify the MET. Insects are often used in hearing research; however, it is important to consider that there is a lot of variety in insect ears. For example, some insects possess similar sound receptors (tympanic membrane), but otherwise have different ear anatomy and physiology. Katydids perceive sound via a tympanal plate on the foreleg, which transmits vibrations through a fluid-filled auditory vesicle that is continuous with a tibial hearing organ. In contrast, the owlet month has a simple ear that detects sound via a tympanum, which vibrates and signals 2 receptor cells that are linked to motor outputs. These outputs produce evasion behaviours responsible for escaping predation by bats (Figure 1.3). See (Stumpner and von Helversen, 2001) for a review that describes the divergent evolution of insect ears.

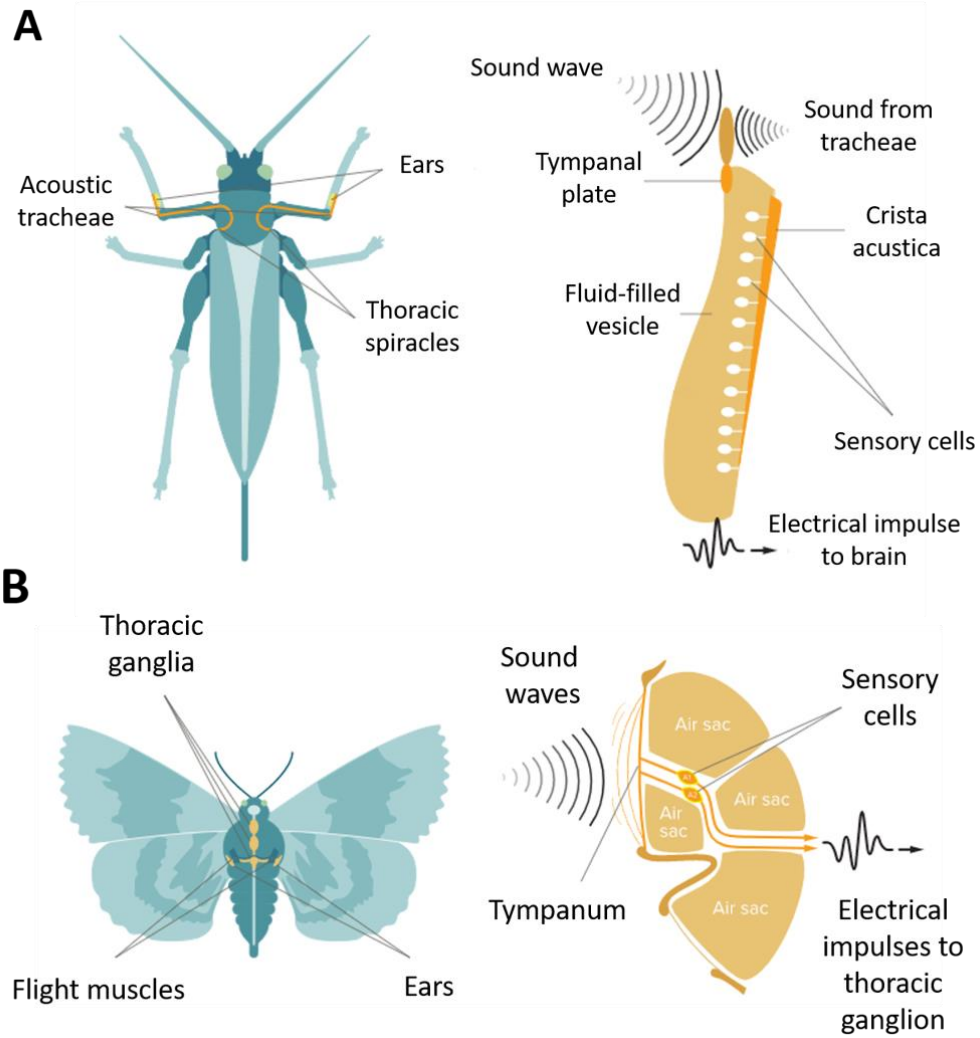

Figure 1.3: Comparison of insect ears. *A: Katydid ears on the foreleg respond to airborne sound (sound waves) and sound transmitted by the acoustic tracheae. Sound is received as vibration of the tympanal plate, and that vibration travels through a fluid-filled vesicle across sensory cells that are tuned to respond to specific frequencies of vibration. These responses are then relayed to the brain. B: Owlet moth ears are simpler than katydid ears. They sit lateral to the flight muscles, and the tympanum of each ear vibrates in response to airborne sound. This vibration is received by specialised sensory cells, A1 and A2, that relay signals to the thoracic ganglia. This direct connection with the ganglia facilitates a fast response to predators (bats, that the moth detects by sound). Figure adapted from (Pain, 2018).*

Insects with antennal ears (*Diptera*) provide a model with many similarities to human hearing. Two of the most common *Diptera* used in research are the mosquito and fruit fly (*Drosophila)*. Both have antennae with a scape (base), pedicel (a2), funiculus (a3) and arista. The arista acts as the sound receiver. It rotates within the pedicel (Gopfert and Robert, 2001), which stimulates the Johnston's organ (JO); a group of ch neurons, or Johnston's organ neurons (JONs), that surrounds the base of the arista. 2-3 JONs and 3-4 support cells combine to form scolopidia, and the total number of scolopidia/ neurons of the JO forms a key difference between the two systems. The *Drosophila* JO features ~200 scolopidia (~500 JONs), whereas the mosquito JO features ~7,500 scolopidia (~15,000 JONs) (Warren, Lukashkin and Russell, 2010; Albert and Gopfert, 2015). Fruit fly and mosquito antennae also differ in that the *Drosophila* arista forms a rotating pendulum with one degree of freedom, while the mosquito antenna is a flagellum that acts like an inverted pendulum with two degrees of freedom (Albert and Kozlov, 2016). The male mosquito exploits its nonlinearity to locate a mate (Jackson and Robert, 2006), however, the reason for the directionality of fly hearing is unclear (Morley *et al.*, 2012). Figure 1.4 shows a fruit fly antenna in detail. Note that whilst it was important to acknowledge the similarities of mosquito and fly hearing, the present research uses *Drosophila* larval chordotonal neurons to model human hearing. Consequently, it is the only *Dipteran* discussed beyond this point.

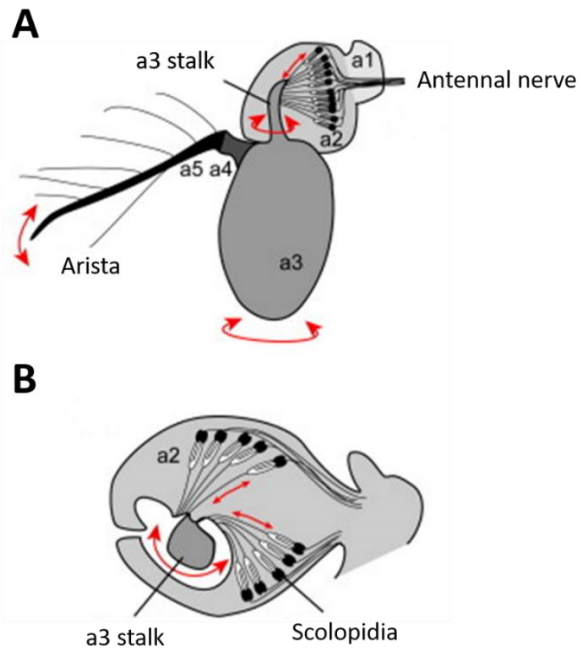

Figure 1.4: Drosophila antenna. *A: Antenna with segments labelled a1-5. The arista vibrates in response to sound, which rotates the a3 (funiculus) stalk inside a2 (pedicel). a2 hosts the Johnston's Organ (JO), which relays sensory information to the brain via the antennal nerve. B: cross-section through a2, showing attachment of scolopidia (groups of Johnston's organ neurons and support cells from JO) to the a2/a3 border. Adapted from (Jarman, 2014).*

Drosophila hearing is like human hearing in several ways. First, hair cells and their *Drosophila* equivalents, ch neurons, arise from precursor cells in response to Notch and bHLH signalling (zur Lage and Jarman, 1999); second, both demonstrate essential nonlinearity that enhances absolute sensitivity to frequency (Eguiluz *et al.*, 2000); third, both have been described by a gating-spring model of mechanosensation (Albert and Kozlov, 2016). In mammals, tension in tip links between stereocilia, created by movement of the hair cell bundle, open MET channels (Albert and Kozlov, 2016) – the lipid bilayer and intracellular proteins (e.g. ankyrin repeat domains of NompC) could perform the same role in insects (Howard and Bechstedt, 2004; Zhang *et al.*, 2015; Liang *et al.*, 2011). I will explore *Drosophila* hearing in greater depth in Chapter 3, which concerns the behavioural role and mechanisms of mechanosensation in ch neurons. For the purpose of this introduction, it is sufficient to establish that *Drosophila* and human hearing are similar.

1.1.2 Proprioception: From mammals to arthropods

The brain-muscle connection was first described in 1826 by Scottish physiologist, Charles Bell. He wrote of a closed-loop system between the brain and muscles which was: "…a circle of nerve; one nerve (ventral roots) conveys influence from the brain to the muscle, another (dorsal roots) gives the sense of condition to the brain" (Bell, 1826). Bell's idea was refined, first by English anatomist Henry Bastian in 1887, then by English neurophysiologist Sir Charles Sherrington in 1906. Bastian introduced the term "kinaesthesia" to describe: "…this complex of sensory impression we are made acquainted with the position and movements of our limbs" (Bastian, 1887). Sherrington formed the definition of proprioception that we use today, which is: "The perception of joint and body movement as well as position of the body, or body segments, in space." (Sherrington, 1906). Proprioception is exemplified in the party game, "pin the tail on the donkey." Players feel where their hand is in space, in relation to a target, while blindfolded. Proprioception is necessary: (1) to protect the joint from excessive and injurious movement via reflex mechanism; (2) to provide information about joint stabilisation during static posture; (3) to aid performance coordination of movement (Knoop *et al.*, 2011).

There are five types of proprioceptors in mammals, all of which exist in or around joints or muscles, namely free nerve endings, Ruffini end organs, Pacinian corpuscles, Golgi tendon organs and muscle spindles. Free nerve endings are stimulated by the deformation of articular tissues surrounding the joint (Lephart, Pincivero and Rozzi, 1998; Swanik, Lephart and Rubash, 2004); Ruffini end organs in the joint capsule report static position, with some feedback on direction of movement (Katonis *et al.*, 2008); Pacinian corpuscles in ligament, meniscus and joint capsule connective tissue relay acceleration of movement (Lephart,

Pincivero and Rozzi, 1998) and Golgi tendon organs are engaged in reflex inhibition of muscle contraction, to prevent muscle damage by excessive force production (Jami, 1992). The final proprioceptor, the muscle spindle, is key to the present research. Muscle spindles are intrafusal muscle fibres that run in parallel with extrafusal muscle fibres. They detect and relay changes in muscle length (Figure 1.5). It is difficult to research spindles in humans (for several reasons including ethical and practical considerations), so much less is known about the cellular mechanisms of muscle length detection than, say, hearing.

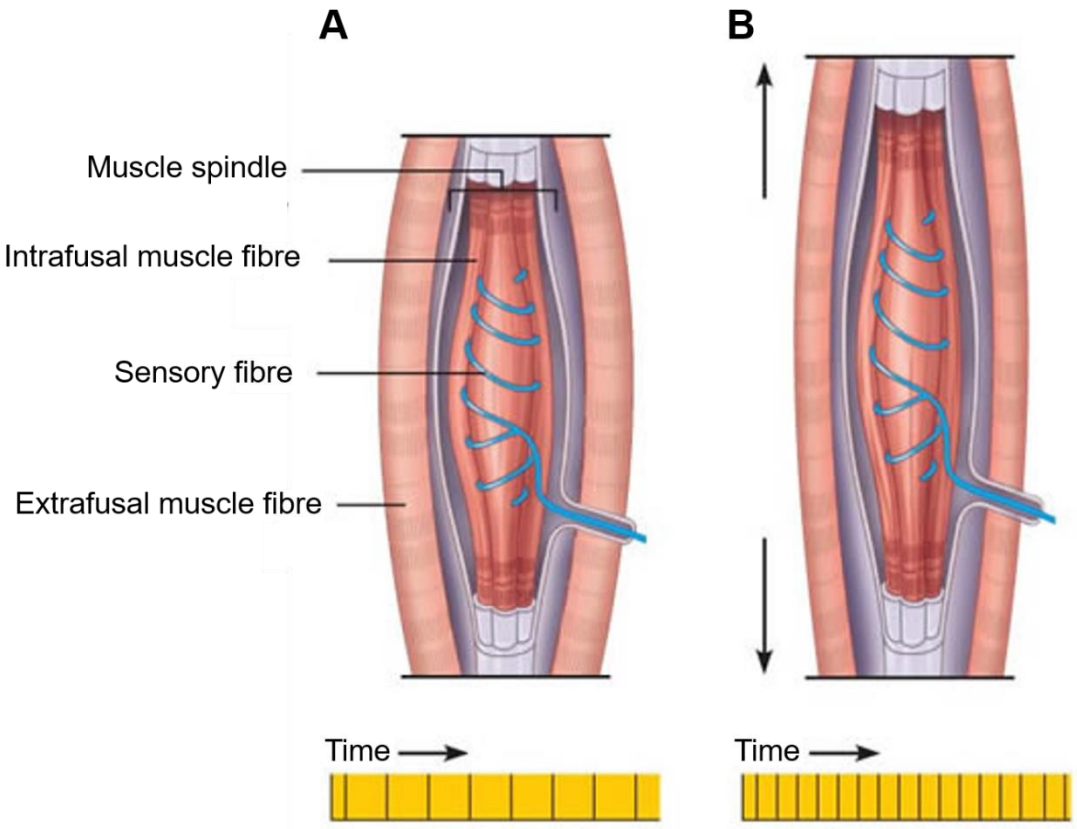

Figure 1.5: Mammalian muscle spindle anatomy and response to stretch. *A: Anatomy of muscle spindle in a relaxed muscle. B: Muscle spindle in a stretched muscle. Black lines in yellow "time" bars below each image depict frequency of action potential firing in each case; spindle action potential frequency increases during stretch. Adapted from (Pearson and Gordon, 2013).*

Most of what is known about the molecular mechanisms of stretch perception comes from work on other mammals. Even in them, recording from the spindle primary fibre terminal is difficult and limits research (Bewick and Banks, 2014). As an alternative, Hunt and colleagues poisoned the principal sensory afferent of feline tail muscle spindles (the sensory nerve fibre) with TTX and recorded from close to its junction with the spindle (Hunt, Wilkinson and Fukami, 1978). This allowed them to show the feline spindle receptor potential (RP) in response to stretch (Figure 1.6), which has a morphology defined by 7 phases (1, baseline; 2, peak initial dynamic response; 3, peak late dynamic response; 4, post-dynamic minimum; 5, static maximum; 6, end static phase; 7, post-release minimum).

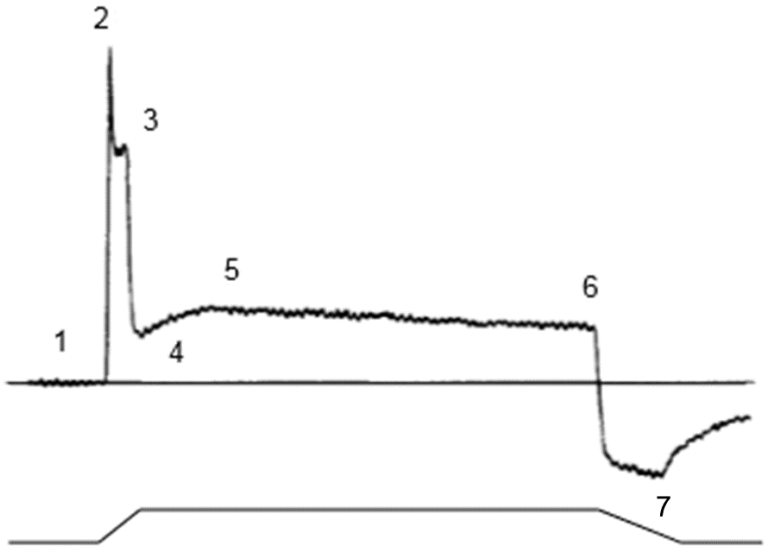

Figure 1.6: Feline spindle receptor potential. *The spindle potential comprises 7 phases (1, baseline; 2, peak initial dynamic response; 3, peak late dynamic response; 4, post-dynamic minimum; 5, static maximum; 6, end static phase; 7, post-release minimum). Horizontal line through trace is resting potential, whilst ramp and hold below trace denotes application of stretch stimulus. Adapted from Hunt, Wilkinson and Fukami, 1978.*

Removing Na^+ and Ca^{2+} from the extracellular solution (replacing Na^+ with Tris, chelating Ca^{2+} with 1.8mM EGTA) used for recordings reduced RP amplitude by ~80% (Hunt, Wilkinson and Fukami, 1978). Removing only Na^+ (leaving 1.8mM Ca^{2+}) reduced RP by ~66%, so sodium current (I_{Na}) is more important for RP generation than calcium current (I_{Ca}). The MET responsible for these currents is unclear. The main candidates for the MET are: Transient receptor potential (TRP), Piezo and degenerin/ epithelial Na (DEG/ENaC) channels. TRP channels are necessary for invertebrate mechanosensation (Gees, Colsoul and Nilius, 2010; Padinjat and Andrews, 2004; Venkatachalam and Montell, 2007), but are more selective for calcium than would fit the I_{Na}-dominant mammalian RP from Hunt *et al.* DmPiezo is required for mechanical nociception in *Drosophila* (Kim *et al.*, 2012) and Piezo2b for light touch in

zebrafish (Faucherre *et al.*, 2013). However, Piezo is not expressed in muscle spindles (Coste *et al.*, 2010; Suslak *et al.*, 2015a). DEG/ENaC channels are the most likely to be the MET; they are highly selective for Na^+ (Garty and Palmer, 1997) and ENaC subunits α, β, γ and δ are expressed in spindles (Simon *et al.*, 2010). ASIC2a (an ENaC superfamily protein) is expressed in spindle terminals where it colocalises with synaptophysin, a marker for synaptic vesicles, which regulate afferent excitability (Bewick and Banks, 2014). ENaC/ ASIC inhibitor amiloride reduces stretch-evoked spindle potentials, whilst ASIC3 is responsible for action potentials generated in response to deformation of the dorsal root ganglion (Bewick and Banks, 2014).

ENaC Na^+ selectivity supports the I_{Na}-dominant model of RP generation from (Hunt, Wilkinson and Fukami, 1978), but suggests another MET is required for of I_{Ca}. This could be a TRP, ASIC1a or Ca_V family channel. TRP channels are expressed in spindles, and TRPM8 agonist AG-3-5 (Wei and Seid, 1983) increases spindle firing (Simon *et al.*, 2010). TRPC and TRPA1 channels are also implicated in mechanotransduction (Trebak, 2010; Suslak, Armstrong and Jarman, 2011). ASIC1a is permeable to calcium, but there is no evidence that it is expressed in spindles (Bewick and Banks, 2014). The L-type calcium channel blocker nifedipine inhibits spindle firing (Fischer and Schafer, 2002) and N-type channels are mechanosensitive in heterologous systems (Calabrese *et al.*, 2002). However, the N-type channel blocker ω-conotoxin GVIA does not affect spindle firing (Simon, Banks and Bewick, 2008). Thus, the identity of the MET responsible for I_{Ca} in spindles remains a mystery.

Arthropod stretch receptor organs (SROs) may be good models of mammalian spindles. The long history of using SROs to model muscle stretch perception began in 1951, when Jerzy Stanislaw Alexandrowicz described the bipolar morphology of sensory terminals that ran in parallel to crustacean skeletal muscle fibres (Alexandrowicz, 1951). Later work showed that the crayfish SRO RP exhibits a mechanosensitive I_{Na} current (Kaila *et al.*, 1987), plus TTX (I_{Na}) and TEA(I_K)-sensitive currents (Figure 1.7 (Ottoson and Swerup, 1982)) like those of the cat tail spindle (Hunt, Wilkinson and Fukami, 1978).

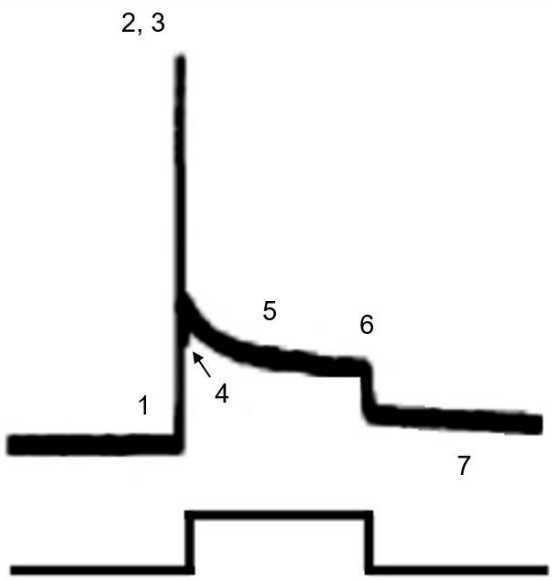

Figure 1.7: Crayfish stretch receptor organ receptor potential. *Like the feline spindle receptor potential, the crayfish SRO potential is comprised of 7 phases (1, baseline; 2, peak initial dynamic response; 3, peak late dynamic response; 4, post-dynamic minimum; 5, static maximum; 6, end static phase; 7, post-release minimum). Ramp and hold below trace denotes application of stretch stimulus. Adapted from Ottoson and Swerup, 1982.*

Shortly after Alexandrowicz reported his findings on crustacean SROs, similar stretch receptors were found in insects (Finlayson and Lowenstein, 1958). These receptors were bipolar, type II (non-ciliated) neurons, that ran in parallel with muscle (Braunig, Cahill and Hustert, 1986) present in the thoracic and abdominal segments of all insect orders investigated (Finlayson and Lowenstein, 1958; Osborne and Finlayson, 1962). More recent work has characterised the anatomy and physiology of the SRO in the caterpillar of the hawkmoth, *Manduca sexta* (Simon and Trimmer, 2009). Specifically, it reported that like crustacean SROs and mammalian spindles, the caterpillar SRO response to displacement is a tonic-phasic, and its amplitude depends on the extent and velocity of stretch (Simon and Trimmer, 2009; Hunt and Ottoson, 1975).

The *Drosophila* larva dorsal bipolar dendritic (dbd) neuron may be a stretch receptor. It has longitudinal dendrites that span each abdominal hemisegment (Figure 1.8) and it runs in parallel to muscle, like SROs and spindles (Suslak and Jarman, 2015). However, these dendrites terminate in a thin strand of connective tissue, so the dbd is not directly associated with muscle in the same way that SROs and spindles are (Schrader and Merritt, 2007). In contrast and so in support of the idea that the dbd is a stretch receptor, they demonstrate similar physiology to SROs. Both exhibit TTX and TEA-sensitive currents (Nair, Bate and Pulver, 2010), so they may share a MET. Similarly, work from the Jarman laboratory posed that the dbd responds to stretch and its MET could be the *Drosophila* orthologue of Piezo,

DmPiezo. Mutating the gene reduced the peak initial dynamic response of the larval dbd neuron receptor potential by ~80% (Suslak *et al.*, 2015b). TRPA1 may contribute the remaining ~20% current as I_{Ca}. Recently, swept confocally aligned planar excitation (SCAPE) microscopy confirmed that the dbd is a stretch receptor (Vaadia *et al.*, 2019). SCAPE facilitates analysis of tissue and cell dynamics in live, behaving animals, by GCaMP (a Ca^{2+} reporter). It showed that dbd neurons are most active in a relaxed or stretched segment during larval crawling, and that this is different to other larval proprioceptors (ddaE, ddaD and dmd1, see section below for a description of these neurons). Chapter 3, *"The role of dorsal bipolar dendritic neurons in proprioception and nociception"*, includes a more detailed account of dbd neuron anatomy and physiology. Its brief introduction here highlights the fact that the dbd neuron and relative simplicity and tractability of fly biology, could be used to model and overcome the difficulty of studying the mechanism~~(s)~~(s) of stretch perception in mammals.

1.2 The *Drosophila* peripheral nervous system and translation of fly research

Since this thesis concerns dbd and ch neurons in *Drosophila* larvae, it is important to review the anatomy of the larval peripheral nervous system (PNS). The PNS branches off from the ventral nerve cord (VNC), in a stereotyped pattern of 45 sensory neurons per abdominal hemisegment (Figure 1.8). Somatosensory organs are grouped into ventral (v), ventral' (v'), lateral and dorsal clusters of either type I (ciliated) or type II neurons (Singhania and Grueber, 2014).

The type I neurons are the external sensory (es) and ch neurons. The es neurons are sensitive to touch (Hartenstein, 1988) and can be identified by either: (1) a campaniform sensillum and papilla; (2) a trichoid sensillum and hair. Ch neurons are as described earlier. Type II neurons are the multidendritic (md) neurons, which are further separated as tracheal dendrite (td), dendritic arborization (da) and dbd neurons. As their name suggests, td neurons innervate trachea (Merritt and Whitington, 1995). There are 15 da neurons per hemisegment, which are subdivided into 4 classes (I-IV). Class I and II neurons have simple branching patterns, and class I neurons are involved in proprioception (Hughes and Thomas, 2007; Cheng *et al.*, 2010; Suslak *et al.*, 2015c). Class II and class III (class III neurons are characterised by 'spikey' protrusions from main branches) express Ripped Pocket, NompC and NMDA receptors and are sensitive to touch (Yan *et al.*, 2013; Tsubouchi, Caldwell and Tracey, 2012). Class IV neurons show extensive dendritic arborisations that span the hemisegment and are responsible for a *ppk26* and *DmPiezo*-dependent mechanism that senses mechanical nociception (Kim *et al.*, 2012; Hwang *et al.*, 2007; Guo *et al.*, 2014). Dbd neurons are as described earlier. Note that the function~~(s)~~(s) of the dbd and ch neurons are not elaborated here; as mentioned above, this is reserved for the introductions of relevant chapters (Chapter 2 and Chapter 3, respectively). Suffice to say that the behavioural role~~(s)~~(s) of, and mechanism~~(s)~~(s) of mechanosensation present in dbd and ch neurons are unclear, in an otherwise reasonably well characterised PNS.

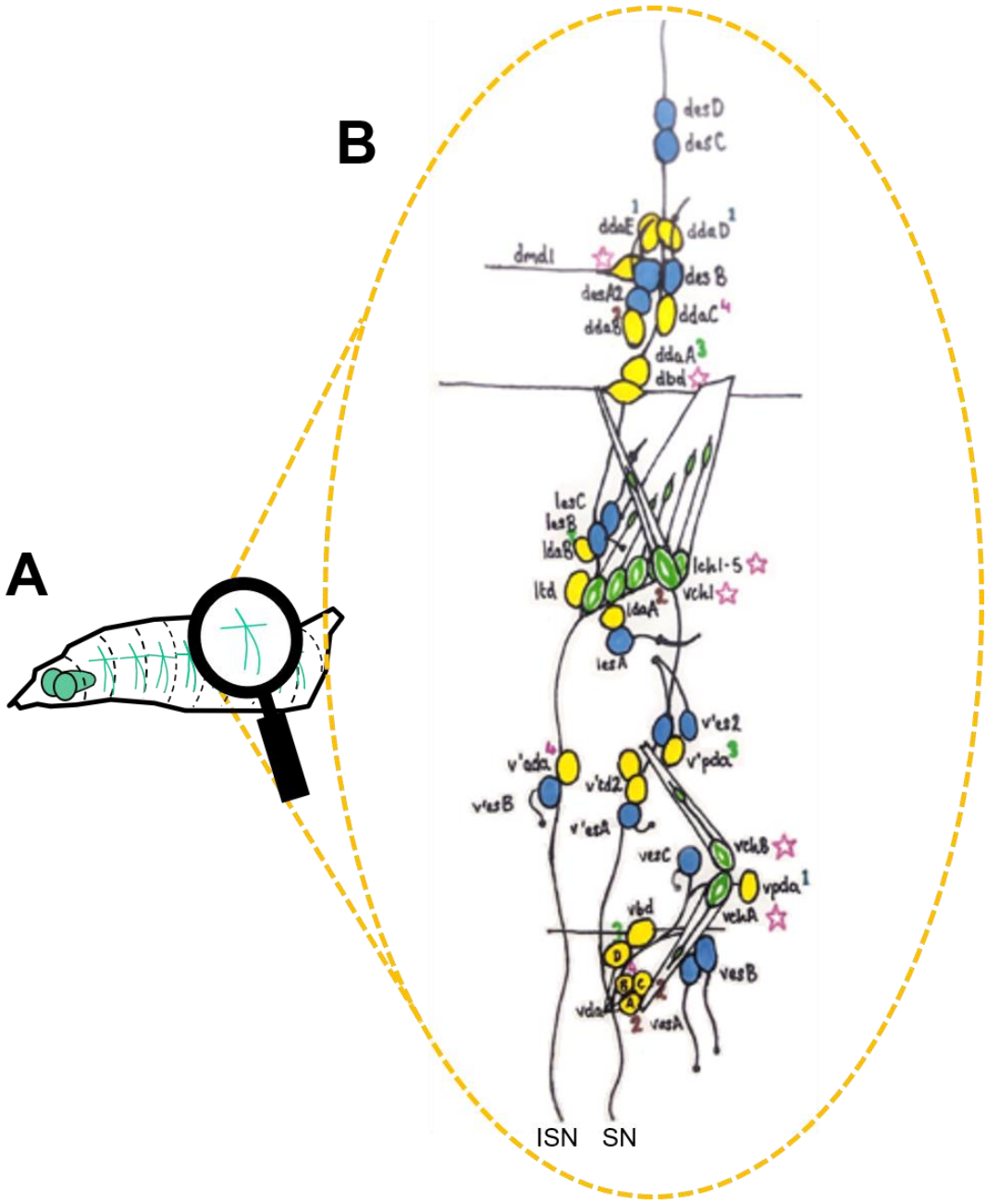

Figure 1.8: Larval nervous system. *A: Larval body plan showing brain lobes and ventral nerve cord (green) at anterior of larvae, and approximate position of peripheral neurons in each of the 8 abdominal hemisegments. B: Colours show types of neuron~~(s)~~(s): Blue is external sensory (es) organs; green is chordotonal (ch) neurons; yellow is multidendritic (md) neurons. Coloured numbers (1-4) highlight classes of da neurons. Stars highlight neurons of interest for the work contained in this Thesis (vchAB, lch1-5, vch1, dbd and dmd1). ISN is intersegmental nerve, which terminates at the posterior root of the anterior fascicle of the CNS; SN is segmental nerve, which terminates as the posterior fascicle of the CNS. Rest of nervous system (motor neurons etc) is omitted for clarity.*

Finally, the fruit fly is one of the most commonly used animal models in nervous system research. Its study has resulted in many novel insights. For example, *Notch* was identified as a gene related to mutations that caused *Drosophila* wing malformation (Morgan and Cattell, 1912). Later research showed that it was necessary for normal embryonic development; loss of *Notch* caused a neurogenic phenotype, characterised by a hypertrophied CNS, then helped identify key genes in differentiation/ cell fate: *neuralized*, *Delta*, *mastermind*, *big brain* and *Enhancer of split* (Camposortega, 1988). Cloning of *Notch* (Wharton *et al.*, 1985) and *Delta* (Vassin *et al.*, 1987) was essential to describe the *Notch* signalling pathway (Artavanistsakonas, Matsuno and Fortini, 1995; Kopan and Ilagan, 2009). Notch is conserved in humans (Ellisen *et al.*, 1991) and most of the signalling pathways identified in flies, exist in mammals (Kopan and Ilagan, 2009). The pathway plays a crucial role in neurogenesis and neuronal differentiation in vertebrates, including cell fate and dendrite morphology in dentate gyrus (Breunig *et al.*, 2007), blood cell and heart development, bone and skin development (Bellen, Tong and Tsuda, 2010) and dysfunction has been linked to cancer (Kopan and Ilagan, 2009). Also, relevant to this thesis, Notch signalling promotes differentiation of proneural cells into hair cells and is one focus of future treatment for hearing loss (Samarajeewa, Jacques and Dabdoub, 2019).

Like Notch, the *achaete-scute* complex is an example of success in translating *Drosophila* research to vertebrates. Complex proteins (comprising four genes: *achaete*, *scute*, *lethal of scute* and *asense* (Ghysen and Damblychaudiere, 1988)) are expressed in neural precursors of the CNS and PNS and are necessary for ectoderm to neural cell fate (Bellen, Tong and Tsuda, 2010). *achaete* and *scute* determine sensory organ specification and *achaete-scute* complex proteins are bHLH transcription factors expressed in ectodermal cells (Cabrera, Martinezarias and Bate, 1987). bHLH proteins, which include Atonal, are necessary to determine neuronal precursors of the fly PNS (Jarman *et al.*, 1993) and homologs are necessary for vertebrate neurogenesis (Lo *et al.*, 1991), specification of vertebrate IHCs (Bermingham *et al.*, 1999), touch receptors (Van Keymeulen *et al.*, 2009; Maricich *et al.*, 2009) and motor neurons (Maricich *et al.*, 2009). While Notch signalling and *achaete-scute* complex research have been discussed here, much more has been discovered using *Drosophila* as a model organism. This includes findings related to the development of the nervous system, the molecular basis of behaviour and proteins that affect the function of the nervous system. Extensive discourse is beyond the scope of this text so for a full review, see (Bellen, Tong and Tsuda, 2010). Suffice to say that *Drosophila* is an established model with a strong record of translation of research findings to humans, so is appropriate to use to achieve the aims of this Thesis.

1.3 Aims

1. Test the hypothesis that crawling and nociception is mediated by dbd neurons, and that this is facilitated by a MET; DmPiezo or TRPA1. I will test the role of the dbd neuron in behaviour with crawling, nociception and optogenetic assays, then attempt to identify the MET by whole-cell patch-clamp electrophysiology. If correct, the hypothesis provides important insight into the *Drosophila* mechanism of stretch perception, which could provide a useful model for understanding human mechanosensation in health and disease.

2. Test the hypothesis that chordotonal neurons are chiefly sound/ vibration sensors that also sense stretch, by a mechanism that requires dyneins. I will use hearing, crawling and GCaMP experiments to assess the role of ch neurons in sound and stretch perception. I will then test the role of dyneins in ch neuron mechanosensation, using GCaMP. If correct, the hypothesis improves our understanding of the *Drosophila* peripheral nervous system and describes a mechanism that highlights the importance of dyneins in ciliary motility, especially as it relates to the function of genes related to human disease (e.g. primary ciliary dyskinesia).

3. Test the hypothesis that ciliary immotility leads to behavioural dysfunction, so that *Drosophila* behavioural assays can screen for gene mutations associated with PCD. I will use crawling and hearing experiments on larvae carrying mutations of, or RNAi knockdown of genes related to dynein assembly, to determine whether the hypothesis is correct. If it is, it offers a useful first step in identifying PCD gene candidates, to guide future treatment of the disease.

2 Materials and methods

2.1 Immunostaining of *Drosophila* larvae

2.1.1 Fillet dissection

Larvae were dissected in a Sylgard dish, filled with HL3.1 (70mM NaCl, 5mM KCl, 1.5mM $CaCl_2$, 4mM $MgCl_2$, 10mM $NaHCO_3$, 5mM Trehalose, 115mM sucrose, 5mM HEPES, pH 7.2 (Feng, Ueda and Wu, 2004)). The tail end of each larva was pinned between the trachea, and the animal was stretched and pinned (again) at the head, avoiding the CNS. Lateral incisions were made at each end of the larvae, to facilitate a longer, lengthways incision between them. Innards (guts, trachea etc.) were scooped out with forceps, leaving only the pelt and nervous system intact. The pelt was pinned out (four-square), to complete the fillet dissection.

2.1.2 Fixing, staining and mounting

Third-instar larvae were fixed in 3.7% formaldehyde in HL3.1 for ≥30 mins, on a mixing platform, in a Sylgard dish covered in tin foil. They were then washed 3 times: First with 4°C PAT3 buffer (0.5% by weight Triton X-100, 5% by volume 10% bovine serum albumin (BSA) in 1 x PBS, where PBS = 1 x PBS tablet (Sigma) in 200ml deionised H_2O) for 15 minutes, then twice with room temperature PAT3 buffer for 15 minutes. Next, pelts were transferred to Eppendorfs and filled with blocking buffer (3% normal goat serum (NGS) in PAT3), then placed on a variable speed tube rotator (VSTR) for 1 hour. After, the Eppendorfs were wrapped in foil, blocking solution was aspirated from, and 1° antibody solution was added to the tubes (e.g. 1:1000 rabbit anti-GFP and 1:200 mouse anti-22C10 as a counterstain, in blocking buffer with PAT3 volume adjusted for antibody concentration). Tubes were placed on a VSTR for 2-4 hours and then nutated for ~20 hours (or overnight) at 4°C. Pelts were washed as after fixing: First with 4°C PAT3 buffer for 15 minutes, then twice with room temperature PAT3 buffer for 15 minutes, before washes were aspirated and 2° antibody solution was added to the tubes (e.g. 1:1000 goat anti-rabbit 488 and 1:1000 goat anti-mouse (22C10), in blocking buffer with PAT3 volume adjusted for antibody concentration). Tubes were placed on a VSTR for 2-4 hours, then washed (once with 4°C PAT3 buffer, twice with room temperature PAT3 buffer (all 15 minutes)), with wash aspirated for mounting. To mount, pelts were positioned on slides and submerged in a drop of Vectashield®, before being covered by a coverslip. Images were taken on a confocal microscope and processed in the public domain imaging software, ImageJ, which can be downloaded at: https://imagej.nih.gov/ij/download.html.

2.2 Optogenetics

2.2.1 Preparation of all-trans retinal food

Eggs were laid and larvae developed in 1mM all-trans retinal (ATR, Sigma) food. Food was made by mixing 60µl of 100mM stock solution (14mg ATR in 486µl 100% ETOH) into 6ml fly food (contents of standard vial), after warming food in microwave. Food was left to cool to room temperature before use.

2.2.2 Behaviour in response to light stimulation

The protocol was based on (Pulver *et al.*, 2011) and (Titlow, Johnson and Pulver, 2015), and setup as shown in Figure 6.1. Larvae were raised on ATR food, which was kept in the dark (to prevent light stimulation of ATR chromophore and/ or larvae). Third-instar larvae were lifted from the walls of the food vial with a damp paintbrush and placed in the centre of a grape agar plate (arena). A camera was set to "record" and simultaneously a timer (on mobile phone, not shown in Figure 2.1) was set to countdown from 120 to 0s, and the experimenter announced: "Start" (to confirm start of experiment on camera recording). 120s was separated into 30s normalisation, for larvae to acclimatise to the arena; 30s pre-stimulation, as control/ for comparison to stimulation; 30s stimulation, to apply red light (by pressing button shown in Figure 6.1); 30s post stimulation, as control/ for comparison to stimulation. The arena was moved by hand during the experiment, to ensure larvae were centred in the recording. Specific parameters were derived from recordings filmed on a Panasonic DMC-T28 (with LEICA 12x optical zoom) camera, played frame-by-frame in Avidemux 2.6 – 64 bit (video player that facilitates milliseconds-accurate playback, available at: http://avidemux.sourceforge.net/download.html) as: (1) crawling speed (CS) = crawling distance (mm)/ time ~~(s)~~(s); (2) peristaltic wave frequency (PWF) = number of peristaltic waves/ 30s, where a peristaltic wave was a contraction that passed along the length of a larva from posterior to anterior (forward movement) or anterior to posterior (backward movement); (3) peristaltic wave duration (PWD) = time ~~(s)~~(s) per peristaltic wave.

When comparisons were made between parameters measured before and after light stimulation, e.g. % change in CS on light stimulation, results for controls and experimental crosses were normalised (expressed on the same scale from 0-100) in GraphPad Prism 7 (trial available at: https://www.graphpad.com/demos/) before being expressed as a % change in behaviour on light stimulation ((e.g. CS on stimulation - CS before stimulation)/ CS before stimulation x 100) in Microsoft Excel. % change in behaviour on light stimulation was then compared by one-way ANOVA with Tukey's post-hoc test in GraphPad Prism 7. Note that in

the case of crawling speed (CS) experiments, the filter shown in Figure 2.1 was removed and a lid was added to the arena. The larval position was tracked on the lid, so that CS could be calculated as above.

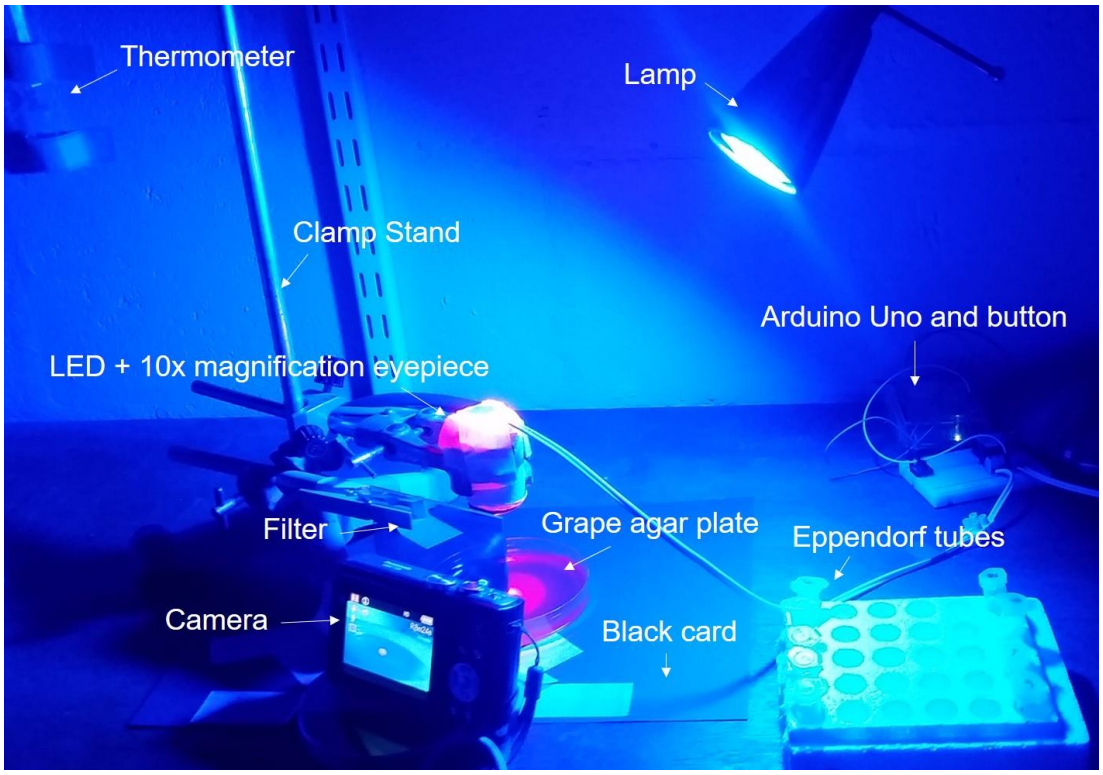

Figure 2.1: Optogenetics experiment setup. *Components and their role~~(s)~~(s) in experiments were as follows: Thermometer fastened to wall of behavioural room, to check temperature was constant across experiments; clamp stand as base to which camera, LED + 10x magnification eyepiece and filter were attached; LED + 10x magnification eyepiece provided stimulating (red) light and focussed that light on the arena; filter prevented glare from arena affecting camera recordings; camera recorded experiments for later analysis; grape agar plate was arena; black card secured to table, beneath arena, reduced glare and increased contrast between arena and larva; lamp provided blue light as background for experiments; Arduino Uno facilitated programming of button, which activated and maintained LED illumination for 30s; Eppendorf tubes were used to separate larvae before and after use in experiments.*

2.3 Pinch experiments

Pinch experiments were used as a novel assay of nociception. The setup was as for optogenetics (Figure 2.1) but only the thermometer, camera, arena and black card were used. Third-instar larvae were removed from food vials using a damp paintbrush and washed, until a total of 16 were collected on a grape agar plate. Larvae were then moved from the plate, one at a time, into the arena. A timer was set to countdown from 150 to 0s, while the experimenter announced: “Start” (to confirm start of experiment on the recording). Larvae crawled freely around the arena during the experiment and every 30s, the posterior of the larvae was ‘pinched’ with forceps (see Figure 3.12). 150s was separated into 30s normalisation, for larvae to acclimatise to the arena; 30s pre-pinch, as control/ for comparison to pinch, pinch applied (x3); 30s post pinch, as control/ for comparison to tone. Analysis was performed by subjective assessment (observation) of the presence or absence, and description of behavioural response to pinch, in videos viewed in Avidemux 2.6 – 64 bit.

2.4 Crawling experiments

The setup was as in Figure 2.2. Third-instar larvae were removed from food vials using a damp paintbrush and washed, until a total of 16 were collected on a grape agar plate. One larva was placed in the centre of the arena, a 20 x 20cm 1% agarose gel plate. A 1cm calibration line was drawn onto the lid of the plate and a timer (a mobile phone application, not shown in Figure 6.2) was set to countdown from 120 to 0s. During this time, larval path was traced using a permanent marker (drawn on lid of plate). Paths (traces) were photographed and analysed by measurement on ImageJ. Specifically, the straight line tool was used to measure the calibrating line and following this calibration, the segmented line tool was used give larval crawling path length. Crawling speed (CS) was then calculated as: CS = larval crawling path length (mm)/ 120, so CS was given in mm/ s. Statistical analysis was performed by comparing means of samples (e.g. *CG34297* +/- vs. *CG34297* -/-) by student *t*-test or one-way ANOVA with Tukey’s post-hoc test on GraphPad Prism 7.

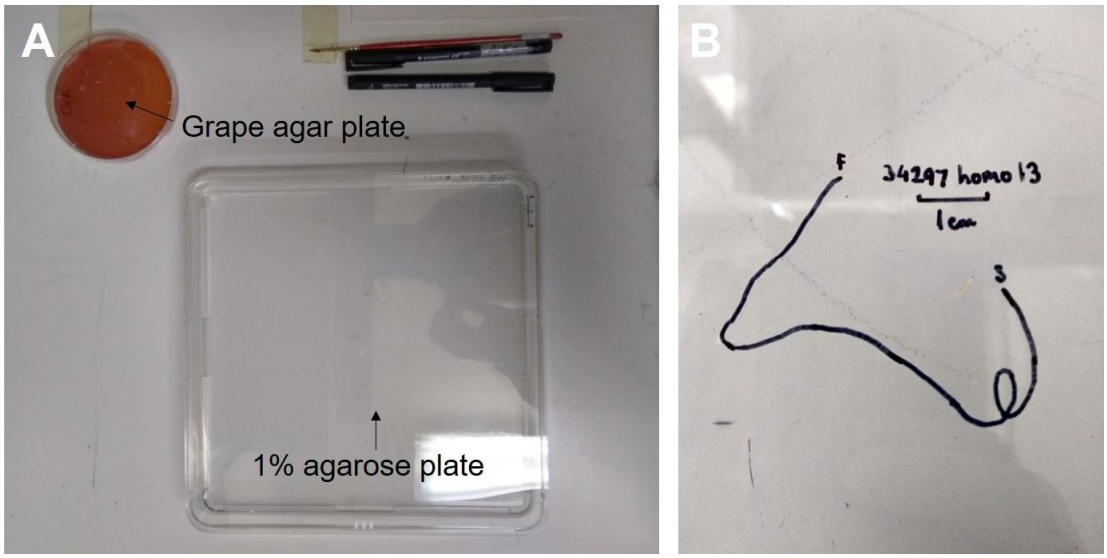

Figure 2.2: Crawling experiment setup. *A: Grape agar plate 'holding pen' for larvae, before they were used in experiments. 1% agarose plate for arena. B: CS trace shown after an experiment (annotation shows CG34297 homozygous larva, number 13. S = start, F = finish).*

2.5 Electrophysiology

The protocol was developed from ((Suslak *et al.*, 2015b). Setup was as in Figure 2.3. Larvae were dissected in HL3.1 in the (fillet) style used for immunostaining, in a custom-made acrylic and wax dish (originally made by Thomas Suslak, later adapted by author). HL3.1 used during dissection was aspirated by Pasteur pipette to remove debris, and fresh HL3.1 was added to the preparation. The preparation was then moved to the electrophysiology rig and viewed at 400x magnification. Muscle overlying the dbd neuron was digested with 1% Type-XIV protease (Sigma-Aldrich), which was applied (and then removed) by large-bore glass electrode. The large-bore electrode was then replaced; whole-cell patch-clamp recordings were made using glass microelectrodes pulled using a P87 puller (Sutter Instruments, USA), with an (electrode) internal solution of 140mM KCH_3SO_3, 2mM $MgCl_2$, 2mM EGTA, 5mM KCl, 20mM HEPES (inspired by (Nair, Bate and Pulver, 2010)).

Electrodes were moved into close proximity of the dbd neuron using a Narishige MC-35 micromanipulator, and gentle suction was applied via syringe to form the seal necessary for whole-cell recordings. Sealing was problematic and values were usually 10-40MΩ - significantly lower than the 1GΩ expected for this type of recording (see Results and Discussion chapters for details). Electrodes were mounted in an Axon Instruments CV201 headstage, connected to an Axopatch 200 amplifier. The amplifier was connected to a computer running Windows 7, via a Digidata 1200, so traces could be recorded using WinWCP (University of Strathclyde, latest version available at: http://spider.science.strath.ac.uk/sipbs/software_ses.htm).

Experiments were mostly current-clamp recordings of voltage change in response to a stretch stimulus, which was delivered to the preparation by either: Tapping on the headstage; a 'puff' of air; piezoelectric wafer; servo driven by Arduino Uno. Results include details of which stretch stimulus was used to produce them. Other work was voltage-clamp recordings of current response to -90mV-60mV steps (Figure 2.41). Traces were uploaded to Clampfit 10.3 (Axon pCLAMP, latest version available at: http://mdc.custhelp.com/app/answers/detail/a_id/20260/~/axon%E2%84%A2-pclamp%E2%84%A2-11-electrophysiology-data-acquisition-%26-analysis-software) which was used to: (1) calculate initial depolarisation of the dbd neuron membrane (dE_m) following stretch: $dE_m = E_p - E_{mrest}$, where E_p was peak depolarisation and E_{mrest} was resting potential; (2) to improve presentation of traces. Comparison of mean dEm (e.g. % difference in W^{1118} vs. *DmPiezo -/-*) was made by calculating: Mean dEm of experimental line/ mean dEm control line x 100, in Microsoft Excel.

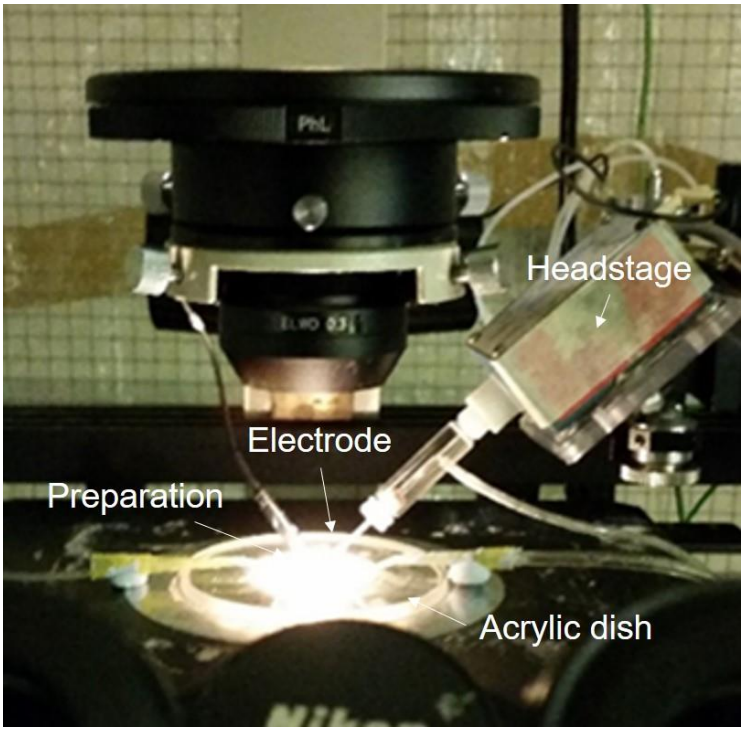

Figure 2.3: Electrophysiology experiment setup. *Image shows key components to clarify their position~~(s)~~(s) in relation to one and other. Note that the setup included an inverted microscope (light source above preparation, lens below).*

2.6 GCaMP imaging

Adapted from (Fushiki, Kohsaka and Nose, 2011). Third-instar larvae were removed from food vials and washed using a damp paintbrush. Larvae were dissected (to fillet preparations) as for immunostaining, with the following modifications: (1) A pin was added between the brain and mouth hook, to fix the position of the VNC (total of 7 pins used here, versus 6 in a normal fillet); (2) Dissection was performed in Ca^{2+}-free saline (140mM NaCl, 2mM KCl, 6mM MgCl2, 5mM Hepes-NaOH, 36mM Sucrose, pH 7.2), as opposed to HL3.1; (3) dissection took place in a Sylgard dish that was smaller and shallower than that used for staining (~30mm diameter x ~10mm deep) and dissection pins were cut short, so that the preparation fit between the lens and platform of the microscope used for recordings. Buffer and debris associated with dissection was aspirated by Pasteur pipette, then the preparation was washed with Ca^{2+}-free saline. Wash saline was aspirated by Pasteur pipette and replaced with 2mM Ca^{2+} Ringer solution (130mM NaCl, 5mM KCl, 2mM $MgCl_2$, 2mM $CaCl_2$, 5mM Hepes-NaOH, 36mM Sucrose, pH 7.3). This solution included 200µM pymetrozine for appropriate experiments.

The dish was fixed to a microscopy slide using Blu Tack, so that the preparation could be imaged on a Zeiss AX10 Examiner A1 fluorescence microscope fitted with a 40x water immersion objective, plus a Q-imaging WLS™ LED illumination unit and Photometrics Prime sCMOS camera. Video was recorded with the following camera settings: 50ms exposure, 20 brightness, 1 x 1 bin (pre-seq); 755 tp @ 53ms/ tp, to give ~20 fps (19.99 fps). The microscope was focussed on the neurons of interest (VNC or chordotonal neurons) and experiments proceeded according to the stimulation used/ observe. Specifically, response to tone videos were filmed over 40s. The first 10s were used to observe neurons under normal conditions (no stimulation); afterwards, a period of stimulation (~1s) was applied every 10s, so that each stimulation was separated from the one prior by ~9s ('recovery' time), until a total of 3 stimulations per preparation (3 x 10s as ~1s stimulation at a specific frequency, separated by ~9s rest per stimulation) was reached. Stimulation was provided using a tuning fork of 256Hz, 512Hz or 1024Hz, applied directly to (touching) the platform of the microscope. Muscle contraction was innate to the preparation (occurred without external stimulation) and spontaneous; contractions did not occur at reliable intervals. Consequently, total times for recordings varied (unlike 40s for response to tone videos) in order to maximise opportunity to record response to 3 contractions in a single preparation (but were usually ≤60s long).

Positive and negative controls were applied to preparations after recording responses to stimulation, to confirm that GCaMP was working properly: 25mM KCl (pipetted into the experimental solution) depolarised neurons so provoked a strong GCaMP response, whereas 2mM EGTA (also pipetted into the experimental solution) chelated Ca^{2+} and so prevented (further) GCaMP response. Analysis of responses to tone and muscle contraction was

performed in stages. First, TIFF files of camera recordings were uploaded to ImageJ, and the "Polygon selection" tool was used to draw around neurons to define a region of interest (ROI). The mean grey value of the ROI was measured across all the images in the TIF stack of each recording, to quantify fluorescence (F). F values were pasted in Microsoft Excel, where they were converted to ΔF/ F0 (%), where ΔF was change in fluorescence ($F-F_0$) and F_0 was either: (1) mean F of (0s - onset of 1st peak) + (end of 1st peak to onset of 2nd peak) + (end of 2nd peak to onset of 3rd peak) for representative peaks, or mean F of 0.5s preceding onset of each peak for peaks used in formulation of mean peak. Finally, ΔF/ F0 (%) traces and bar charts were plotted in GraphPad Prism 7. Comparison of amplitude of mean peak response to stimulation was by t-test, also in GraphPad Prism 7.

2.7 Hearing experiments

The setup was as shown in Figure 3.4. Third-instar larvae were removed from food vials using a damp paintbrush, and placed on a grape agar plate, until five larvae were spaced out equally in the arena. A camera was set to “record” and simultaneously a timer (on laptop) was set to countdown from 150 to 0s, while the experimenter announced: “Start” (to confirm start of experiment on camera recording). Larvae crawled freely around the arena during the experiment and every 30s, a mobile phone tone generator application (not shown in Figure 6.4) and speaker were used to play a 1s, 70dB pure tone of a specific frequency (e.g. 500Hz) to the animals. 150s was separated into: 30s normalisation, for larvae to acclimatise to the arena; 30s pre-tone, as control/ for comparison to tone, tone applied (x3); 30s post tone, as control/ for comparison to tone. Response to tone was defined as the presence of the classical ‘retraction’ phenotype observed when larvae respond to the approach of a parasitic wasp (Hwang *et al.*, 2007); lack of response was defined as an absence of this phenotype. Analysis was performed by calculating the mean number of larval responses to (all 3) tones per experiment, repeated across the 3-5 groups of larvae used per experiment. The median rank of the 3-5 group means was used to compare hearing ability in different genotypes by Mann-Whitney test or Kruskal-Wallis with Dunn’s post-hoc test, performed in GraphPad Prism 7.

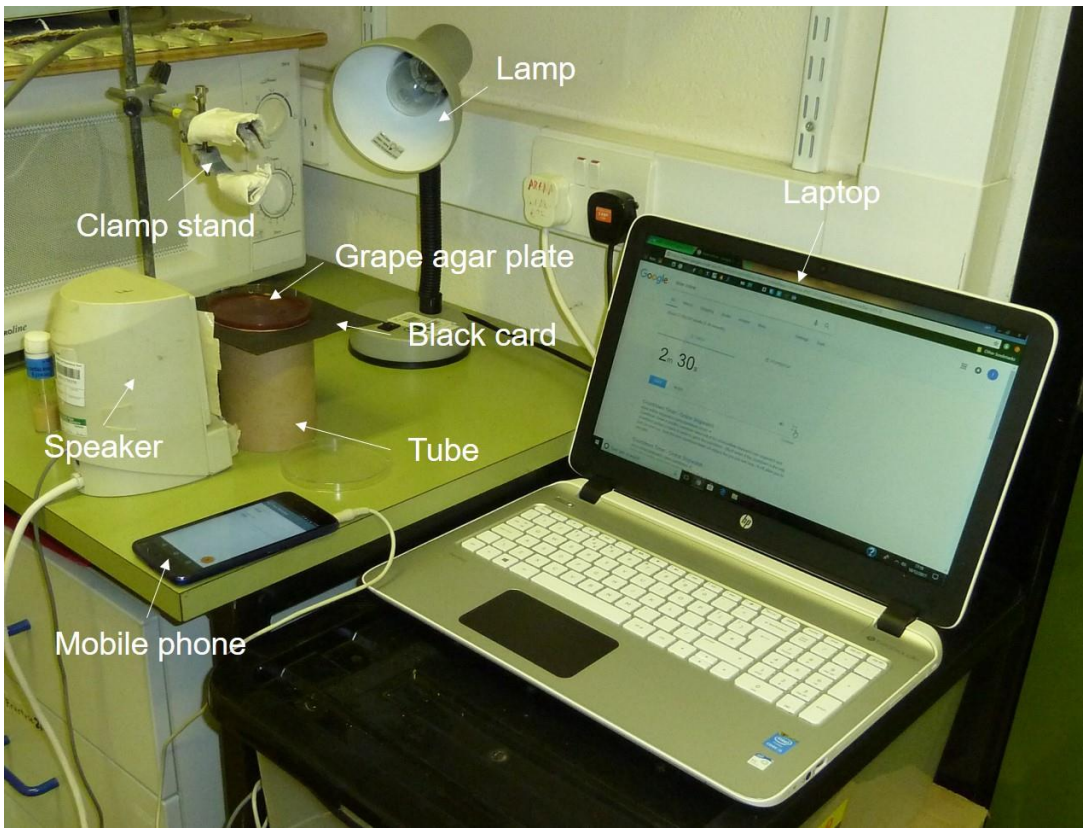

Figure 3.4: Hearing experiment setup. *Components and their role~~(s)~~(s) in experiments were as follows: Clamp stand held camera (latter not shown); grape agar plate was the arena; speaker, pulled out of plastic housing and supported by tube, provided pure tone; black card placed on top of tube, beneath arena, increased contrast between larvae and arena; grape agar plate was arena; mobile phone was used to deliver pure tone using Tone Generator (app); laptop was used to provide a timer.*

3 Role of dorsal bipolar dendritic neurons in proprioception and nociception

3.1 Introduction

The dorsal bipolar dendritic (dbd) neuron is a class I neuron of the *Drosophila* larval peripheral nervous system. The cell body of the dbd neuron is situated towards the dorsal aspect of each hemisegment and dendrites extend from each side of the cell body, to terminate at the boundary of neighbouring segments (Figure 3.1). This anatomy resembles that of the stretch receptor organs (SROs) of other arthropods, so it has been suggested that the dbd neuron is a stretch sensor too (Nair, Bate and Pulver, 2010; Suslak *et al.*, 2015c).

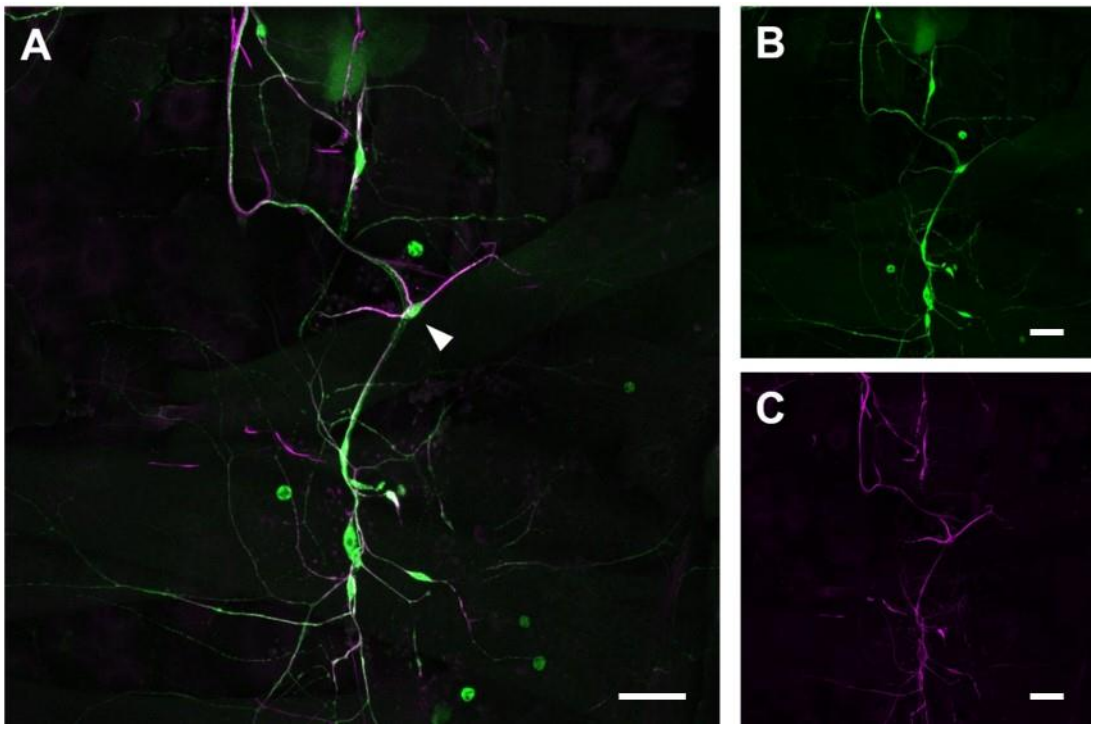

Figure 3.1: Anatomy of the dbd neuron. *Abdominal segment of third instar larva of Sn-Gal4 x UAS-GFP stained with α-GFP and α-22C10 (detects all sensory neurons). A: Larval peripheral nervous system. Arrow indicates position of dbd neuron cell body. B: α-GFP stain only. C: α-22C10 only. Sn-Gal4 is expressed in sensory neurons. Scale bar is 50μm.*

Compared to what is known for other sensory neurons, little is known about the dbd neuron. The proneural gene *amos* is uniquely necessary for the development of dbd and dmd1 neurons, so that dbd is genetically similar to dmd1 and perhaps suggesting functional similarity (Huang, Hsu and Chien, 2000). Whole cell patch clamp electrophysiology revealed that dbd neurons have a TEA sensitive, non-inactivating (I_K) potassium current, a 4-AP sensitive,

inactivating (I_A) potassium current and voltage-gated calcium (I_{Ca}) and sodium (I_{Na}) currents (Nair, Bate and Pulver, 2010). Similarly, dbd neurons produce a receptor potential (RP) in response to stretch that is like the mammalian muscle spindle RP (Hunt, Wilkinson and Fukami, 1978) (Figure 3.2); Silencing *DmPiezo* reduces the initial depolarisation (dEm) phase of this RP by ~80%, whilst silencing TRPA1 reduced it by ~20% (Suslak *et al.*, 2015c). This suggests that the dbd is a stretch sensor (as predicted from its anatomy), and that DmPiezo is the primary mechanoelectrical transducer (MET) in dbd neurons.

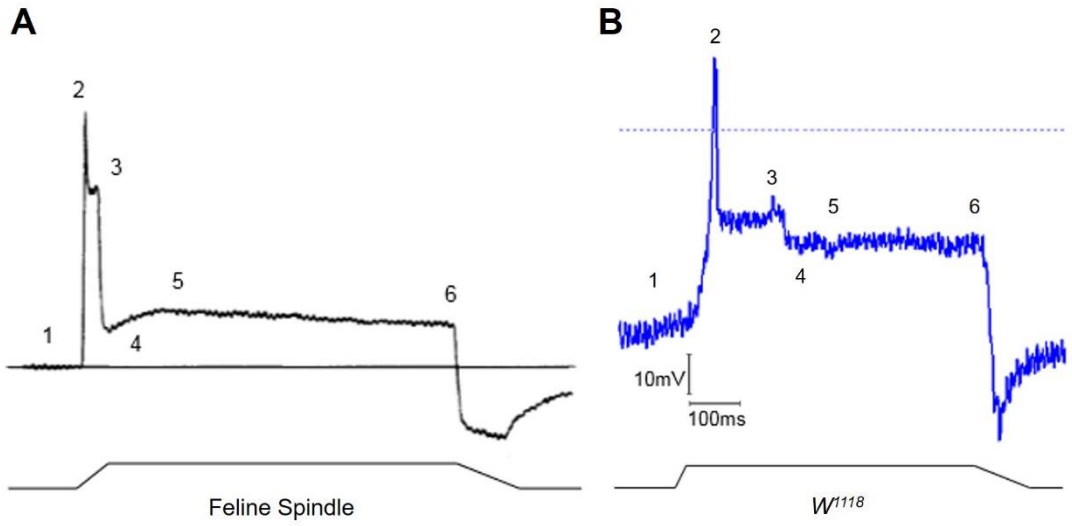

Figure 3.2: Dbd neuron and mammalian muscle spindle receptor potentials are similar. *A: Recording from cat tail muscle spindle, by Hunt et al. 1978. B: Recording from dbd neuron, by Suslak et al., 2015. Numbers show phases of RP conserved across species: 1, pre-stimulation plateau; 2, initial depolarisation; 3, partial repolarisation; 4, establishes hold potential; 5, hold potential; 6, hyperpolarisation. Adapted from Suslak et al., 2015.*

Some behavioural experiments support the idea that the dbd is a stretch receptor by implicating dbd and dmd1 in a normal peristalsis: dbd and dmd1 inhibition by UAS-Shibire^{ts} produces a 'toothpasting' phenotype, related to disordered peristalsis (Hughes and Thomas, 2007)). Others also associate the dbd and dmd1 neurons in crawling, but contrast Suslak *et al.*, by demonstrating that rescuing *NompC* in dbd and dmd1 is sufficient to restore normal locomotion (Cheng *et al.*, 2010). *NompC* encodes a TRPN channel that is required for mechanotransduction in other sensory neurons. A problem with these studies is that they use a Gal4 driver that is not specific to dbd neurons, and so conclusions are provisional.

Several connectomics studies have demonstrated synaptic contacts between dbd neurons and interneurons associated with locomotion control. Based on these connections alone, the dbd neuron has been proposed to impose regulation on locomotion by sending 'mission complete' signals that co-ordinate peristaltic waves during crawling (Schneider-Mizell *et al.*, 2016). In opposition to this work, more direct research in *Manduca* caterpillars has suggested

that dbd neurons have little role in locomotion (Simon and Trimmer, 2009). These researchers surgically ablated the dbd neuron in specific abdominal segments and found that such acute loss of neuron function appeared to have no discernible effect on peristalsis during crawling.

In summary, current understanding is that the dbd neuron is a stretch receptor and that its output regulates peristalsis during crawling, and that either DmPiezo or NompC is the MET. However, there are several limitations uncertainties. First, behavioural data in *Drosophila* largely come from interfering with dbd neuron function using a Gal4 driver that is not specific to this neuron (being also expressed in the dmd1 neuron). Second, detailed models of dbd neuron function in locomotion have been built almost completely on inferences made from connectivity, with little experimental support of function. In short, it is now assumed that dbd neurons are the key receptors for proprioceptive feedback during larval crawling but there is little direct evidence that this is the case. My research described in this chapter attempts to clarify the role of the dbd neuron in behaviour, and support either DmPiezo or NompC as the MET.

3.2 Aims

1. Test the hypothesis that crawling and nociceptive behaviour is mediated by dbd neurons. I will use crawling, nociception and optogenetic to test the hypothesis. If it is correct, it validates findings from other research and demonstrates that the dbd could be used as a model of mammalian muscle spindles.

2. Test the hypothesis that the dbd neuron MET is DmPiezo. I will use crawling experiments and whole-cell patch-clamp electrophysiology to compare the roles of DmPiezo and NompC in the dbd neuron. If it is correct, the hypothesis provides important evidence to confirm DmPiezo as the MET over NompC, an important insight into the mechanism of stretch perception in dbd neurons.

3.3 Results

3.3.1 Optogenetic stimulation of larval peripheral nervous system neurons

Optogenetic experiments were inspired by publications from the Pulver laboratory, which detailed the use of light stimulation to determine the neural basis of flight escape, and to record EJPs at NMJs in *Drosophila* (Pulver *et al.*, 2011; Titlow, Johnson and Pulver, 2015). My research represents the first time optogenetics was used in the Jarman lab, and I worked in conjunction with undergraduate student Aurelija Karaliunaite, to implement, optimise and validate the protocol. The general method was to use red light to activate UAS-csChrimson (red-shifted channelrhodopsin, Titlow *et al.*, 2015) expressed in free moving larvae that are illuminated by blue light for recording purposes. In initial experiments, we used a Gal4 driver with an established expression pattern and related behavioural phenotype. MD-Gal4 was chosen as it is known to be expressed in all four classes of multidendritic (md) neurons. Type IV md neurons are nociceptive, being responsible for a 'rolling' phenotype that aids escape from parasitic wasp attack (Hwang *et al.*, 2007). Specifically, MD-Gal4 control, UAS-csChrimson control and MD-Gal4 x UAS-csChrimson larvae were raised on 1% all-trans retinal food (ATR, a cofactor chromophore necessary for normal csChrimson P_o). Behavioural parameters for third instar larvae were observed and/or measured before and during 30s red light stimulation. Parameters were based on previous research (Hughes and Thomas, 2007; Cheng *et al.*, 2010) and usefulness in validation: (1) phenotype – observation of type of response to light stimulation; (2) % change in crawling speed (CS) before and during stimulation; (3) % change in peristaltic wave frequency (PWF) before and during stimulation.

As expected, MD-Gal4 ATR larvae did not respond to red light (n = 10, Figure 3.3), whereas MD-Gal4 x UAS-csChrimson ATR larvae demonstrated a robust 'rolling' phenotype as expected (n = 10, Figure 3.4) in response to light stimulation. These results agreed with Hwang *et al.*, 2007 and validated the protocol. Unexpectedly, UAS-csChrimson ATR larvae 'froze' (n = 10, Figure 3.5). This 'freezing' was characterised by a sudden and total lack of movement, which may have been caused by endogenous channelrhodopsins binding ATR and reacting to light.

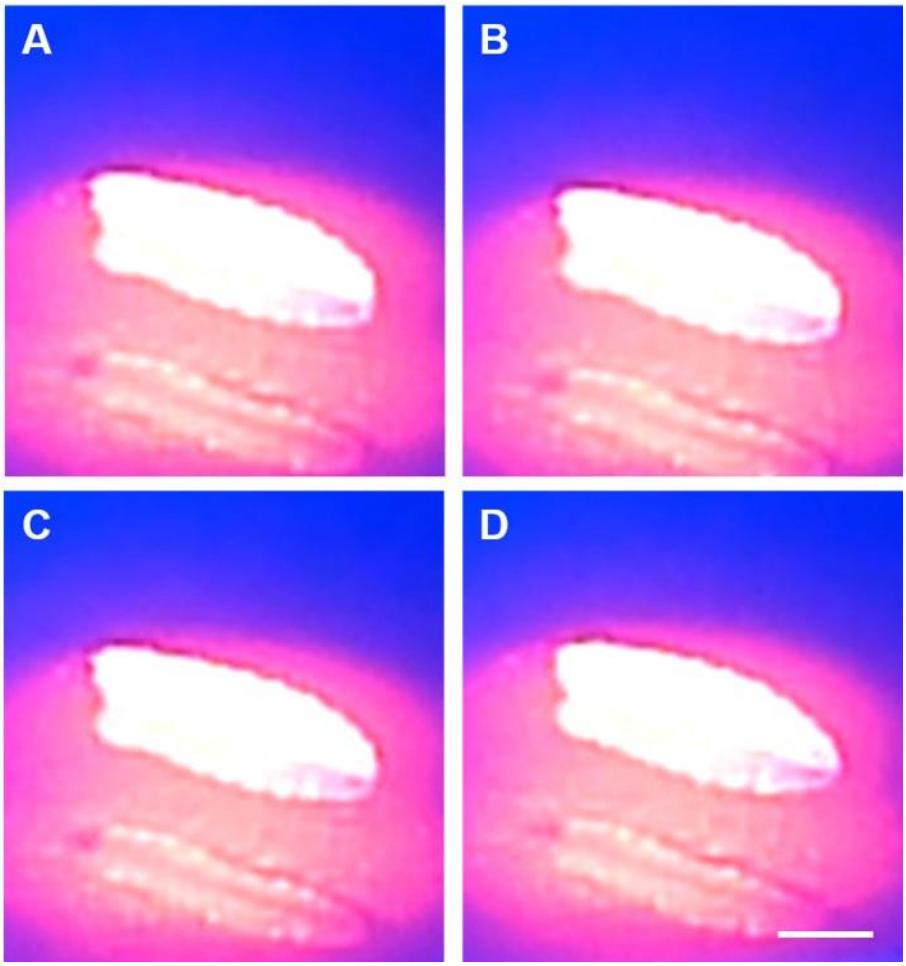

Figure 3.3: MD-Gal4 ATR larvae do not respond to light stimulation. *Representation of phenotype recorded in MD-Gal4 larvae (n = 10) raised on 1% all-trans retinal food, in response to 30s red light stimulation. Larvae crawled on a 200mm x 200mm, 1% grape agar plate in a closed plastic container (23.9-25°C, daylight). Panels A-D show phenotype in stages, (200ms apart) following stimulation. Scale bar is 5mm (shown in one panel for clarity, as all are the same size).*

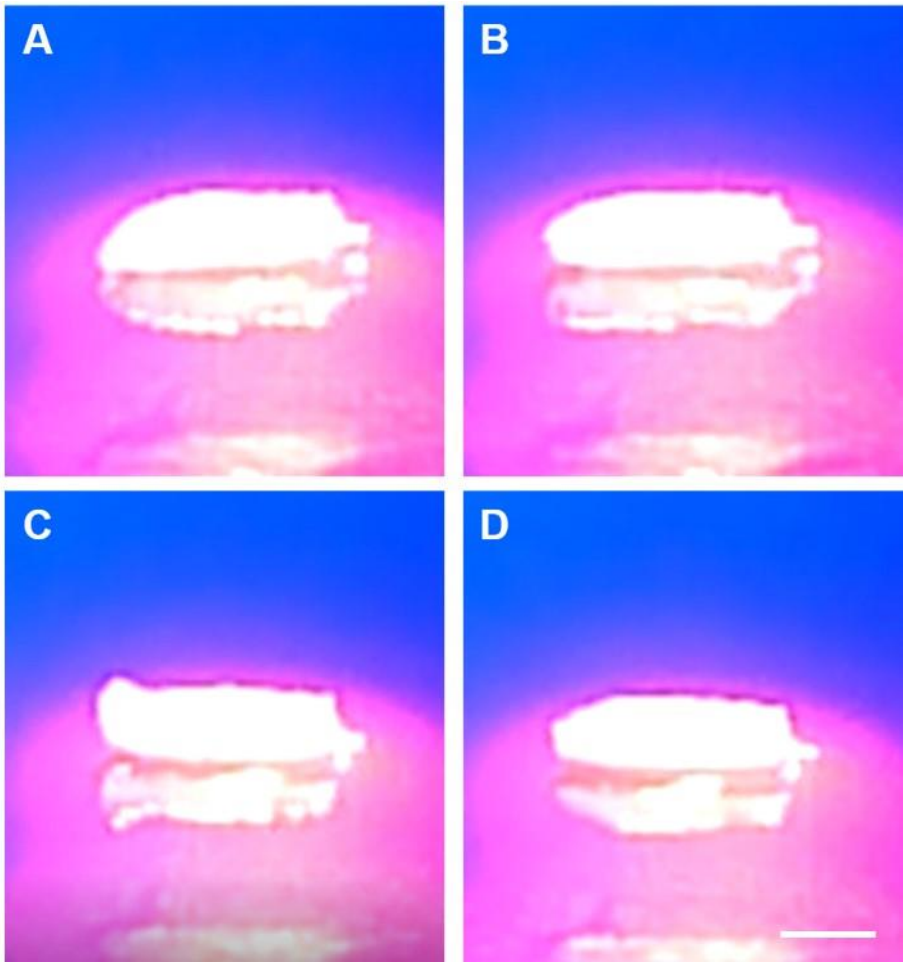

Figure 3.4: MD-Gal4 x UAS-csChrimson ATR larvae demonstrate a 'rolling' phenotype in response to light stimulation. *Representation of phenotype recorded in MD-Gal4 x UAS-csChrimson larvae (n = 10) raised on 1% all-trans retinal food, in response to 30s red light stimulation. Larvae crawled on a 200mm x 200mm, 1% grape agar plate in a closed plastic container (23.9-25°C, daylight). Panels A-D show phenotype in stages, (200ms apart) following stimulation. Scale bar is 5mm (shown in one panel for clarity, as all are the same size).*

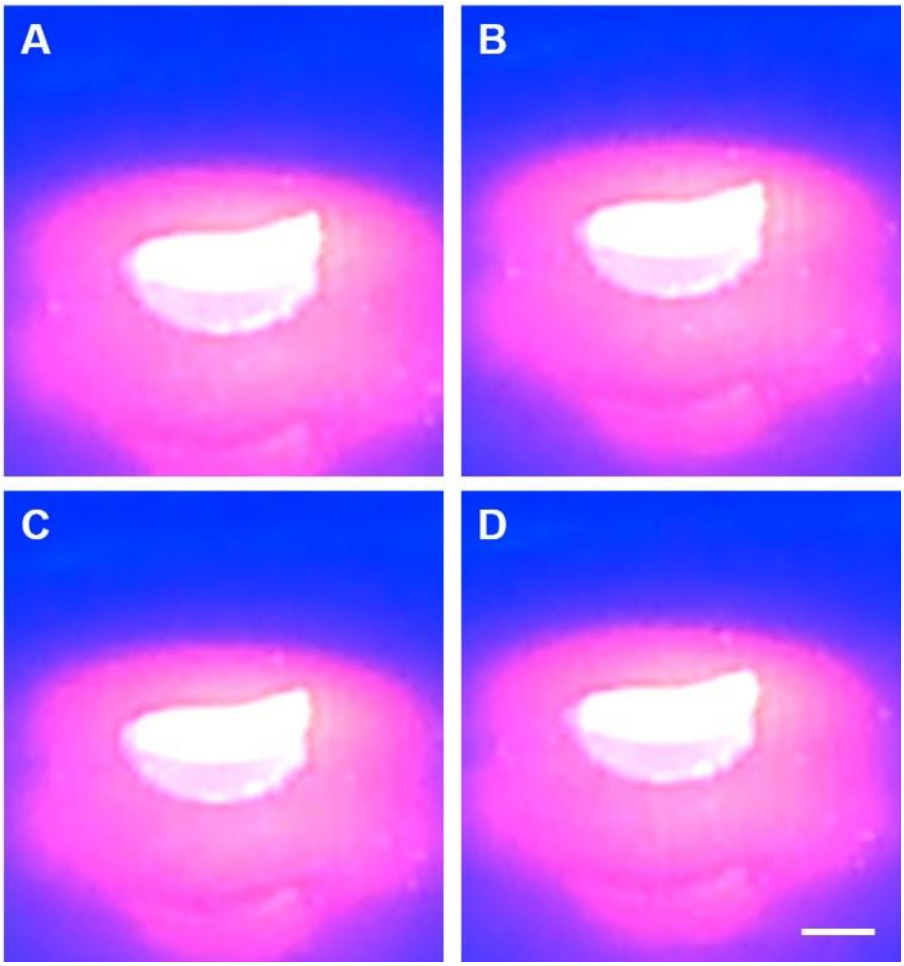

Figure 3.5: UAS-csChrimson ATR larvae 'freeze' in response to light stimulation. *Representation of phenotype recorded in UAS-csChrimson larvae (n = 10) raised on 1% all-trans retinal food, in response to 30s red light stimulation. Larvae crawled on a 200mm x 200mm, 1% grape agar plate in a closed plastic container (23.9-25°C, daylight). Panels A-D show phenotype in stages, (200ms apart) following stimulation. Scale bar is 5mm (shown in one panel for clarity, as all are the same size).*

There was no significant difference in % change in CS between MD-Gal4 x UAS-csChrimson ATR (-5 ± 36.89%; *n* = 10 larvae) and either control; MD-Gal4 ATR (7.58 ± 41.04%; *n* = 10 larvae) and UAS-csChrimson ATR (-45.2 ± 33.58%; *n* = 10 larvae (Figure 3.6)). This lack of difference did not reflect the clear presence of phenotype in MD-Gal4 x UAS-csChrimson ATR and absence in controls; it seemed to originate from generally inactive MD-Gal4 ATR larvae contrasting the 'freeze' phenotype for UAS-csChrimson ATR, shown in Figure 3.5. This also explains the significant difference found between controls ($P \leq 0.05$).

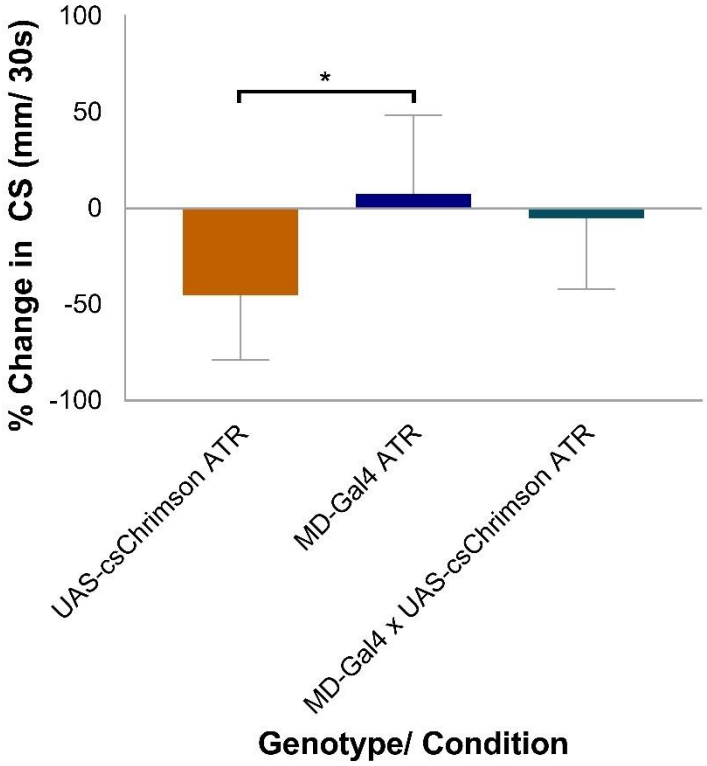

Figure 3.6: Light stimulation of MD neurons does not affect larval crawling speed versus controls. *% Change in crawling speed (CS, where change is difference between pre and during 30s light stimulus) was recorded manually from larvae crawling on a 1% grape agar plate (lid on, 23.9-25°C, daylight). There was a significant difference in % change in CS between UAS-csChrimson ATR (-45.2 ± 33.58%; n = 10 larvae) and MD-Gal4 ATR (7.58 ± 41.04%; n = 10 larvae, P = 0.01). Statistical significance determined by one-way ANOVA with Tukey's multiple comparisons test (threshold for significance: P = 0.05; * = P ≤ 0.05).*

Like % change in CS, there was no significant difference in % change in PWF between MD-Gal4 x UAS-csChrimson ATR (-19.44 ± 35.06%; *n* = 10 larvae) and controls; MD-Gal4 ATR (7.78 ± 26.73%; *n* = 10 larvae) and UAS-csChrimson ATR (-34.55 ± 30.99%; *n* = 10 larvae (Figure 3.7)). Again, this lack of difference did not reflect the rolling phenotype observed in MD-Gal4 x UAS-csChrimson ATR and its absence in controls. It originated from generally inactive MD-Gal4 ATR larvae contrasting the 'freeze' phenotype for UAS-csChrimson ATR, which also explains the significant difference found between controls ($P \leq 0.05$). Results for % change in CS and % change in PWF still supported the use of this protocol to determine the role of specific neurons in behaviour if other sensory neuron driver-expressing larvae were more active than those for MD-Gal4. Thus, MD-Gal4 (phenotype and crawling parameter) results validated the use of optogenetics in this research.

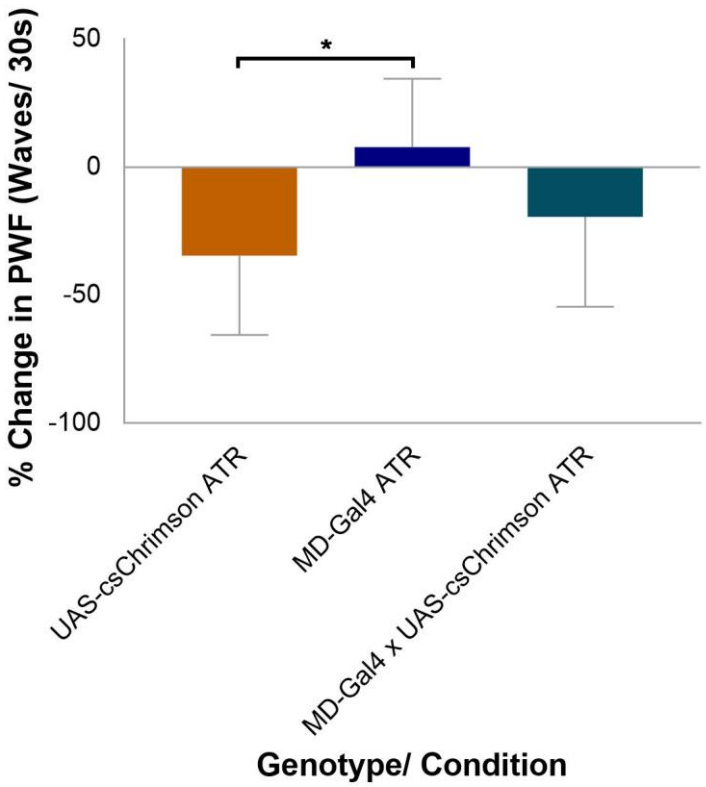

Figure 3.7: Light stimulation of MD neurons does not affect larval peristaltic wave frequency. *% Change in Peristaltic Wave Frequency (PWF, where change is difference between pre and during 30s light stimulus) was recorded manually from larvae crawling on a 1% grape agar plate (lid on, 23.9-25°C, daylight). There was a significant difference in % change in PWF between UAS-csChrimson ATR (-34.55 ± 30.99%; n = 10 larvae) and MD-Gal4 ATR (7.78 ± 26.73%; n = 10 larvae, P = 0.014). Statistical significance determined by one-way ANOVA with Tukey's multiple comparisons test (threshold for significance: P = 0.05; * = P ≤ 0.05).*

3.3.1.1 Role of the dbd neuron in larval behaviour

3.3.1.1.1 Optogenetic activation using the Bd-Gal4 driver line induces a 'strike' behaviour

Once validated, optogenetics was used to investigate the role of the dbd neuron in larval behaviour. To target the dbd neuron, the Bd-Gal4 driver was used, which is said to be expressed in dbd and dmd1 neurons only (in the PNS). This driver has been used in crawling experiments to imply a role for dbd and dmd1 neurons in behaviour (Hughes and Thomas, 2007; Cheng *et al.*, 2010).

UAS-csChrimson ATR phenotype was shown above (larvae 'froze' (*n* = 10) and Bd-Gal4 ATR larvae did not respond (*n* = 10, Figure 3.8). In contrast, Bd-Gal4 x UAS-csChrimson ATR larvae demonstrated a 'strike' phenotype (*n* = 10, Figure 3.9) in response to light stimulation. The strike phenotype was markedly different to the phenotypes of both controls, and was characterised by a violent rearing and arching movement reminiscent of the 'strike' pain response coded for by the stretch receptor organ (SRO) of *Manduca sexta* caterpillar (Simon and Trimmer, 2009). This is a nociceptive response that reportedly protects from parasitic wasps.

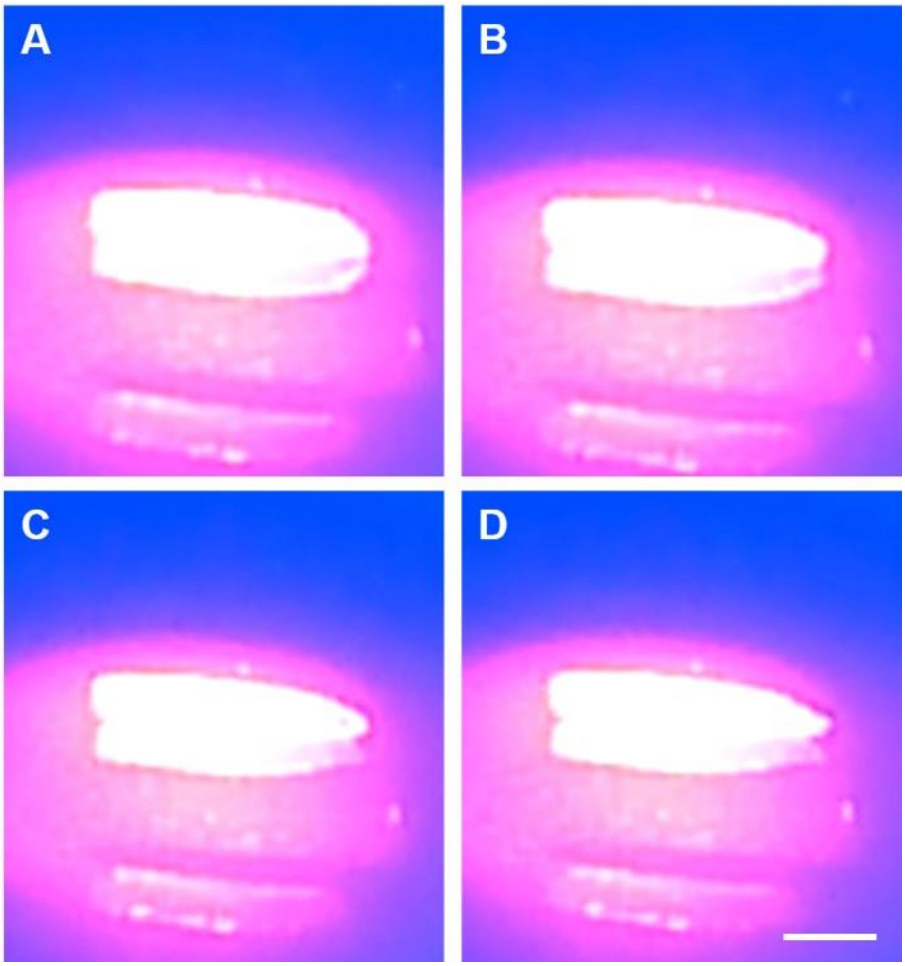

Figure 3.8: Bd-Gal4 ATR larvae do not respond to light stimulation. *Representation of phenotype recorded in Bd-Gal4 larvae (n = 10) raised on 1% all-trans retinal food, in response to 30s red light stimulation. Larvae crawled on a 200mm x 200mm, 1% grape agar plate in a closed plastic container (23.9-25°C, daylight). Panels A-D show phenotype in stages, (200ms apart) following stimulation. Scale bar is 5mm (shown in one panel for clarity, as all are the same size).*

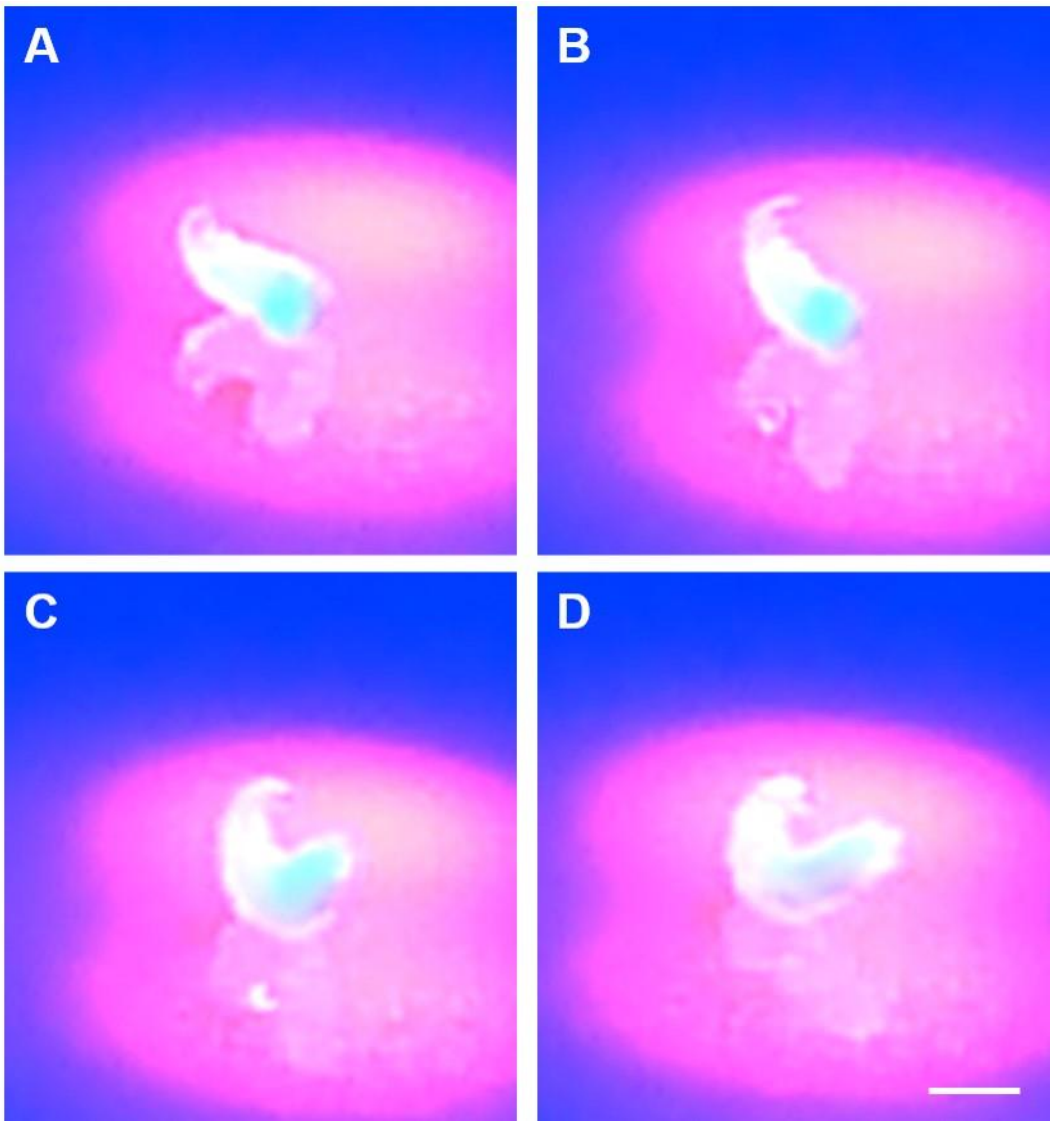

Figure 3.9: Bd-Gal4 x UAS-csChrimson ATR larvae demonstrate a 'strike' phenotype in response to light stimulation. *Representation of phenotype recorded in Bd-Gal4 x UAS-csChrimson larvae (n = 10) raised on 1% all-trans retinal food, in response to 30s red light stimulation. Larvae crawled on a 200mm x 200mm, 1% grape agar plate in a closed plastic container (23.9-25°C, daylight). Panels A-D show phenotype in stages, (200ms apart) following stimulation. Scale bar is 5mm (shown in one panel for clarity, as all are the same size).*

% change in CS reflected these phenotypes: % change in CS for Bd-Gal4 x UAS-csChrimson ATR (-40.81 ± 38.27%; *n* = 10 larvae) was significantly different to Bd-Gal4 ATR (4.35 ± 30.95%; *n* = 10 larvae, *P* ≤ 0.05 (Figure 3.10)). This might suggest that the dbd neuron may be involved in normal crawling speed, but it is also most likely a secondary effect of the strike phenotype. There was a similar significant difference between UAS-csChrimson (-45.2 ± 33.58%; *n* = 10 larvae) and Bd-Gal4 ATR (*P* ≤ 0.01), with no difference between Bd-Gal4 x UAS-csChrimson ATR and UAS-csChrimson ATR because of the 'freeze' phenotype shown in Figure 3.5.

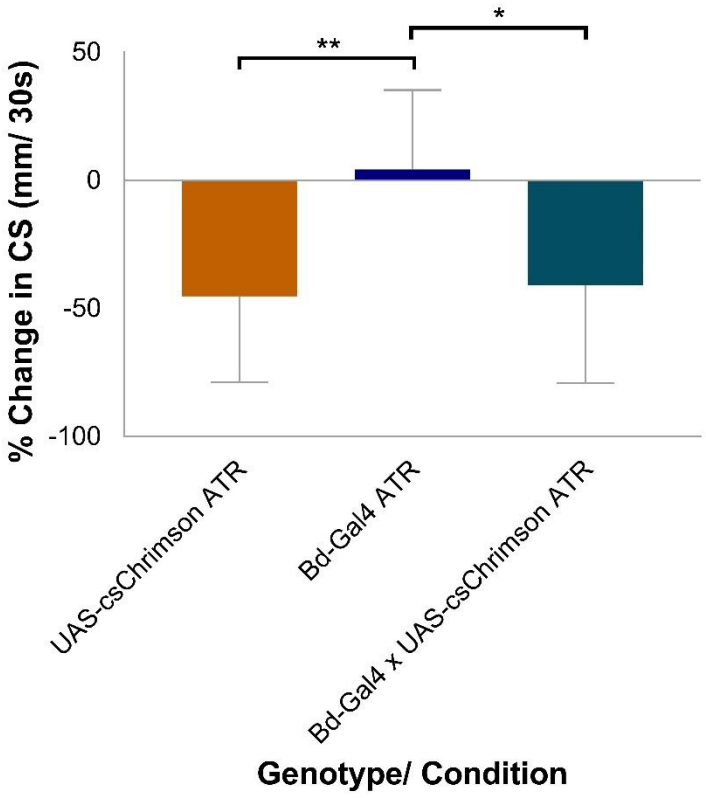

Figure 3.10: Light stimulation of dbd neurons decreases larval crawling speed. *% Change in Crawling Speed (CS, where change is difference between pre and during 30s light stimulus) was recorded manually from larvae crawling on a grape agar plate (lid on, 23.9-25°C, daylight). There was a significant difference in % change in CS between Bd-Gal4 x UAS-csChrimson ATR (-40.81 ± 38.27%; n = 10 larvae) and Bd-Gal4 ATR (4.35 ± 30.95%; n = 10 larvae, P = 0.018). There was also a significant difference between UAS-csChrimson ATR (-45.2 ± 33.58%; n = 10 larvae) and Bd-Gal4 ATR (P = 0.009). Statistical significance determined by one-way ANOVA with Tukey's multiple comparisons test (threshold for significance: P = 0.05; * = P ≤ 0.05, ** = P ≤ 0.01).*

% change in PWF for Bd-Gal4 x UAS-csChrimson ATR (-46.84 ± 28.01%; *n* = 10 larvae) was significantly different to Bd-Gal4 ATR (0.77 ± 17.28%; *n* = 10 larvae, *P* ≤ 0.01 (Figure 3.11). This suggests that the dbd neuron could be involved in normal peristaltic wave frequency, but again could also be a secondary effect of the strike phenotype. There was also a significant difference between UAS-csChrimson (-34.55 ± 30.99%; *n* = 10 larvae) and Bd-Gal4 ATR (*P* ≤ 0.05 (Figure 2.11)) and no difference between Bd-Gal4 x UAS-csChrimson ATR and UAS-csChrimson ATR, due to the 'freeze' phenotype of the latter.

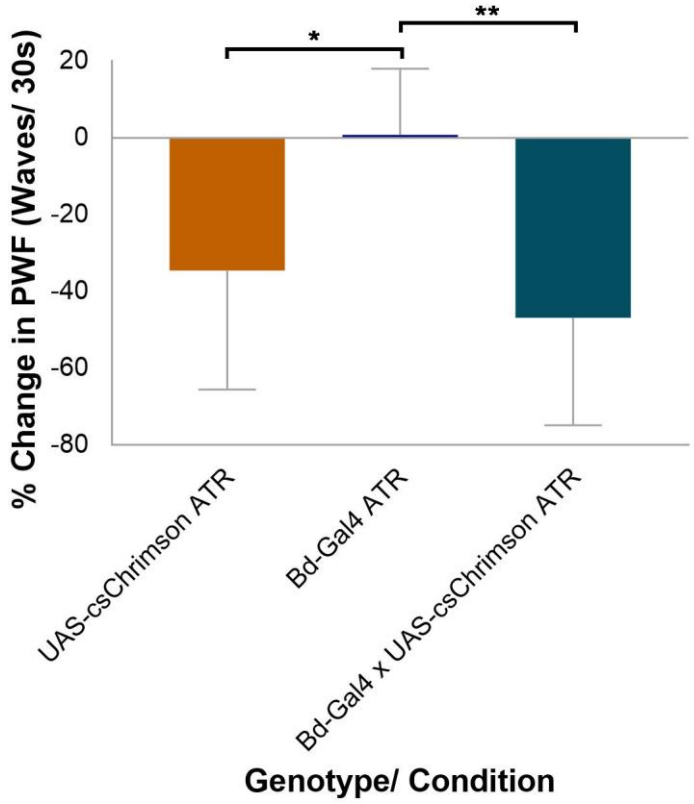

Figure 3.11: Light stimulation of dbd neurons decreases larval peristaltic wave frequency. *% Change in Peristaltic Wave Frequency (PWF, where change is difference between pre and during 30s light stimulus) was calculated from recordings of larvae crawling on a 1% grape agar plate (lid on, 23.9-25°C, daylight). There was a significant difference in % change in PWF between Bd-Gal4 x UAS-csChrimson ATR (-46.84 ± 28.01%; n = 10 larvae) and Bd-Gal4 ATR (0.77 ± 17.28%; n = 10 larvae, P = 0.001). There was also a significant difference between UAS-csChrimson ATR (-34.55 ± 30.99%; n = 10 larvae) and Bd-Gal4 ATR (P = 0.014). Statistical significance determined by one-way ANOVA with Tukey's multiple comparisons test (threshold for significance: P = 0.05; * = P ≤ 0.05, ** = P ≤ 0.01).*

3.3.1.1.2 Role of dbd neuron in response to a nociceptive stimulus

Results from optogenetic experiments raised the possibility of a role for the dbd neuron in *Drosophila* nociception. To explore this further, I made use of a null mutation in the proneural *amos* gene. Dbd and dmd1 neurons are completely absent in *amos* null mutation (*amos*^{1}, zur Lage *et al.*, 2003). Therefore, *amos*^{1} and *Oregon-R* (wild type) control larvae were used in novel pain response experiments to determine whether the presence of dbd (and dmd1) neurons are responsible for nociceptive behaviour in larvae.

Pain stimuli were delivered as a forceps 'pinch' to the posterior (tail) end of larvae. Response to the pinch was recorded and analysed as qualitative data; video was used to observe the presence or absence of a pain response phenotype, and to describe that phenotype when it occurred.

Oregon-R larvae responded to pinch stimulation with a 'strike' phenotype, very similar to that documented in Bd-Gal4 x UAS-csChrimson ATR optogenetic experiments (n = 10, Figure 3.12). As with that phenotype, this response was characterised by a violent rearing and arching movement reminiscent of the 'strike' coded for by the stretch receptor organ (SRO) of *Manduca sexta* caterpillar (Simon and Trimmer, 2009).

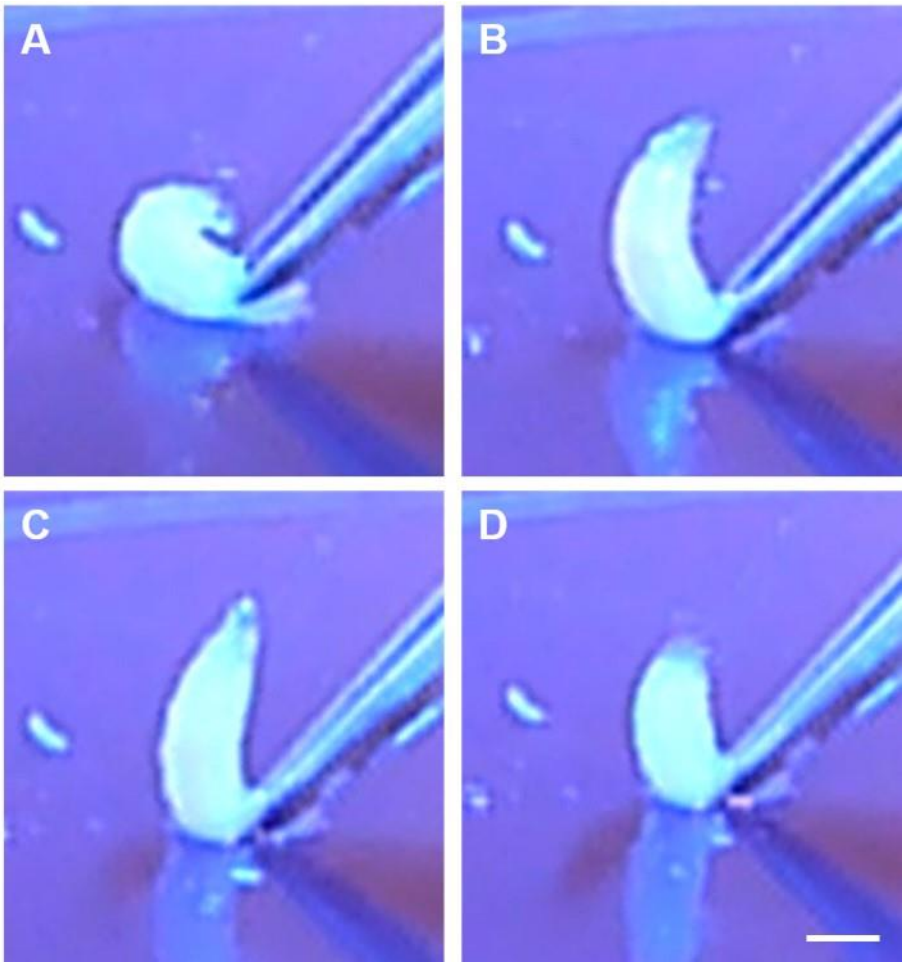

Figure 3.12: Oregon-R larvae demonstrate a 'strike' phenotype in response to nociceptive stimuli. *Representation of phenotype recorded in response to 'pinch' delivered by forceps, to posterior of larvae crawling on a 200mm x 200mm, 1% agar gel in a closed plastic container (23.9-25°C, daylight). Panels A-D show representative phenotype in stages (100ms apart) following pinch. Scale bar is 5mm (shown in one panel for clarity, as all are the same size).*

amos[1] larvae responded to pinch stimulation with the same 'strike' phenotype seen in *Oregon-R* larvae (*n* = 10, Figure 3.13). The similarity in phenotype confirms that the dbd and dmd1 neurons are not responsible for the 'strike' observed in response to pain delivered by this stimulus. This agrees with literature that shows that type IV neurons are responsible for a ppk26 and DmPiezo-dependent mechanism of mechanical nociception in larvae (Kim *et al.*, 2012; Hwang *et al.*, 2007; Guo *et al.*, 2014). However, it does not rule out the possibility that dbd and dmd1 neurons encode nociceptive information from a different form of pain stimulus.

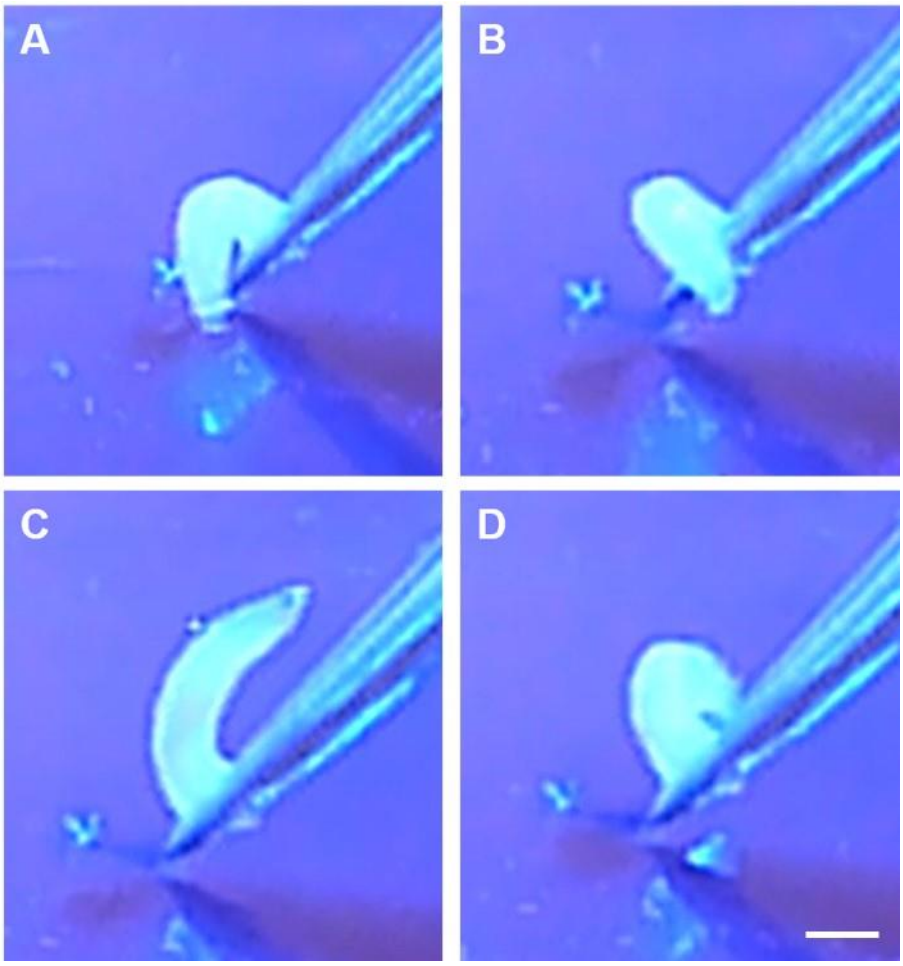

Figure 3.13: amos[1] larvae demonstrate striking phenotype in response to nociceptive stimuli. *Phenotype recorded in response to 'pinch' delivered by forceps, to posterior of larvae crawling on a 200mm x 200mm, 1% agar gel in a closed plastic container (23.9-25°C, daylight). Panels A-D show representative phenotype in stages (100ms apart) following pinch. Scale bar is 5mm (shown in one panel for clarity, as all are the same size).*

3.3.1.1.3 Expression pattern of the Bd-Gal4 driver line

Despite the above findings, the Bd-Gal4 x UAS-csChrimson ATR 'strike' was interesting, and the resemblance to the *Manduca* pain response meant it could represent evidence linking the dbd neuron to nociception from an unknown stimulus. However, this conclusion would require that the driver line is completely specific to dbd neurons, but its expression pattern has not been well characterised (Hughes and Thomas, 2007; Cheng *et al.*, 2010). To check the expression pattern of the Bd-Gal4 driver, immunofluorescence was used. Antibody staining of Bd-Gal4 x UAS-GFP confirmed that Bd-Gal4 drives GFP expression in dbd/ vbd neurons, but also showed expression in dmd1 neurons as previously suggested. However, it also showed expression in many neurons of the ventral nerve cord (VNC, Figure 3.14).

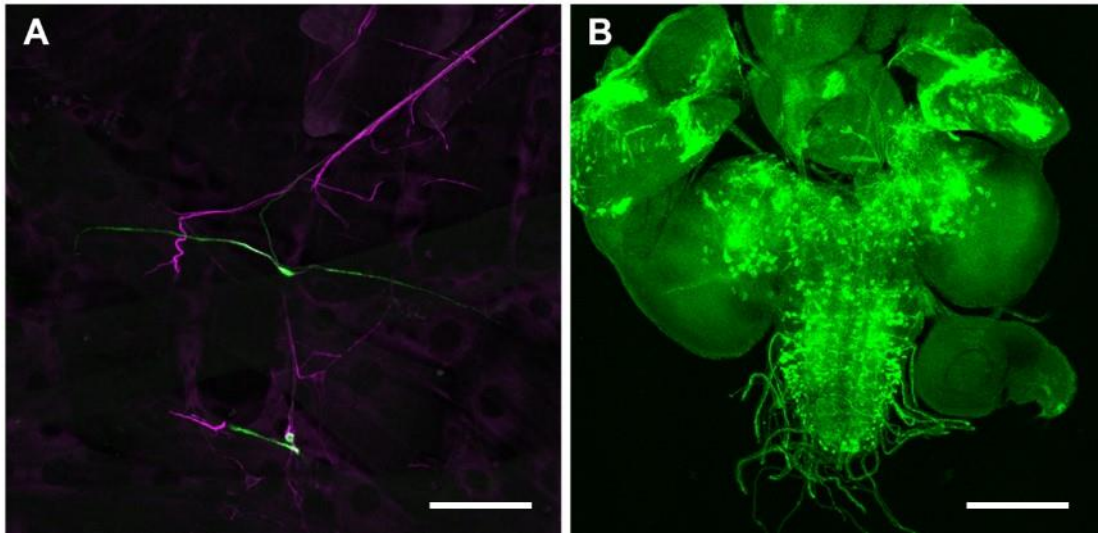

Figure 3.14: Immunostaining of Bd-Gal4 x UAS-GFP with α-GFP and α-22C10. *A: Bd-Gal4 driving GFP expression (green) in dbd and dmd1 neurons, with 22C10 counterstain. dbd neuron is identifiable by its dendrites, which project across centre of panel; dmd1 identifiable as cell body and single dendrite. B: Bd-Gal4 driving GFP expression in VNC. Scale bar is 100µm.*

Supplementary information for Cheng *et al.*, 2010, describes Bd-Gal4 expression as: "bd and a few CNS neurons" (motor neurons in VNC), whilst Hughes and Thomas use different nomenclature ((8-113)-Gal4 in (Hughes and Thomas, 2007)) to describe expression of the same driver as: "dbd, vbd and dmd1 and a few CNS neurons". The staining here and earlier expression data casts doubt on: (1) the neuron/neurons responsible for 'strike' phenotype; (2) the legitimacy of behaviour attributed to the dbd neuron in Cheng and Hughes and Thomas' work.

3.3.1.1.4 Strike behaviour in response to UAS-csChrimson does not require amos-dependent neurons

Unfortunately, there is currently no Gal4 driver that is more specific to dbd neurons (than Bd-Gal4). To define the neurons required for the strike response, I made use of the observation that the proneural gene, amos, is required for the formation of dbd and dmd1 neurons, but not for any CNS neurons ((zur Lage *et al.*, 2003) so in *amos* null mutants (*amos*^{1}) dbd and dmd1 neurons are absent). This mutation was crossed in to the optogenetic experiment lines used above. Experiments were repeated to determine whether dbd and/or dmd1 neuron~~(s)~~(s) were required for the 'strike' phenotype.

Neither *amos*^{1}, UAS-csChrimson ATR (*n* = 10, Figure 3.15) nor *amos*^{1}; Bd-Gal4 ATR control larvae responded to 30s light stimulation (*n* = 10, Figure 3.16). For *amos*^{1}, UAS-csChrimson ATR, this contrasts UAS-csChrimson controls used in earlier experiments and suggests that dbd and dmd1 neurons are necessary for 'freeze' phenotype shown in Figure 2.3. In contrast, *amos*^{1}; Bd-Gal4 x *amos*^{1}, UAS-csChrimson ATR larvae still demonstrated the 'striking' phenotype in response to light stimulation (*n* = 6, Figure 3.17). Dissection and staining of these larvae confirmed the absence of dbd neurons (data not shown). In conclusion, it is activation of CNS neurons, not dbd and dmd1 neurons, that is responsible for the strike phenotype observed in Bd-Gal4 x UAS-csChrimson ATR animals.

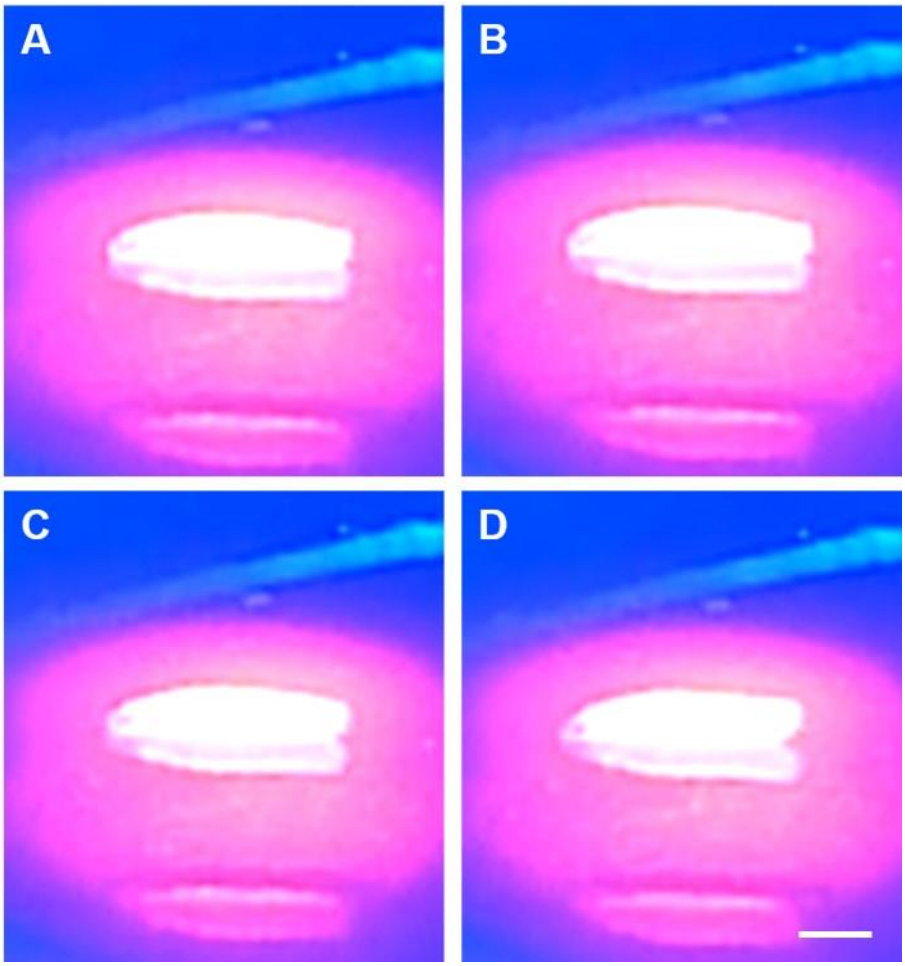

Figure 3.15: amos[1], UAS-csChrimson ATR larvae do not respond to light stimulation. *Representation of phenotype recorded in amos[1], UAS-csChrimson larvae (n = 10) raised on 1% all-trans retinal food, in response to 30s red light stimulation. Larvae crawled on a 200mm x 200mm, 1% grape agar plate in a closed plastic container (23.9-25°C, daylight). Panels A-D show phenotype in stages, (200ms apart) following stimulation. Scale bar is 5mm (shown in one panel for clarity, as all are the same size).*

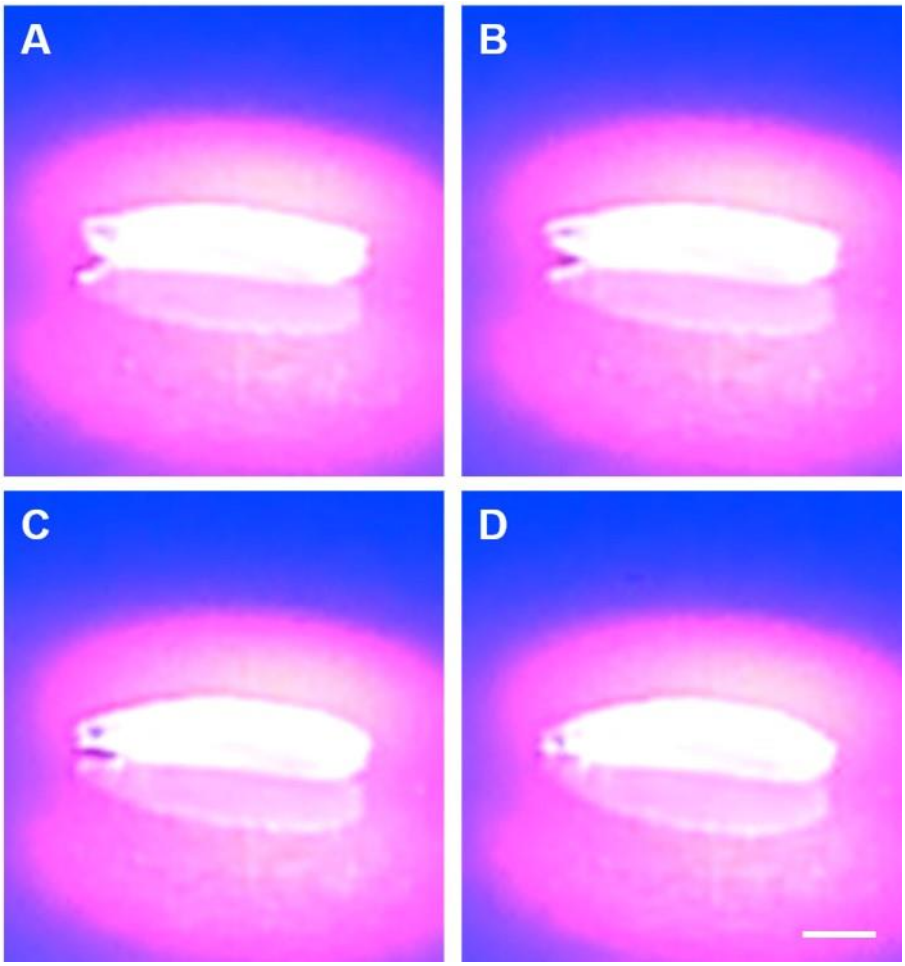

Figure 3.16: amos^{1}; Bd-Gal4 ATR larvae do not respond to light stimulation. *Representation of phenotype recorded in amos1; Bd-Gal4 larvae (n = 10) raised on 1% all-trans retinal food, in response to 30s red light stimulation. Larvae crawled on a 200mm x 200mm, 1% grape agar plate in a closed plastic container (23.9-25°C, daylight). Panels A-D show phenotype in stages, (200ms apart) following stimulation. Scale bar is 5mm (shown in one panel for clarity, as all are the same size).*

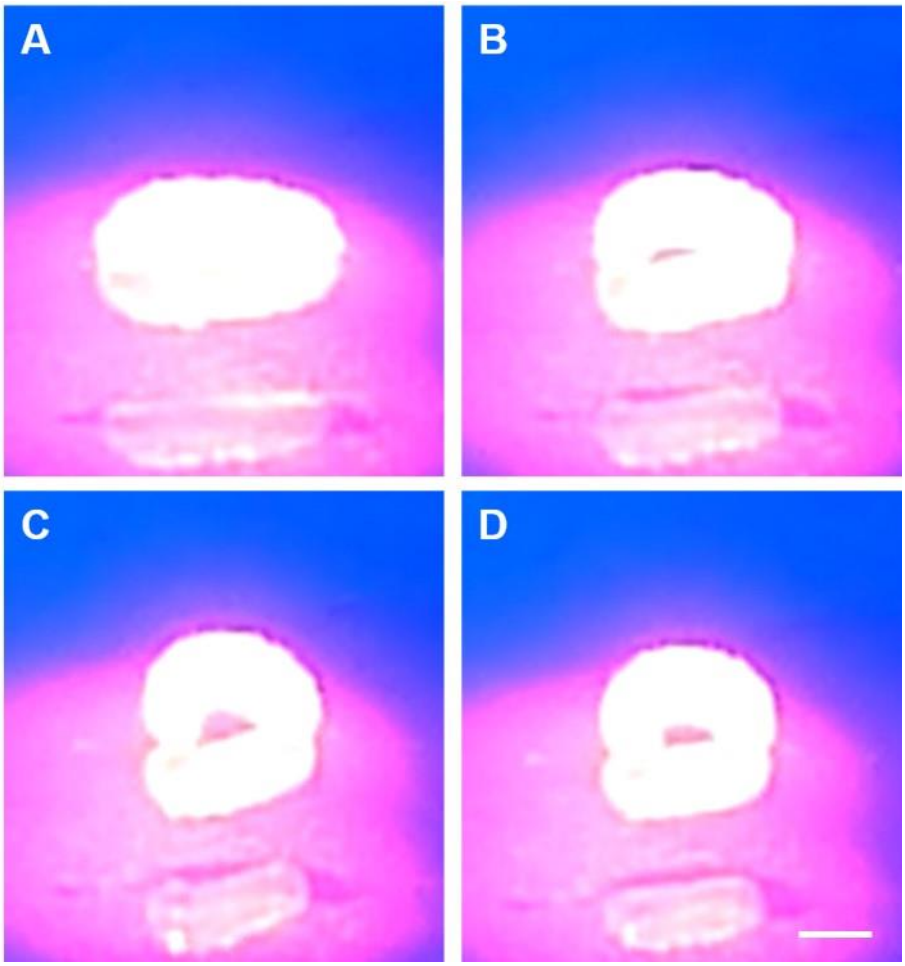

Figure 3.17: amos[1]; Bd-Gal4 x amos[1], UAS-csChrimson ATR larvae demonstrate a 'strike' phenotype in response to light stimulation. *Representation of phenotype recorded in amos1; Bd-Gal4 x amos[1], UAS-csChrimson larvae (n = 10) raised on 1% all-trans retinal food, in response to 30s red light stimulation. Larvae crawled on a 200mm x 200mm, 1% grape agar plate in a closed plastic container (23.9-25°C, daylight). Panels A-D show phenotype in stages, (200ms apart) following stimulation. Scale bar is 5mm (shown in one panel for clarity, as all are the same size).*

There was a significant difference in % change in CS between *amos*[1], Bd-Gal4 x *amos*[1]; UAS-csChrimson ATR (-45.37 ± 34.1%; *n* = 6 larvae) and both controls; *amos*[1]; Bd-Gal4 ATR (7.93 ± 28.94%; *n* = 10 larvae, *P* ≤ 0.01) and *amos*[1], UAS-csChrimson ATR (-12.63 ± 24.96%; *n* = 10 larvae, *P* ≤ 0.01 (Figure 3.18)). This is as expected, given the phenotype for *amos*[1], Bd-Gal4 x *amos*[1]; UAS-csChrimson ATR and is demonstrative of the extent of the effect that acute stimulation of CNS neurons can have on larval locomotion. Similarly, there was a significant difference in % change in PWF between *amos*[1], Bd-Gal4 x *amos*[1]; UAS-csChrimson ATR (-48.96 ± 32.46%; *n* = 6 larvae) and both controls; *amos*[1]; Bd-Gal4 ATR (12.35 ± 24.25%; *n* = 10 larvae, *P* ≤ 0.001) and *amos*[1], UAS-csChrimson ATR (-9.33 ± 19.74%; *n* = 10 larvae, *P* ≤ 0.05 (Figure 3.19)).

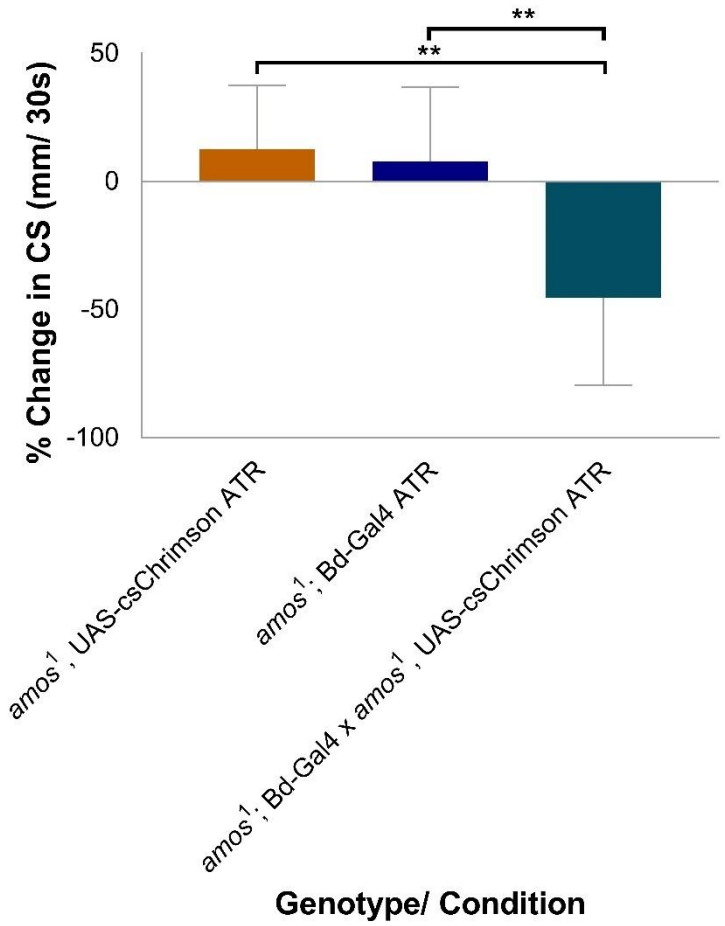

Figure 3.18: Larvae lacking dbd neurons demonstrate reduced crawling speed versus controls in response to light stimulation. *% Change in Crawling Speed (CS, where change is difference between pre and during 30s light stimulus) was recorded manually from larvae crawling on a 1% grape agar plate (lid on, 23.9-25°C, daylight). There was a significant difference in % change in CS between amos¹; Bd-Gal4 x amos¹, UAS-csChrimson ATR (-45.37 ± 34.1%; n = 6 larvae) and amos¹; Bd-Gal4 ATR (7.93 ± 28.94%; n = 10 larvae, P = 0.002) and amos¹; UAS-csChrimson ATR (12.63 ± 24.96%; n = 10 larvae; P = 0.004). Statistical significance determined by one-way ANOVA with Tukey's multiple comparisons test (threshold for significance: P = 0.05; ** = P ≤ 0.01).*

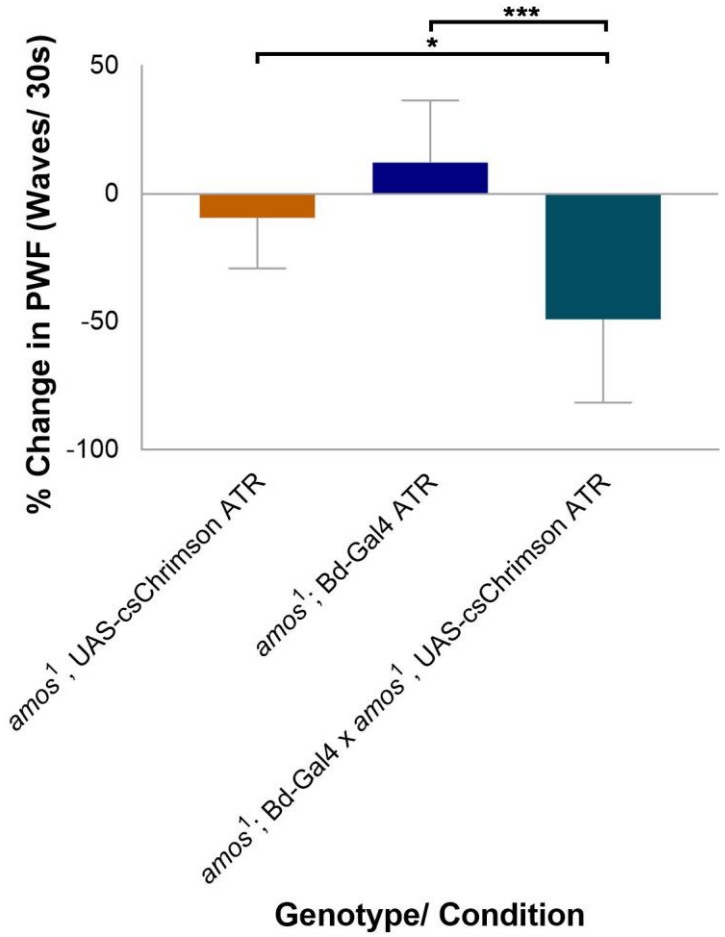

Figure 3.19: Larvae lacking dbd and dmd1 neurons demonstrate reduced peristaltic wave frequency versus controls. *% Change in Peristaltic Wave Frequency (PWF, where change is difference between pre and during 30s light stimulus) was calculated from recordings of larvae crawling on a 1% grape agar plate (lid on, 23.9-25°C, daylight). There was a significant difference in % change in PWF between amos[1]; Bd-Gal4 x amos[1], UAS-csChrimson ATR (-48.96 ± 32.46%; n = 6 larvae) and amos[1]; Bd-Gal4 ATR (12.35 ± 24.25%; n = 10 larvae, P = 0.0002) and amos[1]; UAS-csChrimson ATR (-9.33 ± 19.74%; n = 10 larvae; P = 0.013). Statistical significance determined by one-way ANOVA with Tukey's multiple comparisons test (threshold for significance: P = 0.05; * = P ≤ 0.05, *** = P ≤ 0.001).*

3.3.1.1.5 Effect of absence of dbd and dmd1 neurons on larval crawling behaviour

Finally, I re-examined the recorded data for the *amos* mutant larvae to see if the presence of dbd and dmd1 neurons was required for normal crawling. For this I re-used videos from the above experiment: *amos*[1], UAS-csChrimson ATR, *amos*[1]; Bd-Gal4 ATR and *amos*[1]; Bd-Gal4 x *amos*[1], UAS-csChrimson ATR larvae prior light stimulation (i.e. during 30s of crawling before stimulus was applied). CS, PWF and a new behavioural parameter, peristaltic wave duration (PWD) were used for comparison~~(s)~~(s). There was no significant difference in CS (mm/30s)

for *amos*[1]; Bd-Gal4 x *amos*[1], UAS-csChrimson ATR larvae (8.33 ± 6.43mm/ 30s; *n* = 6 larvae) and either control; *amos*[1]; UAS-csChrimson ATR larvae (8.3 ± 2.67mm/ 30s; *n* = 10 larvae) or *amos*[1]; Bd-Gal4 ATR larvae (7.6 ± 5.07mm/ 30s; *n* = 10 larvae (Figure 3.20)), so dbd and dmd1 neurons are not necessary for normal crawling speed.

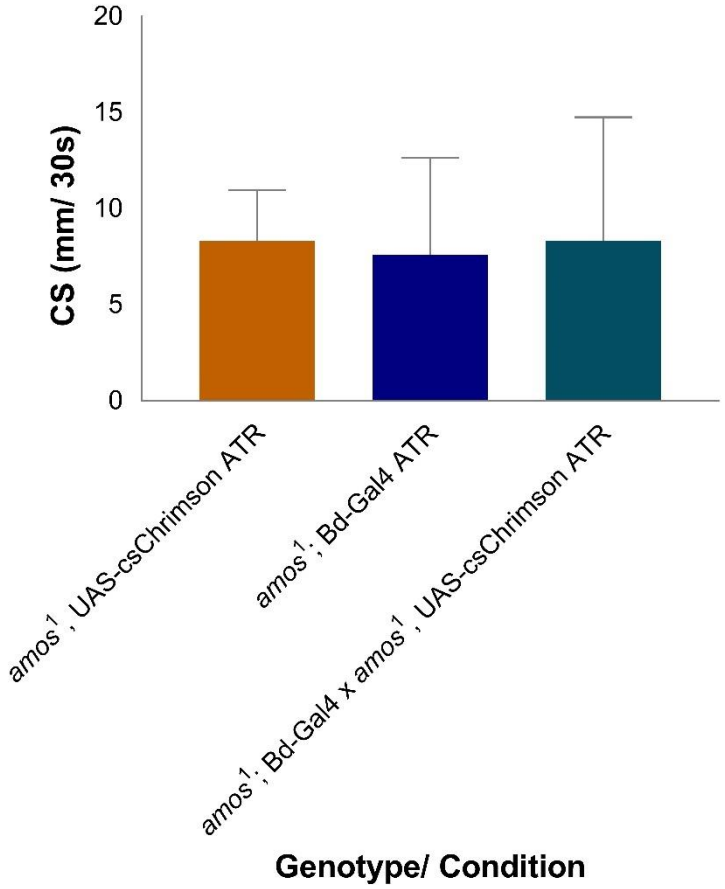

Figure 3.20: Dbd and dmd1 neurons are not necessary for normal crawling speed. *Crawling Speed (CS) was recorded manually from recordings of larvae crawling on a 1% grape agar plate (lid on, 23.9-25°C, daylight). There was no significant difference in CS for amos[1]; Bd-Gal4 x amos[1], UAS-csChrimson ATR larvae (8.33 ± 6.43mm/ 30s; n = 6 larvae) and either control; amos[1]; UAS-csChrimson ATR larvae (8.3 ± 2.67mm/ 30s; n = 10 larvae, P = 0.999) or amos[1]; Bd-Gal4 ATR larvae (7.6 ± 5.07mm/ 30s; n = 10 larvae, P = 0.95). Statistical significance determined by one-way ANOVA with Tukey's multiple comparisons test (threshold for significance: P = 0.05).*

PWF was significantly lower for *amos*[1]; Bd-Gal4 x *amos*[1], UAS-csChrimson ATR larvae (7.83 ± 5.19 waves/ 30s; *n* = 6 larvae) than it was for *amos*[1], UAS-csChrimson ATR (18.1 ± 8.76 waves/ 30s; *n* = 10 larvae, *P* ≤ 0.05) and *amos*[1]; Bd-Gal4 ATR larvae (17.1 ± 3.84 waves/ 30s; *n* = 10 larvae, *P* ≤ 0.05 (Figure 2.21)). This supports the idea that the dbd neuron is (a stretch

receptor) necessary for normal peristalsis (Cheng *et al.*, 2010; Hughes and Thomas, 2007; Suslak *et al.*, 2015c).

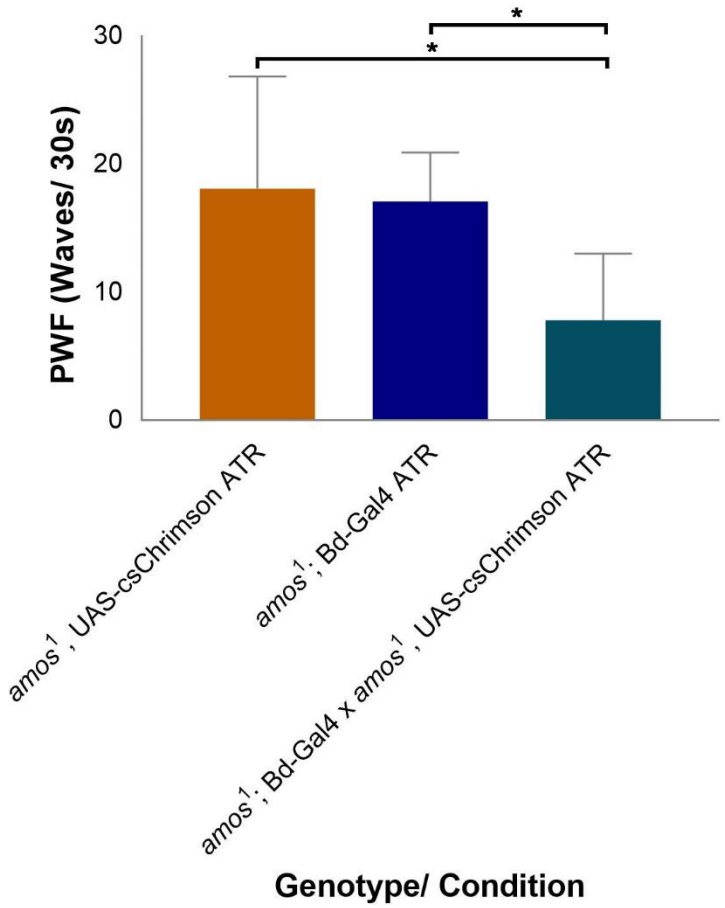

Figure 3.21: Dbd and dmd1 neurons are necessary for normal peristaltic wave frequency. *Peristaltic Wave Duration (PWF) was calculated from recordings of larvae crawling on a 1% grape agar plate (lid on, 23.9-25°C, daylight). There was a significant difference between amos[1]; Bd-Gal4 x amos[1], UAS-csChrimson ATR larvae (7.83 ± 5.19 waves/ 30s; n = 6 larvae) and amos[1], UAS-csChrimson ATR (18.1 ± 8.76 waves/ 30s; n = 10 larvae, P = 0.014) and amos[1]; Bd-Gal4 ATR larvae (17.1 ± 3.84 waves/ 30s; n = 10 larvae, P = 0.028). Statistical significance determined by one-way ANOVA with Tukey's multiple comparisons test (threshold for significance: P = 0.05; * = P ≤ 0.05).*

PWD was significantly longer for *amos*[1]; Bd-Gal4 x *amos*[1], UAS-csChrimson ATR larvae (3.91 ± 1.74s/ wave; *n* = 6 larvae) than it was for *amos*[1], UAS-csChrimson ATR larvae (2.03 ± 0.88s/ wave; *n* = 10 larvae, *P* ≤ 0.0001) and *amos*[1]; Bd-Gal4 ATR larvae (2.43 ± 0.87s/ wave; *n* = 10 larvae, *P* ≤ 0.0002 (Figure 3.22)). Thus, the dbd and/ or dmd1 neuron~~(s)~~(s) is necessary for normal larval peristaltic wave frequency and duration.

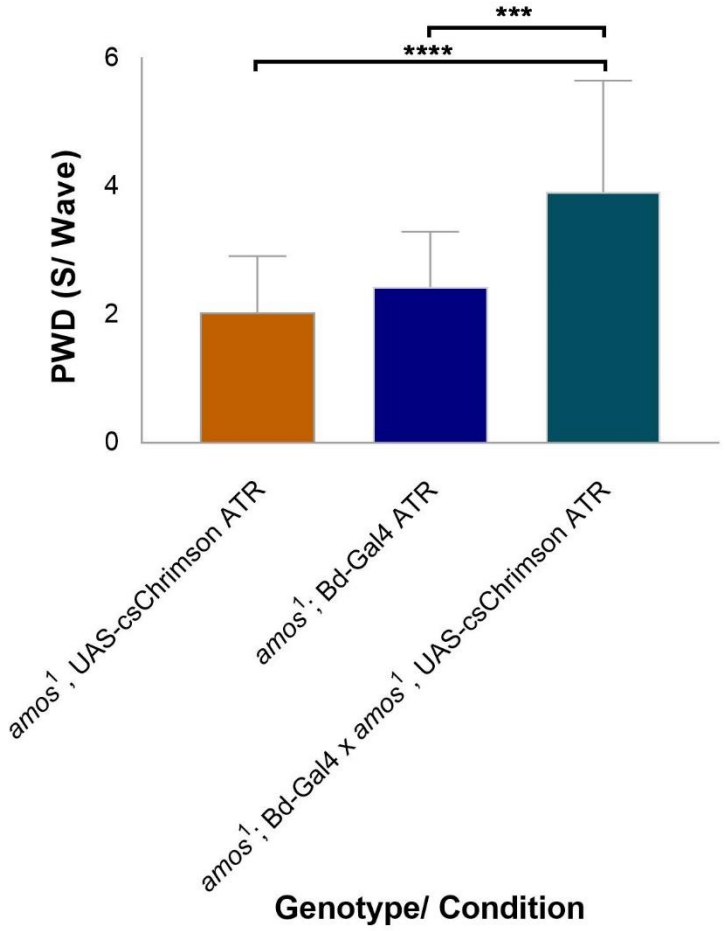

Figure 3.22: Dbd and dmd1 neurons are necessary for normal larval peristaltic wave duration. *Peristaltic Wave Duration (PWD) was timed from recordings of larvae crawling on a 1% grape agar plate (lid on, 23.9-25°C, daylight). There was a significant difference in PWD between amos[1]; Bd-Gal4 x amos[1], UAS-csChrimson ATR (3.91 ± 1.74%; n = 6 larvae) and amos[1], UAS-csChrimson ATR (2.03 ± 0.88s/ wave; n = 10 larvae, P ≤ 0.0001) and amos[1]; Bd-Gal4 ATR larvae (2.43 ± 0.87s/ wave; n = 10 larvae, P = 0.0002). Statistical significance determined by one-way ANOVA with Tukey's multiple comparisons test (threshold for significance: P = 0.05; *** = P ≤ 0.0002, *** = P ≤ 0.0001).*

3.3.1.2 Role of other sensory neurons in larval behaviour

Despite the limitations imposed by the driver, experiments using Bd-Gal4 x UAS-csChrimson ATR confirmed the potential to use optogenetics to identify the behavioural role~~(s)~~(s) of sensory neurons in larval behaviour. As a result, three other drivers: Bd/I-Gal4, NompC-Gal4 and Nan-Gal4, were used in optogenetic experiments.

Bd/I-Gal4 is another driver that has been used to implicate dbd and type I sensory neurons in normal crawling (Hughes and Thomas, 2007; Cheng *et al.*, 2010). Therefore, it was used to determine the prevalence of the strike behaviour identified above. Here, Bd/I-Gal4 x UAS-csChrimson ATR phenotype in response to 30s light stimulation, was recorded and compared to controls (UAS-csChrimson ATR and Bd/I-Gal4 ATR) in the same way as Bd-Gal4. UAS-csChrimson ATR froze (*n* = 10), Bd/I-Gal4 ATR larvae (*n* = 10, Figure 3.23) did not respond to light, whilst Bd/I-Gal4 x UAS-csChrimson ATR demonstrated a variable phenotype in response to stimulation (Figure 3.24). The phenotype was characterised by unpredictable movement ranging from rolling and rearing, to 'striking' like the Bd-Gal4 phenotype. Variability made it difficult to relate the phenotype to normal behaviour.

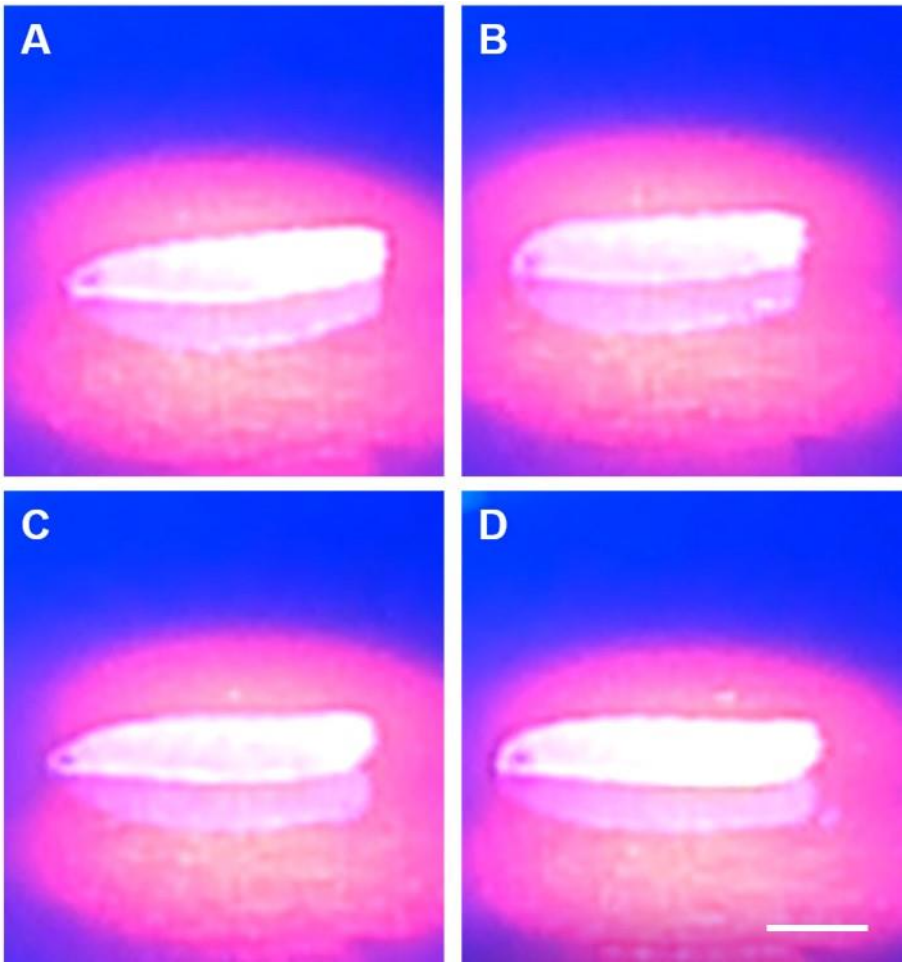

Figure 3.23: Bd/I-Gal4 ATR larvae do not respond to light stimulation. *Representation of phenotype recorded in Bd/I-Gal4 larvae (n = 10) raised on 1% all-trans retinal food, in response to 30s red light stimulation. Larvae crawled on a 200mm x 200mm, 1% grape agar plate in a closed plastic container (23.9-25°C, daylight). Panels A-D show phenotype in stages, (200ms apart) following stimulation. Scale bar is 5mm (shown in one panel for clarity, as all are the same size).*

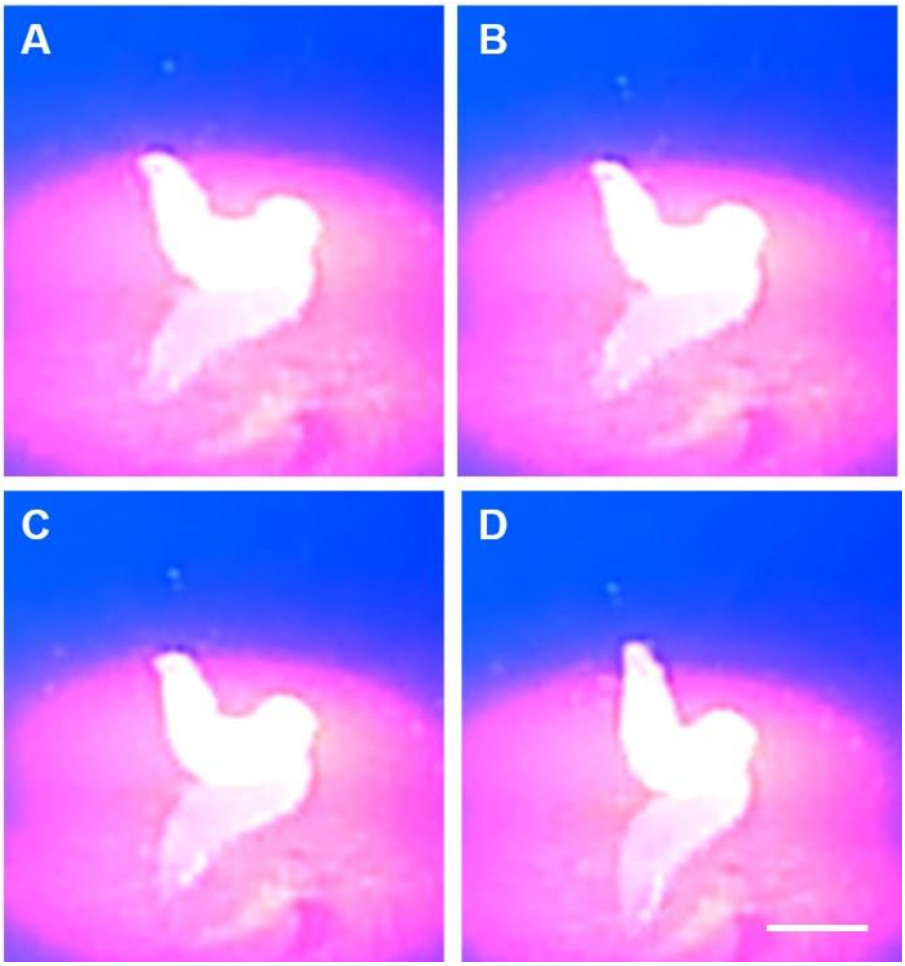

Figure 3.24: Bd/I-Gal4 x UAS-csChrimson ATR larvae demonstrate a variable phenotype in response to light stimulation. *Representation of phenotype recorded in Bd-Gal4/I x UAS-csChrimson larvae (n = 10) raised on 1% all-trans retinal food, in response to 30s red light stimulation. Larvae crawled on a 200mm x 200mm, 1% grape agar plate in a closed plastic container (23.9-25°C, daylight). Panels A-D show phenotype in stages, (200ms apart) following stimulation. Scale bar is 5mm (shown in one panel for clarity, as all are the same size).*

The only significant difference in % change in CS for Bd/I-Gal4 x UAS-csChrimson ATR and its controls was between Bd/I-Gal4 ATR (-1.6 ± 14.35%; *n* = 10 larvae) and UAS-csChrimson ATR (-45.2 ± 33.58%; *n* = 10 larvae; $P \leq 0.01$ (Figure 3.25)). This is: (1) surprising given the Bd/I-Gal4 x UAS-csChrimson ATR phenotype in response to light stimulation, but likely reflects the variability in response (some larvae showed minimal response, and/ or recovered normal crawling quickly); (2) a reflection of the 'freeze' phenotype observed in UAS-csChrimson ATR.

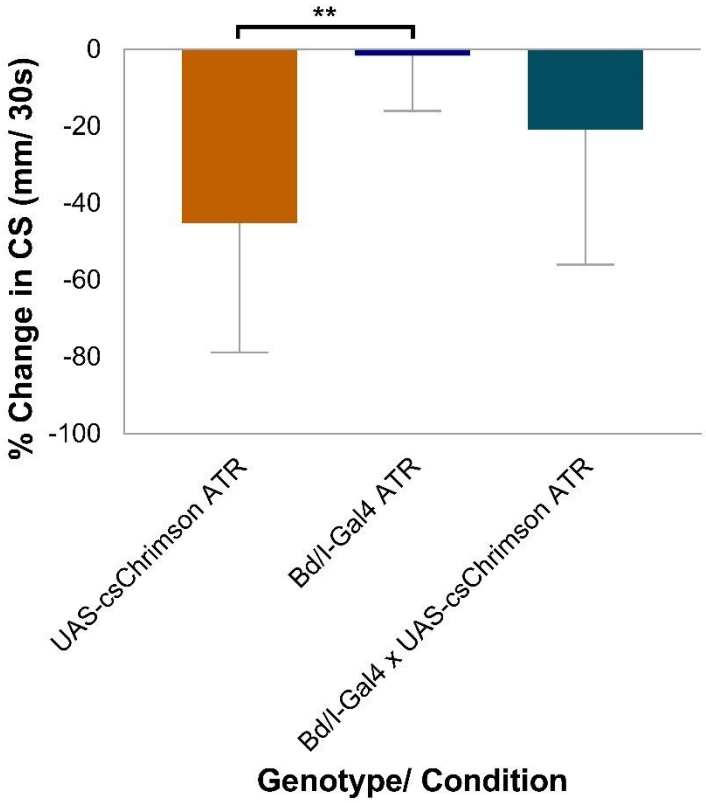

Figure 3.25: Light stimulation of dbd and type I neurons does not affect larval crawling speed versus controls. *% Change in Crawling Speed (CS, where change is difference between pre and during light stimulus) was recorded manually from larvae crawling on a grape agar plate (lid on, 23.9-25°C, daylight). There was a significant difference in % change in CS between Bd/I-Gal4 ATR (-1.6 ± 14.35%; n = 10 larvae) and UAS-csChrimson ATR (-45.2 ± 33.58%; n = 10 larvae; P = 0.007). Statistical significance determined by one-way ANOVA with Tukey's multiple comparisons test (threshold for significance: P = 0.05; ** = P ≤ 0.01).*

As with % change in CS, the only significant difference in % change in PWF for Bd/I-Gal4 x UAS-csChrimson ATR and its controls, was between Bd/I-Gal4 ATR (6.84 ± 12.17%; *n* = 10 larvae) and UAS-csChrimson ATR (-34.55 ± 30.99%; *n* = 10 larvae; *P* ≤ 0.01 (Figure 3.26)). Again, this is surprising given the Bd/I-Gal4 x UAS-csChrimson ATR phenotype, and the lack of significant difference versus controls probably reflects the variability in response to light. Significant difference between controls is due to the 'freeze' phenotype observed in UAS-csChrimson ATR.

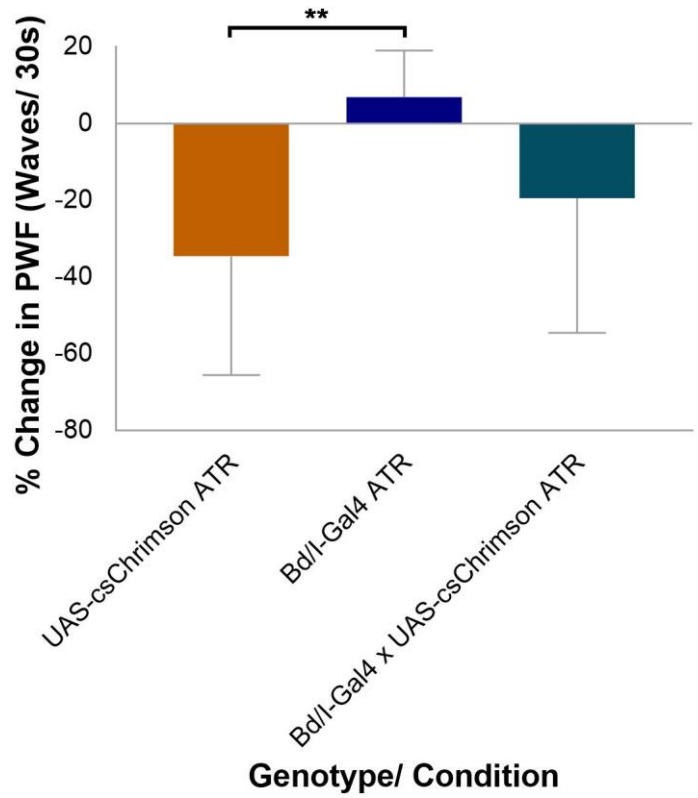

Figure 3.26: Light stimulation of dbd and type I neurons does not affect larval peristaltic wave frequency versus controls. *% Change in Peristaltic Wave Frequency (PWF) was recorded manually from larvae crawling on a grape agar plate (lid on, 23.9-25°C, daylight). There was a significant difference in % change in PWF between UAS-csChrimson ATR (-34.55 ± 30.99%; n = 10 larvae) and Bd/I-Gal4 ATR (6.84 ± 12.17%; n = 10 larvae, P = 0.007). Statistical significance determined by one-way ANOVA with Tukey's multiple comparisons test (threshold for significance: P = 0.05; * = P ≤ 0.05, ** = P ≤ 0.01).*

Given the interesting difference in phenotypes of larvae driven by Bd-Gal4 and Bd/I-Gal4 drivers, and due to the disappointing lack of specificity in Bd-Gal4, Bd/I-Gal4 expression was checked by immunofluoresence. Antibody staining of Bd/I-Gal4 x UAS-GFP showed no GFP expression in dbd or dmd1 neurons, but expression in other MD neurons (Figure 3.27). This difference with expected expression is confusing but explains the difference in phenotypes between the two drivers.

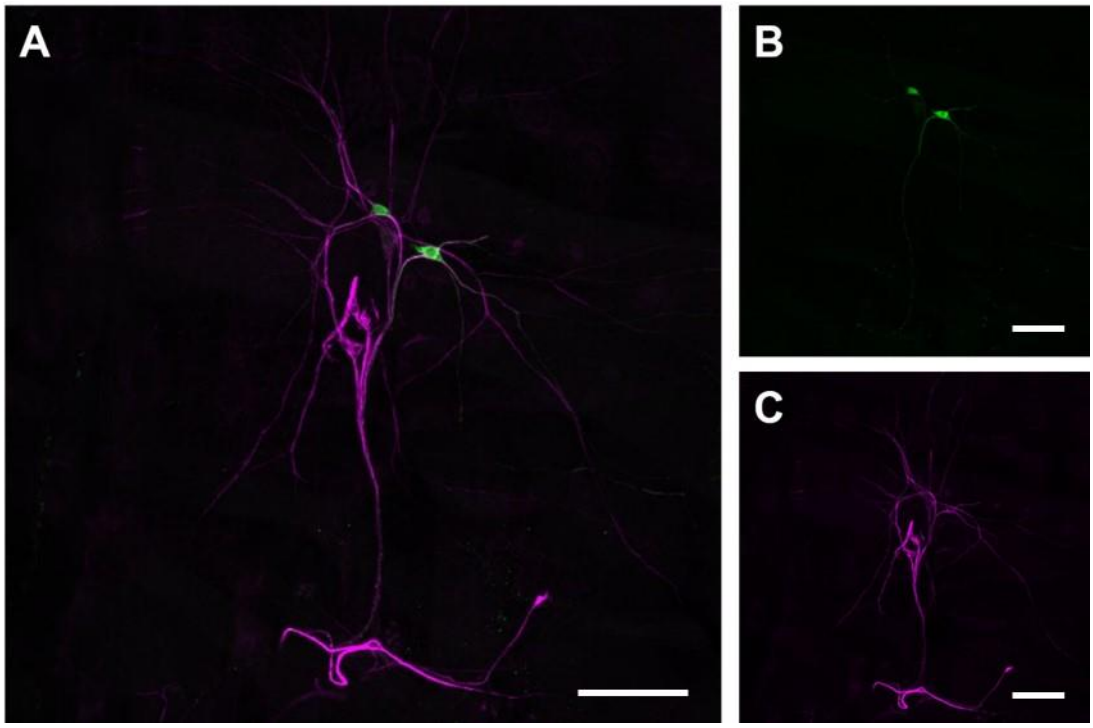

Figure 3.27: Immunostaining of Bd/l-Gal4 x UAS-GFP with α-GFP and α-22C10. *A: Projection of Bd/l-Gal4 driving UAS-GFP expression (green) in MD neurons, with 22C10 counterstain. Note the absence of staining in dbd and dmd1 neurons (dbd is identifiable by its dendrites, which project across bottom of panel; dmd1 is identifiable as cell body and single dendrite more dorsal (closer to top of image) than dbd). B: α-GFP stain only. C: α-22C10 only. Scale bar is 50μm.*

nanchung (nan) encodes a TRPV channel that is expressed in chordotonal (ch) neurons (Kim *et al.*, 2003). Ch neurons are necessary for hearing (Kim *et al.*, 2003; Zhang *et al.*, 2013; zur Lage *et al.*, 2018) and are involved in crawling (Caldwell *et al.*, 2003; Hughes and Thomas, 2007; Cheng *et al.*, 2010; Fushiki, Kohsaka and Nose, 2011). The latter is controversial and is discussed in more detail in Chapter 3. Here I include optogenetic activation of Nan-Gal4 neurons. Nan-Gal4 x UAS-csChrimson ATR phenotype in response to 30s light stimulation, was recorded and compared to controls (UAS-csChrimson ATR and Nan-Gal4 ATR) in the same way as Bd-Gal4. UAS-csChrimson larvae ATR 'froze' (n = 10) on stimulation, whilst Nan-Gal4 ATR larvae (n = 10, Figure 3.28) and Nan-Gal4 x UAS-csChrimson ATR (n = 10, Figure 2.29) did not respond to light. This was surprising, given the research that links ch neurons to locomotion (Caldwell *et al.*, 2003; Hughes and Thomas, 2007; Cheng *et al.*, 2010; Fushiki, Kohsaka and Nose, 2011).

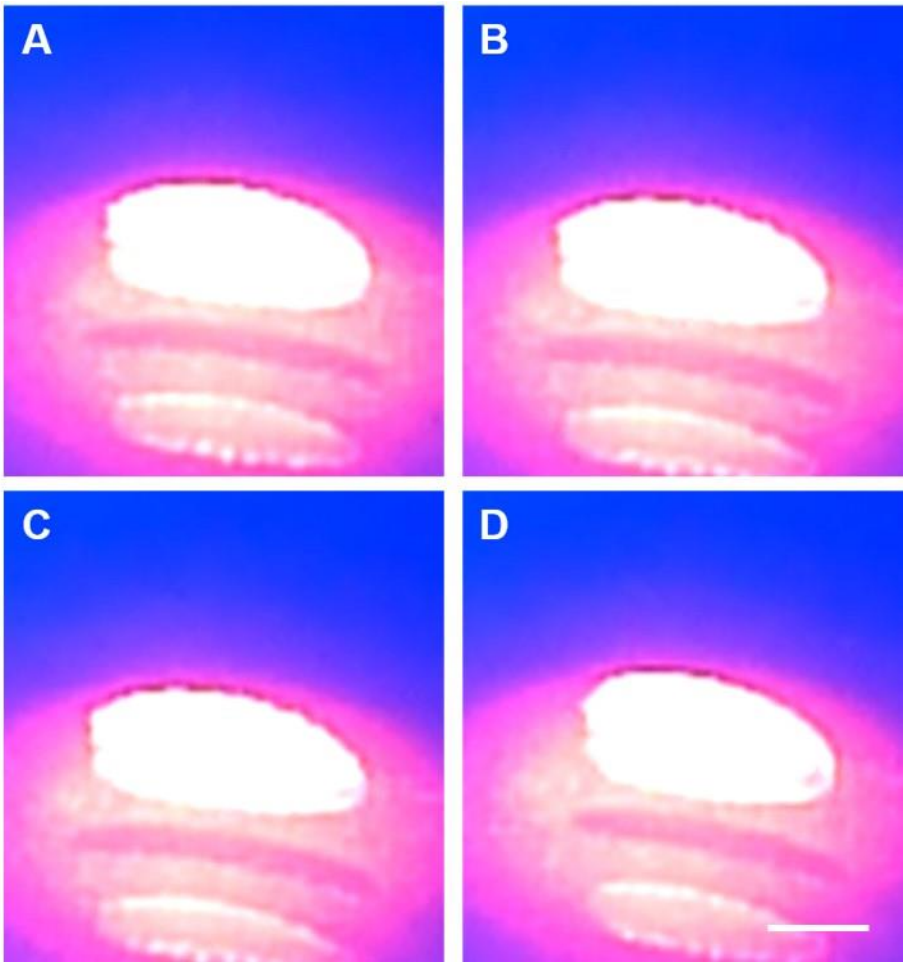

Figure 3.28: Nan-Gal4 ATR larvae do not respond to light stimulation. *Representation of phenotype recorded in Nan-Gal4 larvae (n = 10) raised on 1% all-trans retinal food, in response to 30s red light stimulation. Larvae crawled on a 200mm x 200mm, 1% grape agar plate in a closed plastic container (23.9-25°C, daylight). Panels A-D show phenotype in stages, (200ms apart) following stimulation. Scale bar is 5mm (shown in one panel for clarity, as all are the same size).*

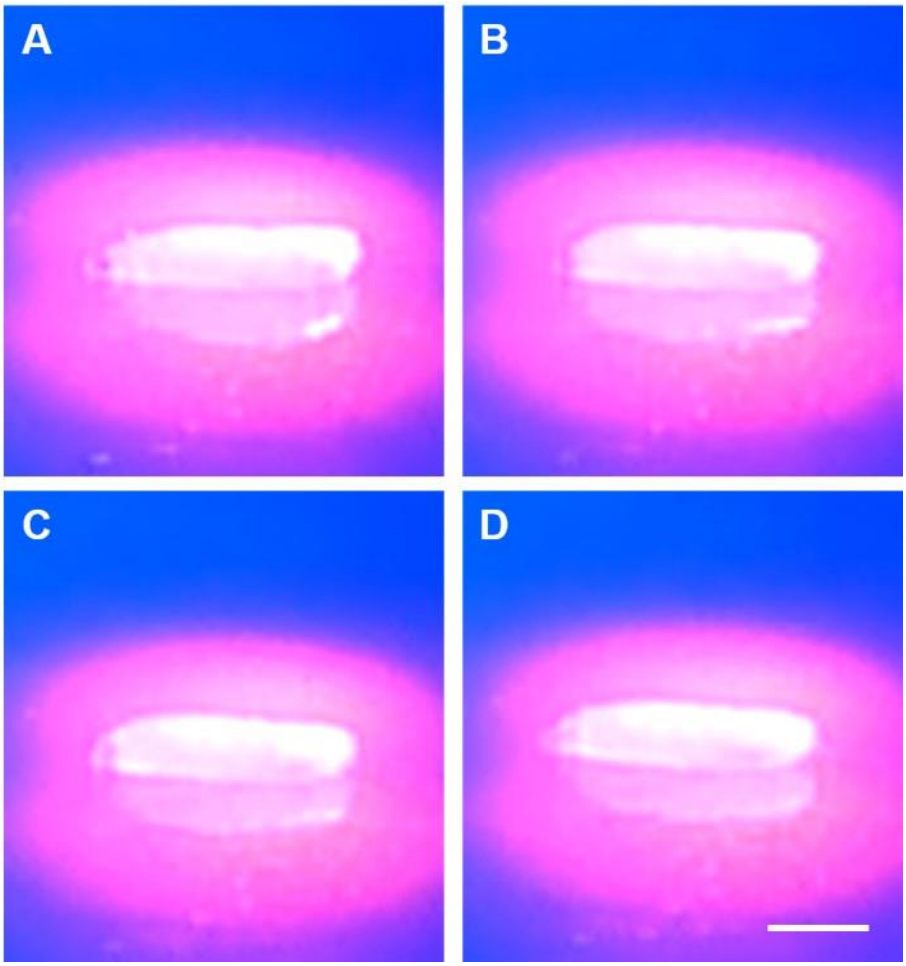

Figure 3.29: Nan-Gal4 x UAS-csChrimson ATR larvae do not respond to light stimulation. *Representation of phenotype recorded in Nan-Gal4 x UAS-csChrimson ATR larvae (n = 10) raised on 1% all-trans retinal food, in response to 30s red light stimulation. Larvae crawled on a 200mm x 200mm, 1% grape agar plate in a closed plastic container (23.9-25°C, daylight). Panels A-D show phenotype in stages, (200ms apart) following stimulation. Scale bar is 5mm (shown in one panel for clarity, as all are the same size).*

There was a significant difference in % change in CS between UAS-csChrimson ATR (-45.2 ± 33.58%; *n* = 10 larvae) and Nan-Gal4 x UAS-csChrimson ATR (-9.41 ± 22.21%; *n* = 10 larvae; P ≤ 0.05) and Nan-Gal4 ATR (-8.61 ± 31.03%; *n* = 10 larvae; P ≤ 0.05 (Figure 3.30)). This is consistent with the 'freeze' phenotype for UAS-csChrimson ATR and lack of phenotype observed in Nan-Gal4 x UAS-csChrimson ATR larvae.

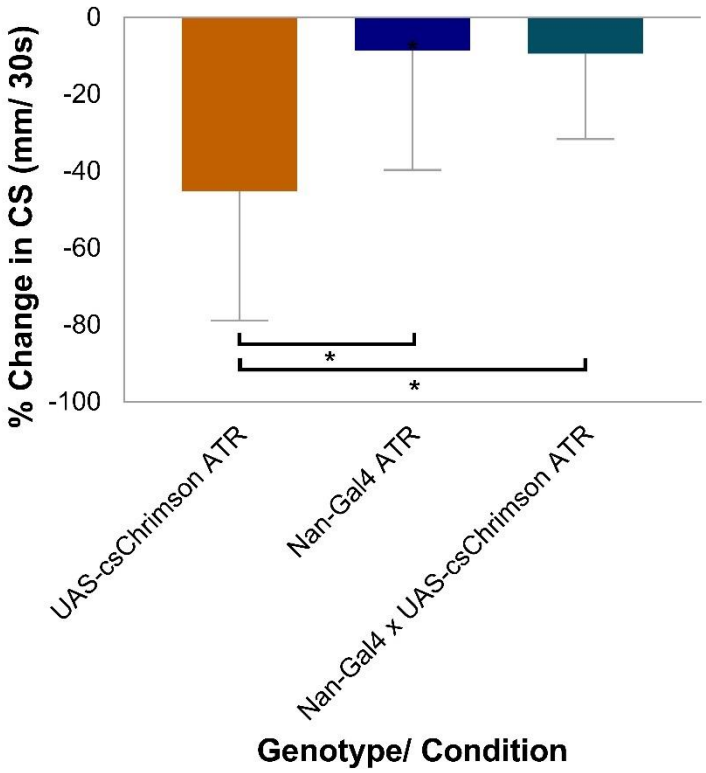

Figure 3.30: Light stimulation of chordotonal neurons does not affect larval crawling speed. *% Change in crawling speed (CS, where change is difference between pre and during light stimulus) was recorded manually from larvae crawling on a grape agar plate (lid on, 23.9-25°C, daylight). There was a significant difference in % change in CS between UAS-csChrimson ATR (-45.2 ± 33.58%; n = 10 larvae) and Nan-Gal4 ATR x UAS-csChrimson ATR (-9.41 ± 22.21%; n = 10 larvae; P = 0.025) and Nan-Gal4 ATR (-8.61 ± 31.03%; n = 10 larvae; P = 0.029). Statistical significance determined by one-way ANOVA with Tukey's multiple comparisons test (threshold for significance: P = 0.05; * = P ≤ 0.05).*

As expected (given % change in CS results), there was a significant difference in % change in PWF between UAS-csChrimson ATR (-34.55 ± 30.99%; n = 10 larvae) and Nan-Gal4 x UAS-csChrimson ATR (0.5 ± 25.87%; n = 10 larvae, P ≤ 0.05) and Nan-Gal4 ATR (2.63 ± 18.77%; n = 10 larvae, P ≤ 0.01 (Figure 3.31)), but not between Nan-Gal4 x UAS-csChrimson ATR and controls. The lack of phenotype for Nan-Gal4 x UAS-csChrimson ATR, and broad (nonspecific) expression of Bd-Gal4 and Bd/I-Gal4 meant that next, Nan-Gal4 expression was checked by immunofluorescence.

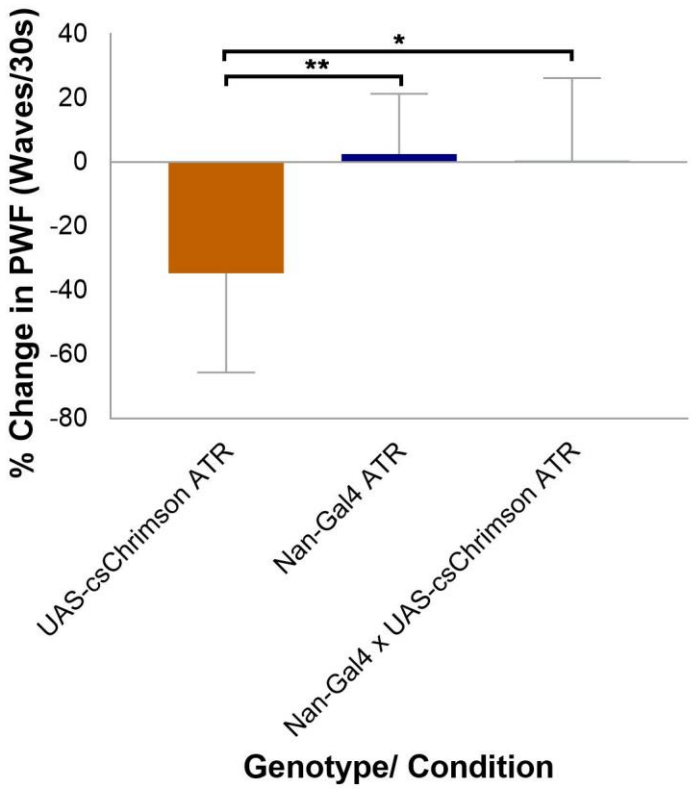

Figure 3.31: Light stimulation of chordotonal neurons does not affect larval peristaltic wave frequency. *% Change in Peristaltic Wave Frequency (PWF, where change is difference between pre and during 30s light stimulus) was recorded manually from larvae crawling on a 1% grape agar plate (lid on, 23.9-25°C, daylight). There was a significant difference in % change in PWF between UAS-csChrimson ATR (-34.55 ± 30.99%; n = 10 larvae) and Nan-Gal4 x UAS-csChrimson ATR (0.5 ± 25.87%; n = 10 larvae, P = 0.014). There was also a significant difference between UAS-csChrimson ATR and Nan-Gal4 ATR (2.63 ± 18.77%; n = 10 larvae, P = 0.009). Statistical significance determined by one-way ANOVA with Tukey's multiple comparisons test (threshold for significance: P = 0.05; * = P ≤ 0.05, ** = P ≤ 0.01).*

Antibody staining of Nan-Gal4 x UAS-GFP showed no GFP expression in ch (or any other) neurons (Figure 3.32). This lack of expression explains the absence of phenotype in Nan-Gal4 x UAS-csChrimson ATR during light stimulation and reinforces the importance of driver line expression/ specificity highlighted by Bd-Gal4 and Bd/I-Gal4.

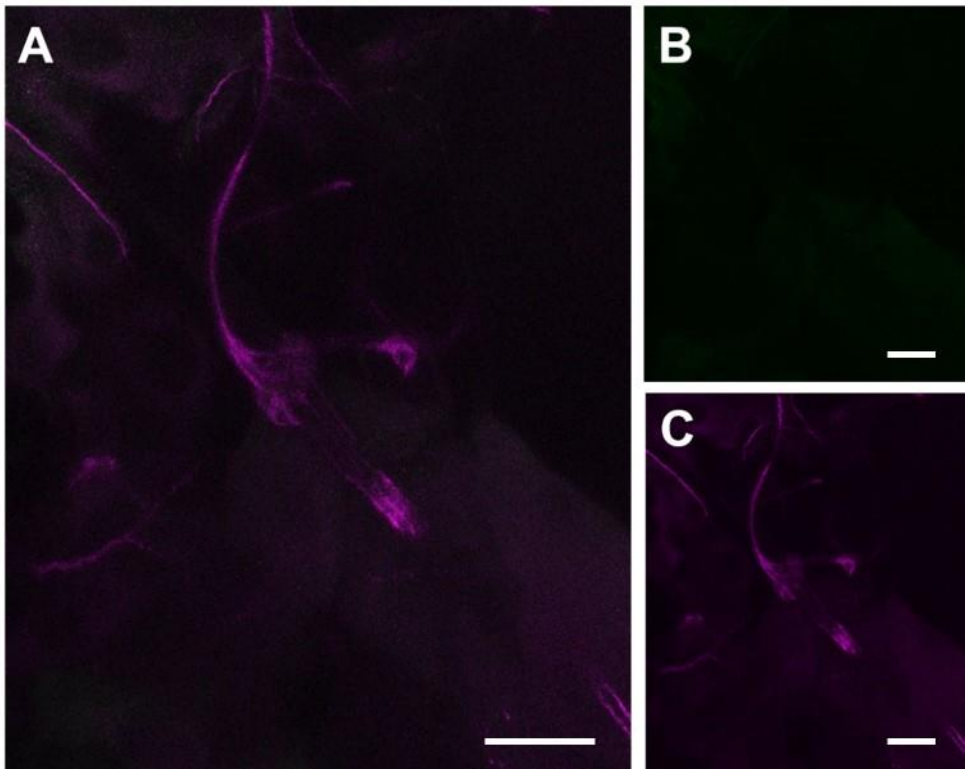

Figure 3.32: Immunostaining of Nan-Gal4 x UAS-GFP with α-GFP and α-22C10. *A: Projection of Nan-Gal4 x UAS-GFP expression in lch1-5 (ch) neurons, stained with α-GFP and α-22C10 counterstain. Note the absence of staining in ch neurons (lch1-5 identified by 5 dendrites seen in centre of panel). B: α-GFP stain only. C: α-22C10 only. Scale bar is 20μm.*

NompC is a mechanosensory cation channel linked to hearing, locomotion and gentle touch sensation, which is expressed in dda (ddaD, ddaE), ch (lch1, lch5, vchA and vchB), dbd, dmd1, vbd and vpda neurons (Cheng *et al.*, 2010; Effertz, Wiek and Gopfert, 2011; Tsubouchi, Caldwell and Tracey, 2012). NompC-Gal4 has been used to suggest that *NompC* is required for bd and type I neuron roles in regulating larval locomotion (Cheng *et al.*, 2010), so was used here to check for a phenotype that would support that suggestion.

NompC-Gal4 x UAS-csChrimson ATR phenotype in response to 30s light stimulation, was recorded and compared to controls (UAS-csChrimson ATR and NompC-Gal4 ATR) in the same way as Bd-Gal4. UAS-csChrimson larvae ATR 'froze' on stimulation (n = 10), whilst NompC-Gal4 ATR larvae did not respond to light (n = 10, Figure 3.33). Nan-Gal4 x UAS-csChrimson ATR produced a variable phenotype that was characterised by a 'tail lift' and reversed peristaltic waves (propagated from head-tail (n = 10, Figure 3.34)), which agrees with a role for NompC in regulation of peristalsis.

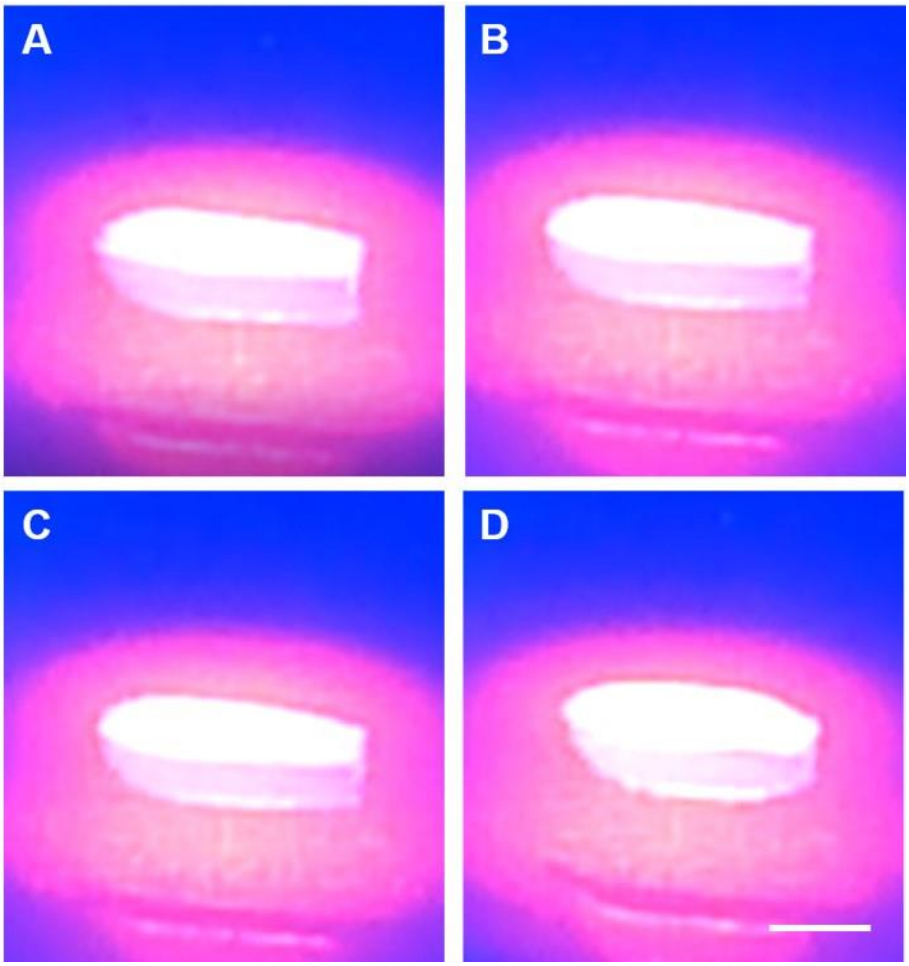

Figure 3.33: NompC-Gal4 ATR larvae do not respond to light stimulation. *Representation of phenotype recorded in NompC-Gal4 larvae (n = 10) raised on 1% all-trans retinal food, in response to 30s red light stimulation. Larvae crawled on a 200mm x 200mm, 1% grape agar plate in a closed plastic container (23.9-25°C, daylight). Panels A-D show phenotype in stages, (200ms apart) following stimulation. Scale bar is 5mm (shown in one panel for clarity, as all are the same size).*

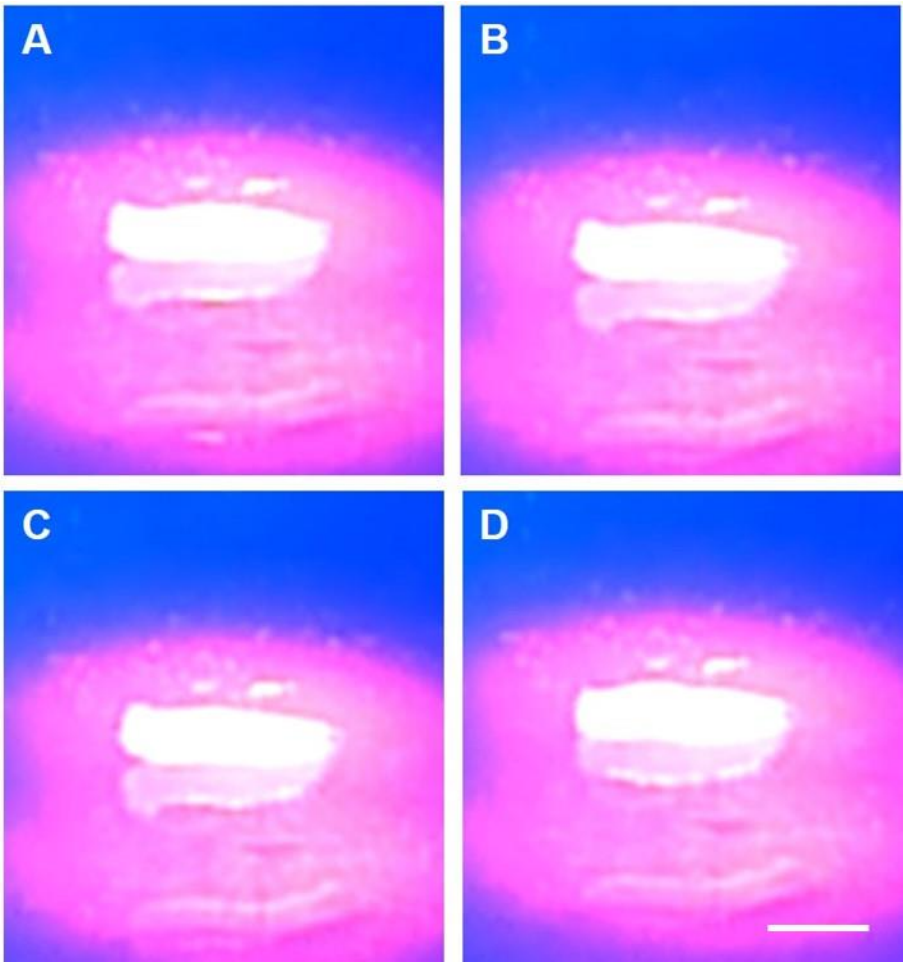

Figure 3.34: NompC-Gal4 x UAS-csChrimson ATR larvae demonstrate a 'tail lift and reverse' phenotype in response to light stimulation. *Representation of phenotype recorded in NompC-Gal4 x UAS-csChrimson larvae (n = 10) raised on 1% all-trans retinal food, in response to 30s red light stimulation. Larvae crawled on a 200mm x 200mm, 1% grape agar plate in a closed plastic container (23.9-25°C, daylight). Panels A-D show phenotype in stages, (200ms apart) following stimulation. Scale bar is 5mm (shown in one panel for clarity, as all are the same size).*

There was no significant difference in % change in CS between NompC-Gal4 x UAS-csChrimson ATR (-30 ± 23.48%; *n* = 10 larvae) and controls. Only the difference between controls, which was consistent across optogenetic experiments due to the 'freeze' phenotype for UAS-csChrimson, was significant; UAS-csChrimson ATR (-45.2 ± 33.58%; *n* = 10 larvae), NompC-Gal4 ATR (8.33 ± 45.21%; *n* = 10 larvae, P ≤ 0.01 (Figure 3.35)). Whilst this contrasts the phenotype observed for NompC-Gal4 x UAS-csChrimson ATR, it is important to note that the difference between the cross and NompC-Gal4 ATR control was large and approaching significance (*P* = 0.055).

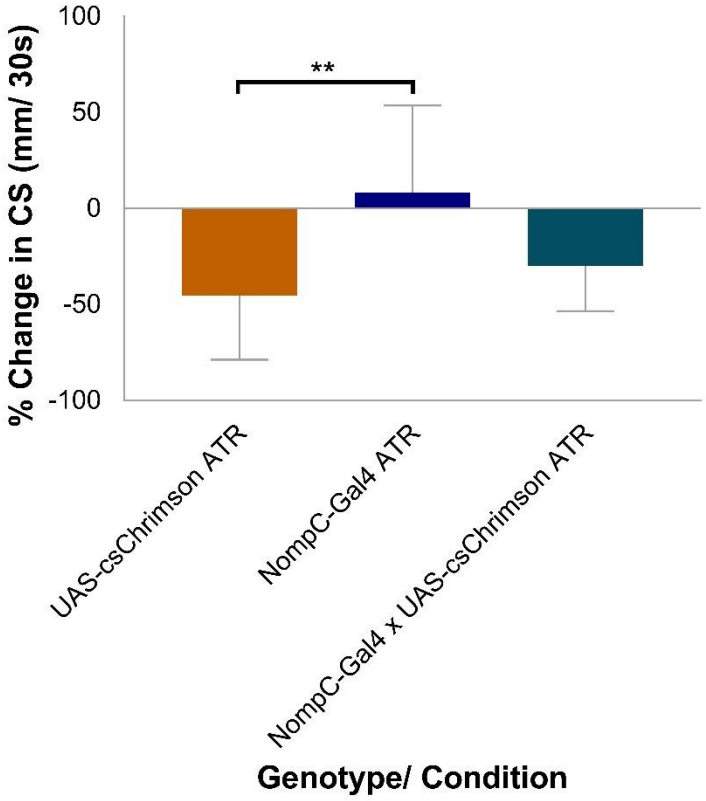

Figure 3.35: Light stimulation of neurons expressing NompC does not affect larval crawling speed. *% Change in crawling speed (CS, where change is difference between pre and during 30s light stimulus) was recorded manually from larvae crawling on a 1% grape agar plate (lid on, 23.9-25°C, daylight). There was a significant difference in % change in CS between UAS-csChrimson ATR (-45.2 ± 33.58%; n = 10 larvae) and NompC-Gal4 ATR (8.33 ± 45.21%; n = 10 larvae, P = 0.006). Statistical significance determined by one-way ANOVA with Tukey's multiple comparisons test (threshold for significance: P = 0.05; ** = P ≤ 0.01).*

There was a significant difference in % change in PWF between NompC-Gal4 x UAS-csChrimson ATR (-41.82 ± 32.48%; *n* = 10 larvae) and NompC-Gal4 ATR (4.58 ± 28.83%; *n* = 10 larvae, *P* ≤ 0.01 (Figure 3.36)). There was also a significant difference between UAS-csChrimson ATR (-41.82 ± 32.48%; *n* = 10 larvae) and NompC-Gal4 ATR (*P* ≤ 0.05). This result is consistent with the NompC-Gal4 x UAS-csChrimson ATR 'tail lift and reverse' phenotype and % change in CS results (if proximity to significance reflects variance that would reduce with greater power), so supports findings that NompC is required for bd and type I neurons' role in regulating larval locomotion.

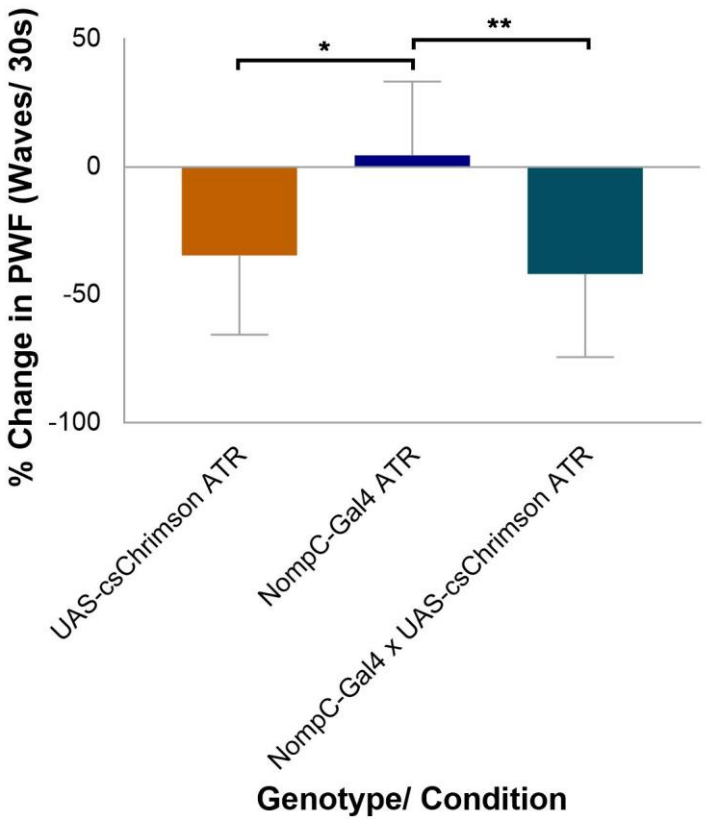

Figure 3.36: Light stimulation of neurons expressing NompC reduces larval peristaltic wave frequency. *% Change in Peristaltic Wave Frequency (PWF, where change is difference between pre and during light stimulus) was recorded manually from larvae crawling on a grape agar plate (lid on, 23.9-25°C, daylight). There was a significant difference in % change in PWF between NompC-Gal4 x UAS-csChrimson ATR (-41.82 ± 32.48%; n = 10 larvae) and NompC-Gal4 ATR (4.58 ± 28.83%; n = 10 larvae, P = 0.006). There was also a significant difference between UAS-csChrimson ATR (-34.55 ± 30.99%; n = 10 larvae) and NompC-Gal4 ATR (P = 0.022). Statistical significance determined by one-way ANOVA with Tukey's multiple comparisons test (threshold for significance: P = 0.05; * = P ≤ 0.05, ** = P ≤ 0.01).*

3.3.1.3 Exploring the molecular mechanism of mechanosensation in dbd neurons

3.3.1.3.1 The role of DmPiezo in larval crawling

Optogenetic experiments showed that dbd and dmd1 neurons are necessary for normal larval PWF and PWD. They also suggested that *NompC* could be the MET, by showing that NompC-expressing neurons (including dbd and dmd1) are necessary for normal crawling. This supports Cheng *et al.*, 2010, which states that NompC expressed in dbd and dmd1 neurons is responsible for crawling speed (CS). However, it contrasts work from the Jarman laboratory, which used electrophysiology to suggest that *DmPiezo* is the primary MET of the dbd neuron (Suslak *et al.*, 2015c). Consequently, *DmPiezo* and *NompC* mutant and RNAi lines were used in crawling experiments to compare the contribution of the channels to locomotion.

Crawling experiments were conducted by measuring the distance travelled by feely-moving larvae, on a 20 x 20cm, 1% agar arena in 120s (so returned a CS as mm/ 120s). *DmPiezo* mutants (*DmPiezo* -/-) were compared to heterozygous controls, and there was a significant difference in CS between *DmPiezo* -/- (83.14 ± 32.21mm/ 120s; *n* = 16 larvae) and *DmPiezo* +/- (124.5 ± 52.44mm/ 120s; *n* = 16 larvae; $P \leq 0.01$ (Figure 3.37).

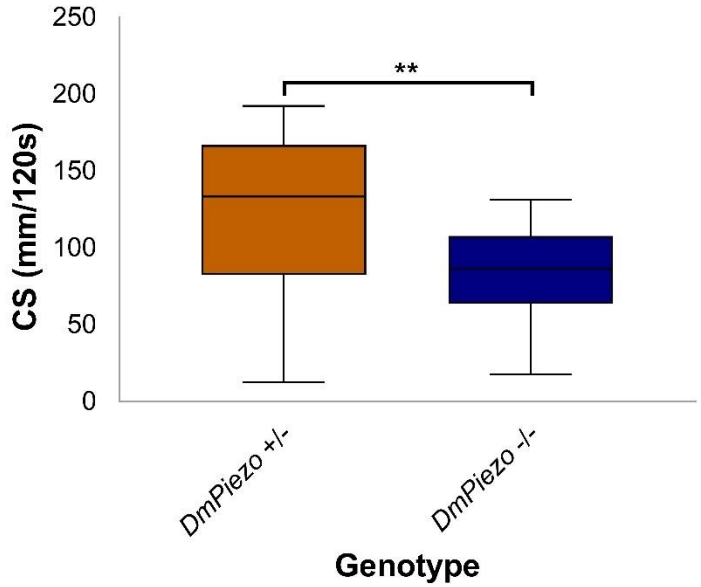

Figure 3.37: DmPiezo is necessary for normal crawling speed. *CS is crawling speed (mm)/ 120s, recorded manually from larvae crawling on a 200mm x 200mm, 1% agar gel in a closed plastic container (23.9-25°C, daylight). There was a significant difference in CS between DmPiezo -/- (83.14 ± 32.21mm/ 120s; n = 16 larvae) and DmPiezo +/- controls (124.5 ± 52.44mm/ 120s; n = 16 larvae; P = 0.007). Shown as whiskers minimum to maximum, horizontal line is median. Statistical significance determined by unpaired t test (threshold for significance: P = 0.05; ** = P ≤ 0.01).*

It was important to confirm whether the requirement for DmPiezo for normal crawling, is specific to the dbd neuron; Bd-Gal4 x UAS-Piezo RNAi larvae were compared to Bd-Gal4 controls (which was possible despite the problem with specificity of this driver, because *DmPiezo* is not expressed in the larval CNS). There was no significant difference in CS between Bd-Gal4 x UAS-Piezo RNAi (117.8 ± 32.56mm/ 120s; *n* = 16 larvae) and Bd-Gal4 larvae (127.1 ± 39.22mm/ 120s; *n* = 16 larvae (Figure 3.38)), which showed that *DmPiezo* expressed in dbd neurons is not responsible for normal crawling. This is of course caveated by the assumption that RNAi knockdown is effective (a subject discussed further in Chapter 4).

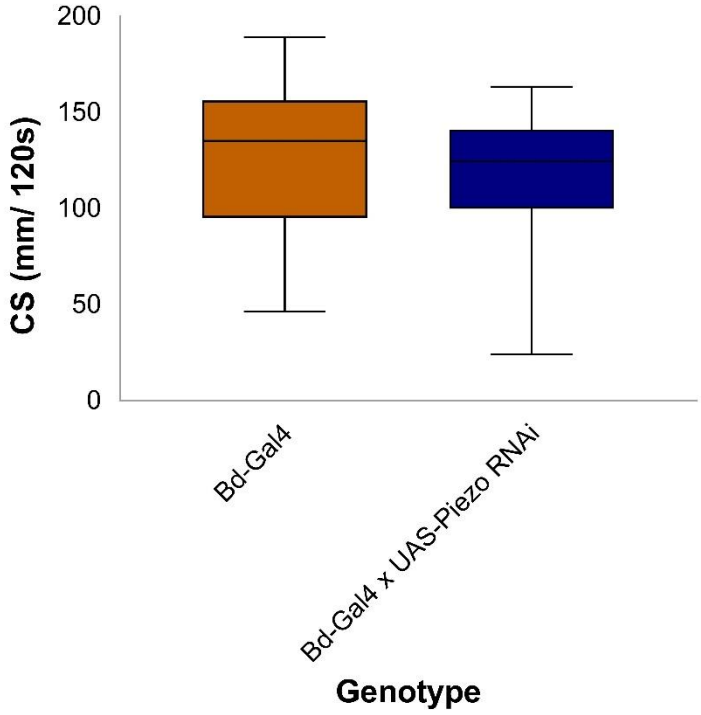

Figure 3.38: RNAi crawling experiments suggest that DmPiezo expressed in dbd neurons is not necessary for normal crawling speed. *CS is crawling speed (mm)/ 120s, recorded manually from larvae crawling on a 200mm x 200mm, 1% agar gel in a closed plastic container (23.9-25°C, daylight). There was no significant difference in CS between Bd-Gal4 x UAS-Piezo RNAi (117.8 ± 32.56mm/ 120s; n = 16 larvae) and Bd-Gal4 controls (127.1 ± 39.22mm/ 120s; n = 16 larvae, P = 0.456). Shown as whiskers minimum to maximum, horizontal line is median. Statistical significance determined by unpaired t test (threshold for significance: P = 0.05).*

Finally, there was a significant difference in CS for *NompC*[1]/[3] (77.64 ± 40.07mm/120s; *n* = 16 larvae) and *NompC*[1]/+ (121.7 ± 28.44mm/ 120s; *n* = 16 larvae, *P* ≤ 0.001) and *NompC*[3]/+ controls (128.6 ± 23.83mm/ 120s; *n* = 16 larvae, *P* ≤ 0.0001 (Figure 4.20 (mentioned here but shown later to benefit flow of Chapter 4)). There was no significant difference between *NompC*[1]/[3] and *Oregon-R* (wild type) controls (90.83 ± 18.65mm/ 120s; *n* = 16 larvae), however, *Oregon-R* crawled significantly less than *NompC*[1]/+ and *NompC*[3]/+ (P ≤ 0.001 for both). The significant difference between *NompC*[1]/[3] and *NompC*[1]/+/ *NompC*[3]/+ supports optogenetics and Cheng *et al.*, 2010, in posing NompC as the MET (or at least one MET) responsible for mechanosensation in dbd and dmd1 neurons. Given that this contradicts data from Suslak *et al.*, 2015, it was decided to pursue electrophysiology to check the published result~~(s)~~(s), and to see whether the same technique could confirm NompC as a MET in dbd neurons.

3.3.2 Electrophysiology to confirm MET responsible for stretch perception in dbd neuron

The electrophysiology protocol described in Suslak *et al.*, 2015, was performed in the Bewick laboratory at the University of Aberdeen. Consequently, my research represents the first time it was attempted at the University of Edinburgh (note: a similar protocol was performed previously, however, important details like the method of imparting a stretch stimulus to the larval preparation, were different (Suslak, 2015)). Thus, with guidance from Thomas Suslak, significant time and effort was spent implementing an electrophysiology protocol for this research and some concessions had to be made, due to availability of equipment. Whole cell patch clamp recordings were taken from the dbd neuron cell body of third-instar larvae, as in the original protocol. Unlike the original, a gentle 'tap' was delivered to the headstage of the recording electrode to provide the mechanical stimulus necessary for a response from the dbd neuron. The published method used a piezoelectric wafer for more accuracy and reliability. However, the wafer: (1) would had to have been submerged in HL3.1 to accommodate the inverted microscope available in Edinburgh; (2) was too large to fit between the dipping lens of the inverted microscope.

Early results were promising: dbd receptor potentials (RP) recorded in W^{1118} larvae in response to 'tap' stimulation, resembled those recorded in response to piezoelectric wafer stimulation (n = 4 larvae, Figure 3.39). Specifically, the RP profiles shared morphology of initial depolarisation and plateau phases (phases detailed in Figure 1.6). Dissimilar aspects of the traces, amplitude (dEm ~60mV in Suslak *et al.*, 2015 versus ~20mV here, where $dEm = E_p - E_{mrest}$) and time (~600ms in Suslak *et al.*, 2015 versus. ~80ms here) were attributed to the difference in means of mechanical stimulation.

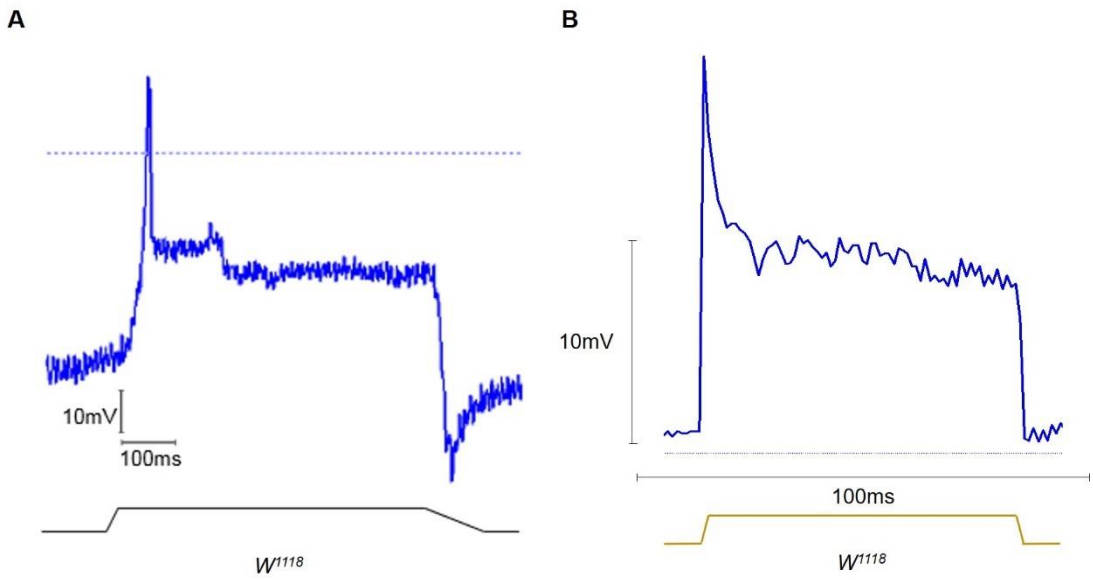

Figure 3.39: w^{1118} dbd neuron receptor potentials generated in response to stretch are reproducible. *A: Representative receptor potential (RP) recorded in W^{1118} larvae in response to stretch imparted by a piezoelectric wafer. Taken from Suslak et al., 2015. B: Representative RP recorded in W^{1118} larvae in response to tap delivered to headstage of recording electrode (n = 4). RPs share morphology of initial depolarisation and later plateau.*

Similarly, recordings of the RP in *DmPiezo* -/- larvae in response to 'tap' stimulation, showed a reduction in RP amplitude like that documented for Piezo-Gal4 x DmPiezo RNAi in Suslak *et al.*; Mean dbd neuron *dEm* of *DmPiezo* -/- larvae was ~88% less than that of W^{1118} larvae (*n* = 4 (Figure 3.40)), whilst *DmPiezo* RNAi produced ~80% reduction in *dEm* (Suslak *et al.*, 2015c). Together, the wild-type and mutant recordings showed that results from Suslak *et al.*, 2015 were reliable, so could have been evidence for *DmPiezo* as the MET in dbd neurons. However, they were subject to a significant error: Testing the seals established with the dbd cell body revealed values of ~10MΩ - significantly below the standard 1GΩ necessary for reliable whole cell patch clamp electrophysiology. Attempts to optimise the seal raised its value to 40MΩ, so were not enough to allow collection of reliable data from this protocol. Seal tests were not performed during *Drosophila* electrophysiology featured in Suslak *et al.*, 2015, so it is difficult to know if the work documented there is accurate.

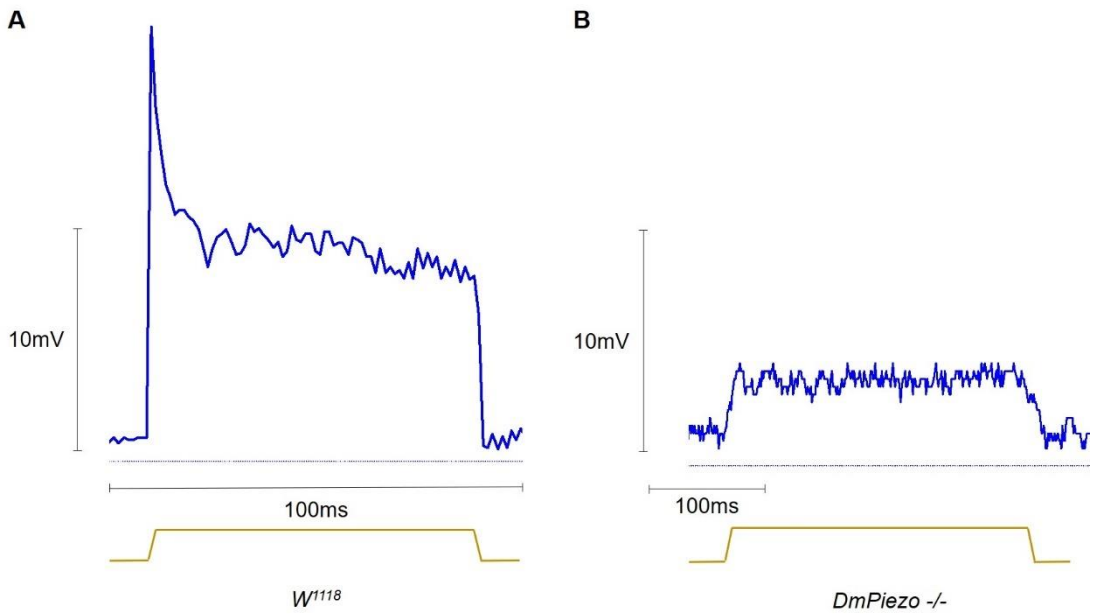

Figure 3.40: Effect of DmPiezo on dbd neuron receptor potentials generated in response to stretch is reproducible. *A: Representative receptor potential (RP) recorded in W^{1118} larvae in response to tap delivered to headstage of recording electrode (n = 4). B: Representative receptor potential (RP) recorded in DmPiezo -/- larvae in response to tap delivered to headstage of recording electrode. Note the ~88% difference in dEm (amplitude of initial depolarisation, where dEm = E_p - E_{mrest}) (n = 4**).***

Other electrophysiology included attempts to replicate voltage clamp recordings from Nair et al, which showed sodium (I_{Na}),inactivating (I_A) and non-inactivating (I_K) currents in dbd neurons of 1st-instar larvae (Nair, Bate and Pulver, 2010). These would be compared to recordings in *DmPiezo* (and *TRPA1*) mutants. As with the attempt to show reliability of findings from Suslak *et al.*, 2015, early efforts were promising; there was some response to change in voltage across *Oregon-R*, DmPiezo -/- and TRPA1 -/- larvae, with what appeared to be a reduction in current in the two latter (Figure 3.41). However, response is muted across genotypes, as experiments were limited by the poor seal of the dbd neuron.

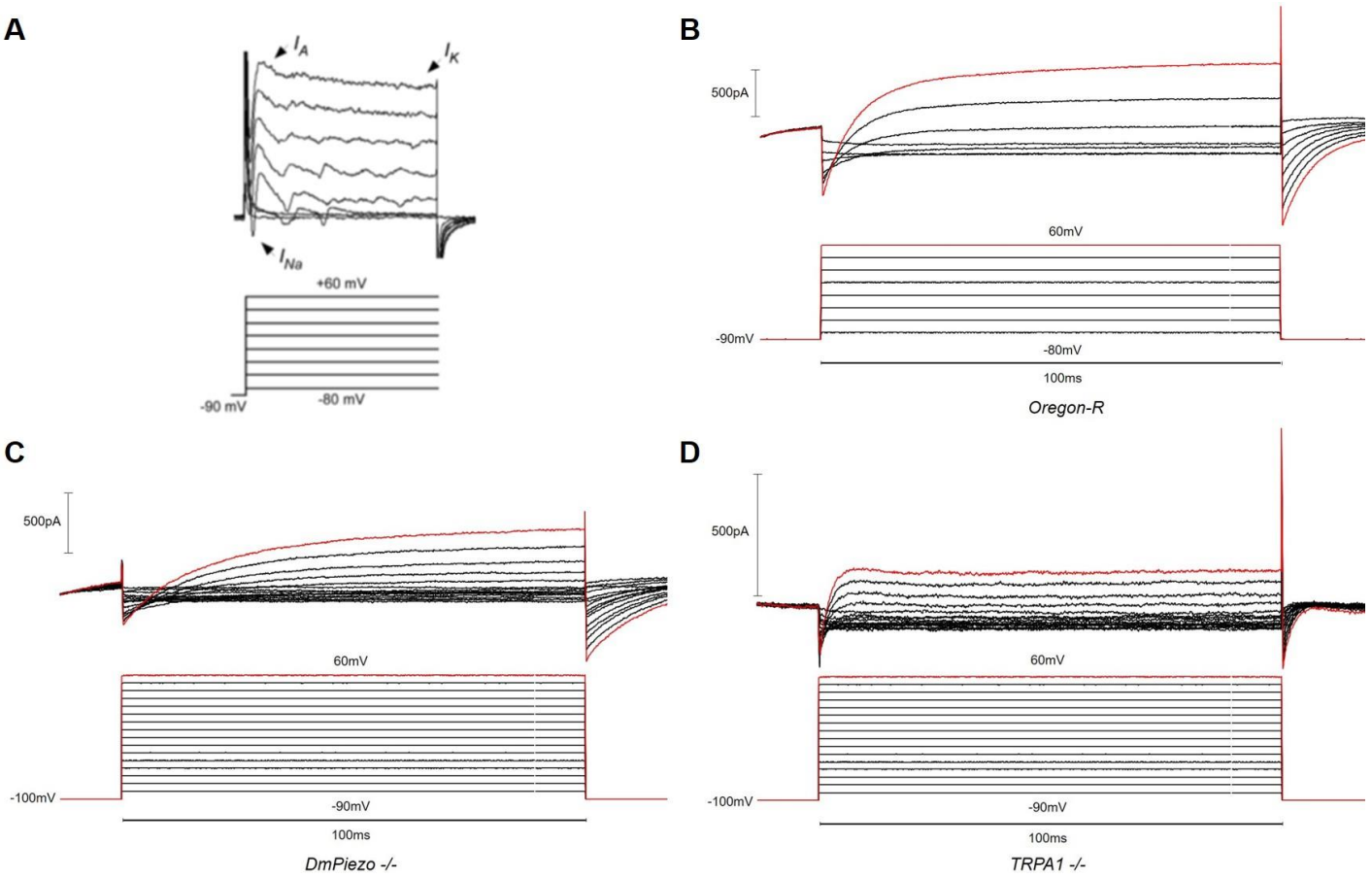

Figure 3.41: Voltage clamp whole cell electrophysiology of dbd neurons. *A: Recording taken from (Nair, Bate and Pulver, 2010), shows current reponse to -90mV-60mV, with shape charateristic of sodium,inactivating and non-inactivating currents (I_{Na}, I_A and I_K currents, respectively). B, C and D: Recordings from this research, with current reponse to -90mV-60mV (B, Oregon-R) or -100mV-60mV (C, DmPiezo -/- and D, TRPA1 -/-) which show a muted response versus A.*

The problem with the seal also affected the ability to improve on the accuracy and reliability of the ‘tap’ stimulus: Implementing a novel means to stretch the larval preparation by using Arduino UNO (a printed circuit board with microcontroller) to drive a servo according to C^{++} code written by the author (Figure 3.42), was redundant unless a proper seal with the dbd was established. This method could, however, provide value to future work. Finally, although further electrophysiological investigation and analysis may have yielded more detailed insights, I decided that more progress could be made in the time available by applying different approaches and techniques: Specifically, behavioural and GCaMP imaging experiments, to investigate the role of ch neurons in mechanosensation (Chapter 4).

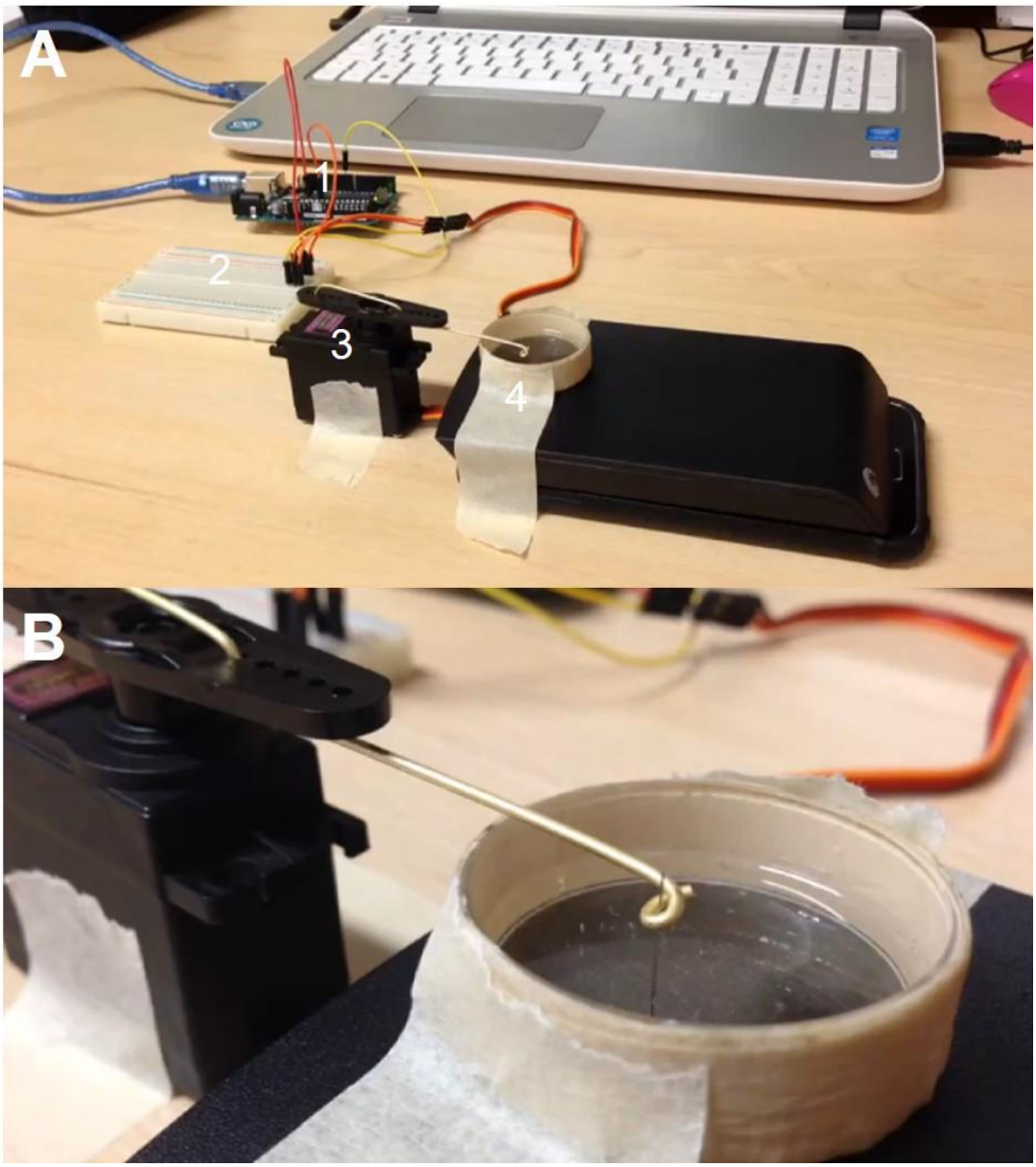

Figure 3.42: A novel method of delivering a stretch stimulus to larval preparations, by microcontroller driving a servo. *A: Zoomed-out view of equipment used to devise novel mechanism to deliver stretch to larval fillet preparation~~(s)~~(s). Components are: 1, Arduino UNO printed circuit board and microcontroller; 2, pegboard for wiring Arduino UNO to servo; 3, servo with arm adapted (extended by paperclip) to accommodate dissection pin; 4, Sylgard dissection dish used for larval preparation, with pin 'head end' dissection pin in place. B: Zoomed-in view of servo and dissection dish. Note that the servo arm moves to push the pin backwards and forwards, and this movement is coded by a modified 'sweep' C++ script uploaded to the microcontroller. The setup is shown at a desk (and not on microscope stage) for clarity.*

3.4 Discussion

This research presents an optogenetics protocol that progresses the case for using the technique in identifying the role of specific neurons in *Drosophila* behaviour, as made by Pulver, Titlow and colleagues (Pulver *et al.*, 2011; Titlow, Johnson and Pulver, 2015). Demonstrating an established nociceptive, type IV md-neuron-dependent, 'rolling' phenotype (Hwang *et al.*, 2007) in response to light stimulation of md neurons (MD-Gal4 x UAS-csChrimson ATR) was important not only to validate this protocol, but because it represents the first time specific behavioural phenotypes have been associated with neurons in larvae in this way. It is disappointing that attempts to apply this technique to identify behaviours associated with dbd, dmd1 and ch were limited by driver expression, particularly because Bd-Gal4 and Bd/I-Gal4 were used to make conclusions about the role of dbd, dmd1 and type I neurons in behaviour that have been published and accepted.

Hughes and Thomas employed acute knockdown of neurons expressing Bd-Gal4 and Bd/I-Gal4 (called *8-113*-Gal4 and *2-21*-Gal4 there, respectively) to state that "the bipolar dendrite and type I md neurons share the feedback role", where feedback refers to regulation of normal crawling (Hughes and Thomas, 2007). Cheng *et al.*, rescued slow larval crawling speed by driving NompC rescue with Bd/I-Gal4 (and cited Hughes and Thomas, 2007), to support the statement: "results indicate that class bd and type I neurons rely on NompC for their function in locomotion" (Cheng *et al.*, 2010). It is difficult to understand how they can make these conclusions, when supplementary information for both publications describes expression of drivers as including "a few CNS neurons". Even more worryingly, the expression pattern evidence presented in this chapter suggests expression in more than 'a few' neurons. This point is amplified by evidence that *amos*^{1} mutants still display the 'strike' phenotype which could have been attributed to dbd and dmd1 neurons had this research not considered specificity carefully.

Conclusions made from Hughes and Thomas, 2007 and Cheng *et al.*, 2010 based on using Bd-Gal4 or Bd/I-Gal4 should be subject to further scrutiny and perhaps disregarded, until there is proper evidence to support them from approaches that do not rely on these Gal4 drivers. With that in mind, I used larvae that lack dbd and dmd1 neurons (possess the *amos*^{1} mutation). These larvae show significantly increased PWF and PWD versus control larvae. This may provide some of the best evidence available that dbd and dmd1 neurons contribute to normal crawling by regulating peristalsis, and I regard this to be the most interesting result of this chapter. However, there is currently no means to separate the functions of the two neurons. Future research should aim to generate specific drivers to separate the two neurons, to better understand their roles in behaviour. It should also exploit *amos*^{1} larvae (as opposed to those

crossed for use in optogenetic experiments here (e.g. amos^{1}; Bd-Gal4 *x* amos^{1}, UAS-csChrimson ATR)), to make comparison to wild-type more straightforward. It should be noted that *amos*^{1} larvae also lack a subset of olfactory sensilla in the head sense organs (zur Lage *et al.*, 2003), but it seems unlikely that this alone would alter crawling behaviour. Importantly, *amos* is not expressed in any CNS neurons.

Optogenetic experiments also revealed a 'tail lift and reverse' phenotype for NompC-Gal4 x UAS-csChrimson ATR larvae on light stimulation, which coincided with a decrease in CS (trend only) and significant decrease in PWF versus controls. Whilst the expression of the driver is so broad it is impossible to attribute the phenotype to specific neurons (NompC-Gal4 is expressed in dda (ddaD, ddaE), ch (lch1, lch5, vchA and vchB), dbd, dmd1, vbd and vpda neurons (Cheng *et al.*, 2010; Effertz, Wiek and Gopfert, 2011; Tsubouchi, Caldwell and Tracey, 2012)), this result adds weight to the validation of the optogenetics protocol and that NompC could be the MET in dbd and dmd1 neurons. Moreover, the specific and reliable appearance of the phenotype, which seems to reflect contraction of dorsal, posterior musculature belies the fact that the anatomy of neurons is conserved across abdominal segments. Future work should clarify the role of NompC in specific neurons by combining suitable drivers with *NompC* RNAi, provided RNAi is effective (more in Chapter 5 regarding RNAi in behavioural experiments).

Provisional connectomics data from Janelia Research Campus suggested that the dbd neuron is connected to pain centres of CNS (personal communication). Experiments performed on *amos*^{1} mutants showed that dbd and dmd1 neurons are not necessary for the pain response observed in *Oregon-R* larvae in response to an applied pinch. This disagrees with the notion that the dbd neuron is involved in nociception and poses the question as to why the axonal connection exists. It is possible that some limitation of the pinch experiments prevented findings confirming a link between dbd and nociception. First, delivery of pain stimulus by forceps may be an insufficient stimulus (did not deliver the specific stimulus dbd responds to). Based on anatomical similarity to other (arthropod) stretch receptors (Suslak and Jarman, 2015) and other data (Suslak *et al.*, 2015c), it seems likely that the stimulus the dbd neuron responds to is stretch; maybe stimulating larvae with the servo developed for electrophysiology would be more appropriate. Second, the wild-type phenotype in response to pinch is complex (comprised of muscle contractions associated with feedback from several sensory neurons), so losing dbd and dmd1 may be insufficient to cause a notable change. This would agree with evidence that response to mechanical nociception occurs as a result of a DmPiezo and ppk26-dependent mechanism (*DmPiezo* is expressed in class III, IV (da), dbd, vbd, dmd1 and *ppk26* is expressed in class IV neurons in larvae (Kim *et al.*, 2012; Guo *et al.*, 2014)). Future research should use *DmPiezo/ ppk26* mutants and silence type IV neurons to assess the effectiveness of using forceps pinch as a pain stimulus, and to confirm the mechanism required for

mechanical nociception. Similarly, it could employ the use of stretch stimuli delivered by servo, to clarify the role of the dbd neuron in nociception.

Crawling data showed that both *NompC* and *DmPiezo* are necessary for normal crawling (CS), which agrees with other research (Cheng *et al.*, 2010; Suslak *et al.*, 2015c). However, knocking down *DmPiezo* in dbd and dmd1 neurons (Bd-Gal4 x UAS-Piezo RNAi) did not affect CS, which makes NompC the best candidate for the MET. It is important to note that this result could be affected by incomplete knockdown (of DmPiezo in dbd and dmd1 neurons) by RNAi, and this seems possible considering that whilst *DmPiezo* is expressed in a number of PNS neurons, it is difficult to imagine any of them being better suited to report PWF and PWD to the CNS than the dbd is. This work must be developed to include Bd-Gal4 x UAS-*NompC* RNAi and measurement of RNAi knockdown efficiency, to compare *NompC* to *DmPiezo*. Again, the effectiveness of using RNAi in behavioural experiments is discussed in more detail in Chapter 5.

It is tempting to leverage the reliability of whole cell patch clamp electrophysiology recordings taken from dbd neurons of w^{1118} and *DmPiezo* -/- larvae to say that this work confirmed DmPiezo is a MET in dbd neurons. Trace morphology and reduction in *dEm* found here were similar to those reported by Suslak *et al.* (morphology of initial depolarisation and later plateau, % reduction in *dEm* was ~88% here versus ~80% in Suslak *et al.*, 2015). However, the electrophysiology protocol was only able to generate a seal 25-100 times less efficient than is necessary for accurate results (10-40MΩ, 1GΩ is standard). Given that the author was taught the protocol by Thomas Suslak, it seems likely that if it had been measured, the seal for earlier experiments would have been very low too.

Much time and effort were expended during this work to try to establish a proper seal between the suction electrode and the dbd neuron. In addition to the author's efforts, Shipston laboratory post-doc Peter Duncan gave advice and allowed the author to practice sealing HEK cells on a different rig (which was straightforward). Other scientists offered levels of help, ranging from email discussion of the problem (as with Amit Nair, who published the Pulver laboratory paper that documented voltage clamp electrophysiology of dbd neurons in 1st-instar larvae (Nair, Bate and Pulver, 2010)) to trying to seal the neuron themselves. Regardless, the seal was always significantly lower than is acceptable, and degraded when a mechanical (tap or servo) stimulus was applied to the preparation. Sealing the dbd neuron of third instar larvae, especially with intent to maintain that seal under stretch, is a technical problem that needs much more work if electrophysiology is to be used as it was intended here. What was useful was the development of the servo-based mechanism to impart stretch (where the servo is driven by microcontroller reading C^{++} code, which allows fine control of speed and extent of

stimulus). This mechanism could be used in future, if a seal is established with the dbd, or in conjunction with other techniques, like GCaMP imaging.

In conclusion, the findings reported here highlight that our understanding of dbd (and dmd1) neuron function is still far from clear, and indeed is less clear than seems to be assumed by others in the field of neuronal control of larval behaviour. I have shown that lack of specificity of Gal4 driver lines can greatly mislead interpretation if not combined with other experimental approaches. This impinges generally on approaches that rely on selective knockdown or optogenetic activation of specific cells combined with whole animal screening of the consequences. Therefore, although I found some evidence from *amos* mutant larvae, the case for dbd and dmd1 neurons as proprioceptors is far from proven, despite what is assumed in connectomics studies to build models of larval locomotion control.

4 Role of chordotonal neurons in hearing and proprioception

4.1 Introduction

Chordotonal (ch) neurons are mechanosensitive, type I (ciliated) neurons of the *Drosophila* peripheral nervous system. In the adult (fly), they are present in the Johnston's organ (JO) of the antennae where they are responsible for hearing and gravitaxis, and the femur where they contribute to coordination (Akitake *et al.*, 2015). In larvae, ch neurons are necessary for larval hearing (Zhang *et al.*, 2013; zur Lage *et al.*, 2018) and are involved in larval locomotion (Caldwell *et al.*, 2003; Hughes and Thomas, 2007; Cheng *et al.*, 2010; Fushiki, Kohsaka and Nose, 2011).

4.1.1 Chordotonal neurons in hearing and proprioception

About 500 ciliated chordotonal neurons (or Johnston's organ neurons, JONs) form the JO in the pedicel of the *Drosophila* adult antenna. JONs are arranged along the distal-proximal axis as: (1) a terminal thread that conveys displacement of the funiculus to the cilium; (2) motile cilium comprised of microtubules (9 + 0 arrangement) and dynein motors, characterised by distal expression of No mechanoreceptor potential C (NompC, a.k.a. TRPN1) and proximal expression of a nanchung-inactive heteromer (nan-iav, both TRPV channels); (3) dendrite, soma and axon that propagate action potentials to the antennal mechanosensory motor centre (AMMC) of the fly's brain ((Jarman, 2014), also see Figure 4.1).

JONs are grouped into subsets, A-E, based on their axonal targets in the AMMC (Kamikouchi, Shimada and Ito, 2006). Subsets may be specialised for particular functions: A and B consist of 200 JONs that are sensitive to ≥ 50nm vibrations (Effertz, Wiek and Gopfert, 2011) and respond to sound, so are necessary for hearing (Yorozu *et al.*, 2009). C and E consist of ~250 JONs that are sensitive to ≥ 250nm vibrations (Effertz, Wiek and Gopfert, 2011) and respond to maintained antennal deflections for gravity and wind detection (Yorozu *et al.*, 2009). D consists of 50 JONs that respond to vibrations and deflections of the antenna, which may be necessary to detect wind and wing beat sounds (Matsuo *et al.*, 2014). It is important to note, however, that this separation could oversimplify a JO response that occurs across a spectrum of frequency and intensity of stimulation (as tonotopy in humans (LeMasurier and Gillespie, 2005)).

The anatomy and physiology of chordotonal neurons present in the *Drosophila* adult femur (fcho) and larval abdomen are less well known than those of the JO. What is known about the about the fcho is: Its ultrastructure (Shanbhag, Singh and Singh, 1992); that proneural gene *atonal* is necessary for fcho (and all other ch neuron) formation (Jarman *et al.*, 1993; Jarman *et al.*, 1994); NompC is expressed in the distal tip of the fcho's motile cilium (Liang *et al.*, 2011) as in JONs, and that passive flexion of the tibio-femoral joint elicits fcho activity in a 'resistance reflex' that leads to contraction of the tibial extensor (Reddy *et al.*, 1997). So, here the ch neuron performs a role reminiscent of the human muscle spindle, by mitigating potential muscle damage caused by excessive stretch. The fcho is not investigated in the present research, so further discussion is beyond the scope of this text.

Larval ch neurons are present in all eight abdominal segments and can be divided into three subpopulations based on the location of their somata: Lateral chordotonal neurons 1-5 (lch1-5), ventral chordotonal neuron 1 (vch1) and ventral chordotonal neurons A and B (vchAB) (Figure 4.1).

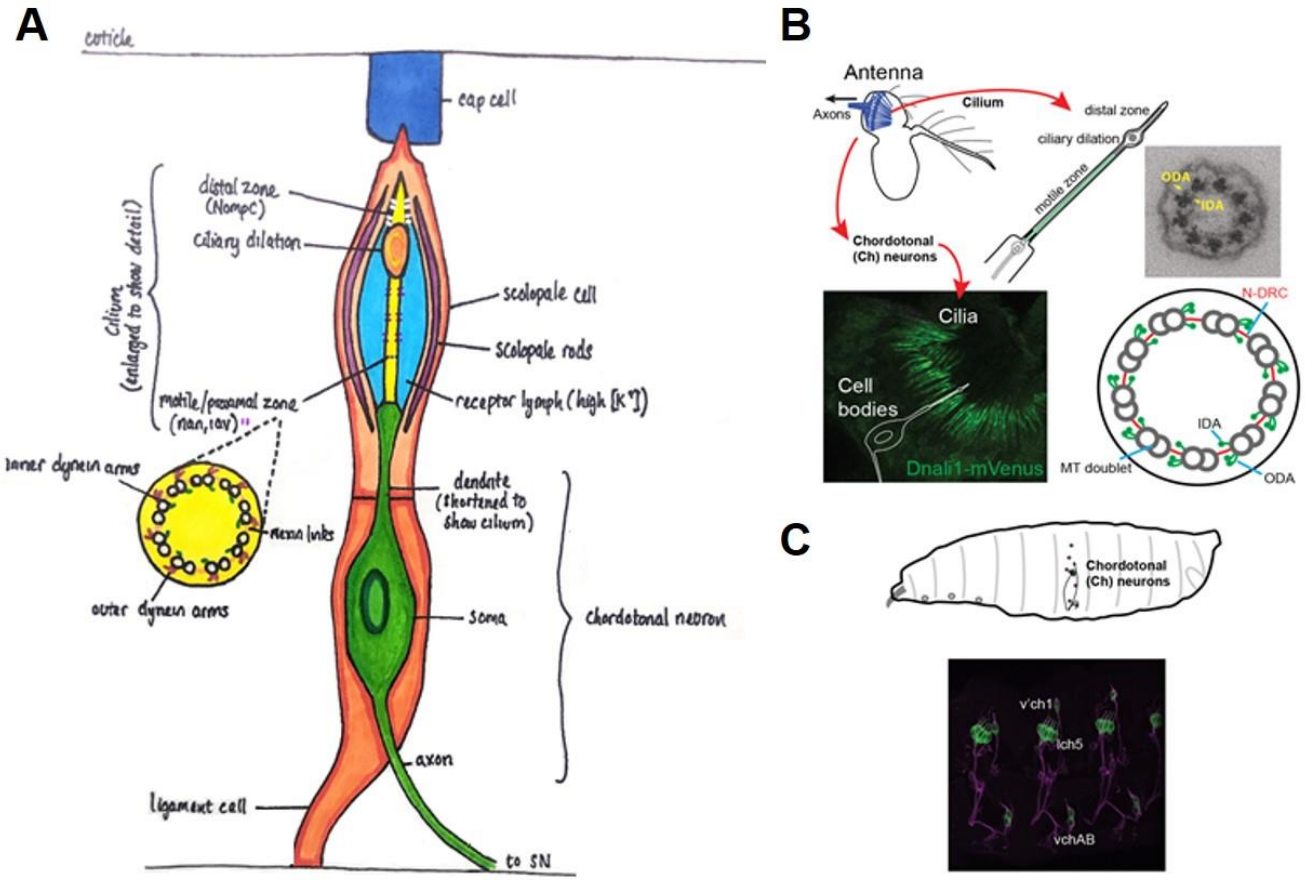

Figure 4.1: Chordotonal neurons in the adult antenna and larval body wall. *A: A generic chordotonal neuron. Note that the dendrite terminates in a mechanosensitive cilium with nine microtubule (MT) doublets, that is characterised by the presence of dynein motors (outer dynein arm, ODA and inner dynein arm, IDA) nexin links (N-DRC). B: JO neurons in the antenna. C: Chordotonal neurons in the body wall of the larva. B and C adapted from zur Lage et al. (2019).*

Most research has treated larval ch neurons as a homogenous population in terms of their physiological function (Caldwell *et al.*, 2003; Hughes and Thomas, 2007; Cheng *et al.*, 2010). GCaMP imaging has shown the impact of mechanical stimulation on larval ch neurons. Zhang *et al.* demonstrated calcium (Ca^{2+}) flux in lch1-5 and vch1 in response to a 500Hz pure tone (Zhang *et al.*, 2013), whilst Fushiki *et al.* documented Ca^{2+} flux in lch1-5 in response to muscle contraction (Fushiki, Kohsaka and Nose, 2011). Thus, unlike the specialised subpopulations in JO, larval chordotonal neurons (at least lch5) appear to respond to both hearing (tonal) and proprioceptive (muscle contraction) stimuli. However, it is not clear if this extends to all larval subpopulations, or even if there are specialisations among the five lch5 neurons. A major motivation of this chapter is to clarify the role of subpopulations of ch neurons in hearing and response to muscle contraction, to investigate if larval ch neurons are tuned (i.e. demonstrate stimulus type sensitivity, plus frequency and temporal sensitivity to a particular stimulus) like those in JONs and human hair cells. Investigating this tuning requires an approach that includes vchAB in analysis, as it has been excluded in previous work.

4.1.1.1 Models of mechanosensation in chordotonal neurons in Drosophila hearing

The mechanism~~(s)~~(s) of mechanosensation present in ch neurons has been researched, but it is still far from clear. Early work posed TRPN channel NompC (TRPN1) as the primary mechano-electrical transducer channel (MET) in *Drosophila*, by demonstrating *nompC*^{1}, *nompC*^{2} and *nompC*^{3} mutants reduced mechanoreceptor responses to microchaete bristle deflection (Walker, Willingham and Zuker, 2000). However, NompC mutation only reduces antennal potential response to 500Hz sine wave stimulation (10 x 2.5 cycles of 500Hz stimulus) by ~40% (Eberl, Hardy and Kernan, 2000). Thus, other proteins must contribute to chordotonal neuron response to sound and NompC may not be the MET. Later, Kim *et al.* established that TRPV family protein nanchung (nan) was expressed in the sensory cilia of chordotonal neurons, mediated hypo-osmotically activated calcium influx in Chinese hamster ovary (CHO-K1) cells and that *nan* mutation abolished antennal potential response to the 500Hz sine wave stimulation protocol (10 x 2.5 cycles of 500Hz stimulus) described by Eberl *et al.* (Kim *et al.*, 2003). This posed nan as a stronger candidate for the MET than NompC and suggested some interaction between the two. Next, the same group found that another TRPV protein, inactive *(*iav), was like nan. iav was expressed in the (proximal) sensory cilium of chordotonal neurons and required nan for normal localisation, mediated hypo-osmotically activated calcium influx in CHO-K1 cells and *iav* mutation (*iav*[3621] hemizygous males) abolished antennal potential response to 500Hz sine wave stimulation (Gong *et al.*, 2004). Consequently, it was proposed that nan and iav formed a heteromultimeric MET (nan-iav) that interacted with NompC.

Several publications have supported a nan-iav MET: *nan*^{36} or *iav*^{1} mutation abolished sound-induced action potential firing (recorded from suction electrodes at distal end of nerve bundle) and Ca^{2+} flux in lch1-5, whilst *NompC* mutation (*NompC*[1]/[3] trans-heterozygote) severely reduced but did not abolish the same indicators of activity (Zhang *et al.*, 2013). *nan*^{36a} and *iav*^{1} mutants were resistant to 200µM pymetrozine (pym, a nan-iav agonist insecticide), which abolishes compound action potentials (CAPs) elicited by the chordotonal neurons of wild-type flies (Nesterov *et al.*, 2015). *nan*^{36a} and *iav*^{1} also abolish spike-mediated sound response and sound-evoked generator currents of adult *Drosophila* chordotonal neurons (response to 100Hz tone measured in the giant fibre neuron (GFN), which is coupled to the JO by gap junctions (Strausfeld and Bassemir, 1983)), whilst *NompC* mutation (*NompC*[1]/[3]) does not. It does, however, reduce normal spike-mediated sound response and sound-induced antennal rotations versus wild-type controls, consistent with a reduction in active amplification (Lehnert *et al.*, 2013). Thus, a 'nan-iav model' of mechanosensation (reviewed in (Albert and Gopfert, 2015)) has been developed to describe nan-iav as the MET and NompC as a component of active amplification for phase locking to high frequency sound (Nadrowski, Albert and Gopfert, 2008).

Further research has challenged the 'nan-iav model' and supported earlier proposals for a 'NompC model' (reviewed in (Albert and Gopfert, 2015)) wherein NompC is the MET. *NompC* mutant, *NompC*[3]/[3], abolished normal antennal nonlinear amplification (~10-fold gain) of low intensity sound, whilst *nan*^{36a} and *iav*^{1} mutants increased the receiver's nonlinear response (~85-fold gain). This increase was mostly rescued by expression of a single wild-type transgene of *iav* (P{*iav*$^{+}$]2.2) in the *iav*^{1} mutant (Gopfert *et al.*, 2006). Moreover, spontaneous oscillations observed in *nan*^{36a} and *iav*^{1} mutants were absent in *NompC*[3]/[3]/ *nan*^{36a} double mutants; it was decided NompC was responsible for amplification and nan-iav were NompC-dependent regulators of amplification gain. Later, a similar group ablated *Drosophila* sound receptors with UAS-ricin toxin A and recorded antennal potential in response to sound, to show that the 'remnant potentials' (~40% antennal potential response to 500Hz sine wave stimulation) reported form *NompC* mutants by Eberl *et al.*, 2000, were due to output from gravity/ wind-receptor cells of the JO and not some other MET for hearing (Effertz, Wiek and Gopfert, 2011). Finally, force-induced antennal displacement militated against a model of mechanotransduction in chordotonal neurons (model from (Albert, Nadrowski and Gopfert, 2007)), implied that *NompC* mutations (*NompC*[2]/[2] and *NompC*[3]/[3]) reduced the initial (peak) CAP response to antennal displacement, which reflects transducer gating (Effertz *et al.*, 2012). Similarly, asymptotic stiffness of the antenna (K_∞, when all transducer channels are open or closed) was defined as equal to linear elasticity of the antennal joint and the neurons that suspend the receiver (K_{lin}), plus the combined stiffness of gating springs (K_{GS}): $K_\infty = K_{lin} + K_{GS}$. This description led the authors to suggest that NompC contributes directly to gating spring stiffness, as *NompC* mutation lowered K_{GS} versus controls (Effertz *et al.*, 2012). Finally,

even supporters of the nan-iav model admit that it is difficult to explain why NompC localises to the distal and nan-iav to the proximal zones of mechanosensory cilia (Lehnert *et al.*, 2013); it seems logical that this would be opposite if the 'nan-iav model' were true, unless NompC is a pre-amplifier for the MET (Albert and Gopfert, 2015). However, it is important that proponents of the nan-iav model feel that most findings supporting a NompC model, also support the former (Lehnert *et al.*, 2013). Similarities between the 'nan-iav model' and 'NompC model' of mechanosensation in *Drosophila* hearing show that nan-iav and NompC are essential to the process. The differences, however, highlight that the identity of the MET and relationship between proteins of the mechanism~~(s)~~(s) is unclear. Indeed, some literature has suggested that DmPiezo, the *Drosophila* homologue of mammalian mechanosensitive channel Piezo (1 and 2), is present in JONs and could play a role in *Drosophila* hearing (Kim *et al.*, 2012). As addressed in Chapter 4, Suslak *et al.* used 30µM ruthenium red (RR) and RNAi experiments to support that DmPiezo is the MET in dbd neurons (stretch receptor assumed to share similar mechanism to ch neurons (Suslak *et al.*, 2015c)). Therefore, a similar role in ch neurons is possible. This, however, is not straightforward: *DmPiezo*^{KO} mutant larvae exhibited a normal 'startle' response to sound, whilst *NompC*, *iav*^{1} and *nan* mutants did not respond (Zhang *et al.*, 2013). Research should clarify the role of DmPiezo using GCaMP imaging in ch neurons, to overcome the limitations of behavioural experiments.

Finally, (as alluded to above) active mechanical amplification is a critical part of mechanotransduction in *Drosophila* hearing. The initial mechanical stimulus provided by sound is amplified not by a chemical second messenger cascade (as in other senses) but by actively driven movement of the antenna in positive feedback. Initial research demonstrated that this active amplification depends on NompA, NompC, Beethoven (btv), touch-insensitive larva B (tilB) and is driven by microtubule-dependent motors (Gopfert and Robert, 2003). It was then proposed that these motors are the axonemal dyneins that are present in the proximal zone of the cilium alongside nan/iav proteins (Senthilan *et al.*, 2012; Newton *et al.*, 2012), and this is consistent with findings in other insects (Warren, Lukashkin and Russell, 2010). Direct evidence for the critical role for dynein motors came from Göpfert's group (Karak *et al.*, 2015). This is supported by further evidence that dynein assembly factors as necessary for normal ch neuron function: *tilB* was found to be a homolog of (human) dynein assembly factor *LRRC6*, which when mutated causes primary ciliary dyskinesia (PCD) (Kott *et al.*, 2012); *CG11253* mutation leads to dynein arm loss and deafness, and its human homologue *ZMYND10* causes ciliary dysmotility and PCD (Moore *et al.*, 2013); *R2TP*-associated factor *CG14353*/*Wdr92* is involved in dynein preassembly and is necessary for ch neuron function (zur Lage *et al.*, 2018); *CG17669* is required for ch neuron function and is a homologue of human dynein assembly factor *DNAAF3* (unpublished, Petra zur Lage); *DNAAF3* mutation leads to PCD in humans (Mitchison *et al.*, 2012). PCD is a chronic disease related to ciliary dysfunction. This will be explored in more depth in the following chapter when I address the

use of *Drosophila* as a model for the disease. For now, suffice to say that research should continue to clarify the role of dyneins in hearing, to further not only our understanding of auditory mechanosensation but also to help understand and treat this human disease.

4.1.1.2 Mechanosensation in chordotonal neurons during larval crawling

Larval locomotion is the result of peristaltic muscle contractions proceeding from posterior segments anteriorly. Whilst there is debate surrounding whether peristalsis is active or passive (Ross, Lagogiannis and Webb, 2015), it is likely that larval locomotion is the product of a central pattern generator (CPG) which drives a process that includes premotor interneuron A27h and inhibitory GABAergic dorsolateral (GD, or A27j2) neurons (Fushiki *et al.*, 2016). Peripheral nervous system (PNS) neurons provide feedback to modulate this process in coordinating contraction and fine-tuning movement (Suster and Bate, 2002). In particular, chordotonal neurons contribute to larval locomotion as stretch receptors (Caldwell *et al.*, 2003; Hughes and Thomas, 2007; Cheng *et al.*, 2010; Fushiki, Kohsaka and Nose, 2011).

Some research supports a major role for chordotonal neurons in larval locomotion. Dynamic Image Analysis (DIAS) of larvae crawling on 1% agar revealed that mutants of genes expressed in chordotonal neurons suffered from locomotor defects (Caldwell *et al.*, 2003). Specifically, *atonal* (*ato*, necessary for ch neuron specification (Jarman *et al.*, 1993)), *btv* (necessary for ch neuron ciliary ultrastructure (Eberl, Duyk and Perrimon, 1997)), *tilB*, *smetana* (*smet*, necessary for normal axonemes (Caldwell and Eberl, 2002)) and *5D10* (necessary for courtship behaviour (Eberl, Duyk and Perrimon, 1997)) mutants all exhibited defects in gross path morphology, rate and extent of peristaltic contraction. Interestingly, Fushiki *et al.* found that Shibire-mediated inhibition of chordotonal neurons (iav-Gal4 x UAS-Shibire^{ts} at 32°^{C}) 16-20h after egg laying (AEL) increased propagation duration in larvae at later stages of development (i.e. second and/ or third-instar larvae demonstrated slower peristalsis than controls). This effect was not observed following inhibition of multidendritic (md) neurons, implying a unique role for chordotonal neurons in <u>*development*</u> of locomotion. Acute knockdown of ch neuron function (iav-Gal4 x UAS-Shibire^{ts} at 32°^{C}) in third-instar larvae also increased propagation duration. Ch neuron response to muscle contraction was recorded by imaging Ca^{2+} flux (GCaMP3) in the ventral nerve cord. The response propagated along neuromeres, concomitant with muscle contractions, in support of a role for acute ch neuron activity in larval crawling (Fushiki, Kohsaka and Nose, 2011).

In contrast to the work by Caldwell *et al.*, 2003 and Fushiki *et al.*, 2011, some research has suggested that chordotonal neurons play a minor role in larval locomotion. Loss of crawling speed and increased stride duration observed in *NompC* mutants (*NompC*[1]/[3]) was rescued

by driving *NompC*-L cDNA expression in sensory neurons (SN-Gal4, a.k.a 5-40-Gal4), md neurons (MD-Gal4, a.k.a. 109(2)80-Gal4) and bd/ dmd1 neurons (bd/I-Gal4, a.k.a. 2-21-Gal4). Thus, NompC expression in bd/dmd1 and not the chordotonal neurons was sufficient for normal larval crawling (Cheng *et al.*, 2010). Cheng *et al.* also employed calcium imaging of *NompC*[1]/[3], MD-Gal4/ UAS-GCaMP3 (MD-Gal4 driving GCaMP in NompC mutant 'background') to reveal that NompC is necessary for the activation of md neurons during peristaltic muscle contractions. Hughes and Thomas conducted similar experiments by imaging muscle contraction (indicated by GFP protein trap of myosin heavy chain, Mhc-GFP^{C110}) during larval crawling. Shibire-mediated knockdown of all sensory neurons (5-40-Gal4 x UAS-Shibire^{ts} at 32°^{C}) or md neurons (MD-Gal4 x UAS-Shibire^{ts} at 32°^{C}) produced a 'toothpasting' phenotype, which was attributed to bd and class I md neurons (NP2225-Gal4 x UAS-Shibire^{ts} at 32°^{C}). 'Toothpasting' was defined by slow peristaltic wave propagation and excessively tight muscle contractions; crucially, toothpasting was absent in acute knockdown of ch neurons (9-20-Gal4 or 8-73-Gal4 x UAS-Shibire^{ts} at 32°^{C}) (Hughes and Thomas, 2007). In summary, the evidence for whether ch neurons play a major or minor role in larval locomotion is contradictory and unclear. They may contribute to development of normal locomotion (Fushiki, Kohsaka and Nose, 2011; Hughes and Thomas, 2007), but their supposed modulation of peristaltic waves in larvae (Eberl, Hardy and Kernan, 2000; Fushiki, Kohsaka and Nose, 2011) is controversial (Hughes and Thomas, 2007; Cheng *et al.*, 2010). Research should continue to try to clarify the role~~(s)~~(s) of chronic and acute activity in chordotonal neurons in larval proprioception.

Finally, given that ch neurons are necessary for hearing and (perhaps) normal crawling, it is important to note that studies have yet to explore directly whether active amplification and dyneins are required for proprioception during muscle contraction. Investigating this would improve understanding of the mechanisms of mechanosensation in *Drosophila*. Specifically, it would confirm the assumption that a single transduction mechanism underlies hearing and proprioception, despite the obvious potential for large differences in frequency and intensity of stimulation of neurons, between hearing and proprioceptive stimuli.

4.2 Aims

1. To characterise larval chordotonal neuron response to sound stimulation

    a. Test the hypothesis that ch neuron peak response is to ~1000Hz stimulation. I will use GCaMP experiments to test the hypothesis, and if it is true, it suggests that (following the protocol described in the present research) neurons are tuned to a higher frequency than is described in other research.

    b. Test the hypothesis that different subpopulations of ch neurons are tuned to different frequencies/ intensities of stimulation. I will use GCaMP imaging to test the hypothesis and if it is true, it evidences tuning (in larval neurons) that has only been observed in adult flies and human hair cells. This would strengthen the case for using *Drosophila* larvae ch neurons to model human hearing.

    c. Test the hypothesis that the nan-iav model represents the MET (nan-iav) responsible for *Drosophila* hearing, using hearing assays. If correct, the hypothesis ends a length debate on the mechanism of mechanosensation in ch neurons, so improves our understanding of a system often used to model our own.

2. To clarify the acute activity of ch neurons in *Drosophila* larval proprioception

    a. Test the hypothesis that acute feedback from ch neurons has a negligible impact on crawling behaviour. I will use optogenetic experiments to test this hypothesis, and if it is true, it suggests a unique role for ch neurons in establishing normal crawling in development. This represents progress in characterising the larval PNS, so informs use of ch neurons in modelling proprioception. Rather, it would pose using different neurons (e.g. dbd) as a better model.

3. To determine whether dyneins contribute to hearing and proprioception in larval ch neurons

    a. Test the hypothesis that dyneins and particularly *CG17669 -/-*, are necessary for larval hearing. I will use hearing and GCaMP experiments to test the hypothesis and if it is correct, it describes a novel insight into the mechanism of mechanosensation affected in PCD.

    b. Test the hypothesis that dyneins and particularly *CG17669 -/-*, are necessary for larval proprioception. I will use crawling and GCaMP experiments to test the hypothesis and if it is correct, it shows that active amplification is necessary for the perception of mechanical stimuli, regardless of their intensity.

4.3 Results

4.3.1 Characterising the response of larval chordotonal neurons to hearing and proprioceptive stimuli

4.3.1.1 Larval chordotonal neurons respond to 1024Hz more than 512Hz and 256Hz tonal stimulation

I recorded aggregate Ca^{2+} influx in the axon termini of all the ch neurons in the ventral nerve cord (VNC) in response to vibration stimuli provided using tuning forks applied to the stage of the microscope, using UAS-GCaMP6f. Tuning forks with frequencies of 1024Hz, 512Hz and 256Hz stimuli were used to determine optimal frequency of stimulation, as a compromise between optimal frequencies of stimulation given in earlier work and availability of tuning forks.

First, ch neuron response to 1024Hz was measured as mean (GCaMP) fluorescence in specified regions of interest (ROI, ch neuron axon terminals) of the VNC of semi-intact iav-Gal4 x UAS-GCaMP6f larvae (Figure 4.2A). These were plotted as ΔF/ F0 (%), where ΔF was change in fluorescence and F_0 was either: (1) mean F of (0s - onset of 1st peak) + (end of 1st peak to onset of 2nd peak) + (end of 2nd peak to onset of 3rd peak) for representative peaks (Figure 4.2B) or mean F of 0.5s preceding onset of each peak for peaks used in formulation of mean peak (Figure 4.2C). Responses were characterised by short duration, high % change peaks (Figure 4.2B and C. Mean Peak ΔF/ F0: 11.47 ± 2.93%; *n* = 39 peaks, 14 larvae) indicative of an intense reaction to 1024Hz stimulation.

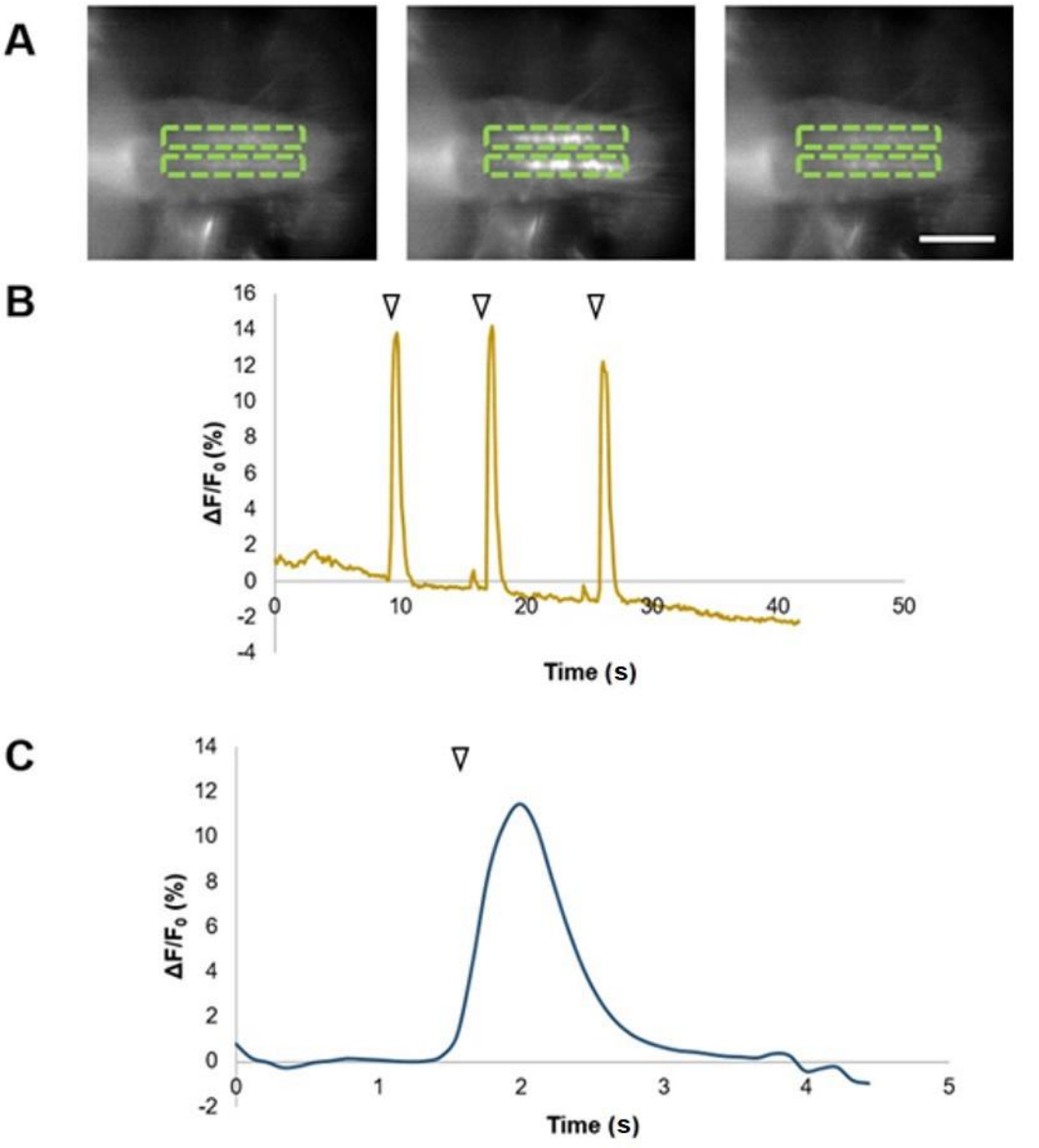
A
B
C
ΔF/F0 (%)
Time (s)
ΔF/F0 (%)
Time (s)

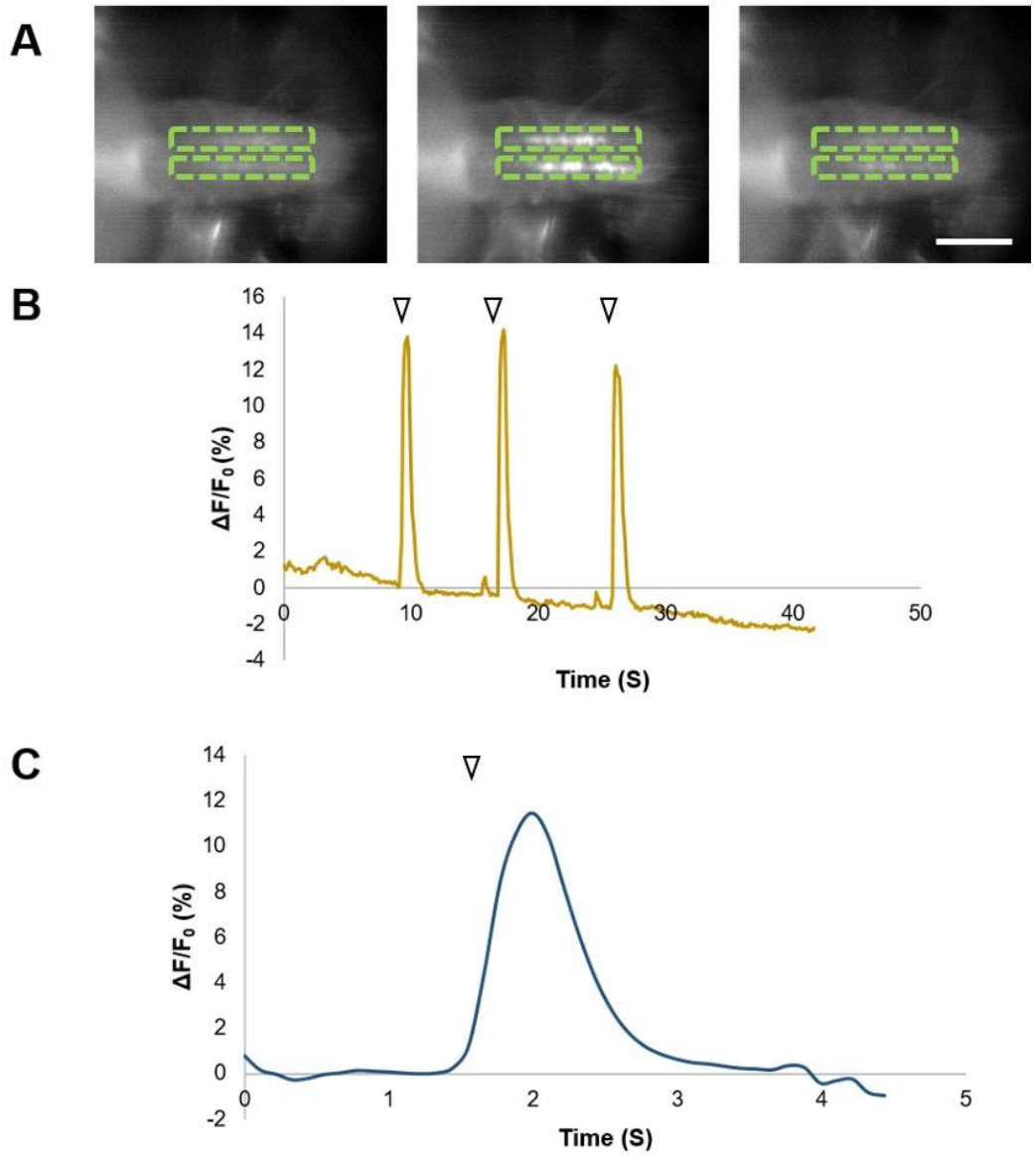

Figure 4.2: Chordotonal neuron response to 1024Hz stimulation, recorded at the ventral nerve cord. *Response as Peak ΔF/ F0 (%) of mean fluorescence of 2 ventral nerve cord (VNC) tracts in semi-intact larval preparations with chordotonal neuron-specific Gal4 driving GCaMP expression (iav-Gal4 x UAS-GCaMP6f), stimulated by 1024Hz tuning fork (52.4 ± 2.8dB). A: Representative images of VNC before, during and after stimulation (left-right, respectively). Dashed lines indicate region of interest defined to produce traces (B, C). B: representative trace (n = 3, 1 larva) where F_0 for ΔF/ F0 (%) is defined as mean F of: (0s - onset of 1st peak) + (end of 1st peak to onset of 2nd peak) + (end of 2nd peak to onset of 3rd peak). C: Mean response to 1024Hz stimulation (11.47 ± 2.93%; n = 39, 14 larvae) generated by aligning all peaks in recordings (from 0.5s before onset of peak to end of peak + 0.5s) where F_0 for ΔF/ F0 (%) is defined as mean F of 0.5s before onset of peak. Arrows in B and C indicate onset of stimulus. Scale bar is 100µm (shown in one panel for clarity, as all panels are the same size).*

Response to 512Hz (Figure 4.3) and 256Hz (Figure 4.4) stimulation was then recorded and quantified as for 1024Hz. 512Hz elicited short duration, small % change peaks (Figure 4.3B and C. 5.9 ± 3.54%; *n* = 15, 6 larvae) whilst 256Hz elicited short duration, moderate % change peaks (9.01 ± 4.07%; *n* = 15, 6 larvae).

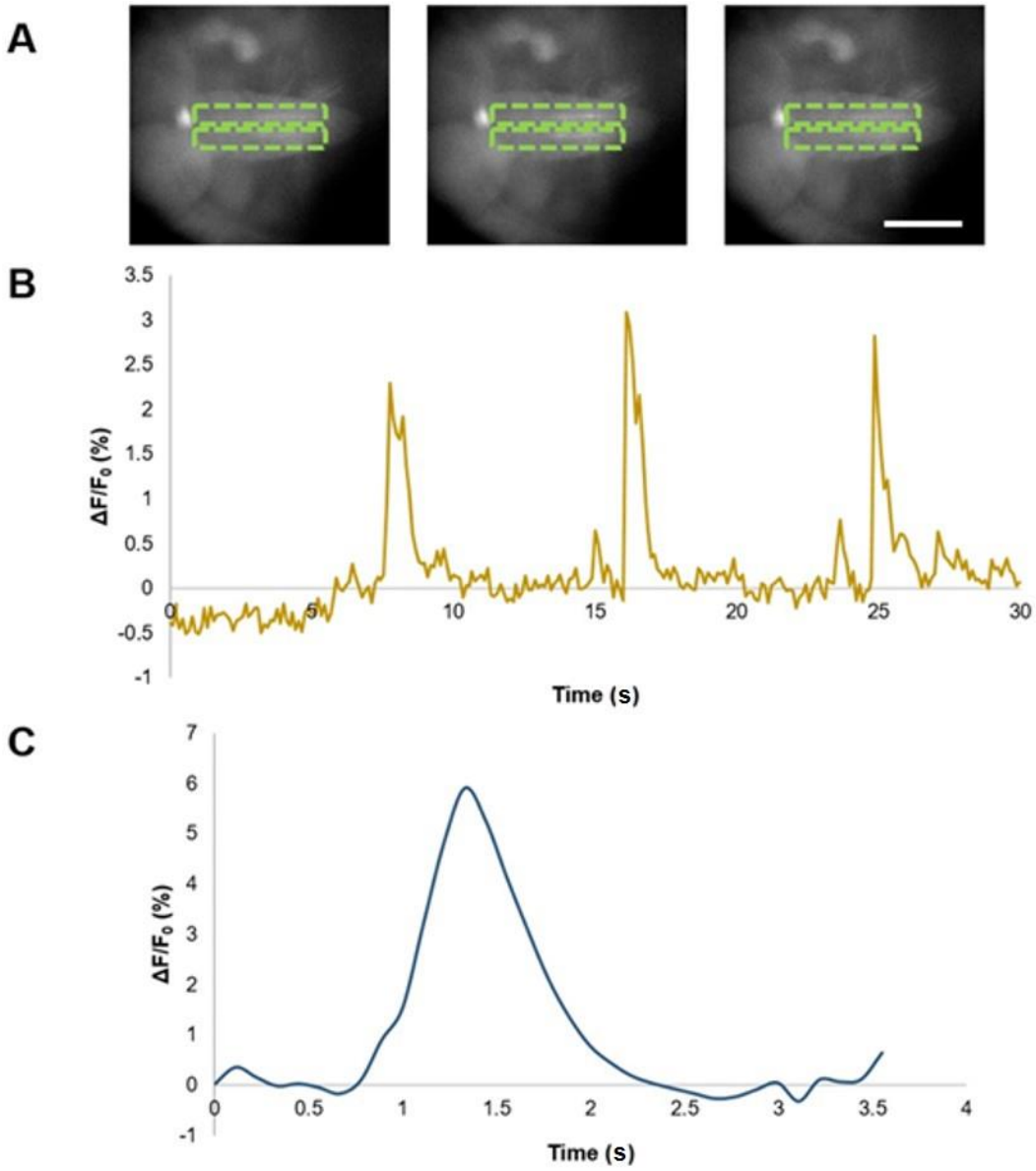

Figure 4.3: Chordotonal neuron response to 512Hz, recorded at the ventral nerve cord. *Response as Peak ΔF/ F0 (%) of mean fluorescence of 2 ventral nerve cord tracts in semi-intact larval preparations with chordotonal neuron-specific Gal4 driving GCaMP expression (iav-Gal4 x UAS-GCaMP6f), stimulated by 512Hz tuning fork (44.3 ± 2.16dB, n = 10 tones). A: Representative images of VNC before, during and after stimulation (left-right, respectively). Dashed lines indicate region of interest defined to produce traces. B: Representative trace (n = 3, 1 larva) where F_0 for ΔF/ F0 (%) is defined as mean F of: (0s - onset of 1st peak) + (end of 1st peak to onset of 2nd peak) + (end of 2nd peak to onset of 3rd peak). C: Mean response to 512Hz (5.9 ± 3.54%; n = 15, 6 larvae) generated by aligning all peaks in recordings (from 0.5s before onset of peak to end of peak + 0.5s) where F_0 for ΔF/ F0 (%) is defined as mean F of 0.5s before onset of peak. Arrows in B and C indicate onset of stimulus. Scale bar is 100µm (shown in one panel for clarity, as all panels are the same size).*

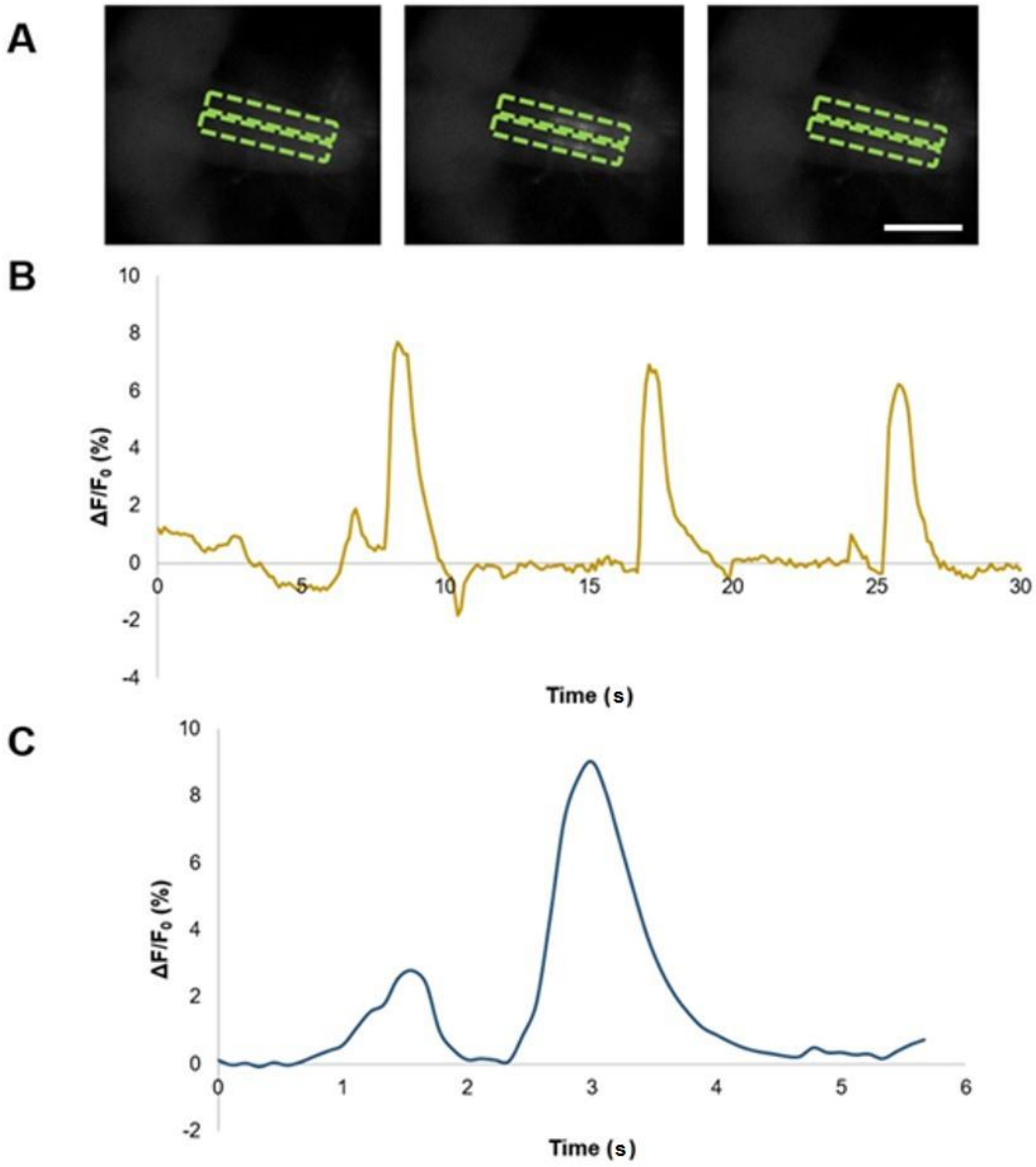

Figure 4.4: Chordotonal neuron response to 256Hz stimulation, recorded at the ventral nerve cord. *Response as Peak ΔF/ F0 (%) of mean fluorescence of 2 ventral nerve cord tracts in semi-intact larval preparations with chordotonal neuron-specific Gal4 driving GCaMP expression (iav-Gal4 x UAS-GCaMP6f), stimulated by 256Hz tuning fork (53.1 ± 3.21dB, n = 10 tones). A: Representative images of VNC before, during and after stimulation (left-right, respectively). Dashed lines indicate region of interest defined to produce traces. B: Representative trace (n = 3, 1 larva) where F_0 for ΔF/ F0 (%) is defined as mean F of: (0s - onset of 1st peak) + (end of 1st peak to onset of 2nd peak) + (end of 2nd peak to onset of 3rd peak). C: Mean response to 256Hz (9.01 ± 4.07%; n = 15, 6 larvae) generated by aligning all peaks in recordings (from 0.5s before onset of peak to end of peak + 0.5s) where F_0 for ΔF/ F0 (%) is defined as mean F of 0.5s before onset of peak. Arrows in B and C indicate onset of stimulus. Scale bar is 100µm (shown in one panel for clarity, as all panels are the same size).*

Comparison of responses (Figure 4.5) revealed a significantly larger response to 1024Hz than 512Hz ($P < 0.0001$) or 256hz ($P < 0.05$), and to 256Hz than 512Hz ($P < 0.05$). The latter was surprising, so the tuning forks were tested for sound intensity: The 256Hz fork was loudest (53.1 ± 3.21dB, $n = 10$ tones), but not significantly louder than 1024Hz (52.4 ± 2.8dB, $n = 10$ tones). Both 256Hz and 1024Hz were significantly louder than 512Hz (44.3 ± 2.16dB, $n = 10$ tones, both $P \leq 0.0001$ by one-way ANOVA with Tukey's multiple comparisons test). Thus, the result that response was higher for 256Hz than 512Hz may be due to volume. However, it seems clear that 1024Hz stimulation elicits the greatest ch neuron response, regardless of differences in tuning fork volume.

Finding that 1024Hz elicits the strongest response in Ch axon termini result supports previous results obtained from larval behavioural responses to sound in the Jarman lab (Jennifer Lennon and Jilly Hope). This contrasts with Zhang *et al.*, 2013, who reported peak larval behaviour response to a 500Hz pure tone (Zhang *et al.*, 2013)). Research should clarify the optimal frequency of stimulation for (the whole population) of ch neurons.

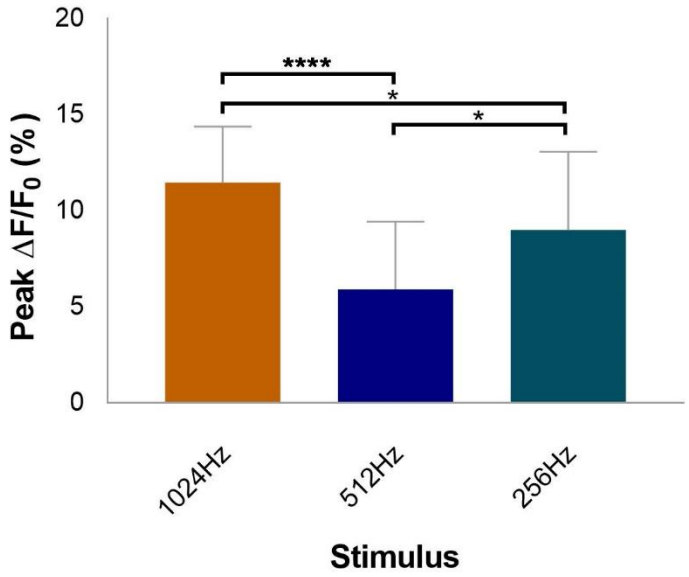

Figure 4.5: Chordotonal neurons are more responsive to 1024Hz stimulation than 512Hz and 256Hz. *Response as Peak ΔF/ F0 (%) of mean fluorescence of 2 ventral nerve cord tracts in semi-intact larval preparations with chordotonal neuron-specific Gal4 driving GCaMP expression (iav-Gal4 x UAS-GCaMP6f). Response to 1024Hz (11.47 ± 2.93%; n = 39, 14 larvae) was significantly greater than to 512Hz (5.9 ± 3.54%; n = 15, 6 larvae, P ≤ 0.0001) and 256Hz (9.01 ± 4.07%; n = 15, 6 larvae, P = 0.046), and response to 256Hz was significantly greater than to 512Hz (P = 0.034), which could reflect volume (dB). Shown as bars of mean ± S.D. Statistical significance determined by one-way ANOVA with Tukey's multiple comparison's test (threshold for significance: P = 0.05; * = P < 0.05, **** = P < 0.0001).*

4.3.1.2 Larval chordotonal neurons are more responsive to a tonal (1024Hz) stimulus than to muscle contraction

With optimal frequency of tonal stimulation determined, I compared the sensitivity of ch neurons to tonal and proprioceptive stimuli. I used the endogenous muscle contractions inherent in a larval preparation following fillet dissection, as the proprioceptive stimulation necessary to elicit a response from the ch neurons (therefore, no external stimulus was applied to preparation).

Response to muscle contraction was measured in the same way as for the 1024Hz experiment. Responses were characterised by long duration, moderate % change peaks (Figure 4.6B and C. 7.56 ± 4.38%; n = 38, 13 larvae) indicative of a definite but less intense response to muscle contraction than to 1024Hz. Indeed, comparison of Mean Peak Response to 1024Hz and muscle contraction revealed a significant difference between responses (Figure 4.7, $P < 0.0001$). This result is significant in that it represents the first demonstration that chordotonal neuron tuning is optimised for hearing and supports the idea that the neurons may be less important than other neurons for crawling (Hughes and Thomas, 2007).

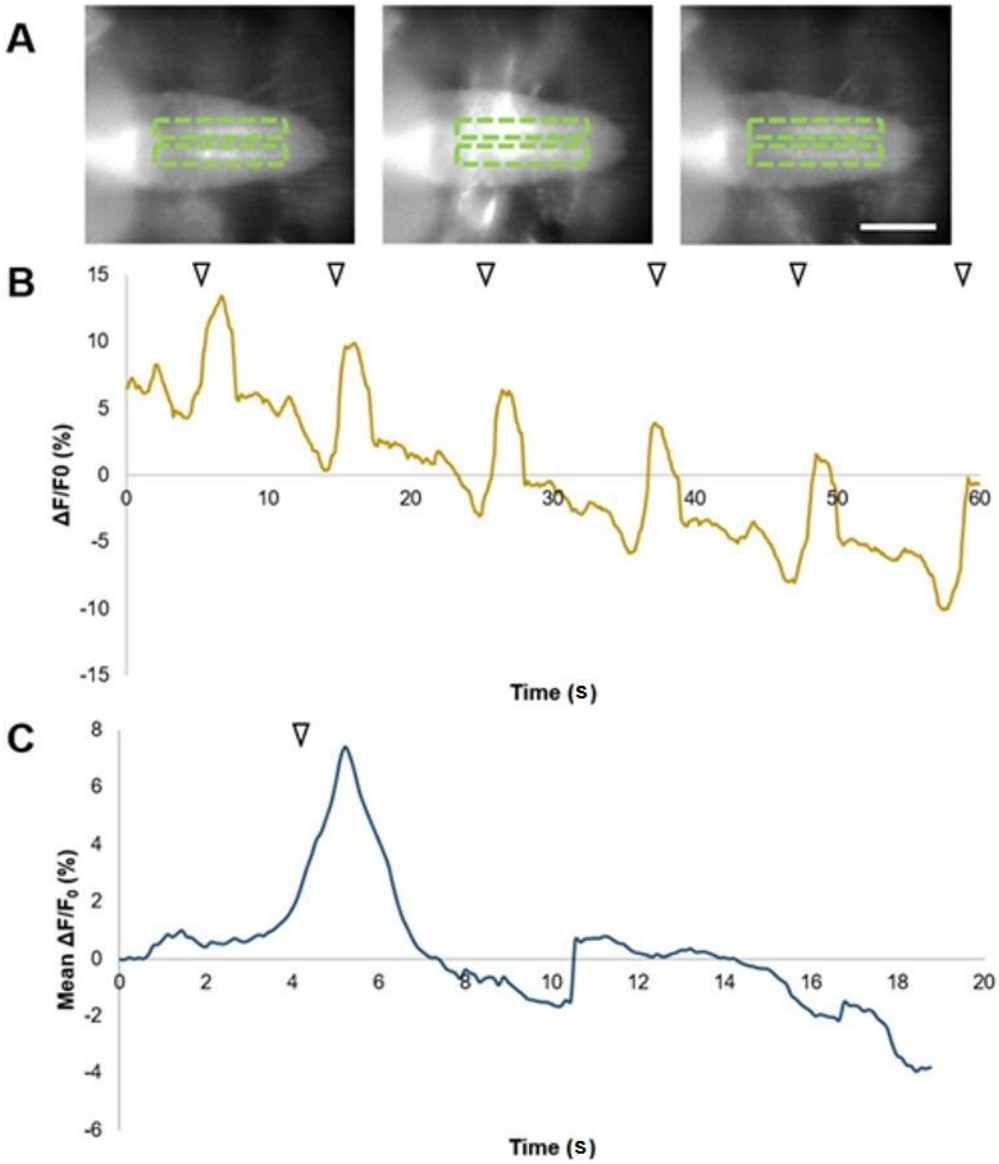

Figure 4.6: Chordotonal neuron response to muscle contraction, recorded at the ventral nerve cord. *Response as Peak ΔF/ F0 (%) of mean fluorescence of 2 ventral nerve cord (VNC) tracts in semi-intact larval preparations with chordotonal neuron-specific Gal4 driving GCaMP expression (iav-Gal4 x UAS-GCaMP6f), stimulated by spontaneous muscle contraction~~(s)~~(s). A: Representative images of VNC before, during and after stimulation (left-right, respectively). Dashed lines indicate region of interest defined to produce traces (B, C). B: Representative trace (n = 3, 1 larva) where F_0 for ΔF/ F0 (%) is defined as mean F of: (0s - onset of 1st peak) + (end of 1st peak to onset of 2nd peak) + (end of 2nd peak to onset of 3rd peak). C: Mean response to muscle contraction (7.56 ± 4.38%; n = 38, 13 larvae) generated by aligning all peaks in recordings (from 0.5s before onset of peak to end of peak + 0.5s) where F_0 for ΔF/ F0 (%) is defined as mean F of 0.5s before onset of peak. Arrows in B and C indicate onset of stimulus. Scale bar is 100µm (shown in one panel for clarity, as all panels are the same size).*

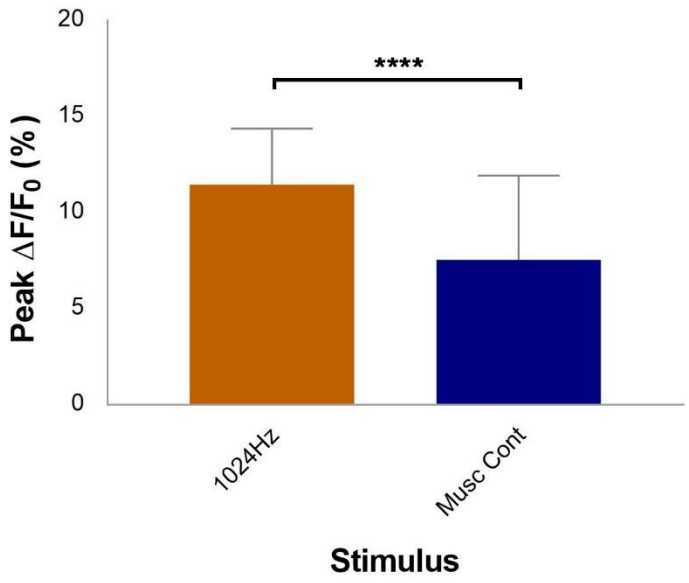

Figure 4.7: Chordotonal neurons are more responsive to 1024Hz stimulation than muscle contraction. *Response as Peak ΔF/ F0 (%) of mean fluorescence of 2 ventral nerve cord tracts in semi-intact larval preparations with chordotonal neuron-specific Gal4 driving GCaMP expression (iav-Gal4 x UAS-GCaMP6f), stimulated by 1024Hz tuning fork or spontaneous muscle contraction~~(s)~~(s). Response to 1024Hz (11.47 ± 2.93%; n = 39, 14 larvae) was significantly greater than to muscle contraction (7.56 ± 4.38%; n = 38, 13 larvae. P ≤ 0.0001), shown by bars of mean ± S.D. Statistical significance determined by unpaired t test (threshold for significance: P = 0.05; **** = P < 0.0001).*

4.3.1.3 Response of individual subpopulations of larval chordotonal neurons to a tonal stimulus

Imaging calcium changes in the VNC does not allow the investigation of individual ch neuron response to stimulation. In order to investigate whether all subpopulations of ch neurons (lch1-5, vch1, vchAB) respond to sound, the GCaMP protocol was adapted to facilitate imaging ch neuron soma. Specifically, an SN-Gal4 (sensory neuron-Gal4 from (Cheng *et al.*, 2010)) driver was crossed to UAS-GCaMP6f, and neurons were imaged in the abdominal hemisegment~~(s)~~(s).

First, lch1-5 response to 1024Hz was recorded and quantified as described for the VNC experiments. Responses in the cell bodies and dendrites were readily detectable (Figure 4.8). Responses were characterised by short duration, high % change peaks (Figure 4.8; Mean Peak ΔF/ F0: 9.54 ± 2.66%; *n* = 12, 4 larvae), like the response to 1024Hz recorded in the VNC. It was, therefore, possible to confirm that lch1-5 responds to sound as documented in (Zhang *et al.*, 2013).

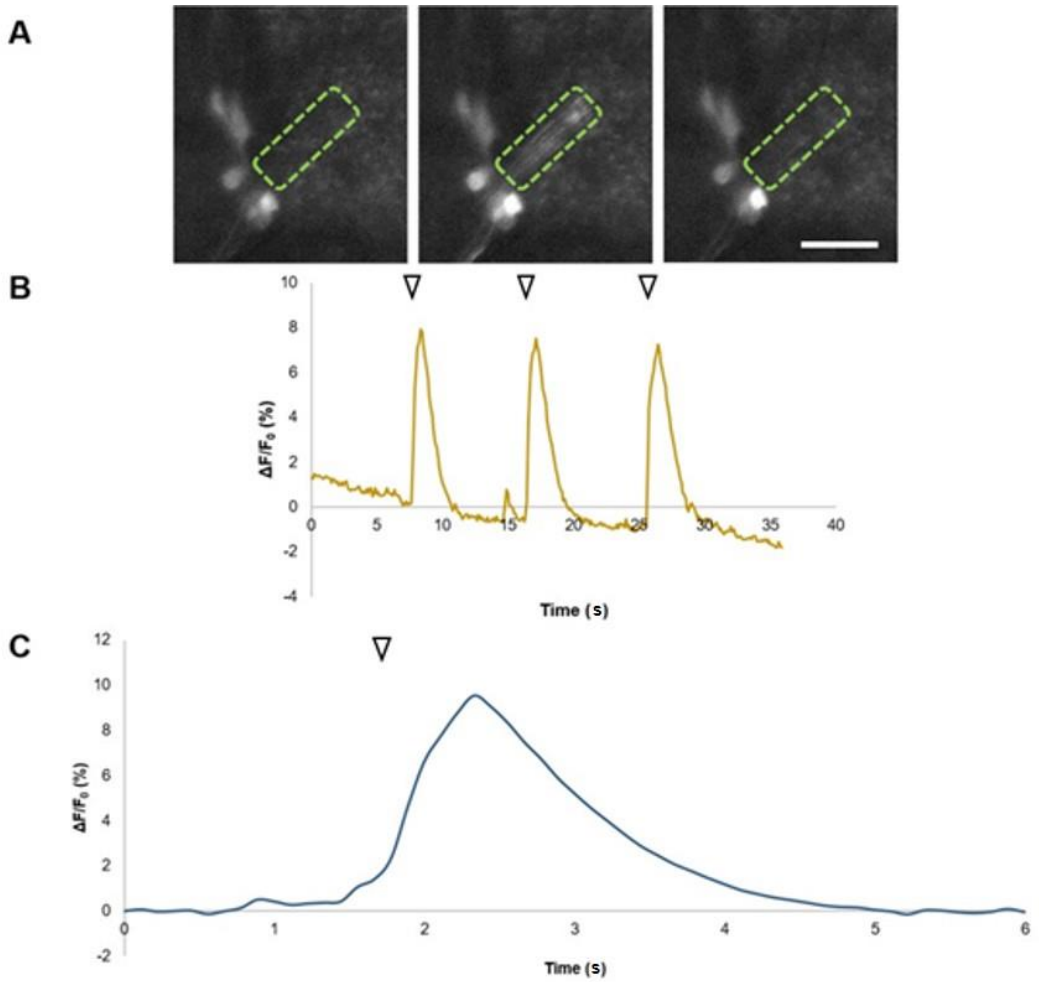

Figure 4.8: Lch1-5 response to 1024Hz stimulation. *Response as Peak ΔF/ F0 (%) of mean fluorescence of Lch1-5 in semi-intact larval preparations with sensory neuron-specific Gal4 driving GCaMP expression (SN-Gal4 x UAS-GCaMP6f), stimulated by 1024Hz tuning fork (52.4 ± 2.8dB, n = 10 tones). A: Representative images of Lch1-5 before, during and after stimulation (left-right, respectively). Dashed lines indicate region of interest defined to produce traces. B: Representative trace (n = 3, 1 larva) where F_0 for ΔF/ F0 (%) is defined as mean F of: (0s - onset of 1st peak) + (end of 1st peak to onset of 2nd peak) + (end of 2nd peak to onset of 3rd peak). C: Mean response to 1024Hz stimulation (9.54 ± 2.66%; n = 12, 4 larvae) generated by aligning all peaks in recordings (from 0.5s before onset of peak to end of peak + 0.5s) where F_0 for ΔF/ F0 (%) is defined as mean F of 0.5s before onset of peak. Arrows in B and C indicate onset of stimulus. Scale bar is 25µm (shown in one panel for clarity, as all panels are the same size).*

Vch1 response to 1024Hz was then recorded and quantified as for lch1-5. Responses were again characterised by short duration, high % change peaks (Figure 4.9, Mean Peak ΔF/ F0: 6.48 ± 4.35%; n = 10, 4 larvae), similar to lch1-5. Thus, both vch1 and lch1-5 respond to sound, supporting previous findings (Zhang *et al.*, 2013).

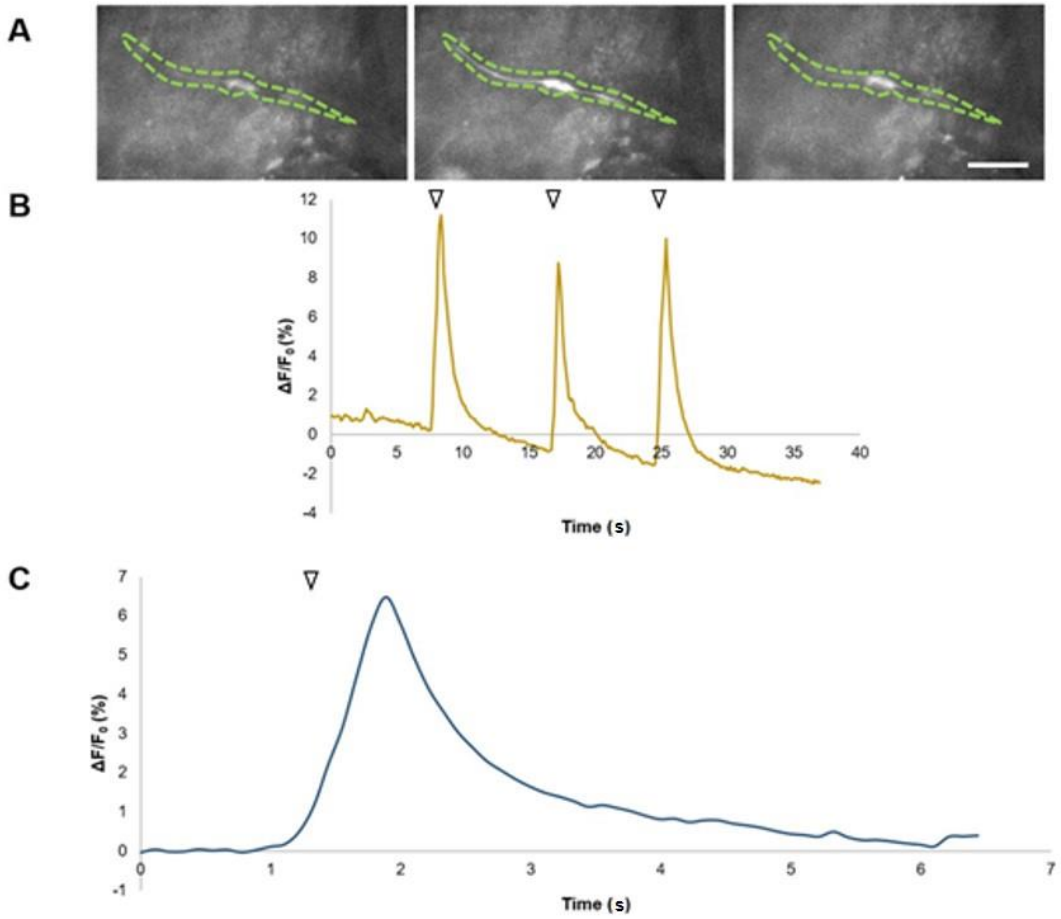

Figure 4.9: Vch1 response to 1024Hz stimulation. *Response as Peak ΔF/ F0 (%) of mean fluorescence of vch1 in semi-intact larval preparations with sensory neuron-specific Gal4 driving GCaMP expression (SN-Gal4 x UAS-GCaMP6f), stimulated by 1024Hz tuning fork (52.4 ± 2.8dB, n = 10 tones). A: Representative images of vch1 before, during and after stimulation (left-right, respectively). Dashed lines indicate region of interest defined to produce traces. B: Representative trace (n = 3, 1 larva) where F_0 for ΔF/ F0 (%) is defined as mean F of: (0s - onset of 1st peak) + (end of 1st peak to onset of 2nd peak) + (end of 2nd peak to onset of 3rd peak). C: Mean response to 1024Hz stimulation (6.48 ± 4.35%; n = 10, 4 larvae) generated by aligning all peaks in recordings (from 0.5s before onset of peak to end of peak + 0.5s) where F_0 for ΔF/ F0 (%) is defined as mean F of 0.5s before onset of peak. Arrows in A and B indicate onset of stimulus. Scale bar is 25µm (shown in one panel for clarity, as all panels are the same size).*

Finally, vchAB response to 1024Hz was recorded and quantified as described for lch1-5. Responses were characterised by short duration, high % change peaks (Figure 4.10. Mean Peak ΔF/ F0: 9.07 ± 4.45%; *n* = 12, 4 larvae) like the response to 1024Hz recorded lch1-5 and vch1. These results confirm that all subpopulations of chordotonal neurons in the peripheral nervous system respond to sound and suggest that none are specialised for proprioception. Thus, it appears that a single mechanism of mechanosensation transduces sound and stretch stimuli in chordotonal neurons.

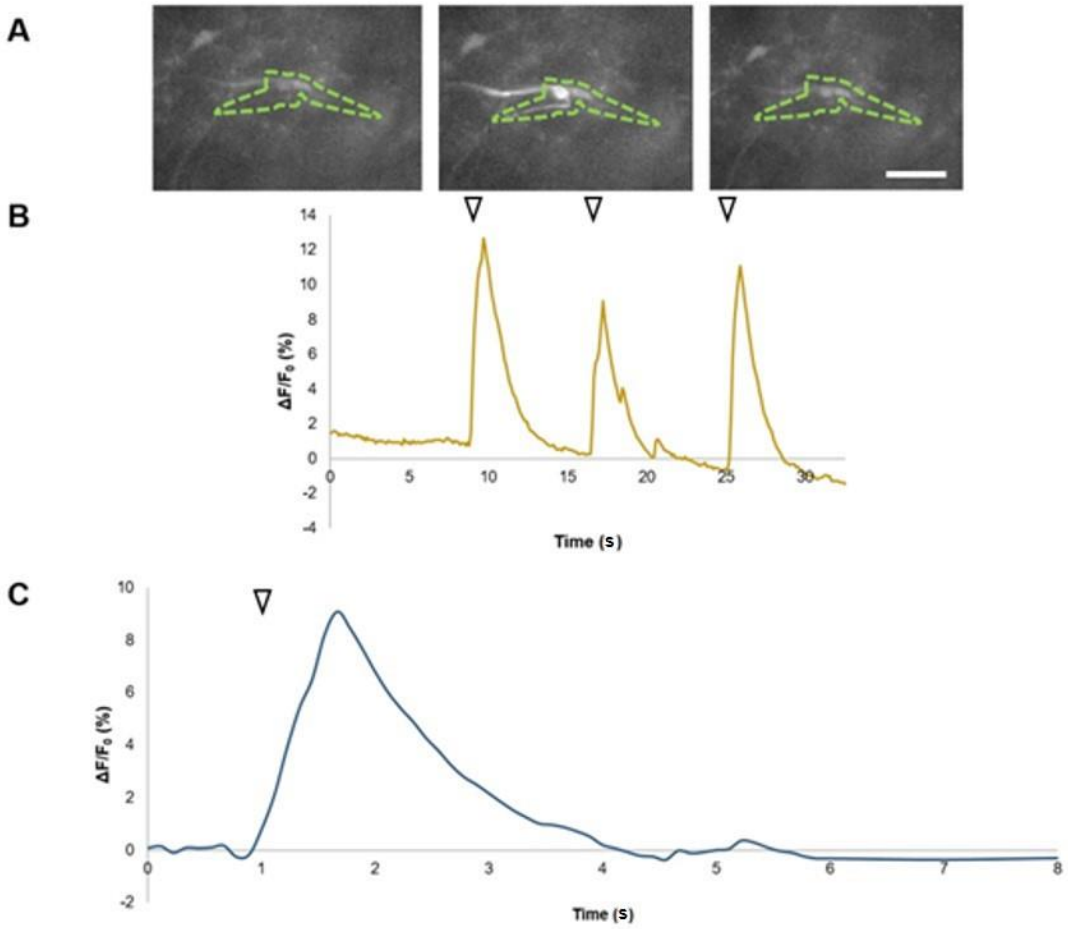

Figure 4.10: VchAB response to 1024Hz stimulation. *Response as Peak ΔF/ F0 (%) of mean fluorescence of vchAB in semi-intact larval preparations with sensory neuron-specific Gal4 driving GCaMP expression (SN-Gal4 x UAS-GCaMP6f), stimulated by 1024Hz tuning fork (52.4 ± 2.8dB, n = 10 tones). A: Representative images of vchAB before, during and after stimulation (left-right, respectively). Dashed lines indicate region of interest defined to produce traces. B: Representative trace (n = 3, 1 larva) where F_0 for ΔF/ F0 (%) is defined as mean F of: (0s - onset of 1st peak) + (end of 1st peak to onset of 2nd peak) + (end of 2nd peak to onset of 3rd peak). C: Mean response to 1024Hz stimulation (9.07 ± 4.45%; n = 12, 4 larvae) generated by aligning all peaks in recordings (from 0.5s before onset of peak to end of peak + 0.5s) where F_0 for ΔF/ F0 (%) is defined as mean F of 0.5s before onset of peak. Arrows in B and C indicate onset of stimulus. Scale bar is 25µm (shown in one panel for clarity, as all panels are the same size).*

4.3.1.4 Individual neurons within lch1-5 and vchAB respond differently to a tonal stimulus

While all subpopulations of ch neurons responded to sound, inspection of lch1-5 and vchAB responses revealed some differences within each subpopulation. Specifically, within the five neurons or lch1-5, lch1 seemed to respond to sound with different dynamics to lch2-5. Similarly, within the vchAB pair, vchA seemed to respond with different dynamics to vchB. The recordings of these subpopulations were, therefore, analysed to investigate this phenomenon.

Lch1 and lch2-5 response~~(s)~~(s) to 1024Hz were recorded and quantified as described for lch1-5. Lch1 responses were characterised by short duration, moderate % change peaks (Figure 4.11. Mean Peak ΔF/ F0: 8 ± 3%; *n* = 12, 4 larvae). Lch2-5 responses were also characterised by short duration, but in contrast to lch1, relatively high % change peaks (Figure 4.12. Mean Peak ΔF/ F_0: 9.54 ± 2.66%; *n* = 12, 4 larvae). This difference was significant (Figure 4.13, P ≤ 0.05) and could point to specialisation of individual neurons.

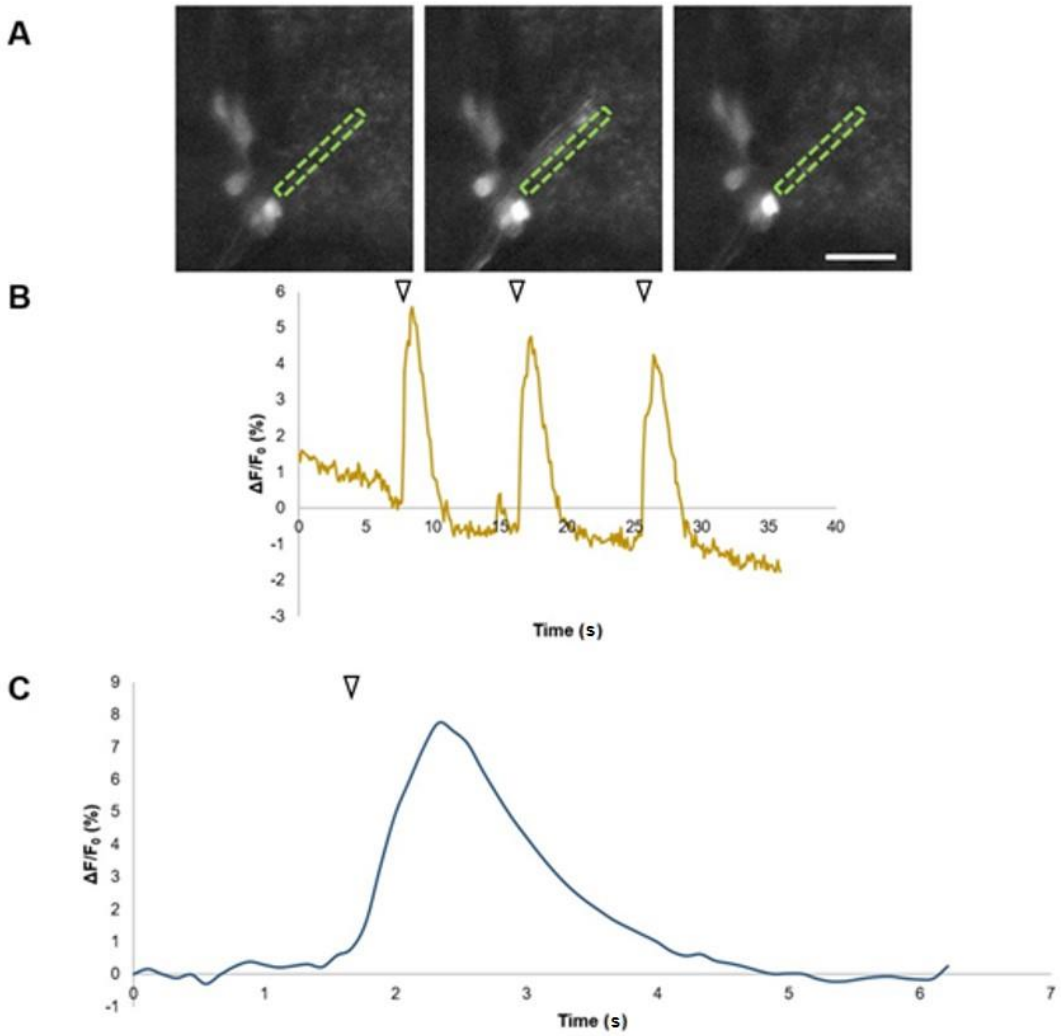

Figure 4.11: Lch1 response to 1024Hz stimulation. *Response as Peak ΔF/ F0 (%) of mean fluorescence of lch1 in semi-intact larval preparations with sensory neuron-specific Gal4 driving GCaMP expression (SN-Gal4 x UAS-GCaMP6f), stimulated by 1024Hz tuning fork (52.4 ± 2.8dB, n = 10 tones). A: Representative images of Lch1 before, during and after stimulation (left-right, respectively). Dashed lines indicate region of interest defined to produce traces. B: Representative trace (n = 3, 1 larva) where F_0 for ΔF/ F0 (%) is defined as mean F of: (0s - onset of 1st peak) + (end of 1st peak to onset of 2nd peak) + (end of 2nd peak to onset of 3rd peak). C: Mean response to 1024Hz stimulation (8 ± 3%; n = 12, 4 larvae) generated by aligning all peaks in recordings (from 0.5s before onset of peak to end of peak + 0.5s) where F_0 for ΔF/ F0 (%) is defined as mean F of 0.5s before onset of peak. Arrows in A and B indicate onset of stimulus. Scale bar is 25µm (shown in one panel for clarity, as all panels are the same size).*

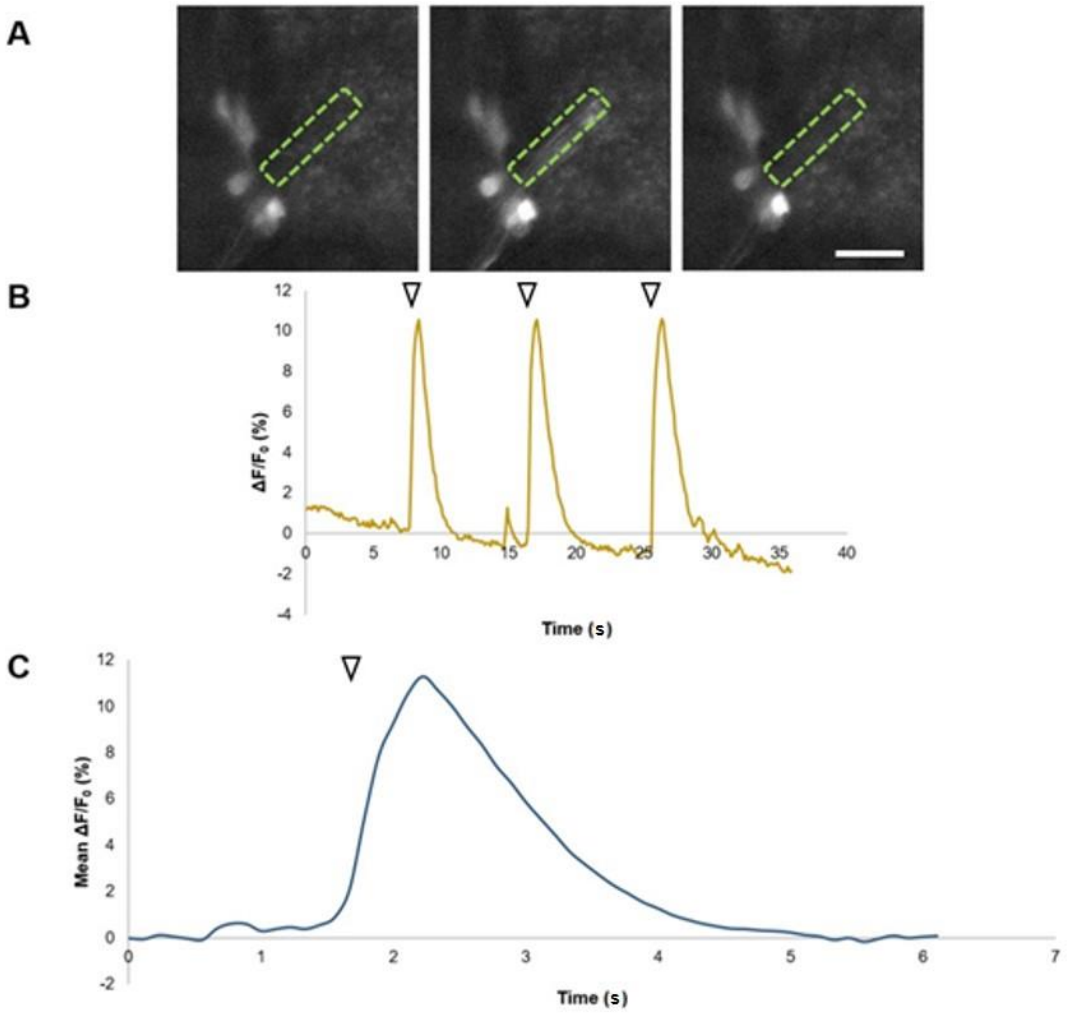

Figure 4.12: Lch2-5 response to 1024Hz stimulation. *Response as Peak ΔF/ F0 (%) of mean fluorescence of lch2-5 in semi-intact larval preparations with sensory neuron-specific Gal4 driving GCaMP expression (SN-Gal4 x UAS-GCaMP6f), stimulated by 1024Hz tuning fork (52.4 ± 2.8dB, n = 10 tones). A: Representative images of lch2-5 before, during and after stimulation (left-right, respectively). Dashed lines indicate region of interest defined to produce traces. B: Representative trace (n = 3, 1 larva) where F_0 for ΔF/ F0 (%) is defined as mean F of: (0s - onset of 1st peak) + (end of 1st peak to onset of 2nd peak) + (end of 2nd peak to onset of 3rd peak). C: Mean response to 1024Hz stimulation (11.28 ± 1.16%; n = 12, 4 larvae) generated by aligning all peaks in recordings (from 0.5s before onset of peak to end of peak + 0.5s) where F_0 for ΔF/ F0 (%) is defined as mean F of 0.5s before onset of peak. Arrows in B and C indicate onset of stimulus. Scale bar is 25µm (shown in one panel for clarity, as all panels are the same size).*

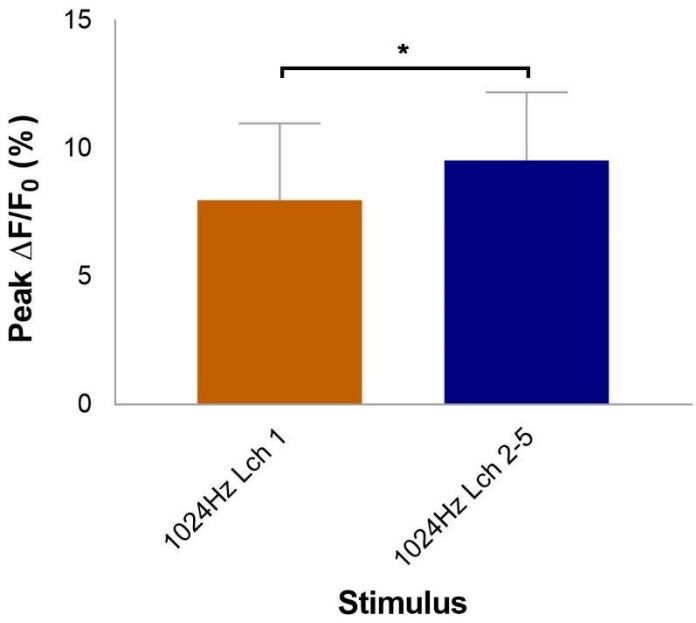

Figure 4.13: Lch1 responds to 1024Hz less than lch2-5 respond to 1024Hz. *Response as Peak ΔF/ F0 (%) of mean fluorescence of lch1 or lch2-5 in semi-intact larval preparations with sensory neuron-specific Gal4 driving GCaMP expression (SN-Gal4 x UAS-GCaMP6f), stimulated by 1024Hz tuning fork (52.4 ± 2.8dB, n = 10 tones). Response of lch1 to 1024Hz (8 ± 3%; n = 12, 4 larvae) was significantly less than response of lch2-5 to1024Hz (11.28 ± 1.16%; n = 12, 4 larvae, P = 0.033) as shown by bars of mean ± S.D. Statistical significance determined by unpaired t test (threshold for significance: P = 0.05; * = P < 0.05).*

Subsequently, vchA and vchB response~~(s)~~(s) to 1024Hz were recorded and quantified as described for lch1-5. VchA responses were characterised by short-moderate duration, high % change peaks (Figure 4.14. Mean Peak ΔF/ F0: 16.53 ± 8.76%; *n* = 12, 4 larvae). VchB responses were characterised by short duration, low % change peaks (Figure 4.15. Mean Peak ΔF/ F_0: 2.87 ± 2.31%; *n* = 12, 4 larvae). The very large difference between the two was significant (Figure 4.16, P ≤ 0.0001) and again suggests some form of fine-tuning specialisation among individual neurons. This research is the first to report this type of specialisation in lch and vch neurons.

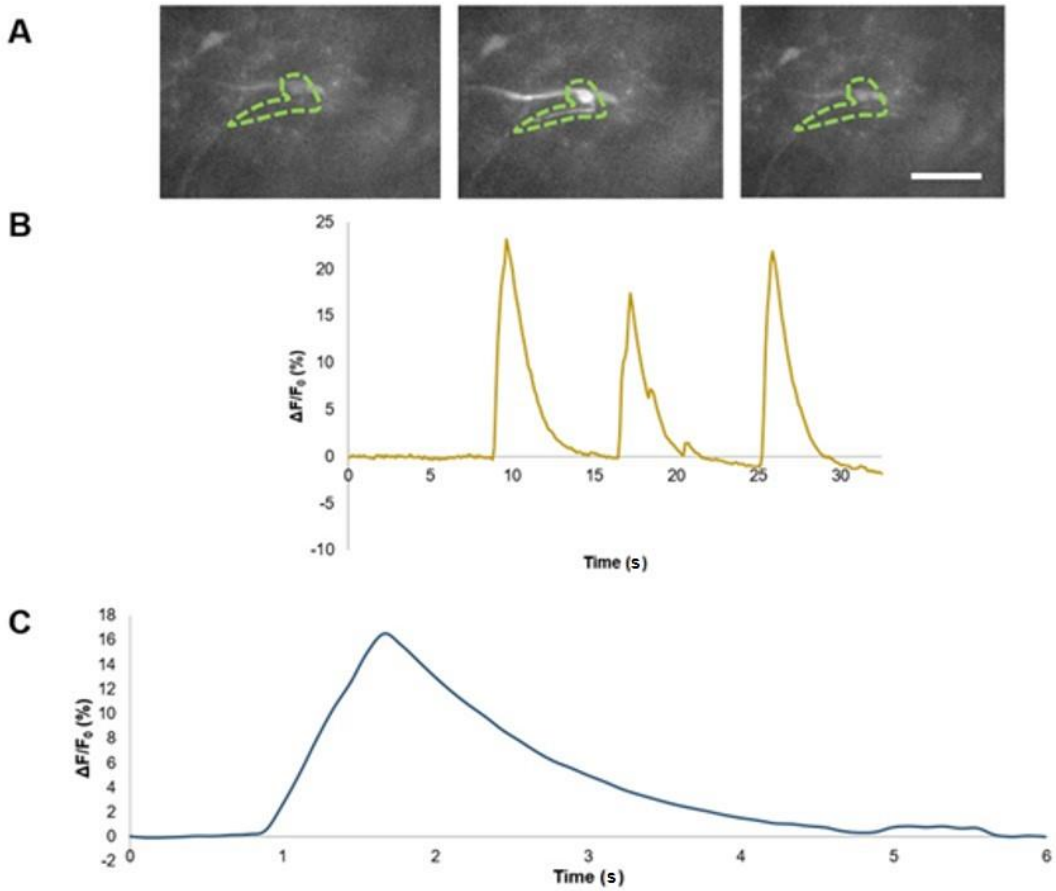

Figure 4.14: VchA response to 1024Hz stimulation. *Response as Peak ΔF/ F0 (%) of mean fluorescence of vchA in semi-intact larval preparations with sensory neuron-specific Gal4 driving GCaMP expression (SN-Gal4 x UAS-GCaMP6f), stimulated by 1024Hz tuning fork (52.4 ± 2.8dB, n = 10 tones). A: Representative images of vchA before, during and after stimulation (left-right, respectively). Dashed lines indicate region of interest defined to produce traces. B: Representative trace (n = 3, 1 larva) where F_0 for ΔF/ F0 (%) is defined as mean F of: (0s - onset of 1st peak) + (end of 1st peak to onset of 2nd peak) + (end of 2nd peak to onset of 3rd peak). C: Mean response to 1024Hz stimulation (16.53 ± 8.76%; n = 12, 4 larvae) generated by aligning all peaks in recordings (from 0.5s before onset of peak to end of peak + 0.5s) where F_0 for ΔF/ F0 (%) is defined as mean F of 0.5s before onset of peak. Scale bar is 25µm (shown in one panel for clarity, as all panels are the same size).*

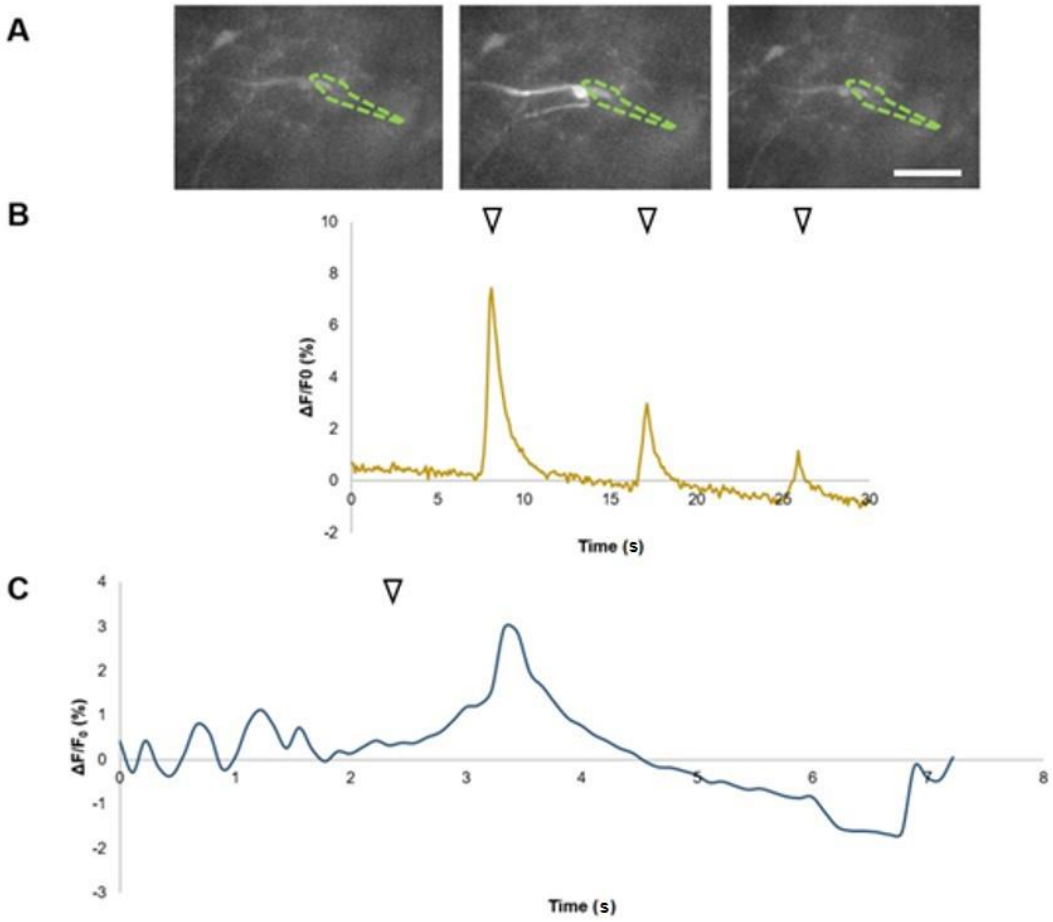

Figure 4.15: VchB response to 1024Hz stimulation. *Response as Peak ΔF/ F0 (%) of mean fluorescence of vchB in semi-intact larval preparations with sensory neuron-specific Gal4 driving GCaMP expression (SN-Gal4 x UAS-GCaMP6f), stimulated by 1024Hz tuning fork (52.4 ± 2.8dB, n = 10 tones). A: Representative images of vchB before, during and after stimulation (left-right, respectively). Dashed lines indicate region of interest defined to produce traces. B: Representative trace (n = 3, 1 larva) where F_0 for ΔF/ F0 (%) is defined as mean F of: (0s - onset of 1st peak) + (end of 1st peak to onset of 2nd peak) + (end of 2nd peak to onset of 3rd peak) or whole trace (to represent absence of peaks). C: Mean response to 1024Hz stimulation (2.87 ± 2.31%; n = 12, 4 larvae) generated by aligning all peaks in recordings (from 0.5s before onset of peak to end of peak + 0.5s) where F_0 for ΔF/ F0 (%) is defined as mean F of 0.5s before onset of peak. Arrows in B and C indicate onset of stimulus. Scale bar is 25µm (shown in one panel for clarity, as all panels are the same size).*

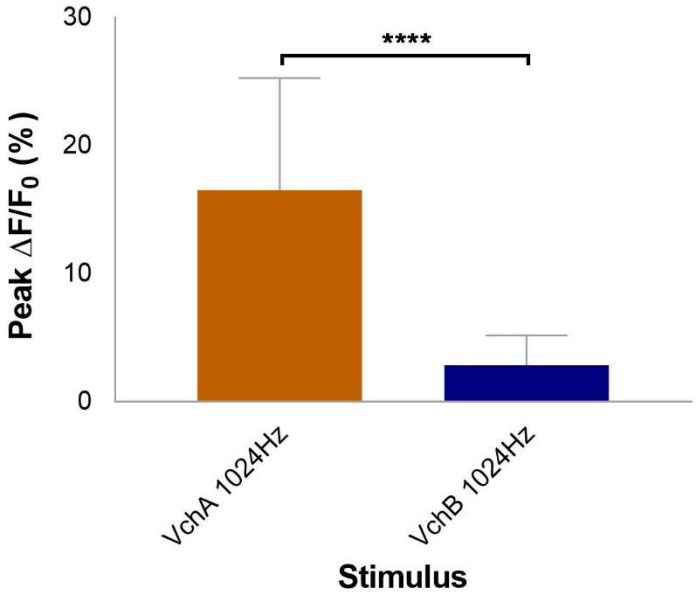

Figure 4.16: VchA responds to 1024Hz significantly more than VchB responds to 1024Hz. *Response as Peak ΔF/ F0 (%) of mean fluorescence of vchA or vchB in semi-intact larval preparations with sensory neuron-specific Gal4 driving GCaMP expression (SN-Gal4 x UAS-GCaMP6f), stimulated by 1024Hz tuning fork (52.4 ± 2.8dB, n = 10 tones). Response of vchA to 1024Hz (16.53 ± 8.76%; n = 12, 4 larvae) was significantly greater than of vchB to 1024Hz (2.87 ± 2.31%; n = 12, 4 larvae, P ≤ 0.0001). Shown by bars of mean ± S.D. Statistical significance determined by unpaired t test (threshold for significance: P = 0.05; **** = P < 0.0001).*

4.3.1.5 Investigation of candidate MET channels for larval hearing and proprioception

In the experiments described in this section, I aimed to use behavioural assays to compare the requirements for candidate ch neuron MET channels in larval hearing and proprioception.

4.3.1.5.1 Confirmation that inactive and NompC are necessary for larval hearing

I used a behavioural assay based on larval response to a tone (RT), to test larval hearing in *iav* and *NompC* mutants. Specifically, freely-crawling larvae were exposed to a 1000Hz pure tone, played through a speaker situated under and in contact with the crawling arena. Larvae were scored in batches of five for their response to the tone – a clear but momentary contraction of the larva. Surprisingly, *iav*[3621] -/- larvae response to 1000Hz (hemizygous mutant males, 0 RT count, given as mean number of larvae responding in each batch of 5*; n* = 5 repeats, 25 larvae) was not significantly different to that of attached-X controls (2.45 ± 0.57 RT count; *n* = 5 repeats, 25 larvae (Figure 4.17)). In contrast, iav[3621] -/- larvae were significantly less responsive than *Oregon-R* (wild-type) controls (5 RT count; *n* = 3 repeats, 15

larvae, both $P \leq 0.05$). The lack of significant difference between iav[3621] -/- and attached-X controls contrasts a body of research that shows that iav is required for *Drosophila* hearing (see Introduction to this chapter). That, in addition to the difference between iav[3621] -/- and *Oregon-R*, suggests this experiment is either underpowered or some genetic background in iav[3621] +/- controls has muted its RT. Again, *iav* is clearly necessary for larval hearing.

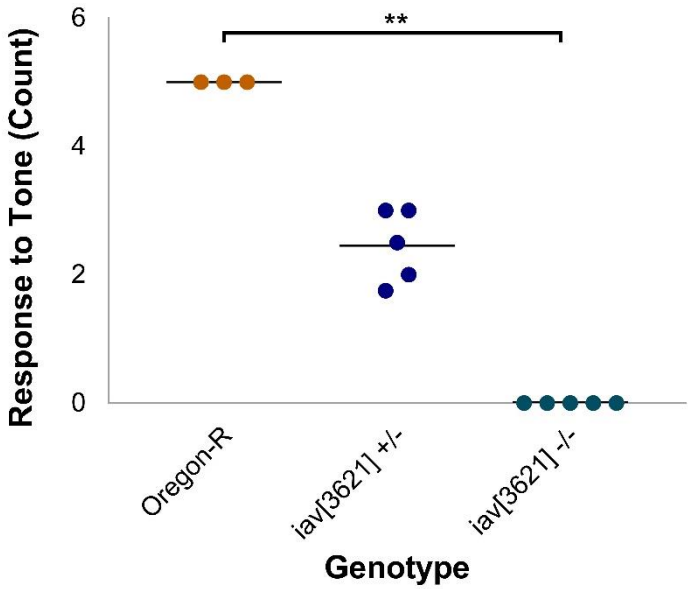

Figure 4.17: inactive may be necessary for larval hearing. *Response to Tone (RT, Count) is clear phenotypic response (e.g. contraction) to a 1000Hz tone observed in larvae crawling on a grape juice agar plate, recorded as mean number/ 5 larvae across 3-5 repeats (23.9-25°C, daylight). iav[3621] -/- RT (0 RT count; n = 5 repeats, 25 larvae) was not significantly different to attached-X controls (2.45 ± 0.57 RT count; n = 5 repeats, 25 larvae, P = 0.106), but was significantly less than Oregon-R (wild-type) controls (5 RT count; n = 3 repeats, 15 larvae, P = 0.003). Shown as scatter plot, horizontal line is mean. Statistical significance determined by Kruskal-Wallis with Duns post-hoc test (threshold for significance: P = 0.05; ** = P ≤ 0.01).*

NompC[1]/*NompC*[3] larvae (trans-heterozygous mutants, 4.8 ± 0.11 RT count; *n* = 5 repeats, 25 larvae) demonstrated significantly less RT than *NompC*[1] +/- (5 RT count; *n* = 5 repeats, 25 larvae, $P \leq 0.05$) and *NompC*[3] +/- controls (5 RT count; *n* = 5 repeats, 25 larvae, $P \leq 0.05$ (Figure 4.18). There was no significant difference between *NompC*[1]/[3] and *Oregon-R* (wild-type) controls (5 RT count; *n* = 3 repeats, 15 larvae) despite *Oregon-R* RT matching that of the *NompC* controls. This is probably due to a low '*n*' (*n* = 3) for *Oregon-R* reducing the power of the statistical analysis. The difference between *NompC*[1]/[3] mutants and *NompC*[1] +/- and *NompC*[3] +/- controls confirms that *NompC* is necessary for hearing and that *NompC*[1]/[3] is a useful mutant to use to compare mechanisms of mechanosensation.

Interestingly, in those mutant larvae that do respond to the tone, the *NompC*[1]/[3] phenotype was markedly different to *iav*[3621]. *NompC*[1]/[3] larvae 'twitched' and returned to normal crawling very quickly; *iav*[3621] mutants contracted completely and took far longer to adapt. This could indicate a more important role for *inactive* than *NompC* in hearing, supporting the 'nan-iav model' of mechanosensation in chordotonal neurons.

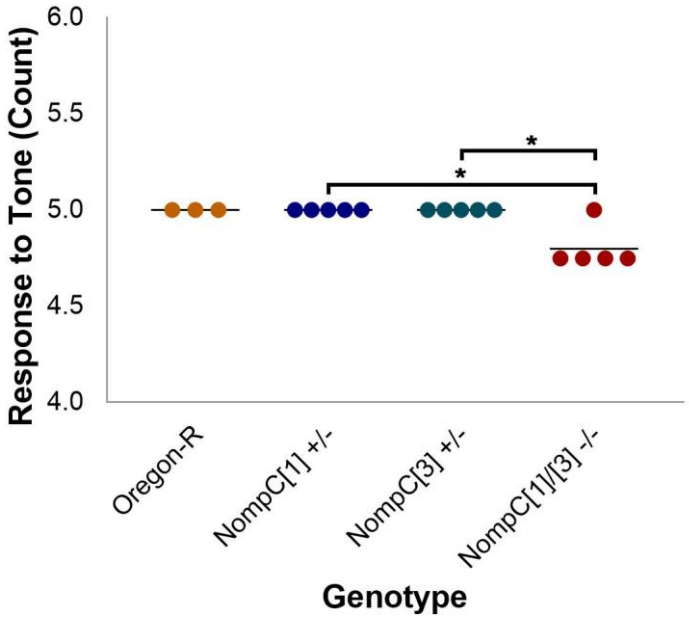

Figure 4.18: NompC is necessary for larval hearing. *Response to Tone (RT, Count) is clear phenotypic response (e.g. contraction) to a 1000Hz tone observed in larvae crawling on a grape juice agar plate, recorded as mean score/ 5 larvae across 3-5 repeats (23.9-25°C, daylight). NompC[1]/[3] -/- RT (4.8 ± 0.11 RT count; n = 5 repeats, 25 larvae) was significantly less than NompC[1] +/- (5 RT count; n = 5 repeats, 25 larvae, P = 0.019) and NompC[3] +/- (5 RT count; n = 5 repeats, 25 larvae, P = 0.019). There was no significant difference between NompC[1] -/-, NompC[3] -/- or NompC[1]/[3] -/- and Oregon-R (wild-type) controls (5 RT count; n = 3 repeats, 15 larvae). Shown as scatter plot, horizontal line is mean. Statistical significance determined by Kruskal-Wallis with Dunn's post-hoc test (threshold for significance: P = 0.05; * = P ≤ 0.05).*

4.3.1.5.2 inactive and NompC may be and are necessary for larval crawling, respectively

Whilst the GCaMP experiments above showed that all ch neurons respond to hearing and (to a lesser extent) proprioceptive stimuli, they could not determine whether different channels were responsible for each response. Thus, the *inactive* and *NompC* mutants were assayed for their requirement in normal larval crawling behaviour to check for possible differences in MET for each stimulus type. In these crawling experiments, I measured larval crawling speed per 120s in a grape agar arena.

For *iav*[3621], there was no significant difference in crawling speed per 120s from and attached-X controls (50.67 ± 18.79mm/ 120s; *n* = 16 larvae vs 55.18 ± 15.04mm/ 120s; *n* = 16 larvae). However, *iav*[3621] and attached-X controls crawled significantly less than *Oregon-R* (wild-type) controls (90.83 ± 18.65mm/ 120s; *n* = 16 larvae, both *P* ≤ 0.0001 (Figure 4.19). These results suggest that *inactive* may not be necessary for normal larval crawling so if *iav*[3621] mutants are deaf (assumes comparison between *iav*[3621] -/- and *Oregon-R* reflects reality), could imply separate *inactive*-dependent and *inactive*-independent mechanisms of mechanosensation in larvae. However, the significant difference between *iav*[3621] +/- and *Oregon-R* suggests an unhealthy background in the *iav*[3621]/ attached-X line, making it hard to reflect on the role of *inactive* in larval crawling.

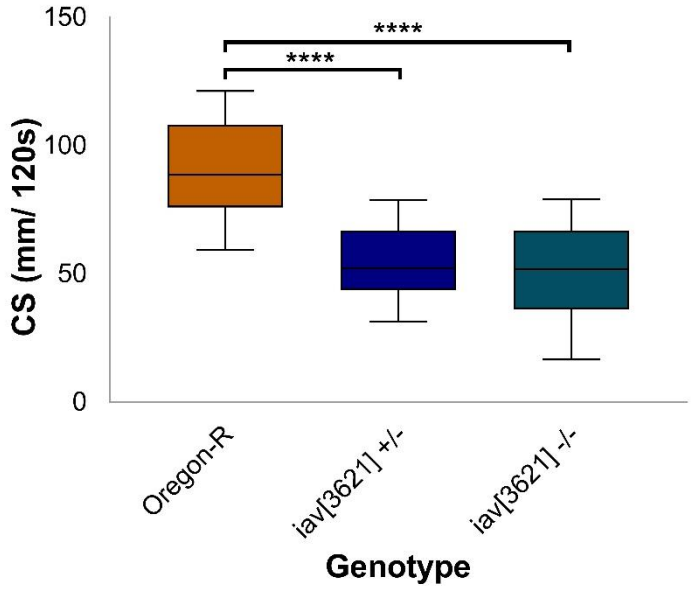

Figure 4.19: inactive may be necessary for normal larval crawling speed. *CS is crawling mm/120s recorded manually from larvae crawling on a 200mm x 200mm, 1% agar gel in a closed plastic container (23.9-25°C, daylight). There was no significant difference in crawling between iav[3621] (50.67 ± 18.79mm/ 120s; n = 16 larvae) and attached-X controls (55.18 ± 15.04mm/ 120s; n = 16 larvae, P = 0.749), whilst iav[3621] and attached-X controls crawled significantly less than Oregon-R (wild-type) controls (90.83 ± 18.65mm/ 120s; n = 16 larvae, P = <0.0001). Shown as whiskers minimum to maximum, horizontal line is median. Statistical significance determined by one-way ANOVA with Tukey's post-hoc test (threshold for significance: P = 0.05; **** = P ≤ 0.0001).*

There was a significant difference in CS between *NompC*[1]/[3] and *NompC*[1]/+ and *NompC*[3]/+ controls (77.64 ± 40.07mm/120s; *n* = 16 larvae, 121.7 ± 28.44mm/ 120s; *n* = 16 larvae, *P* ≤ 0.001, and 128.6 ± 23.83mm/ 120s; *n* = 16 larvae, *P* ≤ 0.0001) (Figure 4.20). There

was no significant difference between *NompC*[1]/[3] and *Oregon-R* (wild type) controls (90.83 ± 18.65mm/ 120s; *n* = 16 larvae), however, *Oregon-R* crawled significantly less than *NompC*[1]/+ and *NompC*[3]/+ (*P* ≤ 0.05 and *P* ≤ 0.01). The significant difference between *NompC*[1]/[3] and *NompC*[1]/+/ *NompC*[3]/+ supports previous research (Cheng *et al.*, 2010) and means that crawling experiments carried out on *inactive* and *NompC* mutants, *iav*[3621] -/- and *NompC*[1]/[3], support the idea that channels established as necessary for hearing, also contribute to normal crawling (caveat by effect of genetic background of *iav*[3621]).

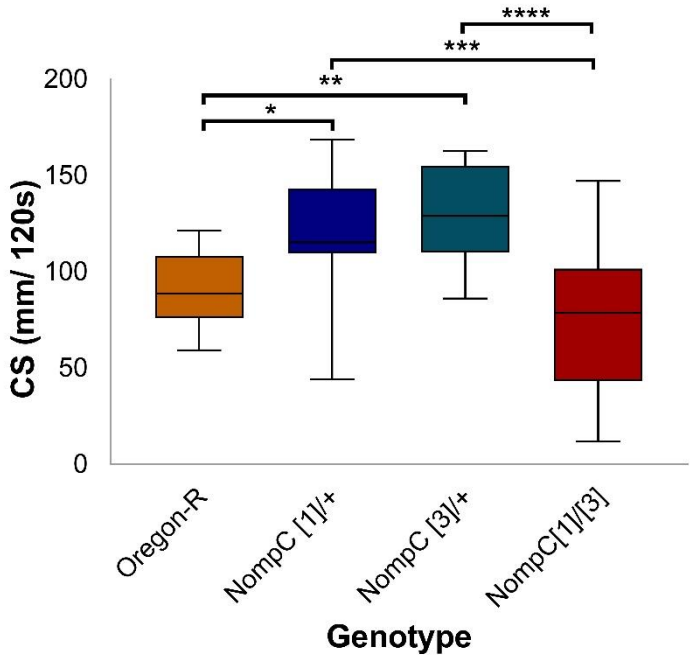

Figure 4.20: NompC is necessary for normal larval crawling speed. *CS is mm/ 120s recorded manually from larvae crawling on a 200mm x 200mm, 1% agar gel in a closed plastic container (23.9-25°C, daylight). NompC[1]/[3] (77.64 ± 40.07mm/120s; n = 16 larvae) crawled significantly less than NompC[1]/+ (121.7 ± 28.44mm/ 120s; n = 16 larvae, P = 0.0003) and NompC[3]/+ controls (128.6 ± 23.83mm/ 120s; n = 16 larvae, P = 0.0001), whilst there was no significant difference between NompC[1]/[3] and Oregon-R (wild type) controls (90.83 ± 18.65mm/ 120s; n = 16 larvae, P = 0.571). Oregon-R crawled significantly less than NompC[1]/+ and NompC[3]/+ (P = 0.019 and 0.0026, respectively). Shown as whiskers minimum to maximum, horizontal line is median. Statistical significance determined by one-way ANOVA with Tukey's post-hoc test (threshold for significance: P = 0.05; * = P ≤ 0.05 ** = P ≤ 0.01, *** = P ≤ 0.001, **** = P ≤ 0.0001).*

4.3.1.5.3 Pilot experiments using nan-iav agonist pymetrozine support a nan-iav MET in chordotonal neurons

Given that hearing and crawling experiments had demonstrated nan-iav and NompC were necessary (or likely necessary) for larval hearing and crawling, it was important to further refine the identity of the MET. Previously the pesticide pymetrozine (pym) has been used as a specific nan-iav agonist to investigate hearing in adult *Drosophila* and the desert locust, *Schistocerca gregaria*. Pymetrozine silences JO (ch) neuron response to sound stimuli, providing evidence for the nan-iav model of mechanosensation (Nesterov *et al.*, 2015; Warren and Matheson, 2018). Consequently, I analysed the effect of pym on ch neuron response to tone and muscle contraction.

Response~~(s)~~(s) to 1024Hz + 200µM pym (Figure 4.21) were recorded and quantified as for 1024Hz previously. In fact, application of 200µM pym alone was enough to stimulate the chordotonal neurons, which produced an intermittent, bright fluorescence in the VNC (Figure 4.21A). Consequently, playing the 1024Hz tone (1024Hz + 200µM pym) produced no clear change in ΔF/ F0 (%) (Figure 4.21B and C. Mean Peak ΔF/ F0 (see C): 0.64 ± 0.36; n = 3, 1 larva). Note that 'peaks' used in calculation of Mean Peak were derived from mean time~~(s)~~(s) of recording that correspond to peaks in 1024Hz, to allow comparison despite lack of peaks present in 1024Hz + 200µM. Comparison of responses revealed a significant difference between the two (Figure 4.22, $P \leq 0.0001$). This pilot supports the idea that chronic stimulation by pym inhibits the acute response to sound stimulus in ch neurons (Ausborn *et al.*, 2005; Nesterov *et al.*, 2015; Warren and Matheson, 2018).

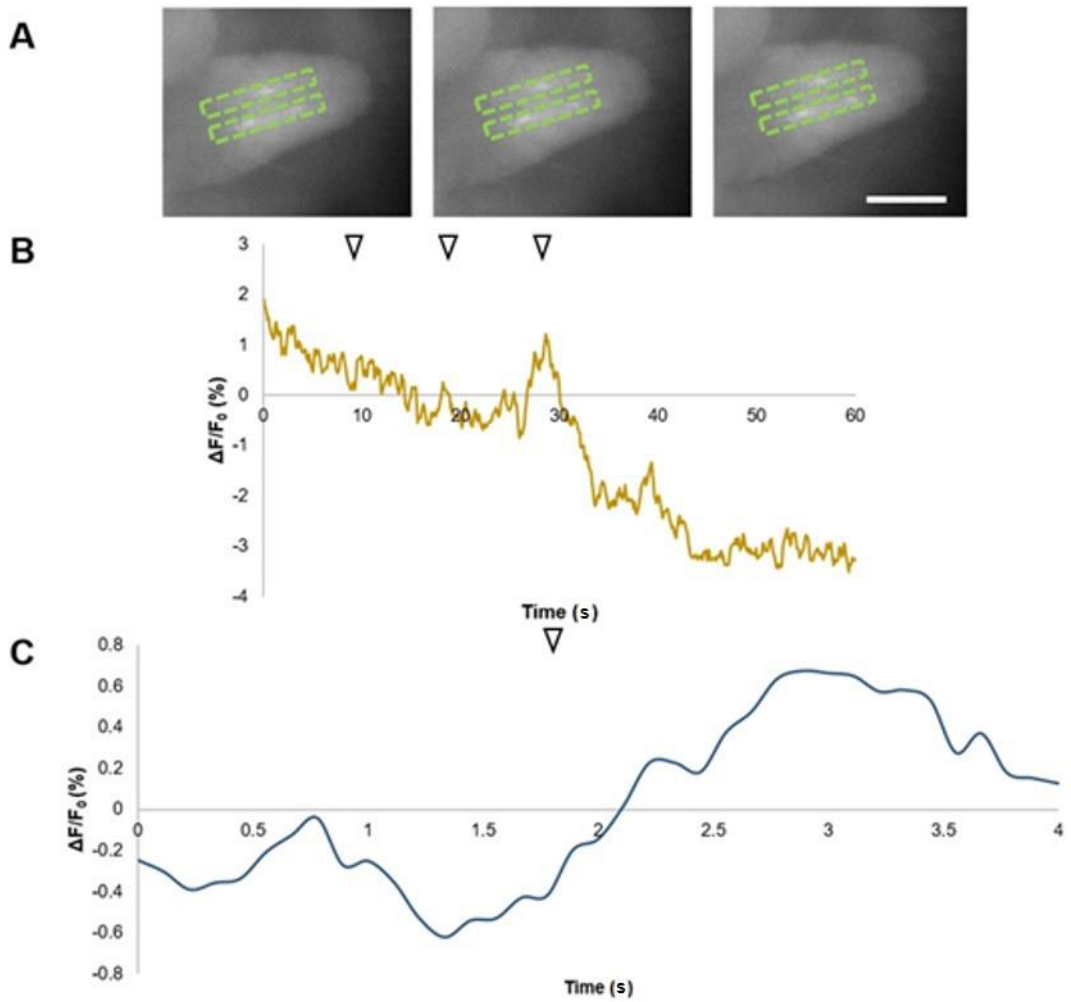

Figure 4.21: Chordotonal neuron response to 1024Hz stimulation + 200µM pymetrozine, recorded at the ventral nerve cord. *Response as Peak ΔF/ F0 (%) of mean fluorescence of 2 ventral nerve cord (VNC) tracts in semi-intact larval preparations with chordotonal neuron-specific Gal4 driving GCaMP expression (iav-Gal4 x UAS-GCaMP6f) + 200µM pymetrozine (pym), stimulated by 1024Hz tuning fork (52.4 ± 2.8dB, n = 10 tones). A, representative images of VNC before, during and after stimulation (left-right, respectively). Dashed lines indicate region of interest defined to produce traces. B, representative trace (n = 3, 1 larva) where F_0 for ΔF/ F0 (%) is defined as mean F of whole trace (to represent absence of peaks). C, mean response to 1024Hz + 200µM pym (0.64 ± 0.36; n = 3, 1 larva) generated by analysing mean times ~~(s)~~(s) of recording that correspond to peaks in 1024Hz (no peaks present in trace of 1024Hz + 200µM pym). Arrows in B and C indicate onset of stimulus. Scale bar is 100µm (shown in one panel for clarity, as all panels are the same size).*

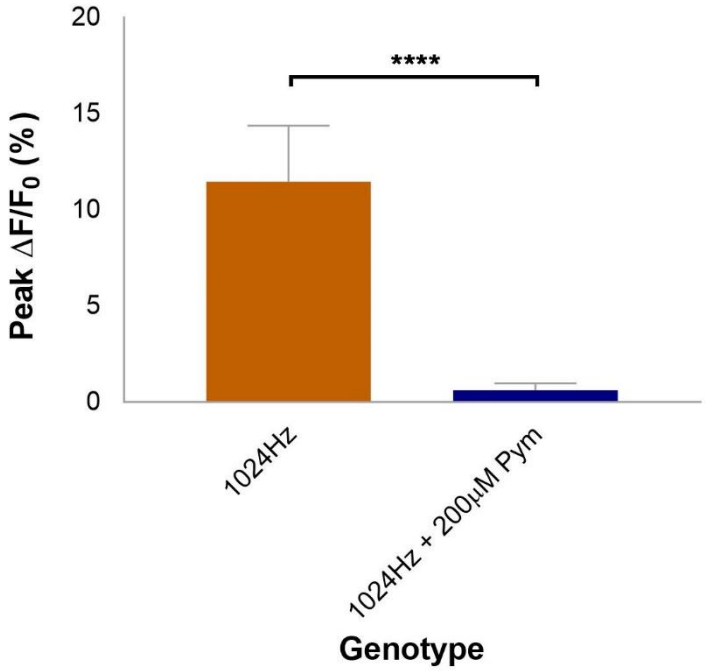

Figure 4.22: 200µM pymetrozine abolishes the chordotonal neuron response to 1024Hz stimulation. *Response as Peak ΔF/ F0 (%) of mean fluorescence of 2 ventral nerve cord tracts in semi-intact larval preparations with chordotonal neuron-specific Gal4 driving GCaMP expression (iav-Gal4 x UAS-GCaMP6f) without or + 200µM pymetrozine (pym), stimulated by 1024Hz (52.4 ± 2.8dB, n = 10 tones). Response of 1024Hz (11.47 ± 2.93%; n = 39, 14 larvae) was significantly greater than of 1024Hz + 200µM pym (0.64 ± 0.36; n = 3, 1 larva, P ≤ 0.0001), which did not respond to stimulation. Shown by bars of mean ± S.D. Statistical significance determined by unpaired t test (threshold for significance: P = 0.05; **** = P ≤ 0.0001).*

Next, the effect of 200µM pym on ch neuron response to spontaneous muscle contraction + 200µM pym were recorded and quantified. As above, 200µM pym alone stimulated the chordotonal neurons, which produced a flickering, bright fluorescence in the VNC (Figure 4.23A). Consequently, muscle contraction (muscle contraction + 200µM pym) produced only a small change in ΔF/ F0 (%) (Figure 4.23B and C. Mean Peak ΔF/ F0 (see C): 1.88 ± 0.3%; *n* = 2, 1 larva). The small peak in fluorescence that was recorded, appeared to be due to movement of the preparation during contraction and did not appear to reflect a response from chordotonal neurons. Comparison of mean Peak ΔF/ F0 to muscle contraction and muscle contraction + 200µM pym revealed no significant difference between responses (Figure 4.24), however, this comparison had very little power as the latter experiment was a pilot (*n* = 2). However, the trend in the difference between muscle contraction and muscle contraction + 200µM pym observed in: (1) the VNC during imaging; (2) traces; (3) Peak ΔF/ F0 all imply significance would be attained if the analysis was conducted with greater power. Thus, pilots (caveated by low power) suggest a single, nan-iav-dependent mechanism of mechanosensation for hearing and proprioception in *Drosophila* larvae.

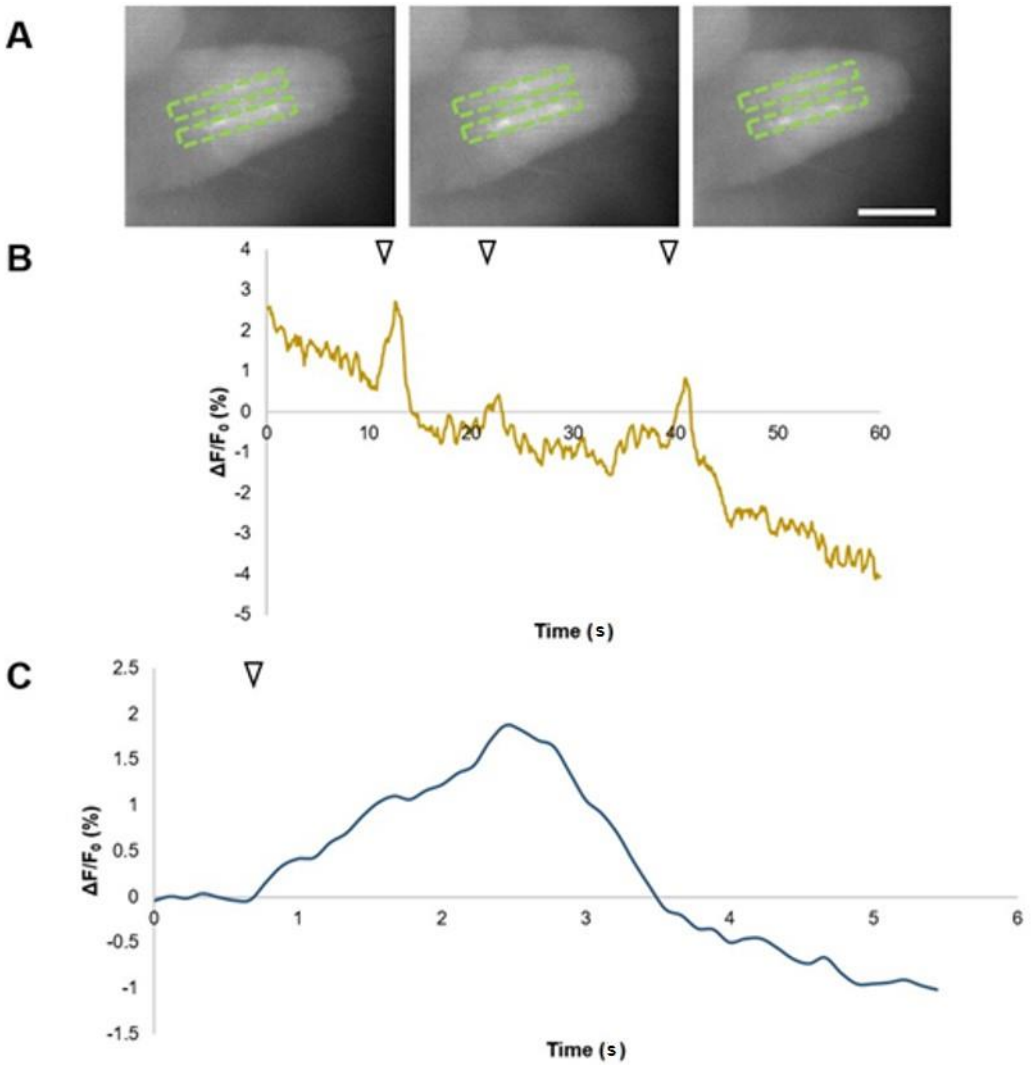

Figure 4.23: Chordotonal neuron response to muscle contraction + 200µM pymetrozine, recorded at the ventral nerve cord. *Response as Peak ΔF/ F0 (%) of mean fluorescence of 2 ventral nerve cord (VNC) tracts in semi-intact larval preparations with chordotonal neuron-specific Gal4 driving GCaMP expression (iav-Gal4 x UAS-GCaMP6f) + 200µM pymetrozine (pym), stimulated by spontaneous muscle contraction~~(s)~~(s). A, representative images of VNC before, during and after stimulation (left-right, respectively). Dashed lines indicate region of interest defined to produce traces. B, representative trace (n = 2, 1 larva) where F_0 for ΔF/ F0 (%) is defined as mean F of: (0s - onset of 1st peak) + (end of 1st peak to onset of 2nd peak). C, mean response to muscle contraction + 200µM pym (1.88 ± 0.3%; n = 2, 1 larva) generated by aligning peaks in recording (from 0.5s before onset of peak to end of peak + 0.5s) where F_0 for ΔF/ F0 (%) is defined as mean F of 0.5s before onset of peak. Arrows in B and C indicate onset of stimulus. Scale bar is 100µm (shown in one panel for clarity, as all panels are the same size).*

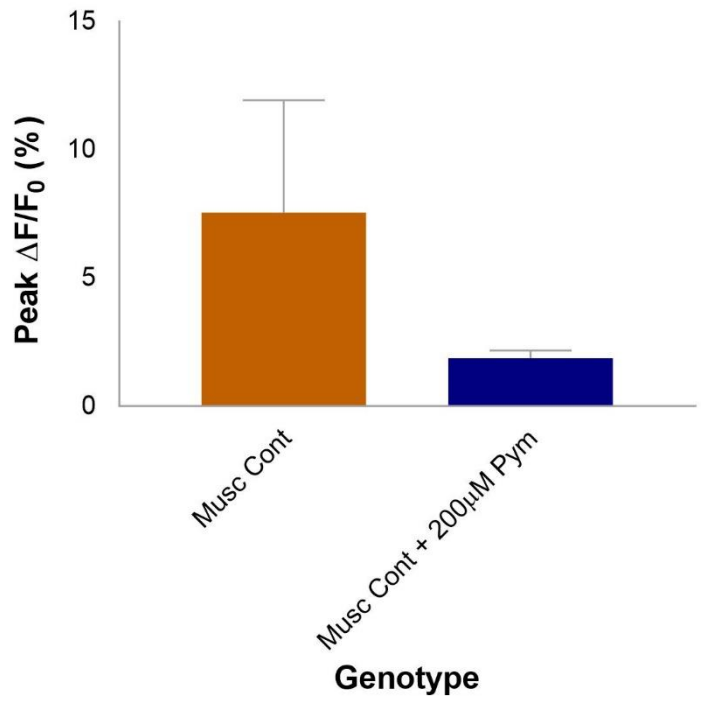

Figure 4.24: 200µM pymetrozine may abolish the chordotonal neurons' response to muscle contraction. *Response as Peak ΔF/ F0 (%) of mean fluorescence of 2 ventral nerve cord tracts in semi-intact larval preparations with chordotonal neuron-specific Gal4 driving GCaMP expression (iav-Gal4 x UAS-GCaMP6f) without or + 200µM pymetrozine (pym), stimulated by spontaneous muscle contraction~~(s)~~(s). Response to muscle contraction (7.56 ± 4.38%; n = 38, 13 larvae) was notably but not significantly different to muscle contraction + 200µM pym (1.88 ± 0.3%; n = 2, 1 larva, P = 0.078), due to a low n number (pilot experiment) resulting in an underpowered test. Shown by bars of mean ± S.D. Statistical significance determined by unpaired t test (threshold for significance: P = 0.05).*

4.3.1.5.4 DmPiezo does not contribute to mechanosensation in larval chordotonal neurons

4.3.1.5.4.1 Broad-spectrum MSC blocker Ruthenium Red does not affect *Drosophila* larval chordotonal response to tonal (1024Hz) or muscle contraction stimuli

DmPiezo has been identified as a candidate MET for hearing due to its expression in embryonic ch neurons (Kim *et al.*, 2012). It has also been identified as a MET in dbd neurons (Suslak *et al.*, 2015c). The latter work used Ruthenium Red (RR) and RNAi techniques to implicate DmPiezo in stretch recaption. RR is a broad-spectrum mechanosensory channel blocker that impairs Piezo activity. As a first experiment to determine whether DmPiezo plays a role in *Drosophila* ch neuron mechanosensation, I investigated whether ch neuron response was sensitive to RR.

Response~~(s)~~(s) to 1024Hz + 30µM Ruthenium Red (Figure 4.25) were recorded and quantified as described previously. 1024Hz + 30µM Ruthenium Red elicited short duration, large % change peaks (Figure 4.25B and C. Mean Peak ΔF/ F0 (see C): 14 ± 3.65%; *n* = 16, 6 larvae) reminiscent of the response for 1024Hz alone. Comparison of responses revealed no significant difference between the two (Figure 4.26). This result is, therefore, in agreement with (Coste *et al.*, 2012) who showed that channels blocked by RR do not play a role in adult *Drosophila* hearing.

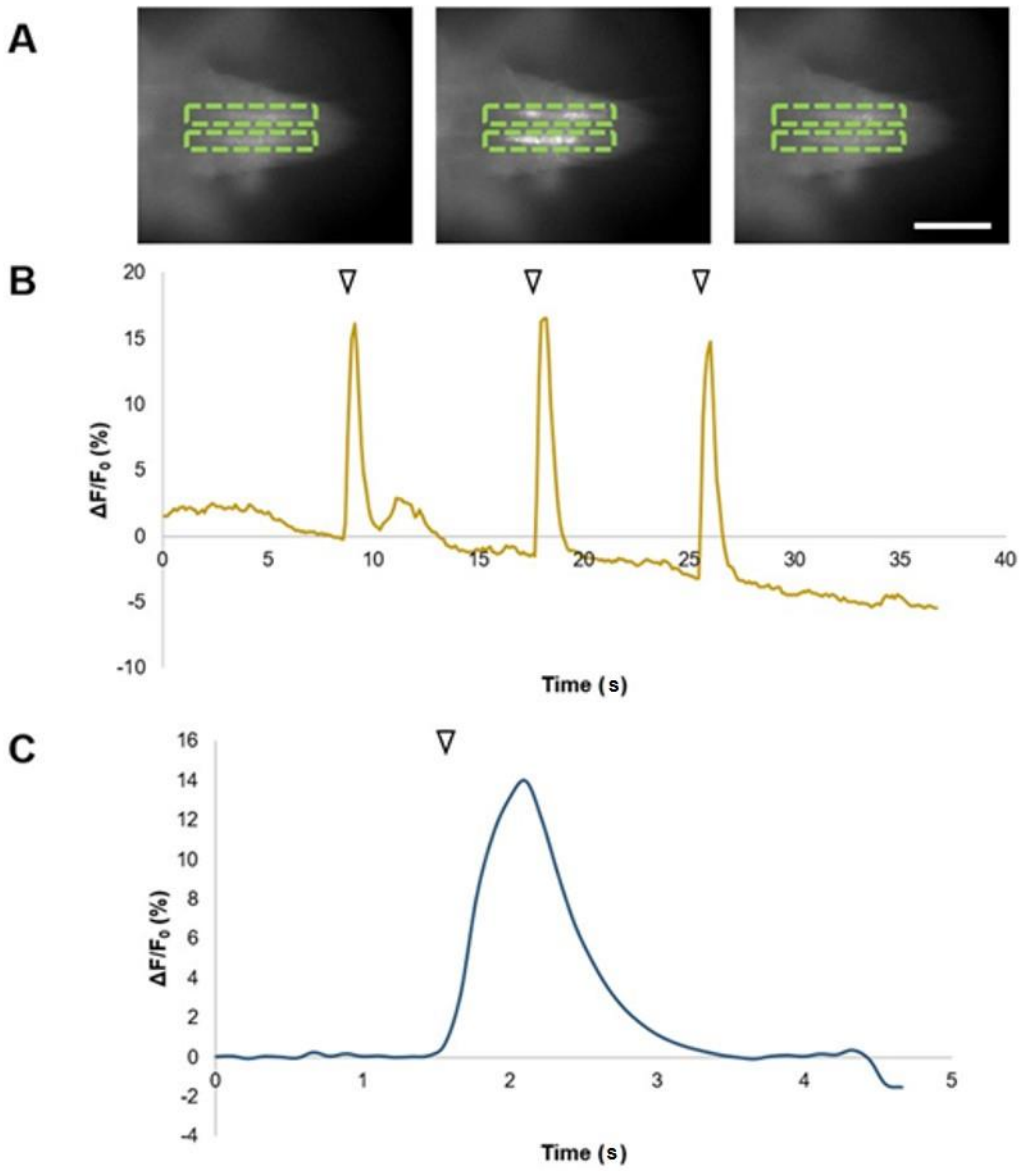

Figure 4.25: Chordotonal neuron response to 1024Hz stimulation + 30µM Ruthenium Red, recorded at the ventral nerve cord. *Response as Peak ΔF/ F0 (%) of mean fluorescence of 2 ventral nerve cord (VNC) tracts in semi-intact larval preparations with chordotonal neuron-specific Gal4 driving GCaMP expression (iav-Gal4 x UAS-GCaMP6f) + 30µM Ruthenium Red, stimulated by 1024Hz tuning fork (52.4 ± 2.8dB, n = 10 tones). A: Representative images of VNC before, during and after stimulation (left-right, respectively). Dashed lines indicate region of interest defined to produce traces. B: Representative trace (n = 3, 1 larva) where F_0 for ΔF/ F0 (%) is defined as mean F of: (0s - onset of 1st peak) + (end of 1st peak to onset of 2nd peak) + (end of 2nd peak to onset of 3rd peak). C: Mean response to 1024Hz + 30µM RR (14 ± 3.65%; n = 16, 6 larvae) generated by aligning all peaks in recordings (from 0.5s before onset of peak to end of peak + 0.5s) where F_0 for ΔF/ F0 (%) is defined as mean F of 0.5s before onset of peak. Arrows in B and C indicate onset of stimulus. Scale bar is 100µm (shown in one panel for clarity, as all panels are the same size).*

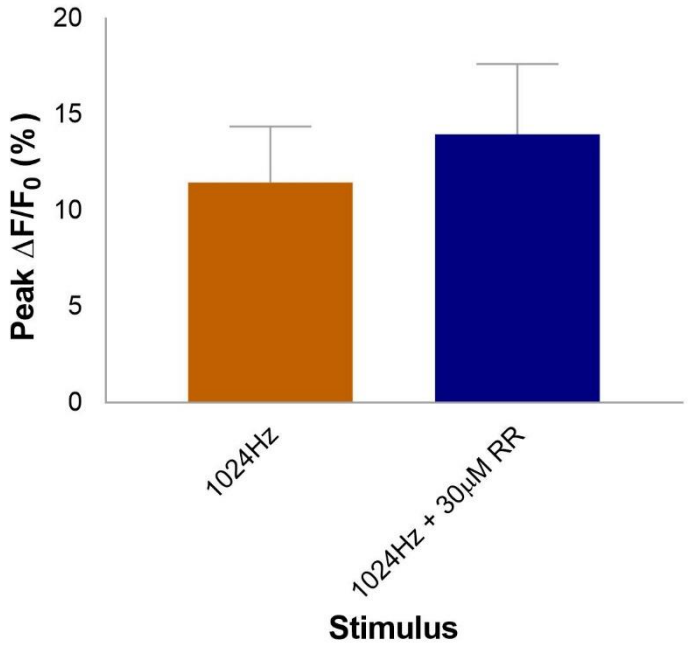

Figure 4.26: 30μM Ruthenium Red does not affect the chordotonal neurons' response to 1024Hz stimulation. *Response as Peak ΔF/ F0 (%) of mean fluorescence of 2 ventral nerve cord tracts in semi-intact larval preparations with chordotonal neuron-specific Gal4 driving GCaMP expression (iav-Gal4 x UAS-GCaMP6f) without or + 30μM Ruthenium Red, stimulated by 1024Hz (52.4 ± 2.8dB, n = 10 tones). Response of 1024Hz (11.47 ± 2.93%; n = 39, 14 larvae) was not significantly different to response of 1024Hz + 30μM RR (14 ± 3.65%; n = 16, 6 larvae, P = 0.08). Shown as bars of mean ± S.D. Statistical significance determined by unpaired t test (threshold for significance: P = 0.05).*

Response to muscle contraction + 30μM RR (Figure 4.27), was measured as before. Responses were characterised by long duration, moderate % change peaks of variable morphology (Figure 4.27B and C. 6.8 ± 3.12%; *n* = 16, 6 larvae), like the response to muscle contraction alone. Comparison of Mean Peak Response to muscle contraction and muscle contraction + 30μM Ruthenium Red revealed no significant difference between responses (Figure 4.28). Thus, 30μM RR does not affect chordotonal neuron response to 1024Hz or muscle contraction, implying that channels blocked by RR do not play a role in *Drosophila* hearing or crawling. This could also support a single mechanism of mechanosensation in chordotonal neurons, if RR blocks DmPiezo and TRPA1 (Suslak *et al.*, 2015c), as these channels are arguably the best candidates for an alternative MET in a nan-iav/ NompC-independent stretch sensitive mechanism in chordotonal neurons.

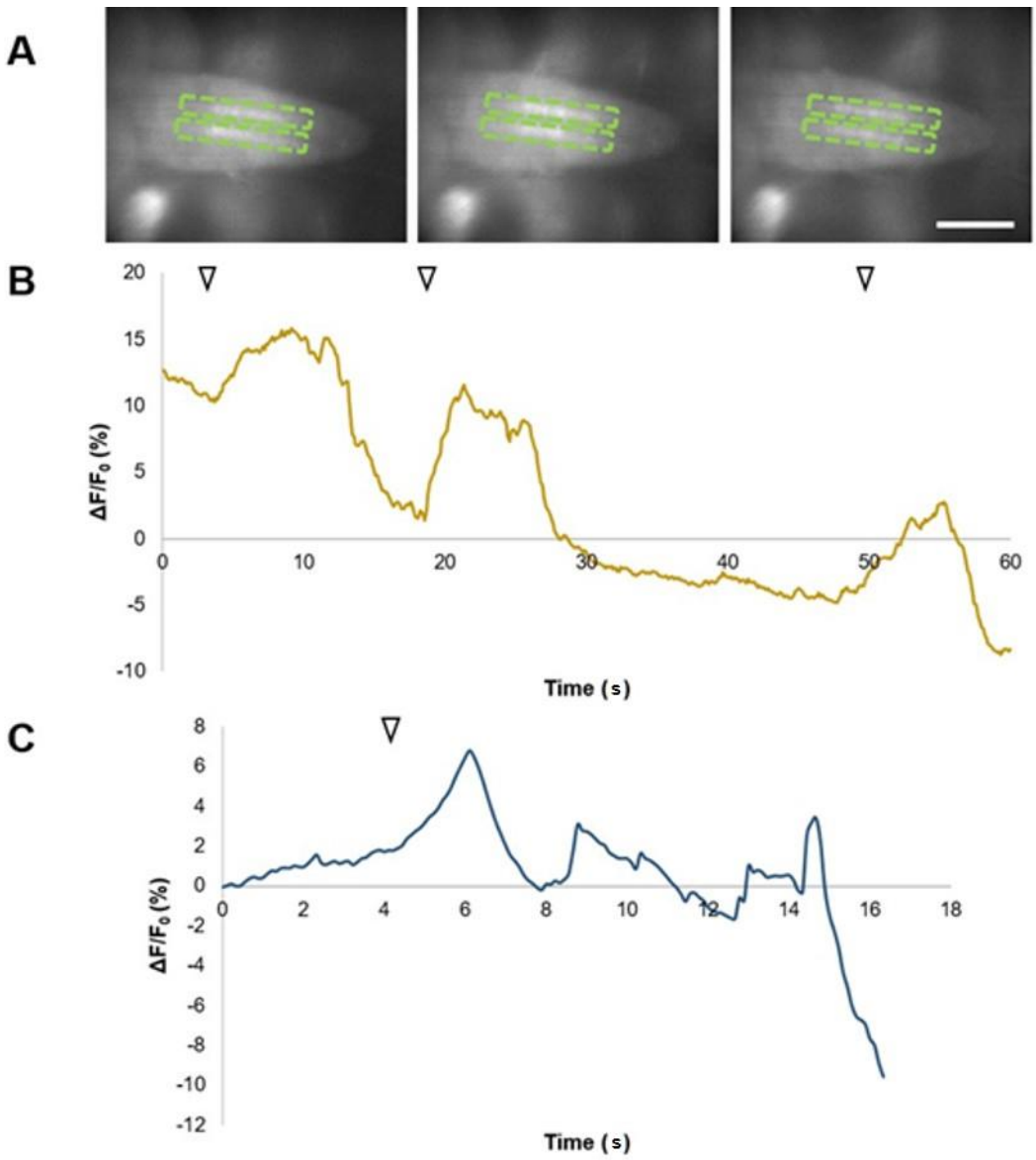

Figure 4.27: Chordotonal neuron response to muscle contraction + 30µM Ruthenium Red, recorded at the ventral nerve cord. *Response as Peak ΔF/ F0 (%) of mean fluorescence of 2 ventral nerve cord (VNC) tracts in semi-intact larval preparations with chordotonal neuron-specific Gal4 driving GCaMP expression (iav-Gal4 x UAS-GCaMP6f) + 30µM Ruthenium Red, stimulated by spontaneous muscle contraction~~(s)~~(s). A: Representative images of VNC before, during and after stimulation (left-right, respectively). Dashed lines indicate region of interest defined to produce traces. B: Representative trace (n = 3, 1 larva) where F_0 for ΔF/ F0 (%) is defined as mean F of: (0s - onset of 1st peak) + (end of 1st peak to onset of 2nd peak) + (end of 2nd peak to onset of 3rd peak). C: Mean response to muscle contraction + 30µM RR (6.8 ± 3.12%; n = 16, 6 larvae) generated by aligning all peaks in recordings (from 0.5s before onset of peak to end of peak + 0.5s) where F_0 for ΔF/ F0 (%) is defined as mean F of 0.5s before onset of peak. Arrows in B and C indicate onset of stimulus. Scale bar is 100µm (shown in one panel for clarity, as all panels are the same size).*

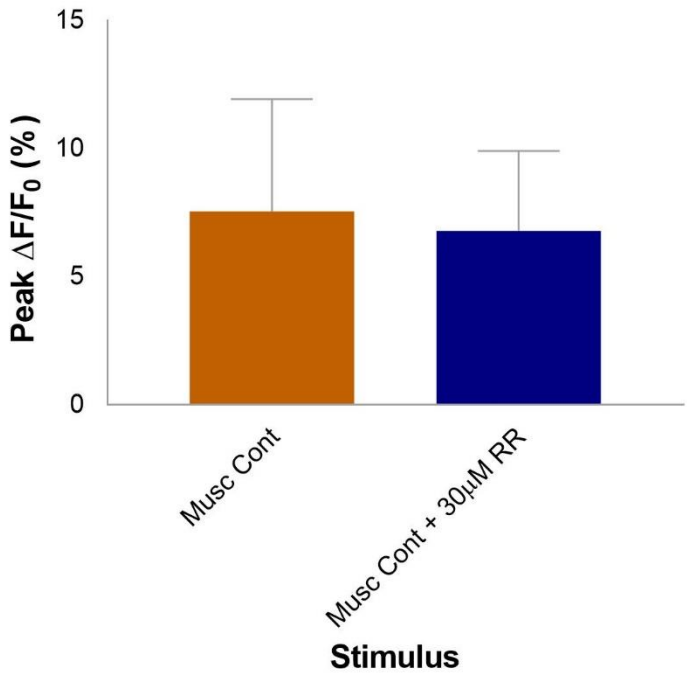

Figure 4.28: 30μM Ruthenium Red does not affect the chordotonal neuron response to muscle contraction. *Response as Peak ΔF/ F0 (%) of mean fluorescence of 2 ventral nerve cord tracts in semi-intact larval preparations with chordotonal neuron-specific Gal4 driving GCaMP expression (iav-Gal4 x UAS-GCaMP6f) without or + 30μM Ruthenium Red (RR), stimulated by spontaneous muscle contraction~~(s)~~(s). Response of muscle contraction (7.56 ± 4.38%; n = 38, 13 larvae) was not significantly different of muscle contraction + 30μM RR (6.8 ± 3.12%; n = 16, 6 larvae, P = 0.531). Shown as bars of mean ± S.D. Statistical significance determined by unpaired t test (threshold for significance: P = 0.05).*

The effect of RNAi knockdown of DmPiezo was investigated, to further refine results gleaned using RR. Knockdown was driven by iav-Gal4 and response to 1024Hz in *DmPiezo* RNAi larvae were recorded and quantified as before. 1024Hz in *DmPiezo* RNAi elicited short duration, large % change peaks (Figure 4.29B and C. Mean Peak ΔF/ F0 (see C): 11.05 ± 3.67; *n* = 18, 6 larvae) reminiscent of the response for 1024Hz and 1024Hz + 30μM Ruthenium Red. Comparison of responses revealed no significant difference between the two (Figure 4.30). Thus, RNAi experiments support the notion that *DmPiezo* does not contribute to sound reception by larval ch neurons.

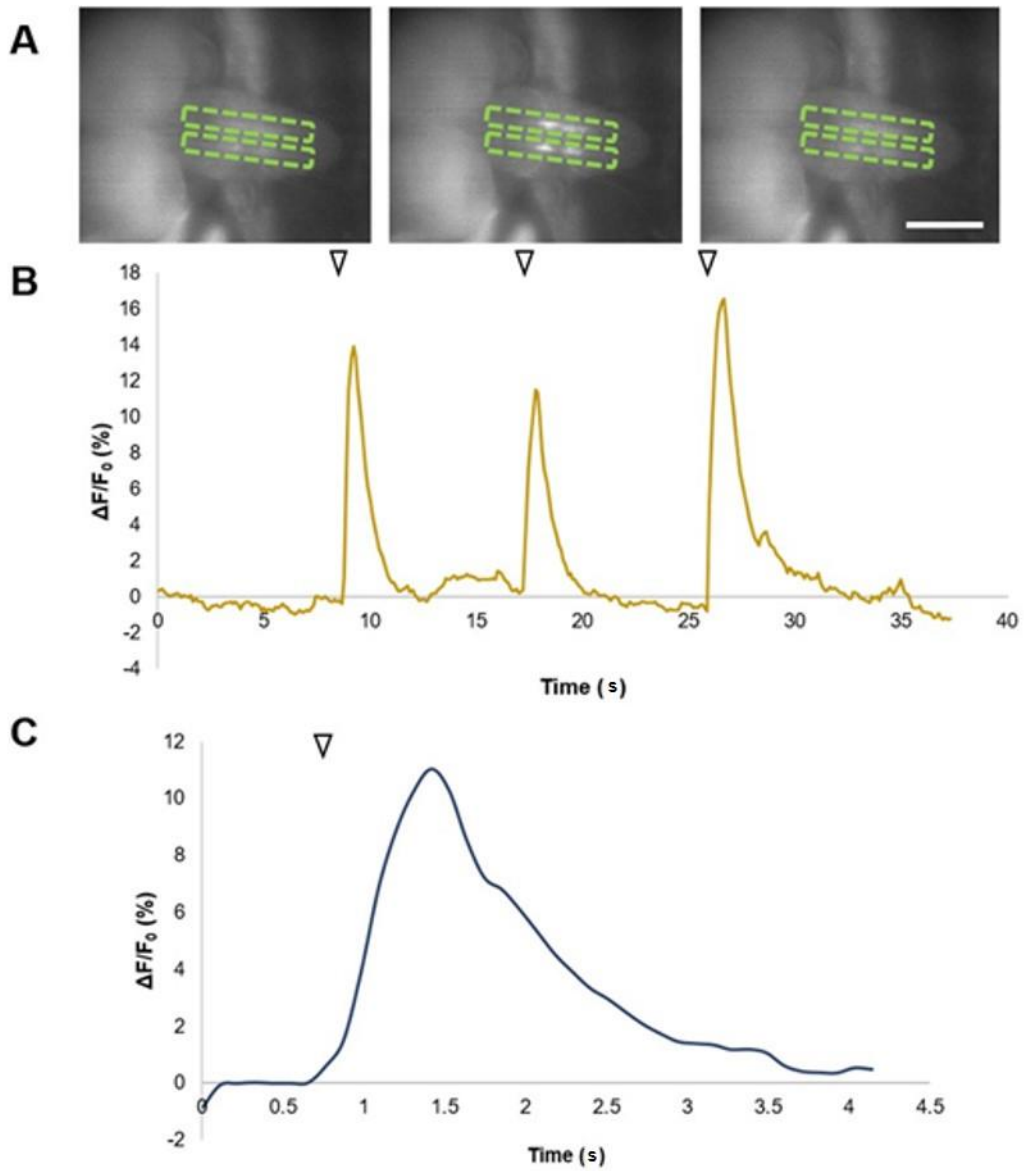

Figure 4.29: Chordotonal neuron response to 1024Hz stimulation in DmPiezo RNAi larvae, recorded at the ventral nerve cord. *Response as Peak ΔF/ F0 (%) of mean fluorescence of 2 ventral nerve cord (VNC) tracts in semi-intact larval preparations with chordotonal neuron-specific Gal4 driving GCaMP expression and DmPiezo RNAi (DmPiezo RNAi/ DmPiezo RNAi; iav-Gal4/ UAS-GCaMP6f), stimulated by 1024Hz tuning fork (52.4 ± 2.8dB, n = 10 tones). A: Representative images of VNC before, during and after stimulation (left-right, respectively). Dashed lines indicate region of interest defined to produce traces. B: Representative trace (n = 3, 1 larva) where F_0 for ΔF/ F0 (%) is defined as mean F of: (0s - onset of 1st peak) + (end of 1st peak to onset of 2nd peak) + (end of 2nd peak to onset of 3rd peak). C: Mean response to 1024Hz in DmPiezo RNAi larvae (11.05 ± 3.67; n = 18, 6 larvae) generated by aligning all peaks in recordings (from 0.5s before onset of peak to end of peak + 0.5s) where F_0 for ΔF/ F0 (%) is defined as mean F of 0.5s before onset of peak. Scale bar is 100µm (shown in one panel for clarity, as all panels are the same size).*

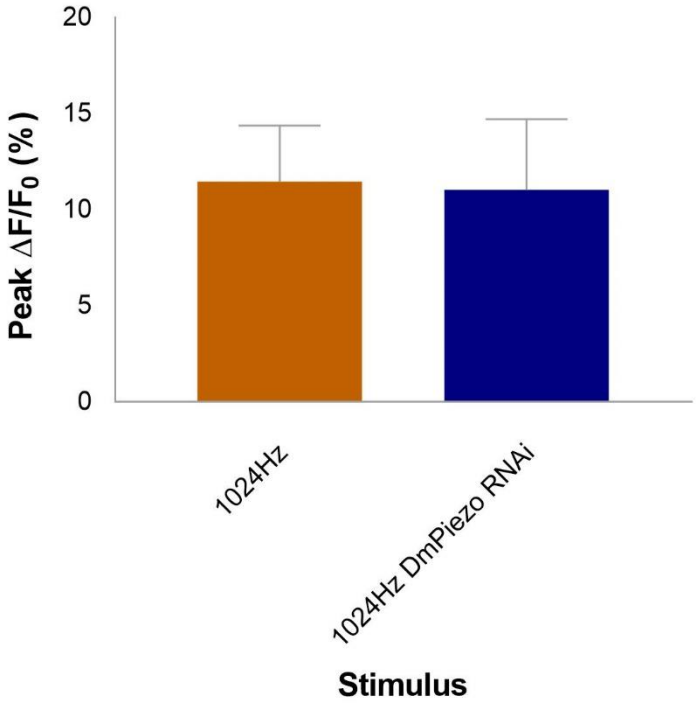

Figure 4.30: DmPiezo RNAi does not affect the chordotonal neuron response to 1024Hz stimulation. *Response as Peak ΔF/ F0 (%) of mean fluorescence of 2 ventral nerve cord tracts in semi-intact larval preparations with chordotonal neuron-specific Gal4 driving GCaMP expression (iav-Gal4 x UAS-GCaMP6f) or GCAMP and DmPiezo RNAi (DmPiezo RNAi/ DmPiezo RNAi; iav-Gal4/ UAS-GCaMP6f), stimulated by a 1024Hz tuning fork (52.4 ± 2.8dB, n = 10 tones). Response of 1024Hz (11.47 ± 2.93%; n = 39, 14 larvae) was not significantly different of 1024Hz DmPiezo RNAi (11.05 ± 3.67; n = 18, 6 larvae, P = 0.639). Shown as bars of mean ± S.D. Statistical significance determined by unpaired t test (threshold for significance: P = 0.05).*

Response to muscle contraction in DmPiezo RNAi was recorded and quantified as 1024Hz. Responses were characterised by long duration, moderate % change peaks of variable morphology (Figure 4.31B and C. 6.8 ± 3.12%; *n* = 16, 6 larvae) like the response to muscle contraction and muscle contraction + 30µM Ruthenium Red. Comparison of Mean Peak Response to muscle contraction and muscle contraction in *DmPiezo* RNAi revealed no significant difference between responses (Figure 4.32). Thus, RNAi suggests that DmPiezo does not function during chordotonal neuron response to 1024Hz or muscle contraction. This supports previous experiments showing that the channel does not play a role in larval hearing or crawling (Zhang *et al.*, 2013).

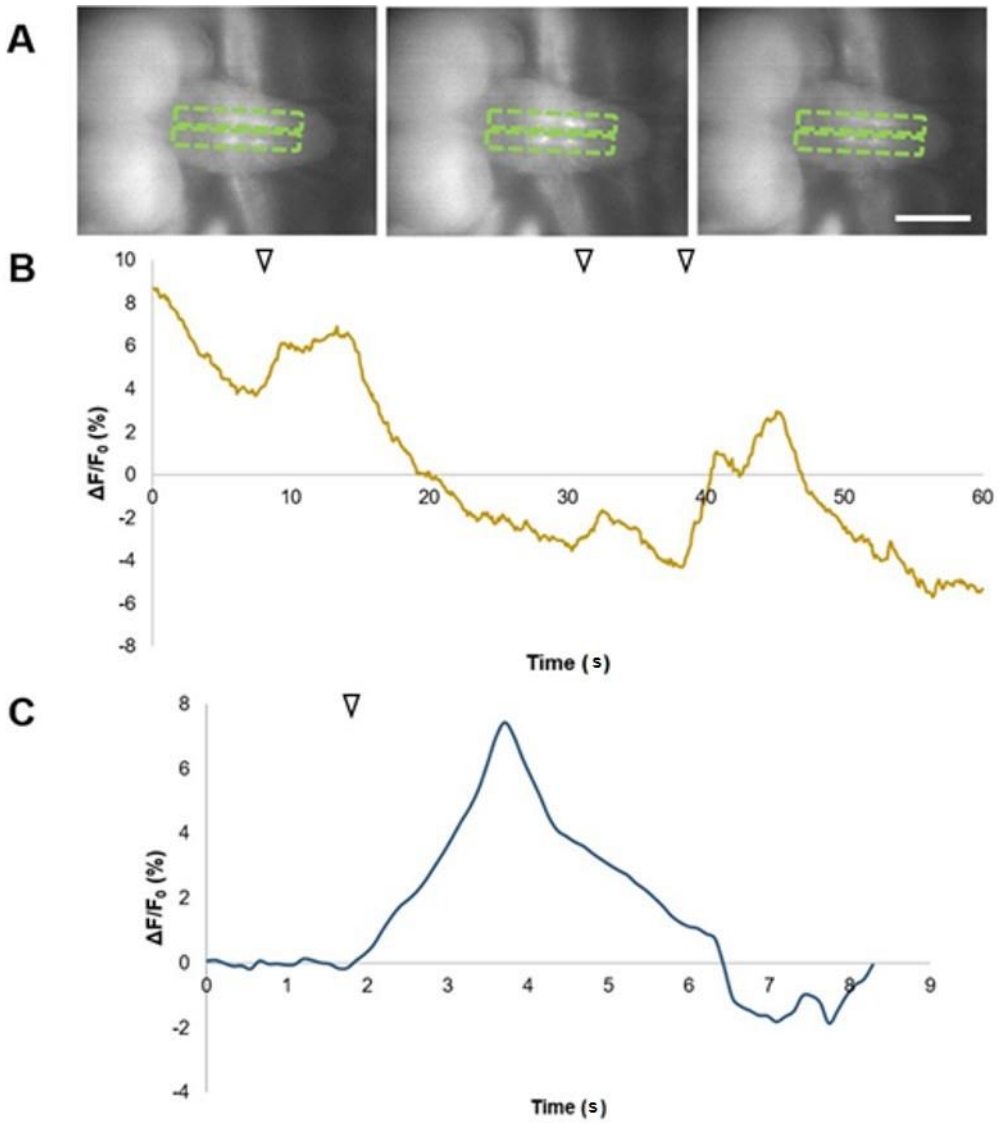

Figure 4.31: Chordotonal neuron response to muscle contraction in DmPiezo RNA$_i$ larvae, recorded at the ventral nerve cord. *Response as Peak ΔF/ F0 (%) of mean fluorescence of 2 ventral nerve cord (VNC) tracts in semi-intact larval preparations with chordotonal neuron-specific Gal4 driving GCaMP expression and DmPiezo RNAi (DmPiezo RNAi/ DmPiezo RNAi; iav-Gal4/ UAS-GCaMP6f), stimulated by spontaneous muscle contraction~~(s)~~(s). A: Representative images of VNC before, during and after stimulation (left-right, respectively). Dashed lines indicate region of interest defined to produce traces. B: representative trace (n = 3, 1 larva) where F_0 for ΔF/ F0 (%) is defined as mean F of: (0s - onset of 1st peak) + (end of 1st peak to onset of 2nd peak) + (end of 2nd peak to onset of 3rd peak). C: mean response to muscle contraction in DmPiezo RNA$_i$ larvae (7.42 ± 3.46%; n = 8, 4 larvae) generated by aligning all peaks in recordings (from 0.5s before onset of peak to end of peak + 0.5s) where F_0 for ΔF/ F0 (%) is defined as mean F of 0.5s before onset of peak. Arrows in B and C indicate onset of stimulus. Scale bar is 100µm (shown in one panel for clarity, as all panels are the same size).*

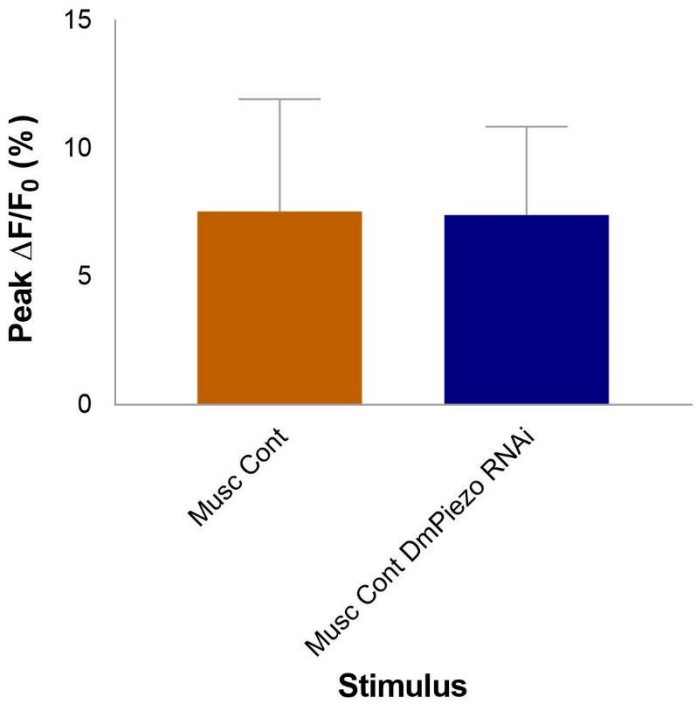

Figure 4.32: DmPiezo RNAi does not affect the chordotonal neuron response to muscle contraction. *Response as Peak ΔF/ F0 (%) of mean fluorescence of 2 ventral nerve cord tracts in semi-intact larval preparations with chordotonal neuron-specific Gal4 driving GCaMP expression (iav-Gal4 x UAS-GCaMP6f) or GCaMP and DmPiezo RNAi (DmPiezo RNAi/ DmPiezo RNAi; iav-Gal4/ UAS-GCaMP6f), stimulated by spontaneous muscle contraction~~(s)~~(s). Response of muscle contraction (7.56 ± 4.38%; n = 38, 13 larvae) was not significantly different of muscle contraction DmPiezo RNAi (7.42 ± 3.46%; n = 8, 4 larvae, P = 0.932). Shown as bars of mean ± S.D. Statistical significance determined by unpaired t test (threshold for significance: P = 0.05).*

4.3.1.6 Optogenetic stimulation of chordotonal neurons does not affect larval crawling

Loss-of-function analyses suggested that ch neurons are required for normal larval locomotion, and my results are consistent with this. In order to explore this function further, I asked whether stimulation of ch neurons affected crawling behaviour. Related experiments were conducted using optogenetic techniques; ch neuron-specific driver nan-Gal4 was crossed to red-shifted channelrhodopsin line, UAS-csChrimson (nan-Gal4 x UAS-csChrimson) to allow specific stimulation of ch neurons in freely-moving larvae. This process is aided by the translucent cuticle, which allows light to pass to neurons. Larvae were grown on food containing 1mM all-trans retinal (ATR), a cofactor chromophore necessary for channelrhodopsin function. Larvae were exposed to a 30s red light stimulus, and measurements were made before and during exposure to calculate % change in crawling speed (% Change in CS), peristaltic wave frequency (% Change in Frequency of Peri. Waves) and peristaltic wave duration (% Change in Peri. Wave Duration).

'Before' and 'during' CSs were normalised prior to calculating % Change in CS. % Change in CS was measured as mean % change in CS (mm/ 30s) of larvae before and during red light stimulation, where red light stimulation depolarised ch neurons. There was no significant difference in % Change in CS between nan-Gal4 x UAS-csChrimson ATR (-9.41 ± 22.21%; n = 10 larvae) and nan-Gal4 ATR controls (-8.61 ± 31.03%; n = 10 larvae), however, there was a significant difference between nan-Gal4 x UAS-csChrimson ATR or nan-Gal4 and UAS-csChrimson ATR (-45.2 ± 33.58%; n = 10 larvae; $P \leq 0.05$ for both (Figure 4.33)). The very large % change in CS for UAS-csChrimson ATR may be due to non-specific expression of channelrhodopsin in neurons that impact crawling, e.g. the bd and/ or type I md neurons (Hughes and Thomas, 2007) or CNS. However, such non-specific expression would not explain how the effect is lost crossing to nan-Gal4. Overall, the results may suggest that acute stimulation of ch neurons does not interfere with crawling behaviour. However, it will be necessary to confirm expression and function of UAS-csChrimson in the ch neurons.

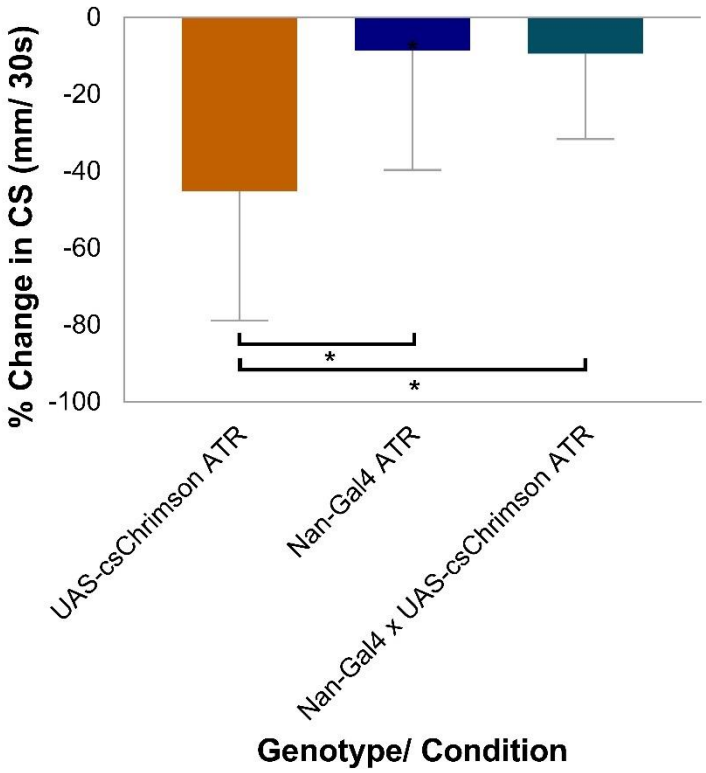

Figure 4.33: Acute stimulation of larval chordotonal neurons does not affect crawling speed. *% Change in CS (mm/ 30s) was % change in normalised crawling speed (CS, mm/ 30s) in background light vs. red light stimulation. There was no significant difference in % Change in CS between Nan-Gal4 x UAS-csChrimson (0.1 ± 5.17% Change in CS; n = 10 larvae) and Nan-Gal4 (-1.85 ± 6.67% Change in CS; n = 10 larvae, P = 0.998). In contrast, there was a significant difference between UAS-csChrimson ATR (-7.6 ± 6.82% Change in CS; n = 10 larvae) and Nan-Gal4 x UAS-csChrimson ATR (P = 0.025) and Nan-Gal4 ATR (P = 0.029). Statistical significance determined by one-way ANOVA (threshold for significance: P = 0.05; * = P ≤ 0.05).*

% Change in Peristaltic Wave Frequency (PWF) was also analysed. 'Before' and 'during' PWFs were normalised prior to calculating % Change in PWF. As for CS, there was no significant difference in % Change in PWF between nan-Gal4 x UAS-csChrimson ATR (0.5 ± 25.87%; *n* = 10 larvae) and nan-Gal4 ATR controls (2.63 ± 18.77%; *n* = 10 larvae), however, there was a significant difference between nan-Gal4 x UAS-csChrimson ATR or nan-Gal4 and UAS-csChrimson ATR (-34.55 ± 30.99%; *n* = 10 larvae; $P \leq 0.05$ or $P \leq 0.01$, respectively) (Figure 4.34).

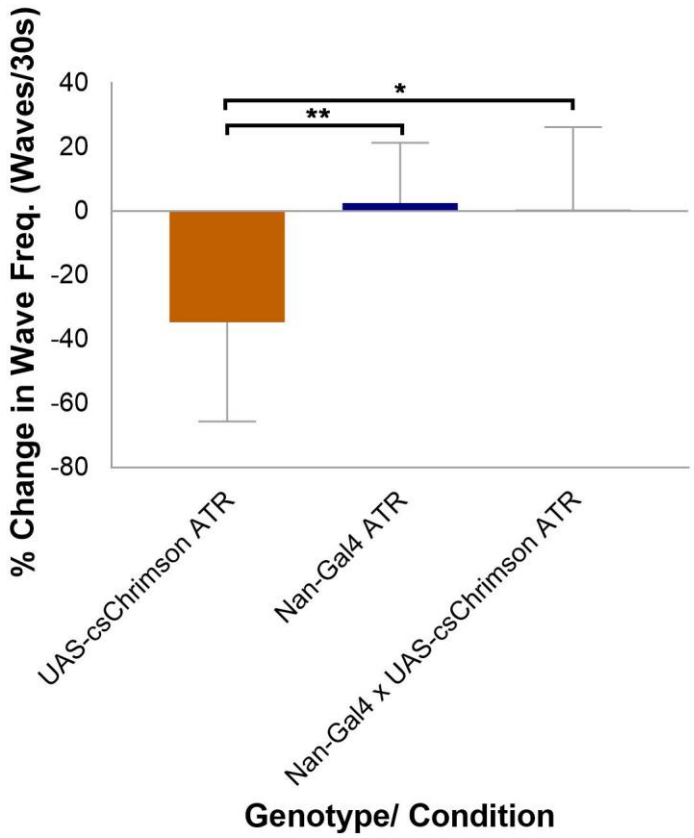

Figure 4.34: Acute stimulation of chordotonal neurons does not affect peristaltic wave frequency in larvae. *% Change in wave freq. (Waves/ 30s) was % change in peristaltic waves/ 30s (waves/ 30s) in background light vs. red light stimulation. There was no significant difference in % change in wave frequency between Nan-Gal4 x UAS-csChrimson (0.5 ± 25.87% Change in CS; n = 10 larvae) and Nan-Gal4 (2.63 ± 18.77% Change in CS; n = 10 larvae, P = 0.981). In contrast, UAS-csChrimson ATR % change in wave frequency (-34.55 ± 30.99% Change in CS; n = 10 larvae) was significantly lower than that of Nan-Gal4 x UAS-csChrimson and Nan-Gal4 ATR (P ≤ 0.014 and P ≤ 0.009, respectively). Statistical significance determined by one-way ANOVA (threshold for significance: P = 0.05; * = P ≤ 0.05, ** = P ≤ 0.01).*

% Change in Peristaltic Wave Duration was measured as mean % change in peristaltic wave duration (PWD, s) of larvae before and during red light stimulation, where red light stimulation depolarised ch neurons. Results from this analysis mirrored the outcomes of CS and PWF above (Figure 4.35). In summary, all three analyses pose that acute activation of ch neurons does not affect crawling in larvae. Thus, these data could support an alternative role for ch neurons in establishing normal crawling behaviour during development (only) (Hughes and Thomas, 2007; Fushiki, Kohsaka and Nose, 2011).

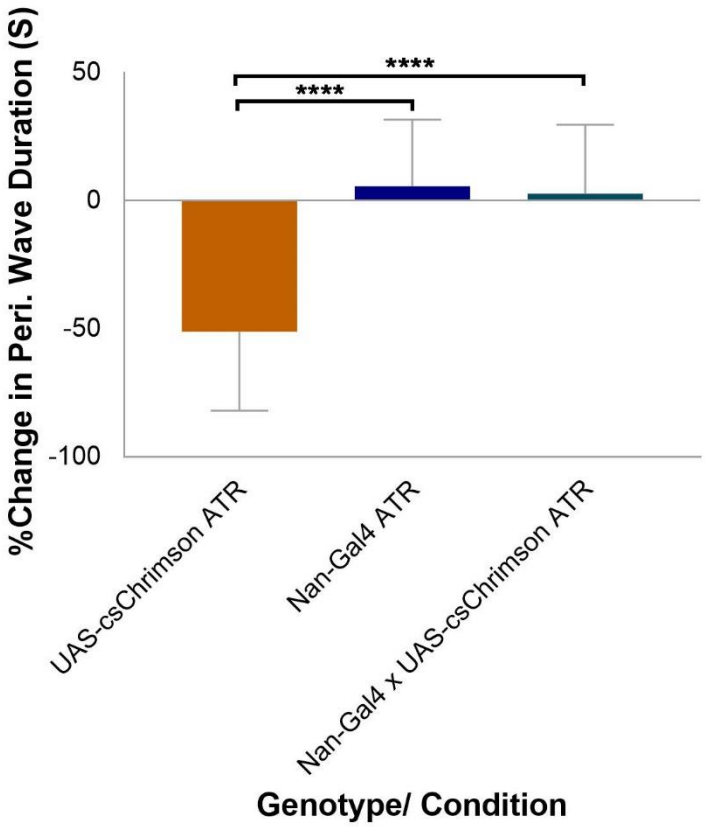

Figure 4.35: Acute stimulation of larval chordotonal neurons does not affect peristaltic wave duration. *% Change in Peri. Wave Duration ~~(s)~~(s) was % change in peristaltic waves duration ~~(s)~~(s) in background light vs. red light stimulation. There was no significant difference in % change in peristaltic wave duration between Nan-Gal4 x UAS-csChrimson (2.77 ± 26.89% change in Peri. Wave Duration; n = 10 larvae) and Nan-Gal4 (5.66 ± 18.77% Change in Peri. Wave Duration; n = 10 larvae, P = 0.916). In contrast, UAS-csChrimson ATR % change in peristaltic wave duration (-51.1 ± 30.9% Change in Peri. Wave Duration; n = 10 larvae) was significantly lower than that of Nan-Gal4 x UAS-csChrimson and Nan-Gal4 ATR (both P ≤ 0.0001). Statistical significance determined by one-way ANOVA (threshold for significance: P = 0.05; **** = P ≤ 0.0001).*

4.3.1.7 Dynein motors are necessary for larval chordotonal neuron function

Although there is evidence for dynein motor function in JO neurons for adult hearing, this has not been tested in larval ch neurons. As mentioned in the introduction to this chapter, *CG17669* is an orthologue of human *DNAAF3* and is necessary for dynein complex preassembly in *Drosophila* (unpublished data from Petra zur Lage). In *CG17669* mutants, dynein motors are completely missing from ch neuron cilia. Consequently, in order to investigate the requirement for dynein motors in larvae, *CG17669* mutant larvae were employed in behavioural and GCaMP experiments.

4.3.1.7.1 Loss of dynein arms in chordotonal neurons abolishes larval response to tone

Hearing assays were conducted on *CG17669* larvae. RT for *CG17669* -/- (0 RT count; *n* = 3 repeats, 15 larvae) was not significantly different to that for *CG17669* +/- (4.44 ± 0.69 RT count; *n* = 3 repeats, 15 larvae), however, this (lack of significance) is clearly due to a lack of power (*n* = 3) in for the heterozygous line. There was a significant difference between *CG17669* -/- and *Oregon-R* (wild-type) controls (5 RT count; *n* = 3 repeats, 15 larvae, $P \leq 0.05$ (Figure 4.36). Despite the lack of power, this comparison represents the first time that *CG17669* has been linked to defective hearing. This is important, as it confirms requirement of DNAAFs/dyneins for larval hearing and adds to the body of evidence that validates *CG17669* as a *Drosophila* model of human PCD (loss of ch neuron axonemal dynein arms, uncoordinated climbing phenotype, unpublished data from Petra zur Lage and Alexander Ahl). It also poses *Drosophila* larva hearing assays as an effective screen for PCD-related genes.

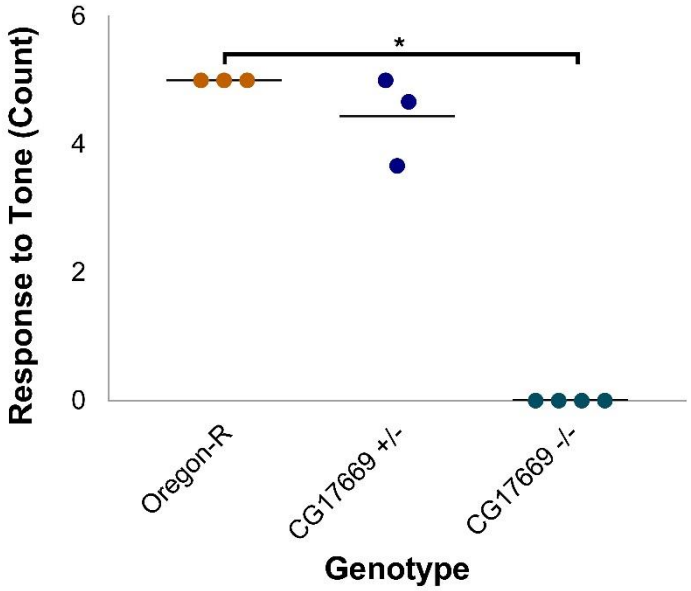

Figure 4.36: CG17669 may be necessary for larval hearing. *Response to Tone (RT, Count) was clear phenotypic response (e.g. contraction) to a 1000Hz tone observed in larvae crawling on a grape juice agar plate, recorded as mean score/ 5 larvae across 3-5 repeats (23.9-25°C, daylight). CG17669 -/- RT (0 RT count; n = 3 repeats, 15 larvae) was not significantly less than CG17669 +/- (4.44 ± 0.69 RT count; n = 3 repeats, 15 larvae, P = 0.2), but was to Oregon-R (wild-type) controls (5 RT count; n = 3 repeats, 15 larvae, P = 0.017). Shown as scatter plot, horizontal line is mean. Statistical significance determined by Kruskal-Wallis with Dunn's post-hoc test (threshold for significance: P = 0.05; * = P ≤ 0.05).*

Crawling experiments were performed on *CG17669* mutant larvae and surprisingly, (given that in this instance, power calculations based on previous work (Suslak, 2015) suggested a power of 0.8) there was no significant difference in CS for *CG17669* -/- (94.31 ± 32.3mm/ 120s; *n* = 16 larvae) and *CG17669* +/- (112.7 ± 21.75mm/ 120s; n = 16 larvae), whilst *Oregon-R* (wild-type) controls (90.83 ± 18.65mm/ 120s; *n* = 16 larvae) crawl significantly less than *CG17669* +/- (*P* ≤ 0.05, Figure 4.37). The contrast between crawling and hearing results for *CG17669* -/- could confuse the (chronic) role of ch neurons in larval locomotion and could make *CG17669* an interesting candidate to study for a possible difference in mechanisms of mechanosensation in chordotonal neurons. However, it is important to note that the crawling result for *CG17669* contradicts that obtained for another dynein assembly factor (*CG14353*, in Chapter 5). This, plus the downward trend and almost significant difference between *CG17669* +/- and *CG17669* -/- (-18.4 ± 9.74mm/ 120s, *P* = 0.1) suggest that despite efforts to prevent one, a type II error has occurred. The difference between the two controls (*Oregon-R* and *CG17669* +/-) is likely a result of genetic background.

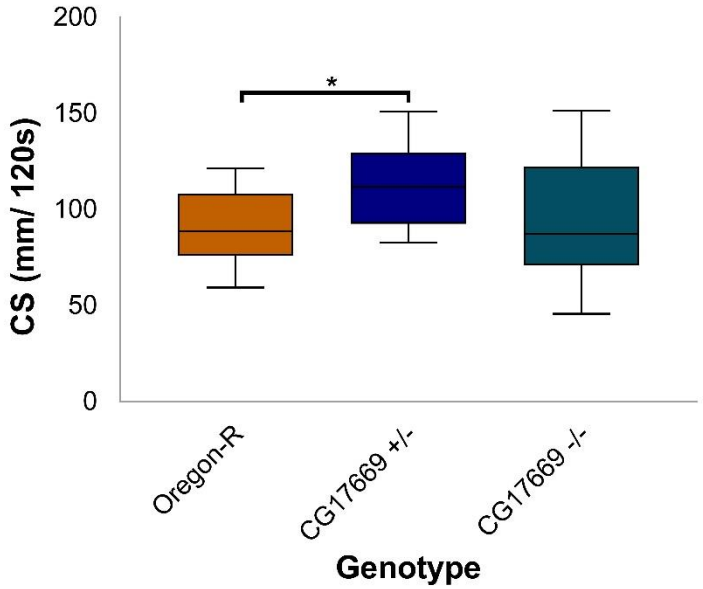

Figure 4.37: CG17669 may be necessary for normal larval crawling. *CS is crawling speed (mm/120s) recorded manually from larvae crawling on a 200mm x 200mm, 1% agar gel in a closed plastic container (23.9-25°C, daylight). There was a notable but insignificant difference in crawling between CG17669 -/- (94.31 ± 32.3mm/ 120s; n = 16 larvae) and CG17669 +/- (112.7 ± 21.75mm/ 120s; n = 16 larvae, P = 0.104), plus 17669 -/- and Oregon-R (wild-type) controls (90.83 ± 18.65mm/ 120s; n = 16 larvae, P ≤ 0.0001, P = 0.918). There was a significant difference between CG17669 +/- and Oregon-R (P = 0.044). Shown as whiskers minimum to maximum, horizontal line is median. Statistical significance determined by one-way ANOVA with Tukey's post-hoc test (threshold for significance: P = 0.05; * = P ≤ 0.05).*

4.3.1.7.2 CG17669 is necessary for larval chordotonal neuron response to tonal and muscle contraction stimuli

The mixed results from *CG17669* -/- behavioural experiments made it important to characterise *CG17669* -/- response to tone and muscle contraction in more detail. Thus, the same GCaMP protocol used previously was employed to investigate the role of *CG17669* (and therefore dyneins) in ch neuron responses.

Response to 1024Hz in *CG17669* +/- (Figure 4.38) and 1024Hz in *CG17669* -/- (Figure 4.39) larvae were recorded and quantified as previously. 1024Hz in *CG17669* +/- elicited short duration, large % change peaks (Figure 4.38, Mean Peak ΔF/ F0: 13.54 ± 3.63%; *n* = 14, 5 larvae) reminiscent of the response for 1024Hz. Homozygous mutation (*CG17669* -/-) abolished the response to 1024Hz (Figure 4.39, Mean Peak ΔF/ F0: 0.25 ± 0.22; *n* = 15, 5 larvae). Note that 'peaks' used in calculation for Mean Peak of *CG17669* -/- were derived from mean time~~(s)~~(s) of recording that correspond to peaks in *CG17669* +/-, to allow comparison despite lack of peaks present in *CG17669* -/-. There was a significant difference between mean Peak ΔF/ F0 (%) for 1024Hz in *CG17669* +/- and 1024Hz in *CG17669* -/- (Figure 4.40, $P \leq 0.0001$). This supports the idea that results from hearing (and crawling) experiments were underpowered and shows that *CG17669* (and therefore dyneins/ciliary motility) is necessary for ch neuron function in larval hearing.

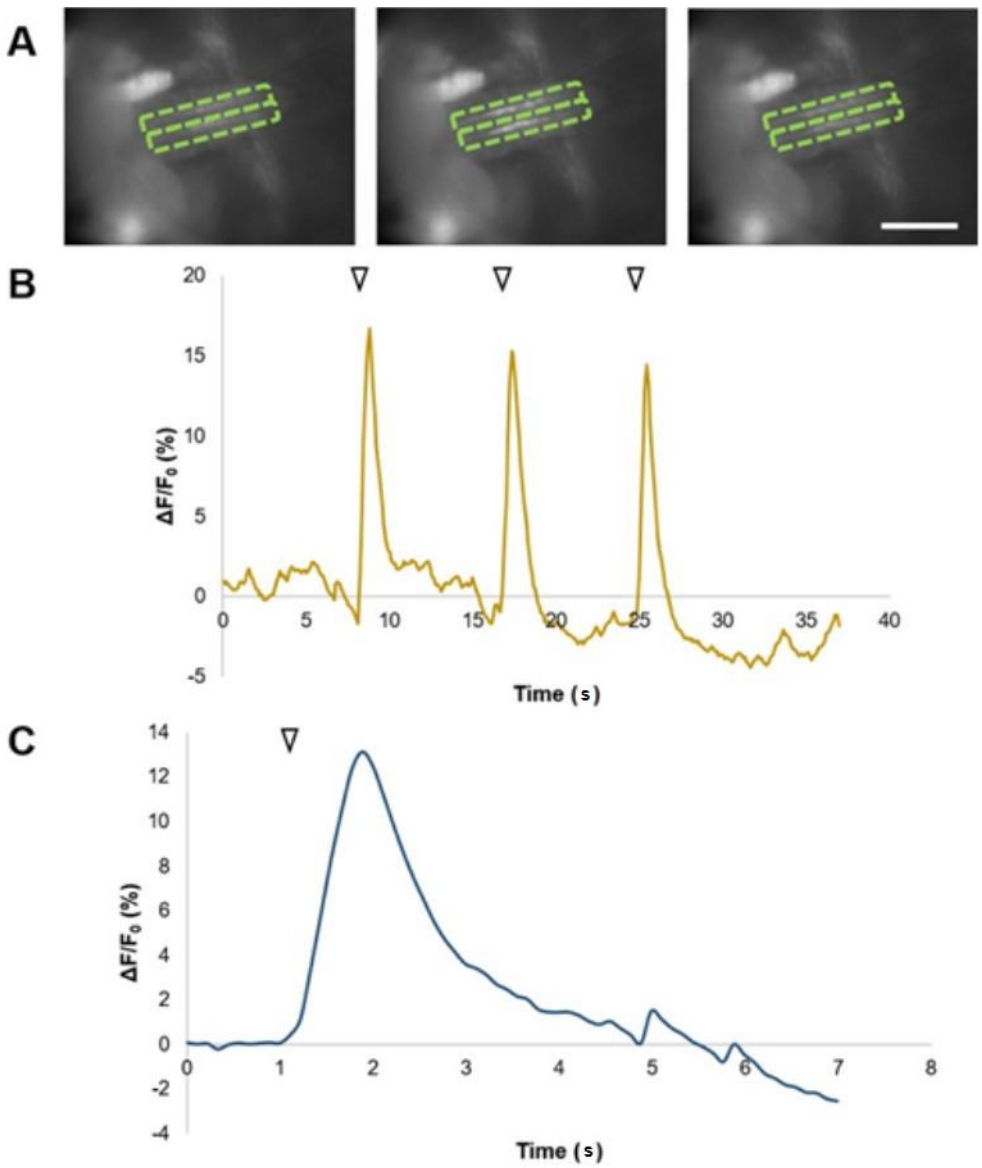

Figure 4.38: Chordotonal neuron response to 1024Hz stimulation in CG17669 +/- larvae, recorded at the ventral nerve cord. *Response as Peak ΔF/ F0 (%) of mean fluorescence of 2 ventral nerve cord (VNC) tracts in semi-intact larval preparations with chordotonal neuron-specific Gal4 driving GCaMP in a CG17669 +/- background (+ / CG17669; iav-Gal4/ UAS-GCaMP6f), stimulated by 1024Hz tuning fork (52.4 ± 2.8dB, n = 10 tones). A: Representative images of VNC before, during and after stimulation (left-right, respectively). Dashed lines indicate region of interest defined to produce traces. B: Representative trace (n = 3, 1 larva) where F_0 for ΔF/ F0 (%) is defined as mean F of: (0s - onset of 1st peak) + (end of 1st peak to onset of 2nd peak) + (end of 2nd peak to onset of 3rd peak). C: Mean response to 1024Hz stimulation in CG17669 +/- larvae (13.54 ± 3.63%; n = 14, 5 larvae) generated by aligning all peaks in recordings (from 0.5s before onset of peak to end of peak + 0.5s) where F_0 for ΔF/ F0 (%) is defined as mean F of 0.5s before onset of peak. Arrows in B and C indicate onset of stimulus. Scale bar is 100µm (shown in one panel for clarity, as all panels are the same size).*

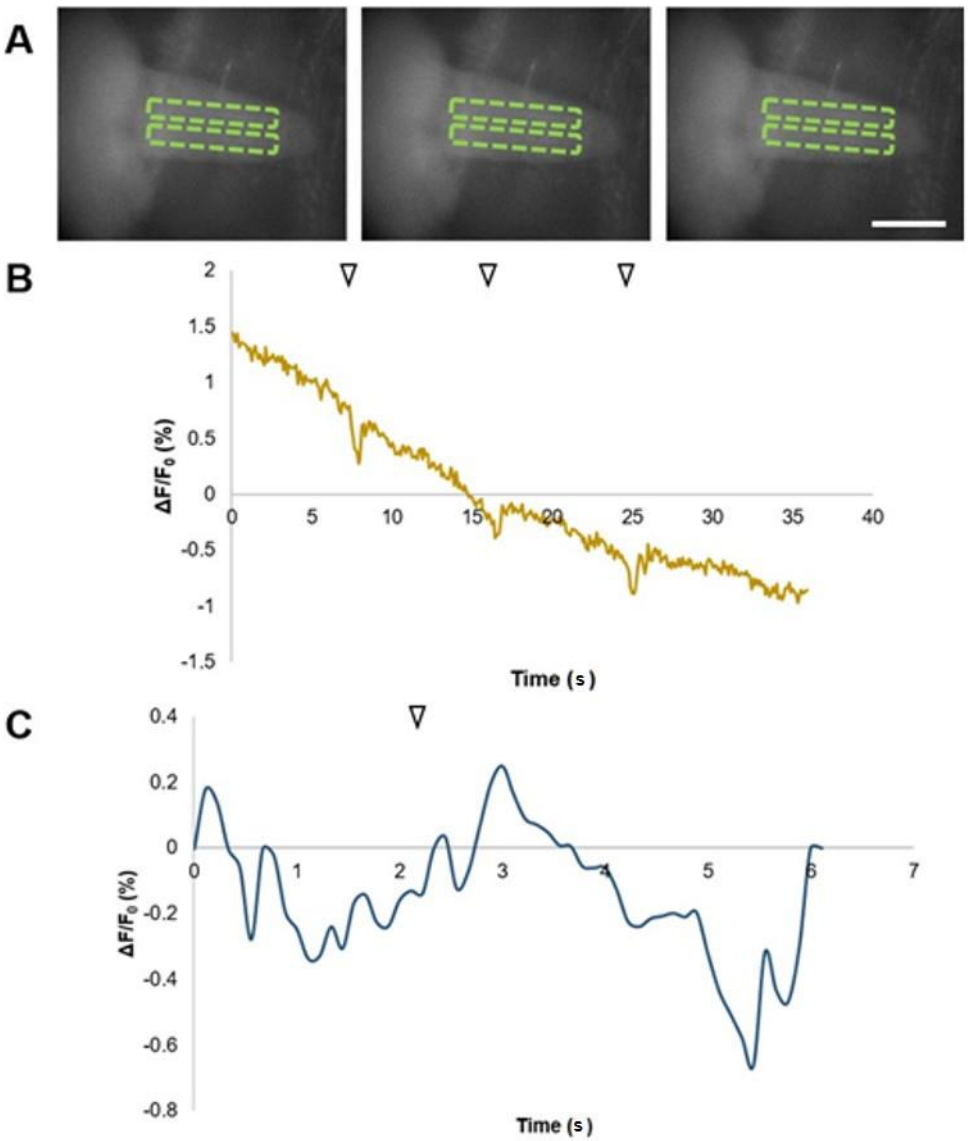

Figure 4.39: Chordotonal neuron response to 1024Hz stimulation in CG17669 -/- larvae, recorded at the ventral nerve cord. *Response as Peak ΔF/ F0 (%) of mean fluorescence of 2 ventral nerve cord (VNC) tracts in semi-intact larval preparations with chordotonal neuron-specific Gal4 driving GCaMP in a CG17669 -/- background (CG17669 / CG17669 ; iav-Gal4/ UAS-GCaMP6f), stimulated by 1024Hz tuning fork (52.4 ± 2.8dB, n = 10 tones). A, representative images of VNC before, during and after stimulation (left-right, respectively). Dashed lines indicate region of interest defined to produce traces. B, representative trace (n = 3, 1 larva) where F_0 for ΔF/ F0 (%) is defined as mean F of whole trace (to represent absence of peaks). C, mean response to 1024Hz stimulation in 17669 -/- larvae (0.25 ± 0.22; n = 15, 5 larvae) generated by analysing mean times (s, including F_0) of recordings that correspond to peaks in 1024Hz CG17669 +/- controls (no peaks present in traces of 1024Hz 17669 -/-). Arrows in B and C indicate onset of stimulus. Scale bar is 100µm (shown in one panel for clarity, as all panels are the same size).*

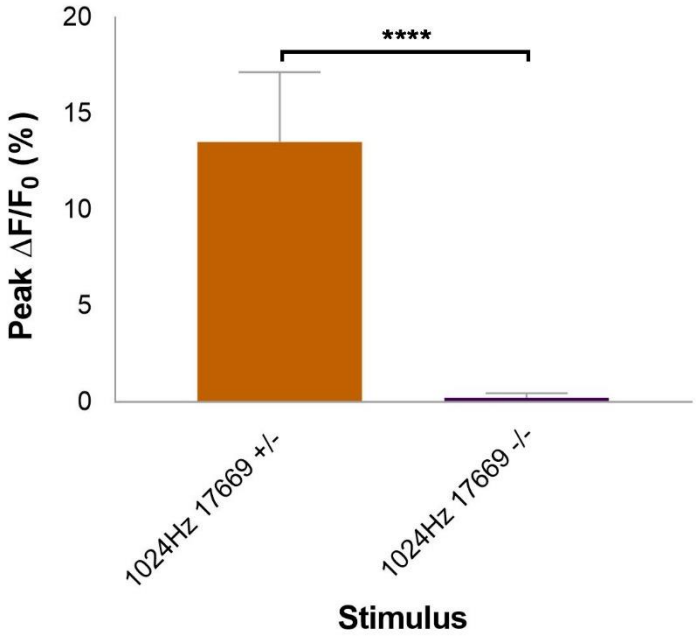

Figure 4.40: CG17669 is necessary for the chordotonal neuron response to 1024Hz stimulation. *Response as Peak ΔF/ F0 (%) of mean fluorescence of 2 ventral nerve cord (VNC) tracts in semi-intact larval preparations with chordotonal neuron-specific Gal4 driving GCaMP in a CG17669 +/- (+ / CG17669; iav-Gal4/ UAS-GCaMP6f) or CG17669 -/- (CG17669/ CG17669; iav-Gal4/ UAS-GCaMP6f) background, stimulated by 1024Hz tuning fork (52.4 ± 2.8dB, n = 10 tones). Response of 1024Hz CG17669 +/- (11.47 ± 2.93%; n = 39, 14 larvae) was significantly greater than of 1024Hz CG17669 -/- (0.25 ± 0.22; n = 15, 5 larvae, P ≤ 0.0001), which did not respond to stimulation. Shown by bars of mean ± S.D. Statistical significance determined by unpaired t test (threshold for significance: P = 0.05; **** = P < 0.0001).*

Response~~(s)~~(s) to muscle contraction in *CG17669* +/- (Figure 4.41) and *CG17669* -/- (Figure 2.42) larvae were recorded and quantified as above. Responses in *CG17669* +/- were characterised by long duration, moderate to large % change peaks of variable morphology (Figure 4.41, Mean Peak ΔF/ F0 (see C): 11.21 ± 4.7%; *n* = 11, 5 larvae), reminiscent of the response to muscle contraction. Homozygous mutation reduced the response, so only a small change in ΔF/ F0 (%) was observed during contraction (Figure 4.42, B and C. Peak ΔF/ F0 (see C): 1.87 ± 1.11%; *n* = 15, 5 larvae). The small peak in fluorescence that was recorded was likely due to movement of the preparation during contraction (Figure 4.42, A) and did not reflect a response from chordotonal neurons. As with above, 'peaks' used in calculation for (mean) Peak ΔF/ F0 of *CG17669* -/- were derived from mean times ~~(s)~~(s) of recording that correspond to peaks in *CG17669* +/-, to allow comparison despite lack of peaks present in *CG17669* -/-). Consistent with the 1024Hz in *CG17669* -/- result~~(s)~~(s), there was a significant difference between mean Peak ΔF/ F0 (%) for muscle contraction in *CG17669* +/- and muscle contraction in *CG17669* -/- (Figure 4.43, $P < 0.0001$). This shows that *CG17669* and so dyneins are necessary for larval proprioception.

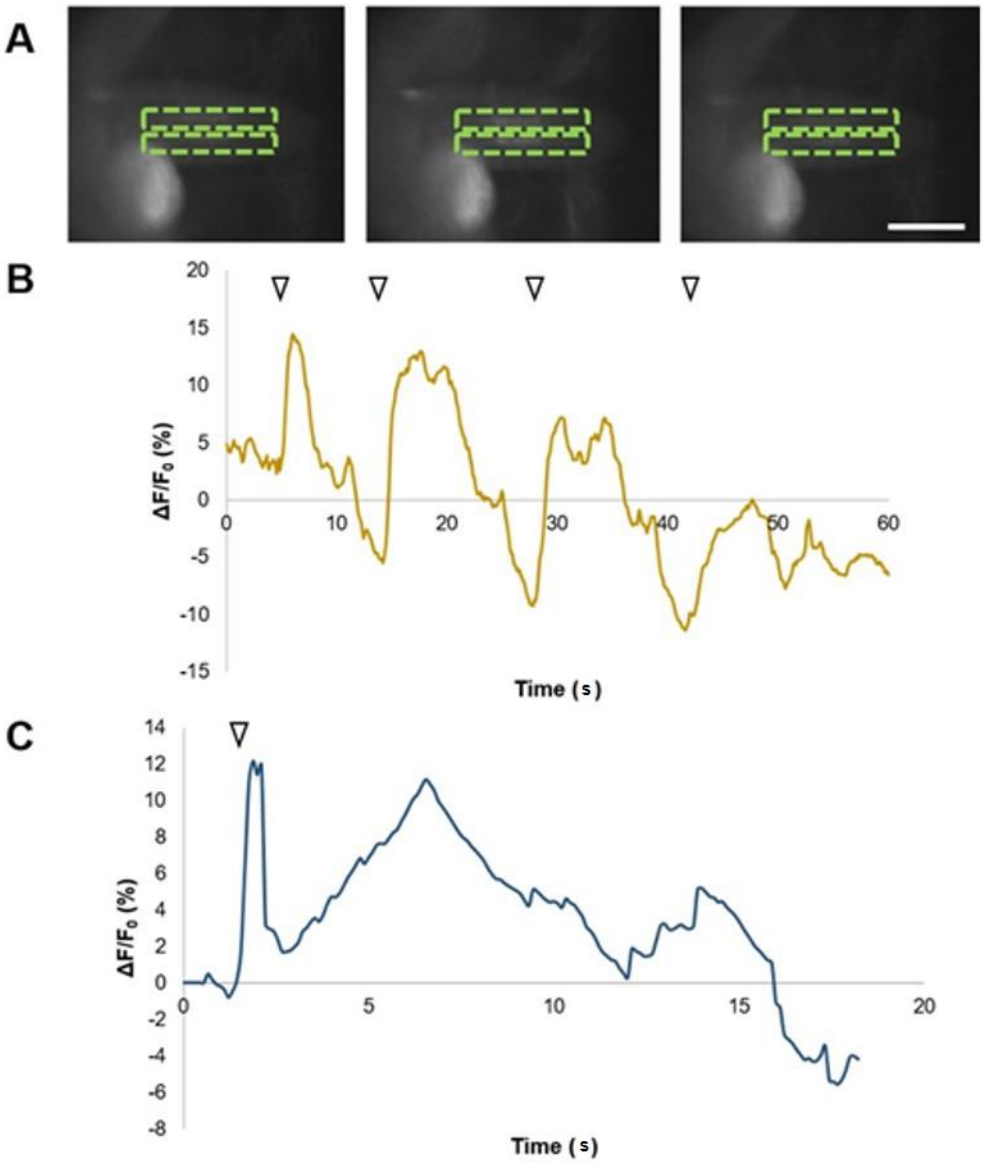

Figure 4.41: Chordotonal neuron response to muscle contraction in CG17669 +/- larvae, recorded at the ventral nerve cord. *Response as Peak ΔF/ F0 (%) of mean fluorescence of 2 ventral nerve cord (VNC) tracts in semi-intact larval preparations with chordotonal neuron-specific Gal4 driving GCaMP in a CG17669 +/- background (+/ CG17669; iav-Gal4/ UAS-GCaMP6f), stimulated by spontaneous muscle contraction~~(s)~~(s). A, representative images of VNC before, during and after stimulation (left-right, respectively). Dashed lines indicate region of interest defined to produce traces. B, representative trace (n = 3, 1 larva) where F_0 for ΔF/ F0 (%) is defined as mean F of: (0s - onset of 1st peak) + (end of 1st peak to onset of 2nd peak) + (end of 2nd peak to onset of 3rd peak). C, mean response to muscle contraction in CG17669 +/- larvae (11.21 ± 4.7%; n = 11, 5 larvae) generated by aligning all peaks in recordings (from 0.5s before onset of peak to end of peak + 0.5s) where F_0 for ΔF/ F0 (%) is defined as mean F of 0.5s before onset of peak). Arrows in B and C indicate onset of stimulus. Scale bar is 100µm (shown in one panel for clarity, as all panels are the same size).*

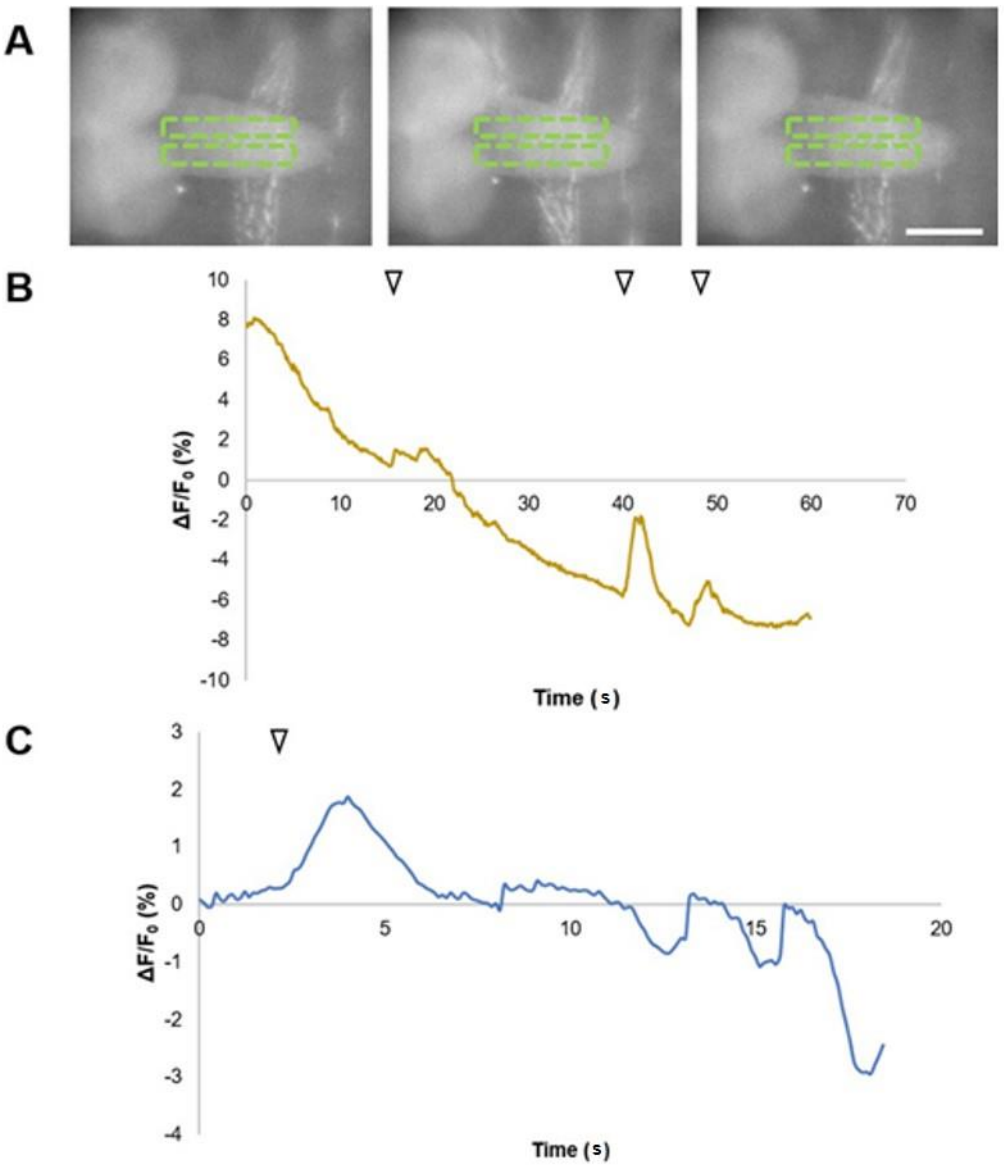

Figure 4.42: Chordotonal neuron response to muscle contraction in CG17669 -/- larvae, recorded at the ventral nerve cord. *Response as Peak ΔF/ F0 (%) of mean fluorescence of 2 ventral nerve cord (VNC) tracts in semi-intact larval preparations with chordotonal neuron-specific Gal4 driving GCaMP in a CG17669 -/- background (CG17669 / CG17669; iav-Gal4/ UAS-GCaMP6f), stimulated by spontaneous muscle contraction~~(s)~~(s). A, representative images of VNC before, during and after stimulation (left-right, respectively). Dashed lines indicate region of interest defined to produce traces. B, representative trace (n = 3, 1 larva) where F_0 for ΔF/ F0 (%) is defined as mean F of: (0s - onset of 1st peak) + (end of 1st peak to onset of 2nd peak) + (end of 2nd peak to onset of 3rd peak). C, mean response to muscle contraction in CG17669 -/- larvae (1.87 ± 1.11%; n = 15, 5 larvae) generated by analysing mean times ~~(s)~~(s) of recordings that correspond to peaks in muscle contraction CG17669 +/- controls (no peaks present in traces of muscle contraction CG17669 -/-). Arrows in B and C indicate onset of stimulus.*

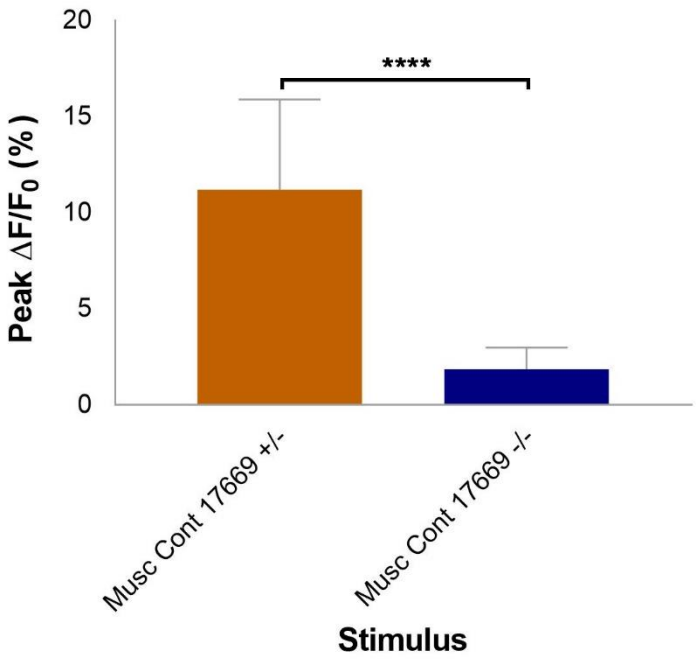

Figure 4.43: CG17669 is necessary for the chordotonal neurons' response to muscle contraction. *Response as Peak ΔF/ F0 (%) of mean fluorescence of 2 ventral nerve cord (VNC) tracts in semi-intact larval preparations with chordotonal neuron-specific Gal4 driving GCaMP in a CG17669 +/- (+ / CG17669; iav-Gal4/ UAS-GCaMP6f) or CG17669 -/- (CG17669 / CG17669; iav-Gal4/ UAS-GCaMP6f) background, stimulated by spontaneous muscle contraction~~(s)~~(s). Response to muscle contraction in CG17699 +/- (11.21 ± 4.7%; n = 11, 5 larvae) was significantly greater than to muscle contraction in CG17699 -/- (1.87 ± 1.11%; n = 15, 5 larvae, P ≤ 0.0001), which did not respond to stimulation. Shown by bars of mean ± S.D. Statistical significance determined by unpaired t test (threshold for significance: P = 0.05; **** = P < 0.0001).*

4.4 Discussion

4.4.1 Chordotonal neuron response to sound stimulation

4.4.2 Optimal frequency for stimulation of chordotonal neurons

GCaMP experiments employed in this research provided evidence to support ~1000Hz as the optimal frequency of stimulation for ch neurons. As mentioned in the results section, this agrees with previous work done in the Jarman laboratory, by Jennifer Lennon and Jilly Hope using behavioural hearing assays. However, it contradicts Zhang *et al.*, 2013, who reported peak response to a 500Hz pure tone. Differences in optimum frequency may be accounted for in contrasting experimental protocols/ genetics used to glean data. Zhang *et al.*, described peak response to 500Hz from: (1) GCaMP recordings of lch1-5 in larvae expressing an undisclosed "chordotonal-specific Gal4" (crossed to GCaMP5), in response to a pure tone; (2) electrophysiological recordings from nerve bundles severed from the VNC of larvae of an undisclosed genotype, in response to a pure tone (Zhang *et al.*, 2013). As detailed above, I recorded fluorescence change in iav-Gal4 x UAS-GCaMP6f larvae, in response to frequency stimulation by tuning forks (applied directly to the platform of the microscope used for recording). It could also be that tones provided by tuning forks are less consistent than electronic pure tones. This does not appear to be the explanation, however, as Lennon and Hope's experiments analysed peak response in freely-moving *Oregon-R* larvae using a pure tone. Zhang *et al.*, 2013 is not explicit about how the pure tone was applied in GCaMP and electrophysiology experiments; it is possible that the tone was played through a speaker that did not contact the surface on which larvae/larval preparations were being tested. In our experiments, the tone was applied with either the tuning fork or speaker in contact with the surface used for testing. This could facilitate a more direct transmission of frequency to ch neurons (than sound waves travelling through air) or could dampen the frequency transmitted. The latter could account for the difference in findings, so future research should use frequency sensors at the site of the larva/ preparation to check for damping.

The fact that Zhang *et al.*, 2013 did not detail the genotype of larvae expressing the "chordotonal-specific Gal4" and those used as wild-type/ controls in electrophysiology experiments, is problematic. It invites speculation on the degree of specificity of the Gal4 lines used. Also, the tuning forks used here, resonated with different intensities (256Hz, 53.1 ± 3.21dB; 512Hz, 44.3 ± 2.16dB; 1024Hz, 52.4 ± 2.8dB) and so complicated results. In future, volume should be fixed to control for accurate assessment of frequency. This is particularly important given that the sound intensity-ΔF/ F0 relationship described in Zhang *et al.*, demonstrates a ~10% change in ch neuron response for 10dB increase in tone volume (60dB

- 70dB, (Zhang *et al.*, 2013)). Finally, Zhang *et al.* describe no response to stimulation at 50dB, which contrasts responses to ~44-53dB here and adds to the validity of questioning the method of application of stimulus in hearing experiments. Thus, future work should control for volume when testing frequency, and be explicit/ consistent in how stimulus is applied.

4.4.3 Specialisation of subpopulations of chordotonal neurons

Ch neuron functional specialisation in adult *Drosophila* is well established. Early work identified specialisation of ch neurons in large insects (Field and Pfluger, 1989; Stein and Sauer, 1999; Sauer and Stein, 1999) and more recent work has documented specialisation of ch neurons in *Drosophila*; JONs are categorised in groups (A-E), based on axonal projections to AMMC (Kamikouchi, Shimada and Ito, 2006), which correspond to sensitivity to sound and vibration (Effertz, Wiek and Gopfert, 2011; Yorozu *et al.*, 2009; Matsuo *et al.*, 2014)). Similarly, fco axons in have been separated into 3 genetically-defined groups – claw, club and hook axons – in the VNC, with specific sensitivity to joint position, bidirectional movement and movement direction, respectively (Mamiya, Gurung and Tuthill, 2018). Of these 3 groups, only club neurons are sensitive to vibration, with a peak sensitivity to 400Hz stimulation encoded in a frequency-specific spatial map visible at axon terminals (Mamiya, Gurung and Tuthill, 2018).
Despite reports of ch neuron specialisation in adult insects, nothing has been published on *Drosophila* larval ch neurons. This is particularly surprising given the potential to exploit the simple layout of larval ch neurons (easier to study than JONs) to improve our understanding of hearing. My GCaMP recordings from ch neuron cell bodies showed that all 3 subpopulations of larval ch neurons (lch1-5, vch1, vchAB) respond to sound. This contrasts with the specialisation of auditory ch neurons reported elsewhere (e.g. group A and B JONs respond to sound, whereas C and E are involved in gravity and wind detection (Yorozu *et al.*, 2009)).
The tone-response results also suggest that no larval ch neurons are specialised for proprioception. This implies that all larval ch neurons are bifunctional, able to respond to vibration and stretch stimuli. However, this has only been demonstrated directly for lch1-5 so far. The intention was to develop this research by recording lch1-5, vch1 and vchAB response to muscle contraction, however, the significant displacement generated by muscle contraction made it impossible to image vch1 and vchAB neurons (they moved out of microscope field of view).

Although all larval ch neurons responded to tones, GCaMP responses showed interesting differences in the amplitude and dynamics of responses in different neurons within the subpopulations. Namely, lch1 response amplitude was significantly lower than lch2-5 response amplitude to 1024Hz stimulation. Similarly, vchB response amplitude was lower than vchA response amplitude to 1024Hz. vchB response also occurred over a shorter time course

(mean response time as onset of peak to cessation was ~2.5s, whereas vchA was ~3s). This could point to tuning of individual neurons within subpopulations, either to specific frequencies (e.g. lch1 and vchB response amplitude may be higher in response to ~500Hz than to ~1000Hz), or to different intensities. Either frequency or sound intensity could be encoded in larvae as different ch neuron responses. Such a mechanism would resemble human hair cells that are tuned to specific frequencies, or human auditory neurons that require different thresholds of stimulus for activation. Another possibility is that the differences are indirect indicators of specialisation to distinct physiological functions. For example, the difference in dynamics between vchA and vchB could equate to phasic and tonic roles observed in *Drosophila* adult fcos (Mamiya, Gurung and Tuthill, 2018). Thus, the reasons for the difference~~(s)~~(s) in amplitude and dynamics of ch neuron responses to 1024Hz need to be elucidated in future research. Specifically, characterising the responses of different ch neurons to different frequencies would serve as a starting point to analyse the sensitivity of individual neurons to frequencies in larval hearing range. These results could also be compared to those for other types of stimulus (e.g. proprioceptive), if the difficulties of recording responses of individual neurons to proprioceptive stimuli were overcome.

4.4.4 Acute versus chronic function~~(s)~~(s) of larval chordotonal neurons as proprioceptors

For a long time, it has been assumed that the primary (classical) role of larval ch neurons as stretch receptors is to provide proprioceptive feedback during larval locomotion. Work on various ch neuron mutants supported this. However, my GCaMP data suggest that ch neurons are more responsive to vibration stimulation than they are too large, slow movement (spontaneous muscle contraction). Similarly, previous research that dissected the requirements of different mechanosensory neurons showed that ch neurons are less important than md and dbd neurons in crawling behaviour (Hughes and Thomas, 2007). One difference that might reconcile these discrepancies is that mutant analyses tend to ablate ch neuron function chronically, whilst GCaMP records acute responses of the neurons. This raises the possibility that ch neurons provide long-term or developmental proprioceptive information rather than ‘real-time’ acute feedback to control peristalsis. In this regard, the results of my attempt to activate ch neurons acutely via optogenetic stimulation in freely moving larvae is interesting. Specifically, the results suggested that ch neuron stimulation does not affect crawling speed, peristaltic wave frequency or peristaltic wave duration. These results are, however, limited by a strange effect observed in UAS-csChrimson ATR larvae; light stimulation of this control resulted in a significant decrease in all 3 parameters versus nan-Gal4 ATR and nan-Gal4 x UAS-csChrimson ATR. This is unexpected, as light sensitivity should only be observed in animals expressing the driver and reporter (nan-Gal4 x UAS-csChrimson ATR),

as opposed to the reporter alone. It is difficult to explain this by non-specific expression of channelrhodopsin in neurons that affect crawling, e.g. bd and/ or type I md neurons. Future work could confirm channelrhodopsin expression in the reporter line, to reflect on the likelihood that this is the case. Potentially, these data support Hughes and Thomas and Cheng *et al.*, in suggesting a negligible acute role for ch neurons in larval crawling (Hughes and Thomas, 2007; Cheng *et al.*, 2010). Furthermore, Cheng *et al.* describes NompC expression in bd/dmd1 neurons as sufficient for normal larval crawling, which is reflected in Piezo KO crawling experiments here (Chapter 3). Thus, this research contributes to the notion that ch neurons are likely involved in development of normal locomotion (Fushiki, Kohsaka and Nose, 2011; Hughes and Thomas, 2007), or perhaps even for homeostasis, but are not as important as other neurons in the modulation of peristaltic waves.

4.4.5 The primary mechanoelectric transducer in mechanosensation

The findings reported here are consistent with other work in showing that *iav* and *NompC* are necessary for larval hearing (Figures 17 and 18; (Gong *et al.*, 2004; Gopfert *et al.*, 2006; Lehnert *et al.*, 2013; Zhang *et al.*, 2013)). The present research also observes that *iav[3621] -/-* hearing phenotype was more severe than that for *NompC*[1]/[3], which could support the nan-iav model of mechanosensation in hearing (reviewed in (Albert and Gopfert, 2015)); the slow-adapting response to tone of *iav* mutants could reflect that nan-iav functions as the primary MET, whilst the fast-adapting response of *NompC* mutants could reflect a role of the protein in active amplification. In addition, supporting prior (hearing) results using the lines: *iav[3621] -/-* and *NompC*[1]/[3], validated their use to compare the role of iav and NompC in hearing to that in crawling. This would indicate whether different mechanisms of mechanosensation in ch neurons, feedback on different physiological functions in larvae.

Like the results for hearing experiments, crawling experiment results showed no significant difference in crawling speed between *iav*[3621] -/- and attached-X controls, but clearly implicated *NompC* in the behaviour. The latter confirms other research (Cheng *et al.*, 2010) and whilst comparison could suggest that *NompC* is necessary for normal crawling and *iav* is not, this is caveated by an unhealthy background in *iav*[3621] larvae; *iav*[3621] +/- animals were noticeably slower than other controls, as confirmed by comparison to *Oregon-R* (55.18 ± 15.04mm/ 120s; n = 16 larvae versus 90.83 ± 18.65mm/ 120s; n = 16 larvae, $P \leq 0.0001$). This makes it difficult to conclude any more than *NompC* is, and *iav* may be, involved in larval crawling. These experiments should be repeated in future, using an *iav* mutant created in a healthy background.

Pilot experiments using nan-iav agonist pymetrozine were promising: 200µM pym abolished ch neuron response to 1024Hz and crucially, abolished ch neuron response to muscle contraction too. This is the first time nan-iav has been linked to larval locomotion explicitly (ch neurons are often implicated without evidence of the mechanism involved (Caldwell *et al.*, 2003; Fushiki, Kohsaka and Nose, 2011)) and is counter to the idea above that ch neurons have a chronic rather than acute role crawling (Hughes and Thomas, 2007; Caldwell *et al.*, 2003; Fushiki, Kohsaka and Nose, 2011). These (pym experiment) results are particularly interesting as they agree with electrophysiology data gleaned from JONs (200µM pym abolishes CAPs of ch neurons in wild-type flies (Nesterov *et al.*, 2015)) and future work should expand on them to confirm the preliminary suggestion of a single, nan-iav-dependent mechanism of mechanosensation shared by hearing and proprioception in ch neurons.

This work was able to further the concept of a single, nan-iav-dependent mechanism of mechanosensation in ch neurons, by contributing to the debate on a role for DmPiezo. Kim *et al.* showed expression of DmPiezo in JONs, suggesting a role for the channel in hearing (Kim *et al.*, 2012); Zhang *et al.* countered this suggestion by showing no change in sound response score in *DmPiezo*^{KO} larvae versus wild-type controls (Zhang *et al.*, 2013). Indeed, DmPiezo is assumed to play a role in larval locomotion (Suslak *et al.*, 2015c) and is not normally associated with hearing. Here, 30µM broad-spectrum MSC blocker RR did not affect ch response to 1024Hz or muscle contraction. DmPiezo knockdown confirmed this finding; DmPiezo RNAi did not affect ch neuron response to 1024Hz or muscle contraction. These results are, therefore, in agreement with Zhang *et al.*, 2013. Note that conclusions made from the RR result are subject to proof that 30µM RR provides an effective block of DmPiezo. Suslak et al, 2015 demonstrate a clear effect on DmPiezo, whereas Coste *et al.*, 2012 report no effect on DmPiezo. This (putative) effect should be clarified by future work.

4.4.6 Dyneins in larval hearing and proprioception

This research demonstrated that dynein assembly factor *CG17669* (homologue of PCD-associated gene *DNAAF3*) is necessary for larval hearing and crawling. Results from behavioural assays were limited by a lack of power but results from GCaMP assays were straightforward: *CG17669 -/-* abolished response to 1024Hz and muscle contraction versus *CG17669 +/-* controls. This agrees with other research that links dynein assembly factors to hearing (Moore *et al.*, 2013; zur Lage *et al.*, 2018), so adds to evidence that dyneins are the motors required for active amplification in adult *Drosophila* (Karak *et al.*, 2015).

The GCaMP data presented here represents the first time dyneins have been linked to proprioception (and so crawling) in *Drosophila*. This is interesting given the focus on dyneins

in hearing ((Karak *et al.*, 2015; Moore *et al.*, 2013; zur Lage *et al.*, 2018)) and confirms that despite the differences in frequency and amplitude of stimulation elicited by hearing and proprioceptive stimuli, ch neurons operate one mechanism of mechanosensation across both. I think that these are the most interesting results of the chapter. Future work should investigate how and why a mechanism that appears to be tuned to hearing frequencies (1024Hz here, 500Hz in (Zhang *et al.*, 2013)) responds to much lower frequency and higher amplitude proprioceptive stimuli with: (1) little utility in larvae (ch neurons only provide negligible contribution to crawling); (2) so much utility in adults. It would also be interesting to pair this with study of remodelling of the PNS during pupation, to shed light on how a relatively simple system of 8 ch neurons (per hemisegment) in larvae, develops to form the (specialised neurons of) complex JOs and fcos.

5 *Drosophila* behavioural experiments as screens for genes associated with primary ciliary dyskinesia

5.1 Introduction

In the previous chapter, I focussed on the physiology of chordotonal neurons as a model for understanding mechanisms of mechanosensation. Since ciliary motility, powered by axonemal dyneins, is central to mechanotransduction by chordotonal neurons, these neurons can also be used as a model for gene discovery and validation for the human disease, Primary Ciliary Dyskinesia (PCD). This chapter addresses that model.

PCD is a congenital reduction or absence of ciliary motility that may affect 1:10,000-1:20,000 births (Kuehni *et al.*, 2010), but is likely more common (prevalence of 1:2,265 in a British Asian cohort (O'Callaghan, Chetcuti and Moya, 2010)). It is a serious disorder associated with chronic respiratory tract infections, glue ear/ hard of hearing, situs inversus (~50% of cases), heart defects and a 5% all-cause mortality rate (Shah *et al.*, 2016). It has a major impact on patients' lives; besides the symptoms, median age for diagnosis is just 5.3 years old (Kuehni *et al.*, 2010) and a patient may experience 50-100 visits to a physician before diagnosis (Sommer *et al.*, 2011). If patients survive long enough for it to be tested, they also show infertility. All these diverse symptoms have a single underlying cellular cause: loss or reduction of ciliary motility. This affects motile cilia in the airways and ear (mucociliary clearance), the embryonic node (left-right organ asymmetry), the fallopian tubes (female infertility) and the sperm flagellum (male infertility).

PCD is caused by mutation of any 1 of at least 40 genes associated with ciliary motility (Mitchison and Valente, 2017) (Figure 5.1). Ciliary motility is driven by dynein motors, comprised of outer and inner dynein arms (ODAs and IDAs). ODAs and IDAs act on 9 microtubule doublets that populate the cilium to generate movement and are made up of heavy chain (HC), intermediate chain (IC) and light chain (LC) proteins that determine the characteristics of the motor (e.g. HCs may determine cilium beat strength and waveform (King and Patel-King, 2015)). Many PCD mutations are in genes that encode dynein subunits. Others are in genes encoding other parts of the motile ciliary machinery, such as radial spokes and nexin links. A third class of PCD mutations affect genes that are required for dynein motor assembly in the cytoplasm or transport (by intraflagellar transport, IFT) into the cilium. Dynein motors are assembled by a group of at least 11 proteins known as dynein assembly factors (DNAAFs, (Mitchison and Valente, 2017)), which were mostly discovered in humans as PCD causative genes. Interestingly, dyneins and dynein assembly factors are well conserved in

eukaryotes, including *Drosophila,* so that model organisms have contributed greatly to discovery and/or validation of new DNAAFs. In *Drosophila*, this conservation includes orthologs of almost all (human) genes associated with PCD (e.g. *ZMYND10*, *CG11253*; *DNAAF3*; *CG17669*; *HEATR2, CG31320*; *Wdr92, CG14353;* genes given as human, *Drosophila* (zur Lage, Newton and Jarman, 2019)). This, in addition to the established benefits of using *Drosophila* as a model organism over alternatives (tractable genetics, low cost, no need for licence to experiment in animals), makes the fruit fly an excellent option for characterising the function of known PCD genes, and for discovery of candidate genes that when mutated, might be considered as a cause of PCD. This is relevant because the underlying mutation is still unknown in some 30% of PCD patients.

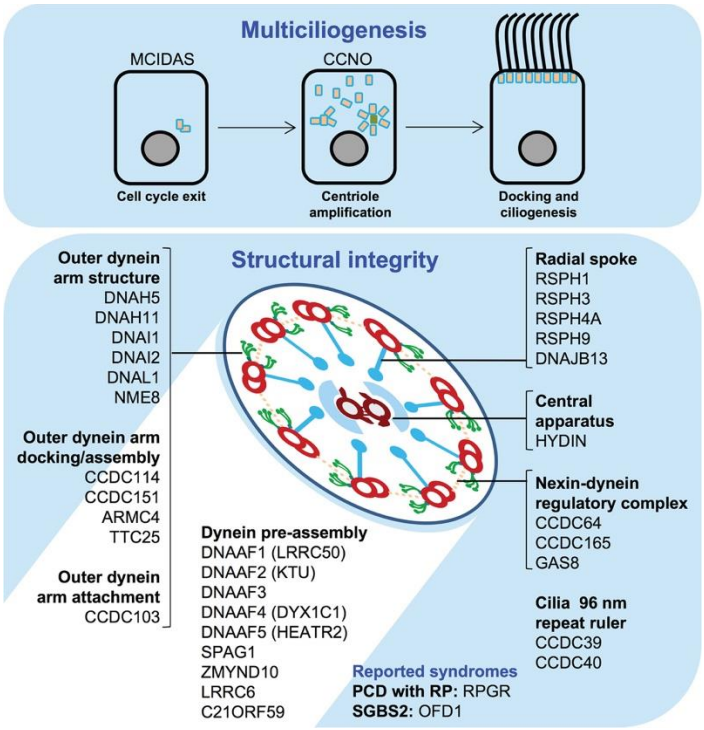

Figure 5.1: Summary of ciliary motility proteins affected by mutations in PCD. *Taken from Mitchison and Valente (2016).*

Focussing on known PCD genes confirms the opportunity to use *Drosophila* to identify new PCD gene candidates. For example, a transcriptome analysis of ch neurons conducted in 2011, identified enriched expression of all known DNAAFs during ch neuron development (Cachero *et al.*, 2011; zur Lage, Newton and Jarman, 2019). This includes, for example, the orthologue of human *DNAAF3, CG17669*. *DNAAF3* mutants lack ODAs and IDAs and suffer PCD (Mitchison *et al.*, 2012) and work in the Jarman lab has confirmed that *CG17669* is involved in dynein assembly (Petra zur Lage and Andrew Jarman, manuscript in preparation). This suggests that the ch neuron transcriptome data could reveal other candidates for DNAAFs and therefore for PCD. Indeed, analysis of the transcriptome data led to the discovery

of new *Drosophila*/human PCD genes *CG11253/ZMYND10* and *CG31320/HEATR2* (Moore *et al.*, 2013; Diggle *et al.*, 2014) and identified enriched expression of *CG14353*, an orthologue of human *Wdr92.* Recent work has shown that *CG14353* interacts with HSP90 cochaperone RT2P to assemble dynein complexes, so that *CG14353* mutants demonstrate a PCD-like phenotype; adults lack ODAs and IDAs, are hard of hearing and uncoordinated (zur Lage *et al.*, 2018).

The Jarman laboratory has identified a further 2 candidate DNAAFs in the ch neuron transcriptome recently, and they are the subject of this chapter. Specifically, the transcriptome analysis revealed enriched expression of *CG34297* and *CG6980* (orthologues of human *TTC12*) in ch neuron development. These genes encode related proteins with TPR domains (tetratricopeptide repeat) that are predicted to interact with the chaperone HSP90 (Haslbeck *et al.*, 2013). This feature, combined with expression restricted to developing ch neurons, suggests that *CG34297* and *CG6980* may be new dynein assembly factors. Preliminary experiments by Alexander Ahl have shown that *CG34297* -/- and *CG6980* -/- mutant adults are uncoordinated and infertile (unpublished, Alexander Ahl). If confirmed, this would make human *TTC12* an excellent candidate gene for PCD. However, in contrast to the complete loss of dynein motor arms in *CG17669* and *CG14353* mutants, TEM of *CG34297* -/- and *CG6980* -/- ch neuron cilia revealed only a partial loss or no loss of dynein motor arms in adult antennae, respectively (unpublished, Alexander Ahl). Thus, the matching phenotypes (uncoordinated and infertile) but contrasting TEM data of *CG17669* and *CG14353* versus *CG34297* and *CG6980* mutants, suggests that more evidence is required to develop the latter two as candidates for PCD.

Clearly, identifying new gene candidates for PCD is an opportunity for earlier diagnosis and treatment, and *Drosophila* represents an excellent model organism to use in this research. Consequently, this chapter focusses on validating and trialling simple behavioural experiments as screens for novel PCD candidate genes identified by microarray. Previously, screening has concentrated on adult proprioceptive and hearing assays as probes of adult ch neuron function. In this chapter, I investigate the use of larval assays as cost- and time-effective alternatives.

5.2 Aims

1. Test the hypothesis that ciliary immotility leads to behavioural dysfunction, by testing hearing and crawling in assumed and establish PCD gene mutants, *CG14353 -/-* and *CG17669 -/-*. If the hypothesis is true, it validates the use of hearing and crawling assays as screens for genes associated with PCD. It also indicates the quality of *Drosophila* as model for PCD research.

2. Test the hypothesis that *CG34297* and *CG6980*, and *CG34297*, *6980* (double) mutant larvae demonstrate a PCD-like phenotype, despite partial or no loss of dynein arms. I will use hearing and crawling assays to test the hypothesis. If it is true, it suggests that the PCD-like phenotype~~(s)~~(s) seen in affected larvae may be due to a mechanism besides loss of motor protein function. It also furthers the case for *CG34297* and *CG6980* to be considered as PCD candidate genes

5.3 Results

Ciliary motility genes identified by the Cachero *et al.*, 2011, were compared to those with an established PCD-like phenotype (*CG14353*) or that are known to cause PCD (*CG17669*), to examine the effectiveness of larval hearing and crawling experiments as screens for PCD-related genes.

5.3.1 CG17669 and CG14353 mutant larvae confirm response to tone assays detect hearing loss in primary ciliary dyskinesia gene mutations

Hearing experiments documented in Chapter 3, demonstrated that *CG17669* mutation abolished Response to Tone (RT) in larvae. This suggests that RT could be used as a simple behavioural readout to screen for other PCD candidate genes. Similar larval hearing loss was reported for *CG14353* -/- by zur Lage *et al.*, 2018. Therefore, here I used *CG14353* -/- larvae in hearing experiments to corroborate the use of RT in screening for PCD candidates.

Hearing experiments were carried out as in Chapter 4, with each condition being replicated 3 times (for 15 larvae each). As expected and shown by zur Lage *et al.*, the was a significant difference between RT for *CG14353* -/- (0 RT count; n = 3 repeats, 15 larvae) and *CG14353* +/- (5 RT count; n = 3 repeats, 15 larvae, P = ≤ 0.05) and *Oregon-R* (wild-type) controls (5 RT count; n = 3 repeats, 15 larvae, P = ≤ 0.05 (Figure 5.2)). This supports the use of RT experiments to screen for PCD candidate genes, following the protocol described in the present research (Chapter 2).

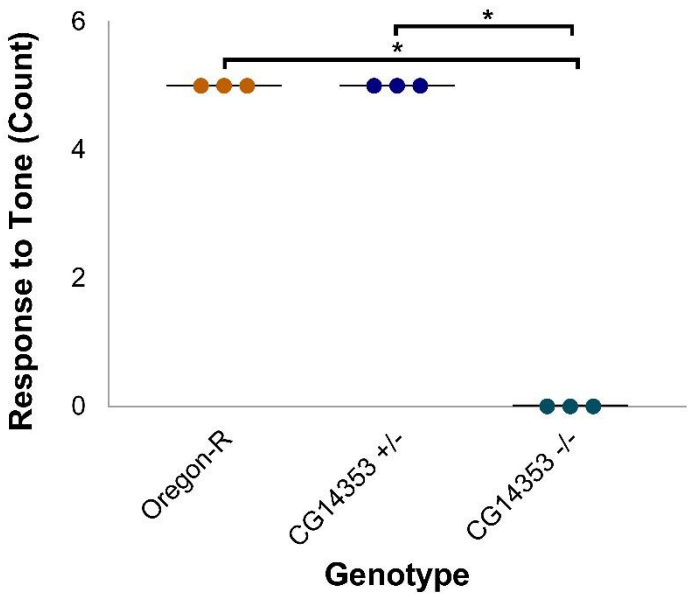

Figure 5.2: Chordotonal neuron function is necessary for larval hearing. *Response to Tone (RT, Count) was scored as clear phenotypic response (e.g. contraction) to a 1000Hz tone observed in larvae crawling on a grape juice agar plate, recorded as mean score per 5 larvae across 3-5 repeats (23.9-25°C, daylight). There was a significant difference in RT between CG14353 -/- (0 RT count; n = 3 repeats, 15 larvae) and CG14353 +/- (5 RT count; n = 3 repeats, 15 larvae, P = 0.043) and Oregon-R (wild-type) controls (5 RT count; n = 3 repeats, 15 larvae, P = 0.043). Shown as scatter plot, horizontal line is mean. Statistical significance determined by Kruskal-Wallis with Dunn's post-hoc test (threshold for significance: P = 0.05; * = P ≤ 0.05).*

5.3.2 Crawling assays of CG17669 and CG14353 mutant larvae confirm reduced crawling speed in primary ciliary dyskinesia gene mutants

Several studies suggest that ch neuron function is required to provide proprioceptive feedback to control larval crawling (Fushiki, Kohsaka and Nose, 2011; Caldwell *et al.*, 2003). Therefore, larval crawling assays may be another means to screen *Drosophila* larvae for PCD-related phenotypes. Crawling data could also support hearing data, validating candidacy posed by either screen alone. However, in Chapter 3, I found that the results of crawling assays performed on *CG17669* -/- mutants were inconclusive. This made it important to confirm the findings of zur Lage *et al.*, 2018 (that *CG14353* -/- larvae are uncoordinated) by using *CG14353* -/- larvae in crawling experiments.

Crawling experiments were carried out as in Chapter 3. CS for *CG14353* -/- (50.77 ± 14.65mm/ 120s; n = 16 larvae) was significantly slower than *CG14353* +/- (107.1 ± 15.64mm/ 120s; n = 16 larvae, $P \leq 0.0001$) and *Oregon-R* (wild-type) controls (90.83 ± 18.65mm/ 120s; n = 16 larvae, $P \leq 0.0001$), whilst *Oregon-R* crawled significantly slower than *CG14353* +/- ($P \leq 0.05$) (Figure 5.3). Therefore, *CG14353* is necessary for normal larval crawling. This agrees with the aforementioned data from (zur Lage *et al.*, 2018) and with the hearing result~~(s)~~(s) from this work. Thus, it suggests that crawling experiments could be used to screen for PCD gene candidates. The difference between the two controls (*Oregon-R* and *CG14353* +/-) is likely a result of genetic background.

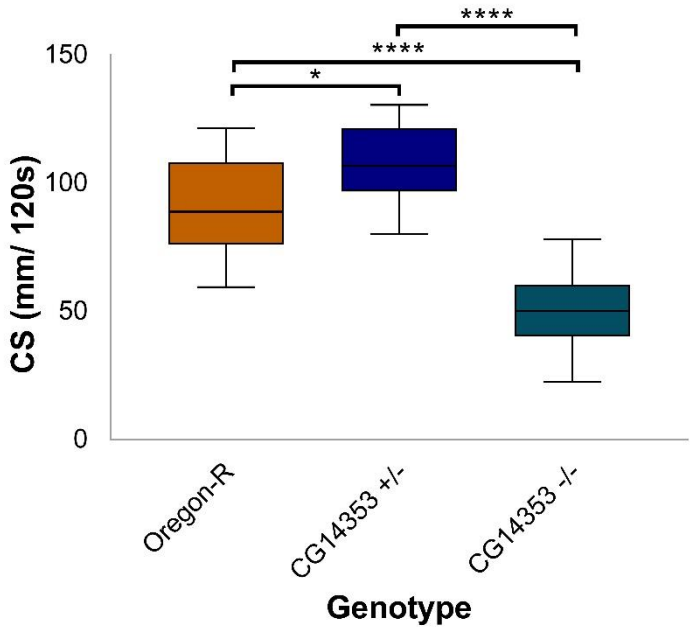

Figure 5.3: Chordotonal neuron function is necessary for normal crawling speed. *CS is crawling speed (mm/120s) recorded manually from larvae crawling on a 200mm x 200mm, 1% agar gel in a closed plastic container (23.9-25°C, daylight). There was a significant difference in crawling between CG14353 -/- (50.77 ± 14.65mm/ 120s; n = 16 larvae) and CG14353 +/- (107.1 ± 15.64mm/ 120s; n = 16 larvae, P ≤ 0.0001) and Oregon-R (wild-type) controls (90.83 ± 18.65mm/ 120s; n = 16 larvae, P ≤ 0.0001). There was also a significant difference between CG14353 +/- and Oregon-R (P = 0.02). Shown as whiskers minimum to maximum, horizontal line is median. Statistical significance determined by one-way ANOVA with Tukey's post-hoc test (threshold for significance: P = 0.05; * = P ≤ 0.05, **** = P ≤ 0.0001).*

Next, *CG14353* -/- and *CG17669* -/- were compared to *fd3F* -/- and *atonal* -/-. *fd3F* encodes a forkhead transcription factor necessary for specialisation of the mechanosensory cilium of ch neurons (Newton *et al.*, 2012) and *atonal* encodes the proneural gene required for formation of ch neurons (Jarman *et al.*, 1993) This experiment was conducted to confirm that the contrasting larval RT and crawling behaviour observed for mutants of the two former genes (*CG17669*, no significant differences detected in mutant; *CG14353,* significant differences in mutant) was due to a type II error. CS was significantly slower for *CG14353* -/- (50.77 ± 14.65mm/ 120s; *n* = 16 larvae) than *CG17669* -/- (94.31 ± 32.3mm/ 120s; *n* = 16 larvae, *P* ≤ 0.0001), and *atonal* -/- (73.42 ± 21.2mm/ 120s; *n* = 16 larvae, *P* ≤ 0.01). In contrast, *fd3F* -/- *fd3F* -/- (64.02 ± 20.32mm/ 120s; *n* = 16 larvae) crawled significantly slower than *CG17669* -/- (*P* ≤ 0.01) (Figure 5.4).

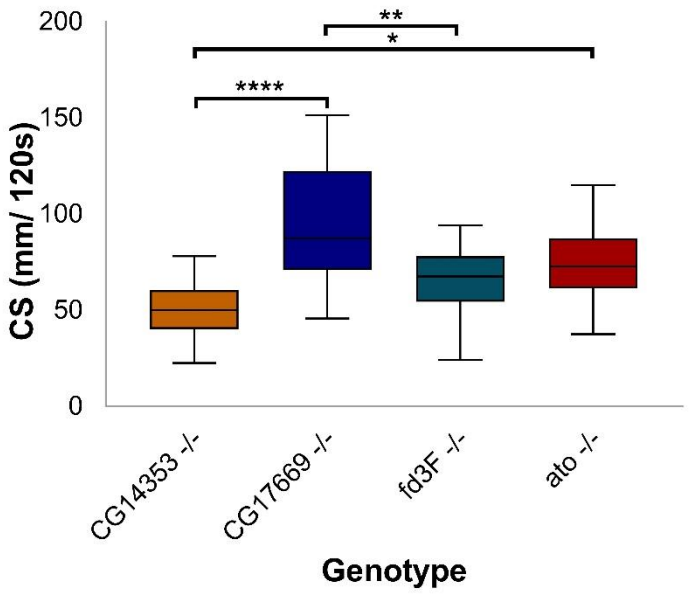

Figure 5.4: Comparison of chordotonal neuron mutants confirms type II error in CG17669 -/- loss-of-function crawling results. *CS is crawling speed (mm/120s) recorded manually from larvae crawling on a 200mm x 200mm, 1% agar gel in a closed plastic container (23.9-25°C, daylight). CG14353 -/- (50.77 ± 14.65mm/ 120s; n = 16 larvae) crawled significantly less than CG17669 -/- (112.7 ± 21.75mm/ 120s; n = 16 larvae, P ≤ 0.0001) and ato -/- (73.42 ± 21.2mm/ 120s; n = 16 larvae, P = 0.035). In contrast, CG17669 -/- crawled significantly faster than fd3F -/- (64.02 ± 20.32mm/ 120s; n = 16 larvae, P = 0.002). Shown as whiskers minimum to maximum, horizontal line is median. Statistical significance determined by one-way ANOVA with Tukey's post-hoc test (threshold for significance: P = 0.05; * = P ≤ 0.05, ** = P ≤ 0.01, **** = P ≤ 0.0001).*

Theoretically, if loss of dynein arms leads to a significant loss-of-function in chordotonal neurons that reduces crawling, *CG14353 -/-, CG17669 -/-, fd3F -/-* and *atonal -/-* should have similar impact~~(s)~~(s) on locomotion (with *atonal* arguably expected to have most as the neurons are completely missing). Thus, the differences seen here could reflect a type II error in *CG17669 -/-* experiments, due to variance in an underpowered experiment; *CG17669 -/-* experiments do not contradict the idea that crawling could be used in screening candidates for PCD (and with enough power, probably support it).

5.3.3 Screening novel primary ciliary dyskinesia gene candidates CG34297 and CG6980 with larval hearing experiments

CG34297 -/- and *CG6980* -/- mutant adults are uncoordinated and infertile (unpublished, Alexander Ahl). In this regard, they resemble *CG14353* (zur Lage *et al.*, 2018) and *CG17669* mutants (unpublished, Petra zur Lage). As mentioned previously, TEM of *CG34297* -/- antennae revealed a partial loss of dynein motor arms in the chordotonal neuron cilia while TEM of *CG6980* -/- revealed no loss of dynein motor arms (unpublished, Alexander Ahl), which contrasts the loss of ODAs and IDAs in *CG14353* and *CG17669* mutants. I therefore examined *CG34297* and *CG6980* mutant larvae for hearing defects to: (1) determine if mutation caused PCD-like phenotype~~(s)~~(s); (2) continue the assessment of *CG34297* and *CG6980* as PCD gene candidates.

Hearing experiments were carried out as above. For *CG34297* -/- larvae, RT (0 RT count; n = 5 repeats, 25 larvae) was not significantly different to that for *CG34297* +/- (4.55 ± 0.37 RT count; n = 5 repeats, 25 larvae). There was, however, a significant difference between *CG34297* -/- and *Oregon-R* (wild-type) controls (5 RT count; n = 3 repeats, 15 larvae; $P \leq 0.01$ (Figure 5.5)). This contrasts with the defects observed in adult coordination and fertility assays (unpublished, Alexander Ahl), and seems to reflect an underpowered experiment, despite efforts to calculate power prior to deciding on sample size. Assuming the difference seen in Figure 5.5 is underpowered, sufficient power should show that *CG34297* is required for ch neuron function in both larva and adult. This supports *CG34297* (and *TTC12*) as a PCD gene candidate, but also raises the question of what the molecular basis for chordotonal neuron dysfunction is in this case, given that dynein arms are only partly lost.

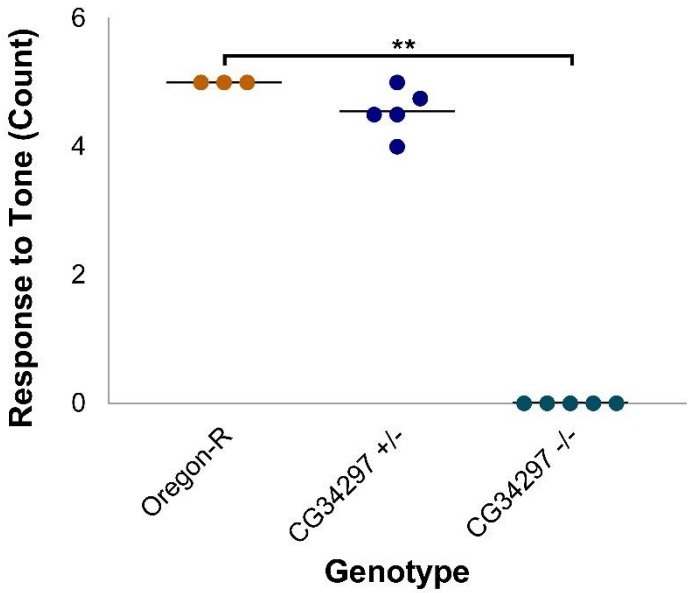

Figure 5.5: CG34297 may be necessary for larval hearing. *Response to Tone (RT, Count) is clear phenotypic response (e.g. contraction) to a 1000Hz tone observed in larvae crawling on a grape juice agar plate, recorded as mean score/ 5 larvae across 3-5 repeats (23.9-25°C, daylight). CG34297 -/- RT (0 RT count; n = 5 repeats, 25 larvae) was significantly less than Oregon-R (wild-type, 5 RT count; n = 3 repeats, 15 larvae, P = 0.005) but not CG34297 +/- (4.55 ± 0.37 RT count; n = 5 repeats, 25 larvae, P = 0.073) controls. Shown as scatter plot, horizontal line is mean. Statistical significance determined by Kruskal-Wallis with Dunn's post-hoc test (threshold for significance: P = 0.05; ** = P ≤ 0.01).*

There was no significant difference between RT for *CG6980* -/- (1 ± 0.58 RT count; *n* = 3 repeats, 15 larvae) and *CG6980* +/- (5 RT count; *n* = 3 repeats, 15 larvae), or between *CG6980* -/- or *CG6980* +/- and *Oregon-R* (wild-type) controls (5 RT count; *n* = 3 repeats, 15 larvae) (Figure 5.6). However, a strong trend to lack of response can be observed. These results are therefore subject to the same caveat as those for *CG34297*: the lack of significance between *CG6980* -/- and controls does not reflect the large trend observed (Figure 5.6) and likely demonstrates a lack of power. An increase in '*n*' number would surely provide the statistical significance seen in other, similar experiments (e.g. *CG1453* -/-) and it is likely that *CG6980* is necessary for larval hearing. Thus, *CG6980* mutation seems to cause PCD-like phenotypes in larvae, so the gene is a legitimate gene candidate for PCD.

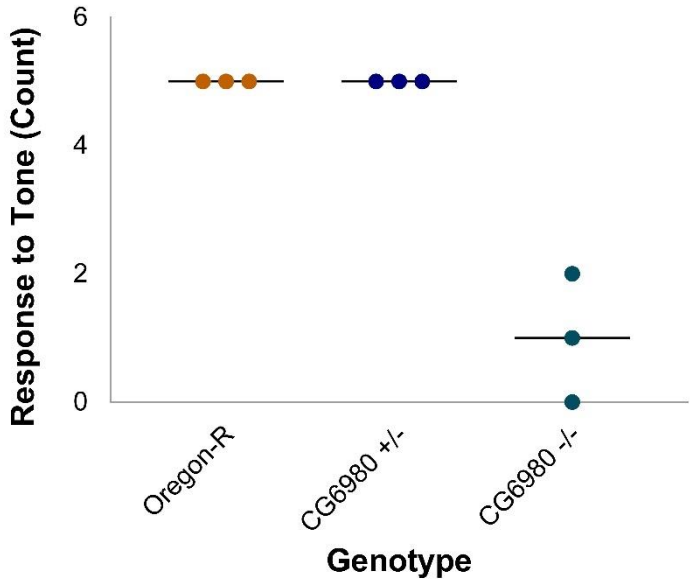

Figure 5.6: CG6980 may be necessary for larval hearing. *Response to Tone (RT, Count) is clear phenotypic response (e.g. contraction) to a 1024Hz tone observed in larvae crawling on a grape juice agar plate, recorded as mean score/ 5 larvae across 3-5 repeats (23.9-25°C, daylight). There was a large downward trend but no significant difference in RT between CG6980 -/- (1 ± 0.58 RT count; n = 3 repeats, 15 larvae) and CG6980 +/- (5 RT count; n = 3 repeats, 15 larvae. P = 0.05). There was also no significant difference between CG6980 -/- and Oregon-R (wild-type) controls (5 RT count; n = 3 repeats, 15 larvae, P = 0.05). Shown as scatter plot, horizontal line is mean. Statistical significance determined by Kruskal-Wallis with Dunn's post-hoc test (threshold for significance: P = 0.05).*

Since *CG34297* and CG6980 are closely related (they are both co-orthologues of human TTC12), there may be some redundancy between the two genes, which could explain TEM results if *CG34297* compensates for loss of *CG6980* in antennae (*CG6980* -/- leads to disruption of axoneme structure in the sperm, unpublished data from Alexander Ahl). Thus, a *CG34297, CG6980* double mutant was assayed for comparison to single mutant results.

RT for *CG34297, 6980* -/- (0.8 ± 0.48 RT count; *n* = 5 repeats, 25 larvae) was significantly less than *CG34297, 6980* +/- (4.85 ± 0.22 RT count; *n* = 5 repeats, 25 larvae, $P \leq 0.05$) and *Oregon-R* (wild-type) controls (5 RT count; *n* = 3 repeats, 15 larvae, $P \leq 0.05$) (Figure 5.7). The insignificant trend for *CG6980* (affected by low '*n*' number) and *CG34297* makes it difficult to reflect on the redundancy, however, it bolsters the argument that the lack of significant difference in RT between each (individual) gene and its heterozygous, was due to insufficient power.

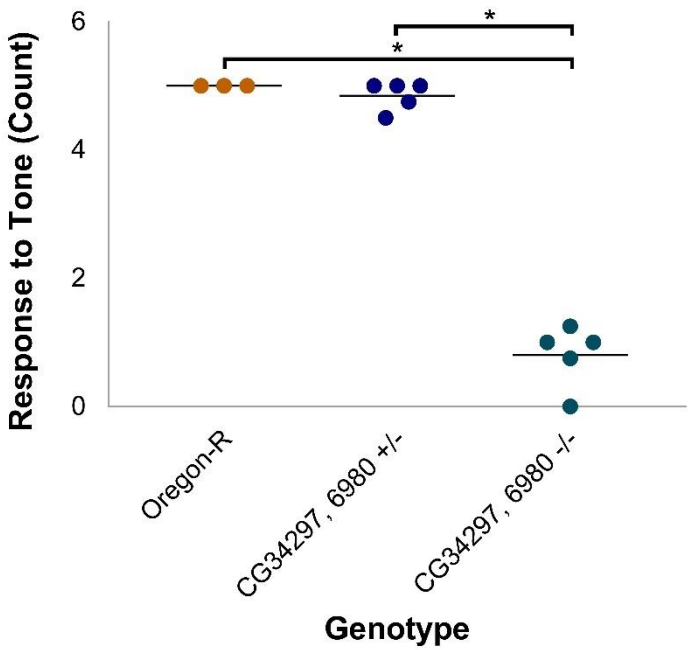

Figure 5.7: CG34297, 6980 is necessary for larval hearing. *Response to Tone (RT, Count) is clear phenotypic response (e.g. contraction) to a 1000Hz tone observed in larvae crawling on a grape juice agar plate, recorded as mean score/ 5 larvae across 3-5 repeats (23.9-25°C, daylight). CG34297, 6980 -/- RT (0.8 ± 0.48 RT count; n = 5 repeats, 25 larvae) was significantly less than CG34297, 6980 +/- (4.85 ± 0.22 RT count; n = 5 repeats, 25 larvae. P = 0.035) and Oregon-R (wild-type) controls (5 RT count; n = 3 repeats, 15 larvae. P = 0.016). Shown as scatter plot, horizontal line is mean. Statistical significance determined by Kruskal-Wallis with Dunn's post-hoc test (threshold for significance: P = 0.05; * = P ≤ 0.05).*

5.3.4 Screening novel primary ciliary dyskinesia gene candidates CG34297 and CG6980 with larval crawling experiments

As for hearing experiments, *CG34297* and *CG6980* were analysed in crawling experiments to: (1) see if mutation caused PCD-like phenotype~~(s)~~(s), given that mutants experience only partial or no loss of dynein arms; (2) continue assessment of *CG34297* and *CG6980* as PCD gene candidates.

Crawling experiments were conducted as before (Chapter 3). CS for *CG34297* -/- (80.03 ± 28.28mm/ 120s; *n* = 16 larvae) was significantly less than *CG34297* +/- (108.1 ± 24.46mm/ 120s; *n* = 16 larvae, $P \leq 0.01$), but was not significantly different to *Oregon-R* (wild-type) controls (90.83 ± 18.65mm/ 120s; *n* = 16 larvae) (Figure 5.8). This result supports crawling assays as an effective screen for PCD gene candidates and agrees with hearing, adult climbing (coordination) and TEM data for *CG34297* -/- (unpublished, Alexander Ahl), plus those for *CG14353* (hearing and crawling from this research, TEM and behavioural data from zur Lage *et al.*, 2018). This shows that *CG34297* mutation produces both hearing and crawling dysfunction resembling PCD and so promotes pursuing the gene as a disease-related candidate. However, the reduction in crawling is not as large as observed for the mutants above, suggesting some retention of chordotonal neuron function. The lack of significant difference between *CG6980* -/- and *Oregon-R* is likely a result of genetic background. Specifically, *CG6980* +/- and *CG6980* -/-share a genetic background that is different to *Oregon-R*.

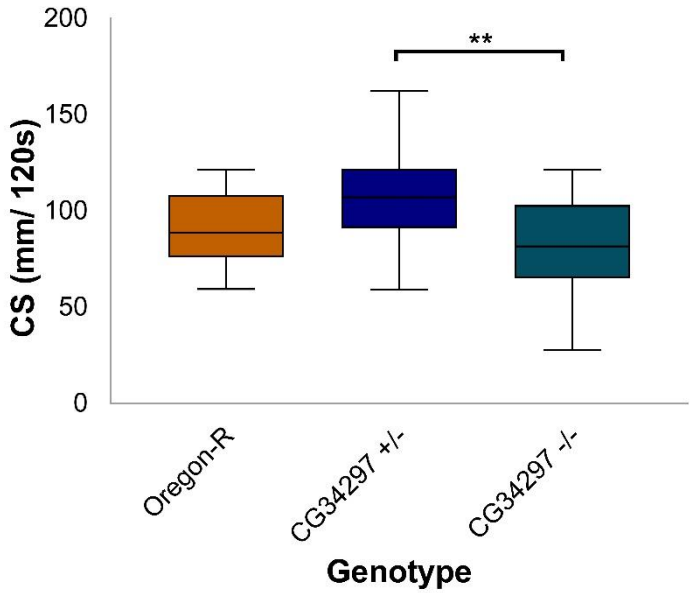

Figure 5.8: CG34297 is necessary for normal larval crawling speed. *CS is crawling speed (mm/ 120s) recorded manually from larvae crawling on a 200mm x 200mm, 1% agar gel in a closed plastic container (23.9-25°C, daylight). There was a significant difference in crawling speed between CG34297 -/- (80.03 ± 28.28mm/ 120s; n = 16 larvae) and CG34297 +/- (108.1 ± 24.46mm/ 120s; n = 16 larvae, P = 0.005). There was no significant difference between CG34297 -/- and Oregon-R (wild-type) controls (90.83 ± 18.65mm/ 120s; n = 16 larvae). Shown as whiskers minimum to maximum, horizontal line is median. Statistical significance determined by one-way ANOVA with Tukey's post-hoc test (threshold for significance: P = 0.05; ** = P ≤ 0.01).*

For *CG6980* -/-, CS (97.6 ± 13.88mm/120s; *n* = 16 larvae) was not significantly different to CS for *CG6980* +/- (110.4 ± 19.71mm/ 120s; *n* = 16 larvae). *Oregon-R* (wild-type) controls (90.83 ± 18.65mm/ 120s; *n* = 16 larvae) crawl significantly slower than *CG6980* +/- (*P* ≤ 0.01) (Figure 5.9). This lack of difference is not obviously due to lack of power, as it was for hearing (no large trend here), but it may be. considering the results of the hearing assays and *CG34207* -/- hearing assay. This is especially important, given that the relatively small reduction in *CG34297* -/- crawling is not as large as observed for the *CG14353*, suggesting some retention of chordotonal neuron function in the former (and so maybe also *CG6980* -/-). Again, the significant difference between the two controls (*Oregon-R* and *CG6980* +/-) is likely a result of genetic background.

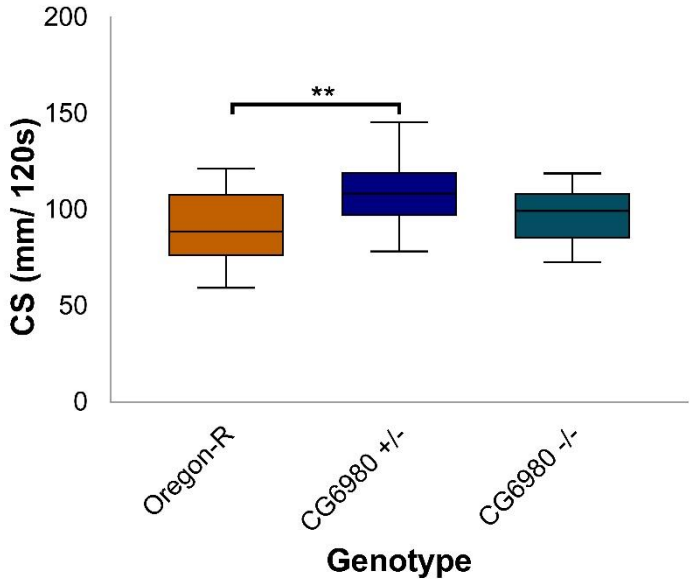

Figure 5.9: CG6980 is not necessary for normal larval crawling speed. *CS is crawling speed (mm/ 120s) recorded manually from larvae crawling on a 200mm x 200mm, 1% agar gel in a closed plastic container (23.9-25°C, daylight). There was no difference in crawling speed between CG6980 -/- (97.6 ± 13.88mm/120s; n = 16 larvae) and either control (CG6980, +/- (110.4 ± 19.71mm/ 120s; n = 16 larvae, P = 0.112; Oregon-R (wild-type), 90.83 ± 18.65mm/ 120s; n = 16 larvae, P = 0.526). However, Oregon-R crawling was significantly slower than CG6980 +/- (P = 0.008). Shown as whiskers minimum to maximum, horizontal line is median. Statistical significance determined by one-way ANOVA with Tukey's post-hoc test (threshold for significance: P = 0.05; ** = P ≤ 0.01).*

In contrast to the (CS) results for *CG34297* -/- and the double mutant results for hearing, there was no significant difference in CS between *CG34297, CG6980* -/- (91.63 ± 23.2mm/ 120s; *n* = 16 larvae) and *CG34297, CG6980* +/- (98.71 ± 30.69mm/ 120s; n = 16 larvae) or *Oregon-R* (wild-type) controls (90.83 ± 18.65mm/ 120s; *n* = 16 larvae (Figure 5.10)). This surprising outcome, which prevents meaningful reflection on redundancy, is almost certainly due to variance. As stated in *CG14353* -/- and *CG17669* -/- hearing results, variance is innately high in behavioural experiments, which means sample size must be large to ensure proper power. As mentioned previously, sample size calculations were conducted in preparation for this work (based on crawling experiments conduct in Suslak, 2015), and they implied that a sample size of 16 was sufficient to exceed the arbitrary power threshold of 0.8 (Jones, Carley and Harrison, 2003).

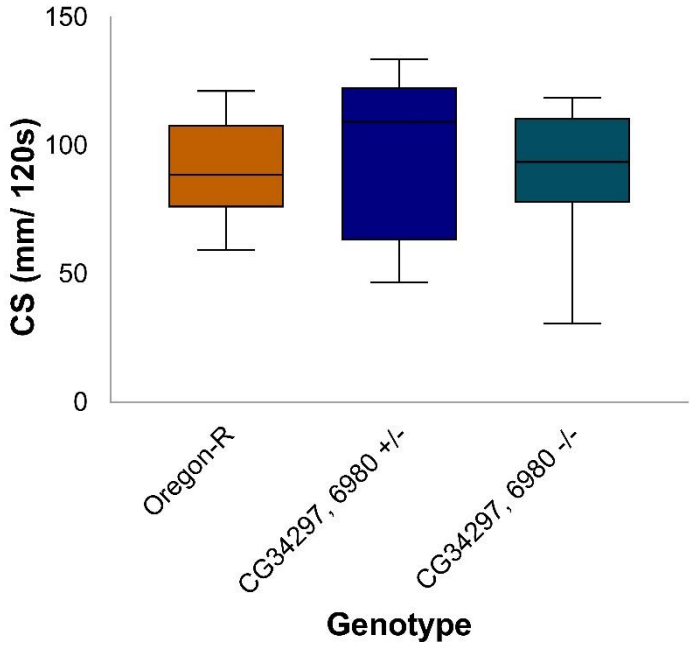

Figure 5.10: CG34297, 6980 is not necessary for normal larval crawling speed*. CS/ 120s (mm) is crawling speed/ 120s (mm) recorded manually from larvae crawling on a 200mm x 200mm, 1% agar gel in a closed plastic container (23.9-25°C, daylight). There was no significant difference in crawling between CG34297, 6980 -/- (91.63 ± 23.2mm/ 120s; n = 16 larvae) and CG34297, 6980 +/- (98.71 ± 30.69mm/ 120s; n = 16 larvae, P = 0.698) or Oregon-R (wild-type) controls (90.83 ± 18.65mm/ 120s; n = 16 larvae, P = 0.995). Shown as whiskers minimum to maximum, horizontal line is median. Statistical significance determined by unpaired t test (threshold for significance: P = 0.05).*

5.3.5 Hearing assays performed on RNAi knockdowns of dynein assembly factors are not effective screens for primary ciliary dyskinesia-associated genes

Despite limitations imposed by a lack of power, experiments using DNAAF mutants suggest that hearing and crawling experiments could be used in screening for genes associated with PCD. An efficient way of screening many candidates is to use Gal4/UAS-driven RNA interference lines to knock down function in chordotonal neurons. Therefore, screening was conducted using RNAi lines for DNAAFs identified as having enriched expression in ch neuron development (Cachero *et al.*, 2011), to assess possible involvement in PCD. RNAi lines were crossed to *scabrous*-Gal4 (*Sca*-Gal4), which is expressed in all developing sensory neurons.

Hearing experiments were carried out as above. RNAi lines were chosen based on: (1) evidence of enrichment in chordotonal neuron development according to microarray analysis (Cachero *et al.*, 2011); (2) availability of RNAi line in laboratory, or to order from Bloomington or Vienna *Drosophila* stock centre~~(s)~~(s). Lines were separated into KK and GD constructs for analysis (Sca-Gal4 x *Oregon-R* as KK control, Sca-Gal4 x w^{1118} as GD control).

7 KK lines were tested against KK Control larvae, but no significant differences were found for any comparison (*CG6980* RNAi, 5 RT count; *CG3723* RNAi, 4.75 ± 0.31 RT count; *CG6971* RNAi, 4.9 ± 0.14 RT count; *CG10958* RNAi, 4.8 ± 0.11 RT count; *CG13202* RNAi, 5 RT count; *CG14353* RNAi, 4.9 ± 0.14 RT count; *CG15804* RNAi, 4.95 ± 0.11 RT count; all *n* = 5 repeats, 25 larvae; KK Control, 4.9 ± 0.14 RT count; *n* = 5 repeats, 25 larvae) (Figure 5.11). This was surprising, at least for *CG14353* RNAi, given that *CG14353* -/- larvae fail this hearing assay and are uncoordinated (above and (zur Lage *et al.*, 2018)). Therefore, the RNAi phenotype is at odds with that observed in the mutant.

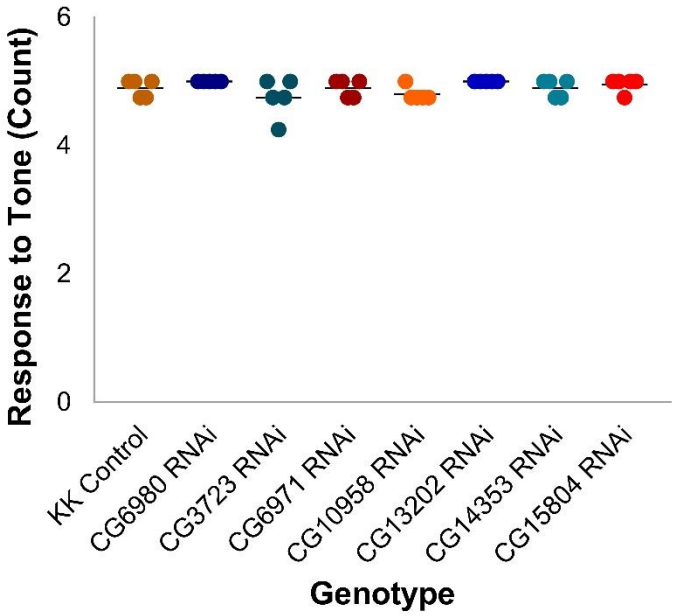

Figure 5.11: KK-line RNAi knockdown of DNAAFs does not affect larval hearing. *Response to Tone (RT, Count) is clear phenotypic response (e.g. contraction) to a 1000Hz tone observed in larvae crawling on a grape juice agar plate, recorded as mean number/ 5 larvae across 3-5 repeats (23.9-25°C, daylight). There was no significant difference between any of the lies tested (CG6980 RNAi, 5 RT count; CG3723 RNAi, 4.75 ± 0.31 RT count; CG6971 RNAi, 4.9 ± 0.14 RT count; CG10958 RNAi, 4.8 ± 0.11 RT count; CG13202 RNAi, 5 RT count; CG14353 RNAi, 4.9 ± 0.14 RT count; CG15804 RNAi, 4.95 ± 0.11 RT count; all n = 5 repeats, 25 larvae) and KK Control (4.9 ± 0.14 RT count; n = 5 repeats, 25 larvae, P >0.999 for all comparisons). All lines were crossed to Sca-Gal4. Shown as scatter plot, horizontal line is mean. Statistical significance determined by Kruskal-Wallis with Dunn's post-hoc test (threshold for significance: P = 0.05).*

1 GD line, *CG30259* RNAi (4.85 ± 0.33 RT count, *n* = 5 repeats, 25 larvae), was tested against w^{1118} (4.9 ± 0.14 count; *n* = 5 repeats, 25 larvae). Again, no significant difference was found between the two (Figure 5.12). Overall, the lack of difference observed across all RNAi lines, especially in context of mutant results for *CG14353*, is disappointing and suggests that RNAi is unsuitable for larval hearing experiments as a screening tool for PCD-related genes.

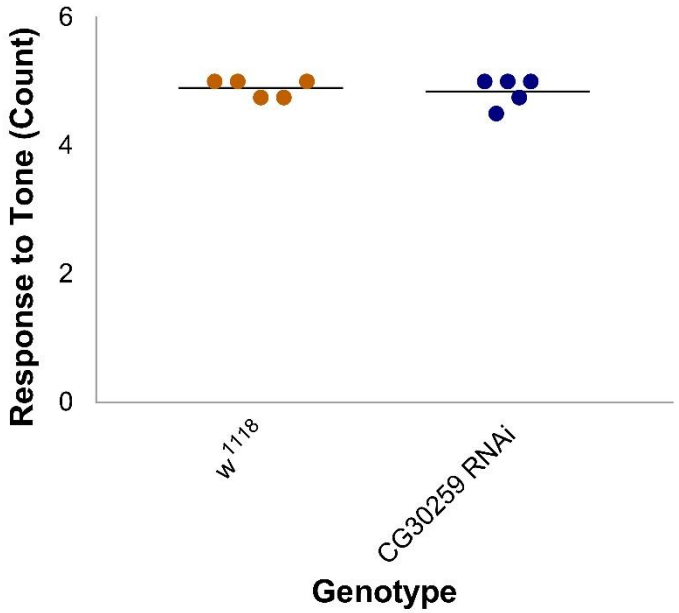

Figure 5.12: GD-line RNAi knockdown of DNAAFs does not affect larval hearing. *Response to Tone (RT, Count) is clear phenotypic response (e.g. contraction) to a 1000Hz tone observed in larvae crawling on a grape juice agar plate, recorded as mean number/ 5 larvae across 3-5 repeats (23.9-25°C, daylight). There was no significant difference between CG30259 RNAi (4.85 ± 0.33 RT count, n = 5 repeats, 25 larvae) and w^{1118} (4.9 ± 0.14 count; n = 5 repeats, 25 larvae, P = >0.999). Both lines were crossed to Sca-Gal4. Shown as scatter plot, horizontal line is mean. Statistical significance determined by Mann-Whitney test (threshold for significance: P = 0.05).*

5.3.6 Crawling assays performed on RNAi knockdowns of dynein assembly factors are not effective screens for Primary Ciliary Dyskinesia-associated genes

Crawling experiments were carried out as above. Lines were chosen on the same basis as for hearing experiments: (1) evidence of enrichment in chordotonal neuron development according to microarray analysis (Cachero *et al.*, 2011); (2) availability in laboratory, or to order from Bloomington or Vienna *Drosophila* stock centre~~(s)~~(s). Lines were separated into KK and GD constructs for analysis (Sca-Gal4 x *Oregon-R* as KK control, Sca-Gal4 x w^{1118} as GD control).

12 KK lines were tested against KK control, and no significant differences were reported in the comparison (*CG14921* RNAi, 114.4 ± 22.73 mm/ 120s; *CG6980 RNAi*, 114.4 ± 22.73 mm/ 120s; *CG34297, 6980* RNAi, 128.5 ± 25.16 mm/ 120s; *CG3723 RNAi*, 120 ± 28.89 mm/ 120s; CG6971 RNAi, 123.8 ± 19.04 mm/ 120s; *CG10958* RNAi, 120.2 ± 12.26 mm/ 120s; *CG13202 RNAi*, 117.4 ± 21.1 mm/ 120s; *CG14353* RNAi, 115.6 ± 24.43 mm/ 120s; *CG15804* RNAi,

139.6 ± 33.8 mm/ 120s; all *n* = 16 larvae; KK control 132.7 ± 26.69 mm/ 120s, *n* = 16 larvae). (Figure 5.13). These results are, once again, surprising as RNAi knockdown should reflect mutant knockout (of *CG14353*).

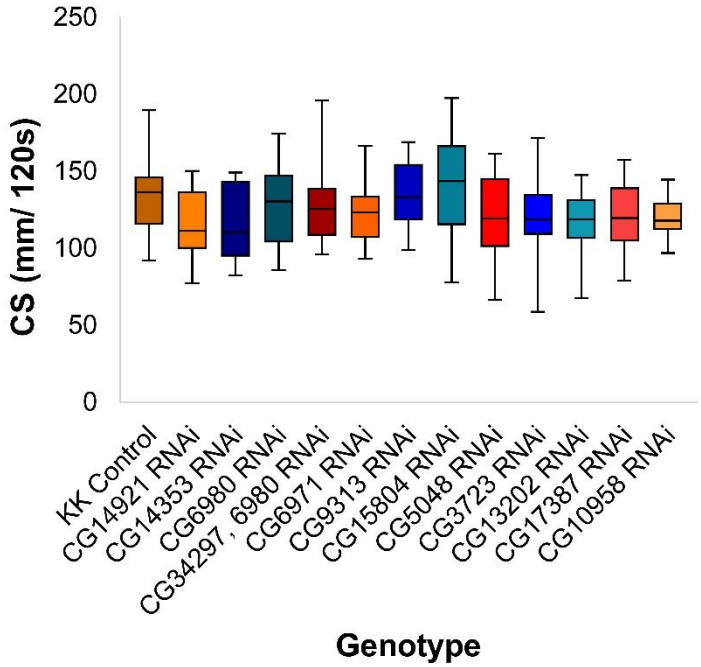

Figure 5.13: KK-line RNAi knockdown of DNAAFs does not affect larval crawling speed. *CS is crawling speed (mm/120s) recorded manually from larvae crawling on a 200mm x 200mm, 1% agar gel in a closed plastic container (23.9-25°C, daylight). There were no significant differences between the control and any of the other lines tested (CG14921, 114.4 ± 22.73 mm/ 120s; CG6980 RNAi, 114.4 ± 22.73 mm/ 120s; CG34297, 6980 RNAi, 128.5 ± 25.16 mm/ 120s; CG3723 RNAi, 120 ± 28.89 mm/ 120s; CG6971 RNAi, 123.8 ± 19.04 mm/ 120s; CG10958 RNAi, 120.2 ± 12.26 mm/ 120s; CG13202 RNAi, 117.4 ± 21.1 mm/ 120s; CG14353 RNAi, 115.6 ± 24.43 mm/ 120s; CG15804 RNAi, 139.6 ± 33.8 mm/ 120s; all n = 16 larvae) and the (KK) control (132.7 ± 26.69 mm/ 120s, n = 16 larvae, P ≤ 0.999 for all comparisons). All lines were crossed to Sca-Gal4. Shown as whiskers minimum to maximum, horizontal line is median. Statistical significance determined by one-way ANOVA with Tukey's post-hoc test (threshold for significance: P = 0.05).*

3 GD lines were compared to Sca-Gal4 x w^{1118} control (*CG17669* RNAi, 121.3 ± 36.17 mm/ 120s; *CG30259* RNAi, 124 ± 23.1 mm/ 120s; *CG14271* RNAi, 115.7 ± 19.03 mm/ 120s; all *n* = 16 larvae; Sca-Gal4 x w^{1118} control, 121.8 ± 19.19 mm/ 120s; *n* = 16 larvae). There were no significant differences found in any of the comparisons (Figure 5.14). Given that it was found in Chapter 4 that *CG17669* mutation probably affects larval crawling, this supports the results for the other RNAi experiments in that knockdown appears to be unsuitable in larval screens for PCD-related genes.

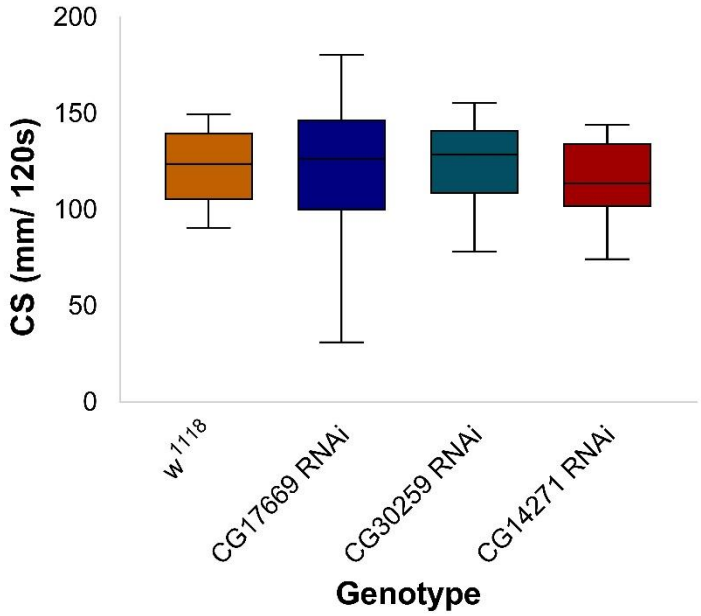

Figure 5.14: GD-line RNAi knockdown of DNAAFs does not affect larval crawling speed. *CS is crawling speed (mm/ 120s) recorded manually from larvae crawling on a 200mm x 200mm, 1% agar gel in a closed plastic container (23.9-25°C, daylight). There was no significant difference between any of the lies tested (CG17669 RNAi, 121.3 ± 36.17 mm/ 120s; CG30259 RNAi, 124 ± 23.1 mm/ 120s; CG14271 RNAi, 115.7 ± 19.03 mm/ 120s; all n = 16 larvae) and w1118 control (121.8 ± 19.19 mm/ 120s; n = 16 larvae, P = >0.999, 0.995 and 0.9030, respectively). All lines were crossed to Sca-Gal4. Shown as whiskers minimum to maximum, horizontal line is median. Statistical significance determined by one-way ANOVA with Tukey's post-hoc test (threshold for significance: P = 0.05).*

5.4 Discussion

5.4.1 Larval behavioural assays for PCD candidate gene analysis

Drosophila has been shown to be a useful model organism for studying PCD-related genes (zur Lage *et al.*, 2019). This is partly due to the inherent advantages of *Drosophila's* genetic toolkit but is also due to the very high conservation of the ciliary motility apparatus across eukaryotes. However, another key factor is the very restricted occurrence of motile cilia in *Drosophila*: They are confined just to chordotonal neurons and the sperm flagellum. This has important consequences in that PCD in *Drosophila* has very restricted phenotypes. The sensory phenotypes are readily assayed through behavioural assays. For many types of gene, locomotion assays would not be very informative because defects could arise from many different causes within the circuit from sensory reception to output: From decision making output to motor control and muscle function. However, the very restricted expression patterns of dynein-related genes (confined to ch neurons) means that the results of such assays are easily interpreted as ch sensory transduction defects. Thus, whole-organism mutants can safely be assayed for incoordination or hearing defects using locomotion behaviour outputs. Generally, adult assays are used, particularly climbing assays for proprioception (Moore *et al.*, 2013; Diggle *et al.*, 2014). However, assessing adult hearing requires specialist equipment (for electrophysiology, or for doppler vibrometry) which makes it unsuitable for larger scale screening.

My results in Chapter 4 posed that larval assays could be effective for screening and general characterisation of PCD candidate genes. Whilst subject to the caveat of insufficient power, hearing assays suggested that fly mutants for known PCD gene *CG17669* (*CG17669* -/-) have defective RT, and crawling experiments detect reduced speed in *CG17669* -/-. Similarly, hearing experiments detected that *CG14353* -/- larvae are hard of hearing, while crawling experiments demonstrated a reduction in speed in *CG14353* -/- versus controls. This agrees with findings in adults from earlier research (zur Lage *et al.*, 2018) and confirms that simple behavioural assays are sufficient to report PCD-like phenotypes in mutant larvae, so can serve as tools in early screening for candidates. Future work could, therefore, deploy hearing and crawling experiments. However, it is clear from results in this chapter that a large sample size is required to increase statistical power. In most of the experiments here, '*n*' was defined by the groups of (5) larvae tested, which reduced 15 larvae to $n = 3$. This reflects a very low number of degrees of freedom and gives statistical tests little power to detect significance in otherwise large differences between genotypes (e.g. *CG17669* -/- mean RT of 0 versus *CG17669* +/- mean RT of 4.44). However, increasing sample size reduces the utility of these simple assays for screening genes.

Mutant stocks of candidate genes are not always available. The mutant stocks used in this chapter mostly were generated in-lab using CRISPR/Cas9 genome engineering. This is a significant investment of time and effort and is only worthwhile if there is clear evidence of a candidate gene's involvement. Instead, initial screening of many genes benefits from using RNA interference by tissue-specific genetically supplied shRNA expression as an alternative. Such screens have been widely used in *Drosophila* using stocks from the VDRC and TRiP projects. In the case of PCD genes, the use of RNAi, targeted to ch neurons or sperm, has been successful for initial validation of *CG17669*, *CG31320*, and *CG14353*, prior to more complete validation after generation of CRISPR-engineered deletion mutants. This success of RNAi screening was based on adult assays for proprioception and hearing. Here I tested its utility in larval assays. In contrast to mutant results, my results show that RNAi does not appear to be effective in (larval) screens. All RNAi results showed no significant difference between ciliary motility knockdown and control lines, which is probably explained by inefficient knockdown by RNAi. Research published by the lab has acknowledged the potential for inefficient knockdown; knocking down dynein heavy chain genes, *Dhc36C* and *Dhc62B,* has a limited effect on fertility and climbing (zur Lage, Newton and Jarman, 2019). Similarly, knocking down *CG17564*, a dynein motor regulator which was expected to be necessary for ciliary motility, had no effect on fertility and climbing. However, the RNAi lines used to knock down gene expression in the assays here, produced significant effects in adult assays using the same Gal4 driver line in the same Jarman laboratory research. For instance, dynein intermediate chain *CG9313* RNAi gave a reduced adult climbing index (0.63 climbing index and fertility in adults (zur Lage, Newton and Jarman, 2019). This could suggest that larval hearing and crawling assays are less sensitive than adult climbing and fertility assays, and/or that knockdown is more impactful in adults than in larvae. It is possible that other driver lines may be more effective in larvae. Also, RNAi knockdown efficiency could be enhanced by crossing in a UAS-Dicer2 line. However, this would complicate the crossing schemes and so would not be conducive to ease of screening.

5.4.2 TTC12 homologues as candidate PCD genes

CG6980 and *CG34297* were included in the analysis in the chapter as further tests of the utility of larval assays for screening PCD genes. Furthermore, as described earlier, data obtained so far for these two candidate genes has been somewhat equivocal concerning their potential role in dynein complex assembly, and so it was hoped that larval phenotypes might provide further illumination. Whilst mutation of other DNAAFs resulted in behavioural defects that correlate with loss of dynein arms by electron microscopy, these two candidates showed only partial loss of dynein arms (*CG34297*) or no effect at all on dynein arms (*CG6980*).

Though limited by a lack of power, here I suggest that both *CG34297* and *CG6980* mutants demonstrate PCD-like phenotypes, despite limited impact on dyneins (*CG34297* -/- and *CG6980* -/- larvae are likely, and *CG34297, 6980* -/- larvae are hard of hearing; *CG34297* -/- crawl slower than controls, and *CG6980* -/- and *CG34297, 6980* larvae probably do the same). Notably, *CG34297* and *CG6980* are orthologs of human *TTC12*. The related *TTC25* has been proposed to link *CCDC151* to IFT, and its mutation is known to cause PCD (Wallmeier *et al.*, 2016). This mutation is characterised by loss of ciliary ODAs, making the lack of impact of *CG34297* and *CG6980* on ch neuron ultrastructure difficult to explain. This difficulty combined with the lack of power affecting behavioural experiments conducted in the present research, means little can be concluded about the two genes; they represent the most open and interesting aspect of this chapter's work. Future experiments should aim to confirm the preliminary findings for these genes. Specifically, the TEM should be repeated to ensure that dynein arm structure is an unaffected as the laboratory's unpublished work suggests. Assuming the ch neuron ultrastructure of *CG34297* and *CG6980* mutants is confirmed, the cellular basis will need to be investigated. It is possible that *CG6980* and *CG34297* affect ciliary motility in a manner not connected directly to dynein structure, for example by regulating motor activity. At this stage, it is even possible that these two genes are required for an aspect of ch neuron function other than ciliary motility, although the ch neuron + sperm nature of their gene expression argues against this. Regardless, these two genes remain as promising candidates for PCD genes for further investigation in *Drosophila* and human PCD families.

6 Discussion

6.1 Summary and implications of key results

This research made a significant contribution to the field of mechanosensation in *Drosophila*. This section summarises that contribution, to guide future research.

6.1.1 Behavioural role and mechanoelectric transducer of the dorsal bipolar dendritic neuron

Behavioural data gleaned from optogenetics experiments showed that dbd and dmd1 neurons are necessary for normal PWF and PWD, but not CS. This is a novel finding; whilst previous work came to a similar conclusion (Hughes and Thomas, 2007; Cheng *et al.*, 2010), it did so based on the use of a driver that is expressed extensively in the VNC. This expression was responsible for a 'strike' phenotype that suggested the change in behaviour reported in Hughes and Thomas, 2007 and Cheng *et al.*, 2010, was not due to dbd and dmd1 activity. Consequently, results presented here validate research formerly based on an assumption. They also provide evidence that NompC is the MET in dbd neurons (supports Cheng *et al.*, 2010 and disputes (Suslak *et al.*, 2015c)), however, this was caveated by a problem regarding RNAi effectiveness (see 5.2.1.2.).

Confirming that dbd and dmd1 neurons are (stretch receptors) necessary for normal PWF and PWD, but not CS, poses the question as to what is responsible for crawling speed. This question is exacerbated by the fact that this work shows ch neurons play only a small role in moderating CS. Results also support using *Drosophila* dbd neurons to model the mammalian spindle to treat spasticity and seizure. This has been attempted but ultimately translation of findings failed: Suslak *et al.*, posed DmPiezo as the MET in dbd neurons, but Piezo is not expressed in murine skeletal muscle spindles (Suslak *et al.*, 2015c). However, this work: (1) brings attention to the potential for inaccuracy in that work due to lack of seal testing; (2) poses that NompC could be the MET.

6.1.2 Behavioural role and mechanoelectric transducer of chordotonal neurons

GCaMP provided considerable insight into the behavioural role~~(s)~~(s) and mechanism of mechanosensation present in ch neurons. It confirmed that optimal frequency of stimulation for ch neurons was ~1024Hz (agrees with Lennon, disagrees with (Zhang *et al.*, 2013) and that all 3 subpopulations of ch neurons respond to sound, which involved showing this in vchAB for the first time. Similarly, this work showed that lch1 responds to 1024Hz with lower amplitude of response than lch2-5, plus vchB responds to 1024Hz with a lower amplitude of response than vchA. Thus, this research is first to offer that individual neurons within subpopulations respond differently to sound, which supports specialisation ('tuning') of PNS neurons in larvae, as exists in humans (Fettiplace, 2017). A variety of GCaMP (DmPiezo inhibition by RR and RNAi; pym pilots) and behavioural (crawling and hearing in *NompC* and *iav* -/- larvae) experiments supported the nan-iav model for the MET, so provided useful results that should push the debate of 'nan-iav model' versus. 'NompC model' (reviewed in (Albert and Gopfert, 2015), towards a resolution. Another novel result was that *CG17669* is probably necessary for hearing and proprioception/ crawling, which adds to the idea dyneins are required for both hearing and proprioception in (larval) ch neurons (zur Lage *et al.*, 2018). Clearly the amplification driven by dynein motors is required by larvae for hearing, and perhaps more interestingly, crawling. While it is easy to see the utility in active amplification of relatively low amplitude stimuli (as in hearing), it is more difficult to imagine why it would be necessary in processing the large amplitude, lower frequency stimulus of stretch in crawling. This should be investigated further, as it is important for understanding the role of dyneins in mechanosensation.

6.1.3 Use of behavioural assays to screen for primary ciliary dyskinesia

Work presented here provided evidence for the utility of larval hearing and crawling experiments in screening gene candidates for PCD. This work was limited by insufficient power and inefficiency of RNAi, however, analysis of results from experiments using mutants was able to associate PCD candidate genes *CG34297* and *CG6980* with PCD-like phenotypes. Thus, this work showed that hearing and crawling experiments could be effective screens for PCD-candidate genes (provided they are conducted with sufficient power). It also developed the case for further investigation of *CG34297* and *CG6980* in PCD.

6.1.4 Complexities of investigating mechanosensation

This section explores the main difficulties encountered while attempting to study mechanosensation and puts them in the context of other work.

6.1.4.1 Limitations of genetic techniques

6.1.4.1.1 Lack of specificity of Gal4 driver lines

Expression of Bd-Gal4, Bd/I-Gal4 and nan-Gal4 limited the conclusions that could be made from optogenetics data. Most impactful to this work was Bd-Gal4; the extent of its expression in the VNC (Figure 3.14) prevented attribution of an otherwise interesting phenotype, to dbd and dmd1 neurons. Expression was even more surprising because Hughes and Thomas, 2007 and Cheng *et al.*, 2010, used Bd-Gal4 to make conclusions on the role of the dbd neuron in behaviour, that have been accepted by the field. Clearly these conclusions should not have been accepted and the fact they were is worrying on several levels. First, researchers must be clear on the requirement for specificity if behaviour is to be attributed to particular neurons; they should not relate neurons to behaviour without it. Second, driver expression should be explicit (with images shown) and not relegated to supplementary information if possible. Third, researchers should not accept claims made in the literature without reading it thoroughly; the description of Bd-Gal4 expression in the supplementary information for Hughes and Thomas, 2007, and Cheng *et al.*, 2010, included “a few CNS neurons.” This description should have warned against citing either as evidence of a role for the dbd and dmd1 in crawling, but many did so regardless. Finally, even if Bd-Gal4 was not limited by expression in the VNC, it is by the fact it is expressed in 2, rather than 1 PNS neuron. Future work should include development of driver lines specific to single neurons (with no expression in VNC), to help determine their role~~(s)~~(s) in behaviour. Bd/I-Gal4 was similar – it was expressed in 2 MD but not dbd or dmd1 neurons, which disagrees with documented expression (Hughes and Thomas, 2007, and Cheng *et al.*, 2010). Finally, nan-Gal4 was not expressed in ch neurons (or any others). Perhaps confusion in husbandry meant that the line was contaminated, and care should be taken to make sure this does not happen in future.

6.1.4.1.2 Incomplete knockdown by RNAi

Chapters 2, 3 and 4 presented surprising results that suggested RNAi was ineffective. This was most obvious in Chapter 4, where (RNAi) knockdown failed to replicate behavioural experiment results that showed *CG14353* is necessary for hearing and crawling. In fact, none of the candidate gene RNAi lines tested in behavioural 'screens' showed a significant difference in behaviour versus control. This is a surprising result, considering that mutation and/ or knockdown of dynein assembly factors identified in the same microarray as those tested here (Cachero *et al.*, 2011), have shown dysfunctional behaviour phenotypes in other work (zur Lage *et al.*, 2018). It seems likely that RNAi knockdown was incomplete (agrees with anomalous results in zur Lage *et al.*, 2018). Future research should either: (1) avoid using RNAi in case knockdown is ineffective or (2) quantify gene expression following RNAi, e.g. by using RT-qPCR. In most cases, (1) is the most effective strategy as (2) is a post-hoc check that is irrelevant if results are null. Thus, future work should use mutants when possible.

6.1.4.2 Stretching and recording from neurons

Most research on mechanosensation focuses on hearing, touch or nociception - relatively little concerns proprioception. This may be due to the difficulty of delivering an accurate and reliable stretch stimulus, then recording the response of the neuron; recording (dbd and ch) neurons' responses to stretch posed a problem, in both electrophysiology and GCaMP experiments. This section explores this issue and how it could be solved in future.

6.1.4.2.1 Delivery of stretch stimulus

Research used 'tap' and innate muscle contraction stimuli to impart stretch into larval preparations. The 'tap' method could be considered a mechanosensitive stimulus that represents stretch, as it was used based on the logical assumption that tapping the headstage elongated the cuticle of hemisegments, like a 'normal' (physiological) stretch does. Clearly it would be preferable to use a more direct/ obvious stretch, and this was the basis for using the piezoelectric wafer in (Suslak *et al.*, 2015c) and developing the servo-driven mechanism shown in Figure 3.42. The latter poses obvious benefits over the former; it is simpler to make fine adjustments to multiple parameters of stretch (speed, amplitude etc.) by modifying code, than it is manipulating current through the wafer. It is also less engineering to transfer movement of the servo arm, than it is the wafer, to the preparation. Therefore, this research suggests that future work should focus on delivering stretch in this way. Whilst innate muscle contraction represents significant progress to the tap (stimulus is physiological), it has been mislabelled in other research (Fushiki, Kohsaka and Nose, 2011). Fushiki and colleagues

describe the innate muscle contractions observed after dissection as “peristaltic waves”, however, this seems unlikely given that they exist in a fillet preparation. More likely, they reflect a nociceptive phenotype. It is important that research considers this difference, before assuming responses here are directly related to locomotion.

6.1.4.2.2 Recording from a moving neuron

Whilst a neuron stays in the same place relative to rest of the larvae (i.e. its anatomy does not change), its absolute position changes significantly during: (1) the movement imposed on a preparation by a man-made mechanism to deliver a stretch stimulus; (2) innate muscle contraction. For electrophysiology, this movement degrades (and breaks) the seal formed between the neuron and recording electrode; even the low resistance seal formed here (maximum of ~40MΩ) regularly dropped to zero on stretch. Researchers will have to develop a highly specific solution to this problem if they want to perform electrophysiology on moving neurons in future; a headstage that moves with very low resistance, to follow and stay sealed to the neuron under stretch, might work. For GCaMP, movement makes it very difficult to image the neuron – its shape changes, is obscured by the cuticle and shifts out of the field of view of the lens. Currently, the most obvious solution to this problem is to record responses at the VNC, which is unaffected by contractions across the abdominal segments. However, this approach is limited by the fact that responses are a ‘proxy’, rather than direct reflection of neuronal activity, so cannot provide the detail available when imaging neurons directly (e.g. evidence given here for tuning of lch1 and lch2-5 in response to 1024Hz). It is also limited by driver line specificity – an issue discussed in depth above. As with electrophysiology, it is difficult to see a good solution for this problem in traditional GCaMP imaging. Recent work (published since the present research was conducted) used SCAPE imaging, a type of high-volume volumetric microscopy discussed in Chapter 1, to describe the contribution of sensory neurons to locomotion (Vaadia *et al.*, 2019). Specifically, SCAPE was used to characterise the relationship between sensory neurons and the cuticle during crawling. It is probably the best way to investigate the mechanisms of proprioception in *Drosophila* larvae, in future.

6.1.5 Comparison of Drosophila and vertebrate mechanosensation

This section explores how findings from the present research relate to and inform the study of vertebrate mechanosensation.

6.1.5.1 Translation of Findings: Drosophila to Vertebrate Proprioception

The key findings of the present research, as they relate to *Drosophila* proprioception, were: (1) support for the dbd neuron as a stretch receptor, even if that support is limited by the poor seal observed in electrophysiology experiments; (2) the dbd is necessary for PWF and PWD, but not CS; (3) NompC may be the MET in dbd neurons. The implication or translation of (1) is straightforward – it adds to a growing body of evidence that supports the dbd as a model of vertebrate/ mammalian muscle spindles. This model is important, because *Drosophila* genetic techniques, anatomy and ethics (i.e. the lack of licence required to experiment on flies) facilitate experiments that would be much more difficult in other organisms. For example, Parkinson's disease (PD) is characterised by a long-latency stretch reflex (LLSR) that contributes to muscle rigidity. This LLSR does not occur due to changes in the primary motor cortex (Pasquereau, DeLong and Turner, 2016) and so must be related to a change in another component of the neuromuscular system. Studying dbd physiology in a *Drosophila* model of PD, could help illuminate the mechanism of LLSR in disease, in a fast and economical way (compared to using other model organisms, such as the macaques used in (Pasquereau, DeLong and Turner, 2016)).

Finding (2) is less easy to translate, in that it describes characteristics specific to larval behaviour. What it does do, is add to what is known about the dbd neuron and so improves our ability to use it as a model as described for (1). It also confirms that the larval nervous system relies on integration of several sensory inputs to regulate crawling (as shown in (Vaadia *et al.*, 2019)). Whilst this may seem obvious, most research has focused on particular roles for specific neurons, like that of dbd and dmd1 on crawling speed ((Hughes and Thomas, 2007; Cheng *et al.*, 2010; Schneider-Mizell *et al.*, 2016) which, of course, contrasts what was reported here). The findings from the present research are a reminder that larval movement occurs with enough complexity to inform the study of the (even more) complex human system (Dietz, 2002). Finally, (3) is interesting and contradicts (1) and (2). The two channels that this research poses as the (possible) MET in dbd neurons, are not candidates for the MET in mammalian muscle spindles. As explained in Chapter 1, DEG/ ENaC superfamily channels are most likely to be the MET in spindles, and Piezo is not expressed in murine spindles (Suslak *et al.*, 2015). Clearly, more work is required to identify the MET in dbd neurons and muscle spindles, to better reflect on the ability to use the fly model to pose mechanisms of proprioception in humans.

6.1.5.2 Translation of Findings: Drosophila to Vertebrate Hearing

The key findings of the present research that relate to *Drosophila* hearing, were: (1) optimal frequency of stimulation for ch neurons is ~1024Hz (which may be specific to the experimental setup described in Chapter 2); (2) all 3 subpopulations of ch neurons respond to sound; (3) the nan-iav model seems more accurate than the NompC model of hearing; (4) lch1 and vchB respond to 1024Hz with a lower amplitude of response than the other ch neurons in their subpopulations (lch2-5 and vchA, respectively); (5) dyneins are necessary for hearing and crawling/ proprioception in fly larvae. Translation of (1)-(3) and (3) here is like that for (1) and (2) findings for proprioception. Specifically, (1)-(3) advance our understanding of the *Drosophila* model used to investigate human mechanosensation. Chapter 4 discusses the similarities between ch neurons and hair cells in depth. This similarity has already been exploited to make important discoveries that guide development of treatments for hearing loss. 17 years ago, Jarman laboratory principal investigator, Professor Andrew Jarman, published that a*tonal* is a proneural gene necessary for chordotonal organ formation (Jarman *et al.*, 1993). Translation of this finding led to a recent Phase I/II drug trial by Novartis, that aimed to recover hearing loss in humans (Novartis, 2019). Continuing to develop our understanding of mechanosensation in ch neurons will surely lead to (other) novel treatments for its dysfunction.

Finding (4) also improves our understanding of the *Drosophila* (ch neuron) model of hearing, but also has a fairly direct translation to the human system. Tuning of individual neurons, like that observed within lch1-5 and vchAB, exists in the human ear. Inner hair cells are tuned to a narrow frequency range, which relates to their position in the coiled duct of the cochlea (Figure 1.1, (Fettiplace, 2017)). Perhaps ch neuron tuning also relates to anatomical position; lch1 is anterior to lch2-5, whilst vchB is ventral to vchA, and it may convey some advantage (like predator detection) to sense different frequency or sound intensity in each position. It may be less important in larval behaviour, and instead it reflects the tuning observed in the (adult) JO (Effertz, Wiek and Gopfert, 2011; Yorozu *et al.*, 2009; Matsuo *et al.*, 2014). Regardless, once bolstered by a deeper investigation than the one included in the present research, proof of tuning of larval ch neurons could provide even more utility to an already well-regarded model of human hearing.

Confirming that dyneins are required for hearing and proprioception (5) is key to the value of the present research, particularly as it relates to *CG17669*. This is because GCaMP imaging of *CG17669* -/- larval ch neurons (Figures 4.38-4.43) provided novel insight into the mechanism of dysfunction present in humans suffering from PCD, caused by mutation of its orthologue, *DNAAF3* (Mitchison *et al.*, 2012). Other research has reported ch neurons missing dynein arms, following mutation of a dynein assembly-related gene, *CG14353* (zur Lage *et al.*,

2018)). However, this work did not show the physiological consequence of this loss (i.e. that dyneins are required for ch neuron function) besides in whole-animal behaviour (adult climbing) and fertility, and it did not do so in for a gene with an orthologue related to PCD. Thus, the present research is the first to demonstrate that loss of dynein function causes PCD symptoms and offer a target for therapy. Continuing the search for orthologues of PCD-related genes in *Drosophila* and using them in GCaMP experiments (and perhaps even SCAPE for a more accurate assessment of the impact on proprioception), will allow researchers to confirm the link between dyneins and the disease. This link will inform a list of dynein assembly factor gene targets for gene therapy, and so will help treat patients in future.

7 References

Akitake, B., Ren, Q. T., Boiko, N., Ni, J. F., Sokabe, T., Stockand, J. D., Eaton, B. A. and Montell, C. (2015) 'Coordination and fine motor control depend on *Drosophila* TRP gamma', *Nature Communications,* 6.

Albert, J. T. and Gopfert, M. C. (2015) 'Hearing in *Drosophila*', *Current Opinion in Neurobiology,* 34, pp. 79-85.

Albert, J. T. and Kozlov, A. S. (2016) 'Comparative aspects of hearing in vertebrates and insects with antennal ears', *Current Biology,* 26(20), pp. R1050-R1061.

Albert, J. T., Nadrowski, B. and Gopfert, M. C. (2007) 'Mechanical signatures of transducer gating in the *Drosophila* ear', *Current Biology,* 17(11), pp. 1000-1006.

Artavanistsakonas, S., Matsuno, K. and Fortini, M. E. (1995) 'Notch signaling', *Science,* 268(5208), pp. 225-232.

Askew, C., Rochat, C., Pan, B. F., Asai, Y., Ahmed, H., Child, E., Schneider, B. L., Aebischer, P. and Holt, J. R. (2015) 'Tmc gene therapy restores auditory function in deaf mice', *Science Translational Medicine,* 7(295).

Assad, J. A., Shepherd, G. M. G. and Corey, D. P. (1991) 'Tip-link integrity and mechanical transduction in vertebrate hair-cells, *Neuron,* 7(6), pp. 985-994.

Ausborn, J., Wolf, H., Mader, W. and Kayser, H. (2005) 'The insecticide pymetrozine selectively affects chordotonal mechanoreceptors', *Journal of Experimental Biology,* 208(23), pp. 4451-4466.

Bellen, H. J., Tong, C. and Tsuda, H. (2010) 'TIMELINE 100 years of *Drosophila* research and its impact on vertebrate neuroscience: A history lesson for the future', *Nature Reviews Neuroscience,* 11(7), pp. 514-+.

Bermingham, N. A., Hassan, B. A., Price, S. D., Vollrath, M. A., Ben-Arie, N., Eatock, R. A., Bellen, H. J., Lysakowski, A. and Zoghbi, H. Y. (1999) 'Math1: An essential gene for the generation of inner ear hair cells', *Science,* 284(5421), pp. 1837-1841.

Beurg, M., Evans, M. G., Hackney, C. M. and Fettiplace, R. (2006) 'A large-conductance calcium-selective mechanotransducer channel in mammalian cochlear hair cells', *Journal of Neuroscience,* 26(43), pp. 10992-11000.

Beurg, M., Kim, K. X. and Fettiplace, R. (2014) 'Conductance and block of hair-cell mechanotransducer channels in transmembrane channel-like protein mutants', *Journal of General Physiology,* 144(1), pp. 53-67.

Beurg, M., Nam, J. H., Crawford, A. and Fettiplace, R. (2008) 'The actions of calcium on hair bundle mechanics in mammalian cochlear hair cells', *Biophysical Journal,* 94(7), pp. 2639-2653.

Beurg, M., Xiong, W., Zhao, B., Muller, U. and Fettiplace, R. (2015) 'Subunit determination of the conductance of hair-cell mechanotransducer channels', *Proceedings of the National Academy of Sciences of the United States of America,* 112(5), pp. 1589-1594.

Bewick, G. and Banks, R. 2014. Mechanotransduction in the muscle spindle. Special Issue on Physiological Aspects of Mechano-sensing ed.: European Journal of Physiology.

Blair, E. and Watson, L. (2006) 'Epidemiology of cerebral palsy', *Seminars in Fetal & Neonatal Medicine,* 11(2), pp. 117-125.

Breunig, J. J., Silbereis, J., Vaccarino, F. M., Sestan, N. and Rakic, P. (2007) 'Notch regulates cell fate and dendrite morphology of newborn neurons in the postnatal dentate gyrus', *Proceedings of the National Academy of Sciences of the United States of America,* 104(51), pp. 20558-20563.

Burke, R. E. (2007) 'Sir Charles Sherrington's The integrative action of the nervous system: a centenary appreciation', *Brain,* 130, pp. 887-894.

Cabrera, C. V., Martinezarias, A. and Bate, M. (1987) 'The expression of 3 members of the achaete-scute gene-complex correlates with neuroblast segregation in *Drosophila*', *Cell,* 50(3), pp. 425-433.

Cachero, S., Simpson, T. I., Lage, P. I. Z., Ma, L. N., Newton, F. G., Holohan, E. E., Armstrong, J. D. and Jarman, A. P. (2011) 'The gene regulatory cascade linking proneural specification with differentiation in *Drosophila* sensory neurons', *Plos Biology,* 9(1).

Calabrese, B., Tabarean, I. V., Juranka, P. and Morris, C. E. (2002) 'Mechanosensitivity of N-type calcium channel currents', *Biophysical Journal,* 83(5), pp. 2560-2574.

Caldwell, J. C. and Eberl, D. F. (2002) 'Towards a molecular understanding of *Drosophila* hearing', *Journal of Neurobiology,* 53(2), pp. 172-189.

Caldwell, J. C., Miller, M. M., Wing, S., Soll, D. R. and Eberl, D. F. (2003) 'Dynamic analysis of larval locomotion in *Drosophila* chordotonal organ mutants', *Proceedings of the National Academy of Sciences of the United States of America,* 100(26), pp. 16053-16058.

Camposortega, J. A. (1988) Cellular interactions during early neurogenesis of *Drosophila-melanogaster*', *Trends in Neurosciences,* 11(9), pp. 400-405.

Cheng, L. E., Song, W., Looger, L. L., Jan, L. Y. and Jan, Y. N. (2010) 'The role of the TRP channel NompC in *Drosophila* larval and adult locomotion', *Neuron,* 67(3), pp. 373-380.

Corns, L. F., Jeng, J. Y., Richardson, G. P., Kros, C. J. and Marcotti, W. (2017) 'TMC2 modifies permeation properties of the mechanoelectrical transducer channel in early postnatal mouse cochlear outer hair cells', *Frontiers in Molecular Neuroscience,* 10.

Coste, B., Mathur, J., Schmidt, M., Earley, T. J., Ranade, S., Petrus, M. J., Dubin, A. E. and Patapoutian, A. (2010) 'Piezo1 and Piezo2 are essential components of distinct mechanically activated cation channels', *Science,* 330(6000), pp. 55-60.

Coste, B., Xiao, B., Santos, J. S., Syeda, R., Grandl, J., Spencer, K. S., Kim, S. E., Schmidt, M., Mathur, J., Dubin, A. E., Montal, M. and Patapoutian, A. (2012) 'Piezo proteins are pore-forming subunits of mechanically activated channels', *Nature,* 483(7388), pp. 176-U72.

Crawford, A. C., Evans, M. G. and Fettiplace, R. (1989) Activation and adaptation of transducer currents in turtle hair-cells', *Journal of Physiology-London,* 419, pp. 405-434.

Daousi, C., MacFarlane, I. A., Woodward, A., Nurmikko, T. J., Bundred, P. E. and Benbow, S. J. (2004) 'Chronic painful peripheral neuropathy in an urban community: A controlled comparison of people with and without diabetes', *Diabetic Medicine,* 21(9), pp. 976-982.

Eberl, D. F., Duyk, G. M. and Perrimon, N. (1997) 'A genetic screen for mutations that disrupt an auditory response in *Drosophila melanogaster*', *Proceedings of the National Academy of Sciences of the United States of America,* 94(26), pp. 14837-14842.

Eberl, D. F., Hardy, R. W. and Kernan, M. J. (2000) 'Genetically similar transduction mechanisms for touch and hearing in *Drosophila*', *Journal of Neuroscience,* 20(16), pp. 5981-5988.

Effertz, T., Nadrowski, B., Piepenbrock, D., Albert, J. T. and Gopfert, M. C. (2012) 'Direct gating and mechanical integrity of *Drosophila* auditory transducers require TRPN1', *Nature Neuroscience,* 15(9), pp. 1198-U43.

Effertz, T., Wiek, R. and Gopfert, M. C. (2011) 'NompC TRP channel Is essential for *Drosophila* sound receptor function', *Current Biology,* 21(7), pp. 592-597.

Eguiluz, V. M., Ospeck, M., Choe, Y., Hudspeth, A. J. and Magnasco, M. O. (2000) 'Essential nonlinearities in hearing', *Physical Review Letters,* 84(22), pp. 5232-5235.

Ellisen, L. W., Bird, J., West, D. C., Soreng, A. L., Reynolds, T. C., Smith, S. D. and Sklar, J. (1991) 'TAN-1, The human homolog of the *Drosophila Notch* gene, is broken by chromosomal translocations in T-lymphoblastic neoplasms', *Cell,* 66(4), pp. 649-661.

Farris, H. E., LeBlanc, C. L., Goswami, J. and Ricci, A. J. (2004) 'Probing the pore of the auditory hair cell mechanotransducer channel in turtle', *Journal of Physiology-London,* 558(3), pp. 769-792.

Faucherre, A., Nargeot, J., Mangoni, M. E. and Jopling, C. (2013) 'piezo2b regulates vertebrate light touch response', *Journal of Neuroscience,* 33(43), pp. 17089-17094.

Feng, Y. F., Ueda, A. and Wu, C. F. (2004) 'A modified minimal hemolymph-like solution, HL3.1, for physiological recordings at the neuromuscular junctions of normal and mutant *Drosophila* larvae', *Journal of Neurogenetics,* 18(2), pp. 377-402.

Fettiplace, R. (2017) 'Hair cell transduction, tuning, and synaptic transmission in the mammalian cochlea', *Comprehensive Physiology,* 7(4), pp. 1197-1227.

Field, L. H. and Pfluger, H. J. (1989) 'The femoral chordotonal organ – a bifunctional orthopteran (*Locusta-migratora*) sense-organ', *Comparative Biochemistry and Physiology a-Physiology,* 93(4), pp. 729-743.

Fischer, M. and Schafer, S. S. (2002) 'Effects of the calcium antagonist nifedipine on the afferent impulse activity of isolated cat muscle spindles', *Brain Research,* 954(2), pp. 256-276.

Frolenkov, G. I., Belyantseva, I. A., Friedman, T. B. and Griffith, A. J. (2004) 'Genetic insights into the morphogenesis of inner ear hair cells', *Nature Reviews Genetics,* 5(7), pp. 489-498.

Fushiki, A., Kohsaka, H. and Nose, A. (2011) 'Role of sensory experience in functional development of *Drosophila* motor circuits', *Neuroscience Research,* 71, pp. E251-E251.
Fushiki, A., Zwart, M. F., Kohsaka, H., Fetter, R. D., Cardona, A. and Nose, A. (2016) 'A circuit mechanism for the propagation of waves of muscle contraction in *Drosophila*', *Elife,* 5.
Garty, H. and Palmer, L. G. (1997) 'Epithelial sodium channels: Function, structure, and regulation', *Physiological Reviews,* 77(2), pp. 359-396.
Gees, M., Colsoul, B. and Nilius, B. (2010) 'The role of transient receptor potential cation channels in Ca^{2+} signaling', *Cold Spring Harbor Perspectives in Biology,* 2(10).
Geleoc, G. S. G., Lennan, G. W. T., Richardson, G. P. and Kros, C. J. (1997) 'A quantitative comparison of mechanoelectrical transduction in vestibular and auditory hair cells of neonatal mice', *Proceedings of the Royal Society B-Biological Sciences,* 264(1381), pp. 611-621.
Ghysen, A. and Damblychaudiere, C. (1988) From DNA to form – the achaete-scute complex', *Genes & Development,* 2(5), pp. 495-501.
Gillespie, P. G. and Muller, U. (2009) 'Mechanotransduction by hair cells: Models, molecules, and mechanisms', *Cell,* 139(1), pp. 33-44.
Gong, Z. F., Son, W. S., Chung, Y. D., Kim, J. W., Shin, D. W., McClung, C. A., Lee, Y., Lee, H. W., Chang, D. J., Kaang, B. K., Cho, H. W., Oh, U., Hirsh, J., Kernan, M. J. and Kim, C. S. (2004) 'Two interdependent TRPV channel subunits, inactive and Nanchung, mediate hearing in *Drosophila*', *Journal of Neuroscience,* 24(41), pp. 9059-9066.
Gopfert, M. C., Albert, J. T., Nadrowski, B. and Kamikouchi, A. (2006) 'Specification of auditory sensitivity by *Drosophila* TRP channels', *Nature Neuroscience,* 9(8), pp. 999-1000.
Gopfert, M. C. and Robert, D. (2003) 'Motion generation by *Drosophila* mechanosensory neurons', *Proceedings of the National Academy of Sciences of the United States of America,* 100(9), pp. 5514-5519.
Guo, Y. M., Wang, Y. P., Wang, Q. X. and Wang, Z. R. (2014) 'The role of PPK26 in *Drosophila* larval mechanical nociception', *Cell Reports,* 9(4), pp. 1183-1190.
Hartenstein, V. (1988) 'Development of *Drosophila* larval sensory organs – spatiotemporal pattern of sensory neurons, peripheral axonal pathways and sensilla differentiation', *Development,* 102(4), pp. 869-886.
He, D. Z. Z., Jia, S. P. and Dallos, P. (2004) 'Mechanoelectrical transduction of adult outer hair cells studied in a gerbil hemicochlea', *Nature,* 429(6993), pp. 766-770.
Howard, J. and Bechstedt, S. (2004) 'Hypothesis: A helix of ankyrin repeats of the NOMPC-TRP ion channel is the gating spring of mechanoreceptors', *Current Biology,* 14(6), pp. R224-R226.
Huang, M. L., Hsu, C. H. and Chien, C. T. (2000) 'The proneural gene amos promotes multiple dendritic neuron formation in the *Drosophila* peripheral nervous system', *Neuron,* 25(1), pp. 57-67.
Hughes, C. L. and Thomas, J. B. (2007) 'A sensory feedback circuit coordinates muscle activity in *Drosophila*', *Molecular and Cellular Neuroscience,* 35(2), pp. 383-396.

Hunt, C. C. and Ottoson, D. (1975) ‘Impulse activity and receptor potential of primary and secondary endings of isolated mammalian muscle-spindles', *Journal of Physiology-London,* 252(1), pp. 259-281.

Hunt, C. C., Wilkinson, R. S. and Fukami, Y. (1978) ‘Ionic basis of receptor potential in primary endings of mammalian muscle-spindles', *Journal of General Physiology,* 71(6), pp. 683-698.

Hwang, R. Y., Zhong, L. X., Xu, Y. F., Johnson, T., Zhang, F., Deisseroth, K. and Tracey, W. D. (2007) 'Nociceptive neurons protect *Drosophila* larvae from parasitoid wasps', *Current Biology,* 17(24), pp. 2105-2116.

Ivanusic, J. J. (2017) 'Molecular mechanisms that contribute to bone marrow pain', *Frontiers in Neurology,* 8.

Jami, L. (1992) ‘Golgi tendon-organs in mammalian skeletal-muscle - functional-properties and central actions', *Physiological Reviews,* 72(3), pp. 623-666.

Jarman, A. (2014) 'Development of the auditory organ (Johnston’s Organ) in *Drosophila*', *Development of Auditory and Vestibular Systems*: Elsevier, pp. 562.

Jarman, A. P., Grau, Y., Jan, L. Y. and Jan, Y. N. (1993) ‘Atonal is a proneural gene that directs chordotonal organ formation in the *Drosophila* peripheral nervous system', *Cell,* 73(7), pp. 1307-1321.

Jarman, A. P., Grell, E. H., Ackerman, L., Jan, L. Y. and Jan, Y. N. (1994) ‘Atonal is the proneural gene for *Drosophila* photoreceptors’, *Nature,* 369(6479), pp. 398-400.

Jia, S. P., Dallos, P. and He, D. Z. Z. (2007) 'Mechanoelectric transduction of adult inner hair cells', *Journal of Neuroscience,* 27(5), pp. 1006-1014.

Kaila, K., Rydqvist, B., Swerup, C. and Voipio, J. (1987) ‘Stimulation-induced changes in the intracellular sodium activity of the crayfish stretch-receptor, *Neuroscience Letters,* 74(1), pp. 53-57.

Kamikouchi, A., Shimada, T. and Ito, K. (2006) 'Comprehensive classification of the auditory sensory projections in the brain of the fruit fly *Drosophila* melanogaster', *Journal of Comparative Neurology,* 499(3), pp. 317-356.

Karak, S., Jacobs, J. S., Kittelmann, M., Spalthoff, C., Katana, R., Sivan-Loukianova, E., Schon, M. A., Kernan, M. J., Eberl, D. F. and Gopfert, M. C. (2015) 'Diverse roles of axonemal dyneins in *Drosophila* auditory neuron function and mechanical amplification in hearing', *Scientific Reports,* 5, pp. 12.

Katonis, P., Papoutsidakis, A., Aligizakis, A., Tzanakakis, G., Kontakis, G. M. and Papagelopoulos, P. J. (2008) 'Mechanoreceptors of the posterior cruciate ligament', *Journal of International Medical Research,* 36(3), pp. 387-393.

Kawashima, Y., Geleoc, G. S. G., Kurima, K., Labay, V., Lelli, A., Asai, Y., Makishima, T., Wu, D. K., Della Santina, C. C., Holt, J. R. and Griffith, A. J. (2011) 'Mechanotransduction in mouse inner ear hair cells requires transmembrane channel-like genes', *Journal of Clinical Investigation,* 121(12), pp. 4796-4809.

Kennedy, H. J., Evans, M. G., Crawford, A. C. and Fettiplace, R. (2003) 'Fast adaptation of mechanoelectrical transducer channels in mammalian cochlear hair cells', *Nature Neuroscience,* 6(8), pp. 832-836.

Kim, J., Chung, Y. D., Park, D. Y., Choi, S. K., Shin, D. W., Soh, H., Lee, H. W., Son, W., Yim, J., Park, C. S., Kernan, M. J. and Kim, C. (2003) 'A TRPV family ion channel required for hearing in *Drosophila*', *Nature,* 424(6944), pp. 81-84.

Kim, K. X. and Fettiplace, R. (2013) 'Developmental changes in the cochlear hair cell mechanotransducer channel and their regulation by transmembrane channel-like proteins', *Journal of General Physiology,* 141(1), pp. 141-148.

Kim, S. E., Coste, B., Chadha, A., Cook, B. and Patapoutian, A. (2012) 'The role of *Drosophila* Piezo in mechanical nociception', *Nature,* 483(7388), pp. 209-212.

King, S. M. and Patel-King, R. S. (2015) 'The oligomeric outer dynein arm assembly factor *CCDC103* is tightly integrated within the ciliary axoneme and exhibits periodic binding to microtubules', *Journal of Biological Chemistry,* 290(12), pp. 7388-7401.

Knoop, J., Steultjens, M. P. M., van der Leeden, M., van der Esch, M., Thorstensson, C. A., Roorda, L. D., Lems, W. F. and Dekker, J. (2011) 'Proprioception in knee osteoarthritis: a narrative review', *Osteoarthritis and Cartilage,* 19(4), pp. 381-388.

Kopan, R. and Ilagan, M. X. G. (2009) 'The canonical notch signaling pathway: Unfolding the activation mechanism', *Cell,* 137(2), pp. 216-233.

Kott, E., Duquesnoy, P., Copin, B., Legendre, M., Dastot-Le Moal, F., Montantin, G., Jeanson, L., Tamalet, A., Papon, J. F., Siffroi, J. P., Rives, N., Mitchell, V., de Blic, J., Coste, A., Clement, A., Escalier, D., Toure, A., Escudier, E. and Amselem, S. (2012) 'Loss-of-function mutations in *LRRC6*, a gene essential for proper axonemal assembly of inner and outer dynein arms, cause primary ciliary dyskinesia', *American Journal of Human Genetics,* 91(5), pp. 958-964.

Kros, C. J., Rusch, A. and Richardson, G. P. (1992) 'Mechanoelectrical transducer currents in hair-cells of the cultured neonatal mouse cochlea', *Proceedings of the Royal Society B-Biological Sciences,* 249(1325), pp. 185-193.

Kuehni, C. E., Frischer, T., Strippoli, M. P. F., Maurer, E., Bush, A., Nielsen, K. G., Escribano, A., Lucas, J. S. A., Yiallouros, P., Omran, H., Eber, E., O'Callaghan, C., Snijders, D., Barbato, A. and Dys, E. R. S. T. F. P. C. (2010) 'Factors influencing age at diagnosis of primary ciliary dyskinesia in European children', *European Respiratory Journal,* 36(6), pp. 1248-1258.

Kurima, K., Peters, L. M., Yang, Y. D., Riazuddin, S., Ahmed, Z. M., Naz, S., Arnaud, D., Drury, S., Mo, J. H., Makishima, T., Ghosh, M., Menon, P. S. N., Deshmukh, D., Oddoux, C., Ostrer, H., Khan, S., Deininger, P. L., Hampton, L. L., Sullivan, S. L., Battey, J. F., Keats, B. J. B., Wilcox, E. R., Friedman, T. B. and Griffith, A. J. (2002) 'Dominant and recessive deafness caused by mutations of a novel gene, *TMC1*, required for cochlear hair-cell function', *Nature Genetics,* 30(3), pp. 277-284.

Lehnert, B. P., Baker, A. E., Gaudry, Q., Chiang, A. S. and Wilson, R. I. (2013) 'Distinct roles of TRP channels in auditory transduction and amplification in *Drosophila*', *Neuron,* 77(1), pp. 115-128.

LeMasurier, M. and Gillespie, P. G. (2005) 'Hair-cell mechanotransduction and cochlear amplification', *Neuron,* 48(3), pp. 403-415.

Lephart, S. M., Pincivero, D. M. and Rozzi, S. L. (1998) 'Proprioception of the ankle and knee', *Sports Medicine,* 25(3), pp. 149-155.

Liang, X., Madrid, J., Saleh, H. S. and Howard, J. (2011) 'NOMPC, a member of the TRP channel family, Localizes to the tubular body and distal cilium of *Drosophila* campaniform and chordotonal receptor cells', *Cytoskeleton,* 68(1), pp. 1-7.

Lo, L. C., Johnson, J. E., Wuenschell, C. W., Saito, T. and Anderson, D. J. (1991) 'Mammalian achaete-scute homolg-1 is transiently expressed by spatially restricted subsets of early neuroepithelial and neural crest cell', *Genes & Development,* 5(9), pp. 1524-1537.

Action on Hearing Loss, (2011) *Facts and Figures on Hearing Loss and Tinnitus*. Available at: file:///C:/Users/Iain/Downloads/Facts%20and%20figures%20on%20deafness%20and%20tinnitus%20July%202011.pdf.

Maeda, R., Kindt, K. S., Mo, W. K., Morgan, C. P., Erickson, T., Zhao, H. Y., Clemens-Grisham, R., Barr-Gillespie, P. G. and Nicolson, T. (2014) 'Tip-link protein protocadherin 15 interacts with transmembrane channel-like proteins *TMC1* and *TMC2*', *Proceedings of the National Academy of Sciences of the United States of America,* 111(35), pp. 12907-12912.

Mahendrasingam, S., Fettiplace, R., Alagramam, K. N., Cross, E. and Furness, D. N. (2017) 'Spatiotemporal changes in the distribution of *LHFPL5* in mice cochlear hair bundles during development and in the absence of PCDH15', *Plos One,* 12(10).

Mamiya, A., Gurung, P. and Tuthill, J. C. (2018) 'Neural coding of leg proprioception in *Drosophila*', *Neuron,* 100(3), pp. 636-+.

Maricich, S. M., Wellnitz, S. A., Nelson, A. M., Lesniak, D. R., Gerling, G. J., Lumpkin, E. A. and Zoghbi, H. Y. (2009) 'Merkel cells are essential for light-touch responses', *Science,* 324(5934), pp. 1580-1582.

Matsuo, E., Yamada, D., Ishikawa, Y., Asai, T., Ishimoto, H. and Kamikouchi, A. (2014) 'Identification of novel vibration- and deflection-sensitive neuronal subgroups in Johnston's organ of the fruit fly', *Frontiers in Physiology,* 5.

Merritt, D. J. and Whitington, P. M. (1995) 'Central projections of sensory neurons in the *Drosophila* embryo correlate with sensory modality, soma position, and proneural gene-function', *Journal of Neuroscience,* 15(3), pp. 1755-1767.

Mitchison, H. M., Schmidts, M., Loges, N. T., Freshour, J., Dritsoula, A., Hirst, R. A., O'Callaghan, C., Blau, H., Al Dabbagh, M., Olbrich, H., Beales, P. L., Yagi, T., Mussaffi, H., Chung, E. M. K., Omran, H. and Mitchell, D. R. (2012) 'Mutations in axonemal dynein assembly factor *DNAAF3* cause primary ciliary dyskinesia', *Nature Genetics,* 44(4), pp. 381-U186.

Mitchison, H. M. and Valente, E. M. (2017) 'Motile and non-motile cilia in human pathology: from function to phenotypes', *Journal of Pathology,* 241(2), pp. 294-309.

Moore, D. J., Onoufriadis, A., Shoemark, A., Simpson, M. A., zur Lage, P. I., de Castro, S. C., Bartoloni, L., Gallone, G., Petridi, S., Woollard, W. J., Antony, D., Schmidts, M., Didonna, T., Makrythanasis, P., Bevillard, J., Mongan, N. P., Djakow, J., Pals, G., Lucas, J. S., Marthin, J. K., Nielsen, K. G., Santoni, F., Guipponi, M., Hogg, C., Antonarakis, S. E., Emes, R. D., Chung, E. M. K., Greene, N. D. E., Blouin, J. L., Jarman, A. P. and Mitchison, H. M. (2013) 'Mutations in *ZMYND10*, a gene essential for proper axonemal assembly of inner and outer dynein arms in humans and flies, cause primary ciliary dyskinesia', *American Journal of Human Genetics,* 93(2), pp. 346-356.

Morgan, T. H. and Cattell, E. (1912) 'Data for the study of sex-linked inheritance in *Drosophila*', *Journal of Experimental Zoology,* 13(1), pp. 79-101.

Nadrowski, B., Albert, J. T. and Gopfert, M. C. (2008) 'Transducer-based force generation explains active process in *Drosophila* hearing', *Current Biology,* 18(18), pp. 1365-1372.

Nair, A., Bate, M. and Pulver, S. R. (2010) 'Characterization of voltage-gated ionic currents in a peripheral sensory neuron in larval *Drosophila*', *BMC research notes,* 3, pp. 154-154.

Nesterov, A., Spalthoff, C., Kandasamy, R., Katana, R., Rankl, N. B., Andres, M., Jahde, P., Dorsch, J. A., Stam, L. F., Braun, F. J., Warren, B., Salgado, V. L. and Gopfert, M. C. (2015) 'TRP channels in insect stretch receptors as insecticide targets', *Neuron,* 86(3), pp. 665-671.

Newton, F. G., zur Lage, P. I., Karak, S., Moore, D. J., Gopfert, M. C. and Jarman, A. P. (2012) 'forkhead transcription factor *Fd3F* cooperates with *Rfx* to regulate a gene expression program for mechanosensory cilia specialization', *Developmental Cell,* 22(6), pp. 1221-1233.

Nicolson, T., Rusch, A., Friedrich, R. W., Granato, M., Ruppersberg, J. P. and Nusslein-Volhard, C. (1998) 'Genetic analysis of vertebrate sensory hair cell mechanosensation: the zebrafish circler mutants', *Neuron,* 20(2), pp. 271-283.

O'Callaghan, C., Chetcuti, P. and Moya, E. (2010) 'High prevalence of primary ciliary dyskinesia in a British Asian population', *Archives of Disease in Childhood,* 95(1), pp. 51-52.

Odding, E., Roebroeck, M. E. and Stam, H. J. (2006) 'The epidemiology of cerebral palsy: Incidence, impairments and risk factors', *Disability and Rehabilitation,* 28(4), pp. 183-191.

Ohmori, H. (1985) 'Mechano-electrical transduction currents in isolated vestibular hair-cells of the chick', *Journal of Physiology-London,* 359(FEB), pp. 189-&.

Orgogozo, V. and Grueber, W. B. (2005) 'FlyPNS, a database of the *Drosophila* embryonic and larval peripheral nervous system', *Bmc Developmental Biology,* 5.

Ottoson, D. and Swerup, C. (1982) 'Studies on the role of calcium in adaptation of the crustacean stretch-receptor - effects of intracellular injection of calcium, EGTA and TEA', *Brain Research,* 244(2), pp. 337-341.

Padinjat, R. and Andrews, S. (2004) 'TRP channels at a glance', *Journal of Cell Science,* 117(24), pp. 5707-5709.

Pan, B. F., Geleoc, G. S., Asai, Y., Horwitz, G. C., Kurima, K., Ishikawa, K., Kawashima, Y., Griffith, A. J. and Holt, J. R. (2013) 'TMC1 and TMC2 are components of the mechanotransduction channel in hair cells of the mammalian inner ear', *Neuron,* 79(3), pp. 504-515.

Pearson, K. and Gordon, J. (2013) *Principles of Neural Science.* 5th edn.: McGraw Hill Medical.

Peng, I. F. and Wu, C. F. (2007) '*Drosophila* cacophony channels: A major mediator of neuronal Ca2+ currents and a trigger for K^+ channel homeostatic regulation', *Journal of Neuroscience,* 27(5), pp. 1072-1081.

Pulver, S. R., Hornstein, N. J., Land, B. L. and Johnson, B. R. (2011) 'Optogenetics in the teaching laboratory: Using channelrhodopsin-2 to study the neural basis of behavior and synaptic physiology in *Drosophila*', *Advances in Physiology Education,* 35(1), pp. 82-91.

Qiu, X. F. and Muller, U. (2018) 'Mechanically gated ion channels in mammalian hair cells', *Frontiers in Cellular Neuroscience,* 12.

Reddy, S., Jin, P., Trimarchi, J., Caruccio, P., Phillis, R. and Murphey, R. K. (1997) 'Mutant molecular motors disrupt neural circuits in *Drosophila*', *Journal of Neurobiology,* 33(6), pp. 711-723.

Ricci, A. J., Crawford, A. C. and Fettiplace, R. (2003) 'Tonotopic variation in the conductance of the hair cell mechanotransducer channel', *Neuron,* 40(5), pp. 983-990.

Ross, D., Lagogiannis, K. and Webb, B. (2015) 'A model of larval biomechanics reveals exploitable passive properties for efficient locomotion', *Biomimetic and Biohybrid Systems, Living Machines 2015,* 9222, pp. 1-12.

Samarajeewa, A., Jacques, B. E. and Dabdoub, A. (2019) 'Therapeutic potential of Wnt and Notch signaling and epigenetic regulation in mammalian sensory hair cell regeneration', *Molecular Therapy,* 27(5), pp. 904-911.

Sauer, A. E. and Stein, W. (1999) 'Sensorimotor pathways processing vibratory signals from the femoral chordotonal organ of the stick insect', *Journal of Comparative Physiology a-Sensory Neural and Behavioral Physiology,* 185(1), pp. 21-31.

Schneider-Mizell, C. M., Gerhard, S., Longair, M., Kazimiers, T., Li, F., Zwart, M. F., Champion, A., Midgley, F. M., Fetter, R. D., Saalfeld, S. and Cardona, A. (2016) 'Quantitative neuroanatomy for connectomics in *Drosophila*', *Elife,* 5.

Schwander, M., Kachar, B. and Muller, U. (2010) 'The cell biology of hearing', *Journal of Cell Biology,* 190(1), pp. 9-20.

Senthilan, P. R., Piepenbrock, D., Ovezmyradov, G., Nadrowski, B., Bechstedt, S., Pauls, S., Winkler, M., Mobius, W., Howard, J. and Gopfert, M. C. (2012) '*Drosophila* auditory organ genes and genetic hearing defects', *Cell,* 150(5), pp. 1042-1054.

Shah, A., Shoemark, A., MacNeill, S. J., Bhaludin, B., Rogers, A., Bilton, D., Hansell, D. M., Wilson, R. and Loebinger, M. R. (2016) 'A longitudinal study characterising a large adult primary ciliary dyskinesia population', *European Respiratory Journal,* 48(2), pp. 441-450.

Shanbhag, S. R., Singh, K. and Singh, R. N. (1992) 'Ultrastructure of the femoral chordotonal organs and their novel synaptic organization in the legs of *Drosophila*-melanogaster meigen (diptera, drosophilidae)', *International Journal of Insect Morphology & Embryology,* 21(4), pp. 311-322.

Simon, A., Banks, R. W. and Bewick, G. S. 2008. K_{Ca} channels regulate stretch-evoked afferent firing from muscle spindles. Proceedings Physiological Society.

Simon, A., Shenton, F., Hunter, I., Banks, R. W. and Bewick, G. S. (2010) 'Amiloride-sensitive channels are a major contributor to mechanotransduction in mammalian muscle spindles', *Journal of Physiology-London,* 588(1), pp. 171-185.

Simon, M. A. and Trimmer, B. A. (2009) 'Movement encoding by a stretch receptor in the soft-bodied caterpillar, *Manduca sexta*', *Journal of Experimental Biology,* 212(7), pp. 1021-1031.

Singhania, A. and Grueber, W. B. (2014) 'Development of the embryonic and larval peripheral nervous system of *Drosophila*', *Wiley Interdisciplinary Reviews-Developmental Biology,* 3(3), pp. 193-210.

Sommer, J. U., Schafer, K., Omran, H., Olbrich, H., Wallmeier, J., Blum, A., Hormann, K. and Stuck, B. A. (2011) 'ENT manifestations in patients with primary ciliary dyskinesia: prevalence and significance of otorhinolaryngologic co-morbidities', *European Archives of Oto-Rhino-Laryngology,* 268(3), pp. 383-388.

Stein, W. and Sauer, A. E. (1999) 'Physiology of vibration-sensitive afferents in the femoral chordotonal organ of the stick insect', *Journal of Comparative Physiology a-Sensory Neural and Behavioral Physiology,* 184(3), pp. 253-263.

Strausfeld, N. J. and Bassemir, U. K. (1983) 'Cobalt-coupled neurons of a giant fiber system in diptera', *Journal of Neurocytology,* 12(6), pp. 971-991.

Suslak, T. J. (2015) *There and back again: A stretch receptor's tale.* Ph.D. Thesis, University of Edinburgh.

Suslak, T. J., Armstrong, J. D. and Jarman, A. P. (2011) 'A general mathematical model of transduction events in mechano-sensory stretch receptors', *Network-Computation in Neural Systems,* 22(1-4), pp. 133-142.

Suslak, T. J., Hunter, I., Armstrong, D., Bewick, G. and Jarman, A. 'Mechanisms of mechanosensation in proprioceptors', *ScotFly (4th Scottish Fly Meeting)*, St. Andrews, Scotland.

Suslak, T. J. and Jarman, A. P. 2015. Stretching the imagination beyond muscle spindles - stretch-sensitive mechanisms in arthropods. Journal of Anatomy (in press).

Suslak, T. J., Watson, S., Thompson, K. J., Shenton, F. C., Bewick, G. S., Armstrong, J. D. and Jarman, A. P. (2015b) 'Piezo is essential for amiloride-sensitive stretch-activated mechanotransduction in larval *Drosophila* dorsal bipolar dendritic sensory neurons', *Plos One,* 10(7).

Suster, M. L. and Bate, M. (2002) 'Embryonic assembly of a central pattern generator without sensory input', *Nature,* 416(6877), pp. 174-178.

Swanik, C. B., Lephart, S. M. and Rubash, H. E. (2004) 'Proprioception, kinesthesia, and balance after total knee arthroplasty with cruciate-retaining and posterior stabilized prostheses', *Journal of Bone and Joint Surgery-American Volume,* 86A(2), pp. 328-334.

Titlow, J. S., Johnson, B. R. and Pulver, S. R. (2015) 'Light activated escape circuits: a behavior and neurophysiology lab module using *Drosophila* optogenetics', *Journal of undergraduate neuroscience education : JUNE : a publication of FUN, Faculty for Undergraduate Neuroscience,* 13(3), pp. A166-73.

Trebak, M. (2010) 'The puzzling role of *TRPC3* channels in motor coordination', *Pflugers Archiv-European Journal of Physiology,* 459(3), pp. 369-375.

Tsubouchi, A., Caldwell, J. C. and Tracey, W. D. (2012) 'Dendritic Filopodia, Ripped Pocket, NOMPC, and NMDARs contribute to the sense of touch in *Drosophila* larvae', *Current Biology,* 22(22), pp. 2124-2134.

Van Keymeulen, A., Mascre, G., Youseff, K. K., Harel, I., Michaux, C., De Geest, N., Szpalski, C., Achouri, Y., Bloch, W., Hassan, B. A. and Blanpain, C. (2009) 'Epidermal progenitors give rise to Merkel cells during embryonic development and adult homeostasis', *Journal of Cell Biology,* 187(1), pp. 91-100.

Vassin, H., Bremer, K. A., Knust, E. and Camposortega, J. A. (1987) 'The neurogenic gene-delta Of *Drosophila-melanogaster* is expressed in neurogenic territories and encodes a putative transmembrane protein with EGF-like repeats', *Embo Journal,* 6(11), pp. 3431-3440.

Venkatachalam, K. and Montell, C. (2007) 'TRP channels', *Annual Review of Biochemistry,* 76, pp. 387-417.

Vreugde, S., Ereven, A., Kros, C. J., Marcotti, W., Fuchs, H., Kurima, K., Wilcox, E. R., Friedman, T. B., Griffith, A. J., Balling, R., de Angelis, M. H., Avraham, K. B. and Steel, K. P. (2002) '*Beethoven*, a mouse model for dominant, progressive hearing loss *DFNA36*', *Nature Genetics,* 30(3), pp. 257-258.

Walker, R. G., Willingham, A. T. and Zuker, C. S. (2000) 'A *Drosophila* mechanosensory transduction channel', *Science,* 287(5461), pp. 2229-2234.

Wallmeier, J., Shiratori, H., Dougherty, G. W., Edelbusch, C., Hjeij, R., Loges, N. T., Menchen, T., Olbrich, H., Pennekamp, P., Raidt, J., Werner, C., Minegishi, K., Shinohara, K., Asai, Y., Takaoka, K., Lee, C., Griese, M., Memari, Y., Durbin, R., Kolb-Kokocinski, A., Sauer, S., Wallingford, J. B., Hamada, H. and Omran, H. (2016) '*TTC25* deficiency results in defects of the outer dynein arm docking machinery and primary ciliary dyskinesia with left-right body asymmetry randomization', *American Journal of Human Genetics,* 99(2), pp. 460-469.

Warren, B., Lukashkin, A. N. and Russell, I. J. (2010) 'The dynein-tubulin motor powers active oscillations and amplification in the hearing organ of the mosquito', *Proceedings of the Royal Society B-Biological Sciences,* 277(1688), pp. 1761-1769.

Warren, B. and Matheson, T. (2018) 'The role of the mechanotransduction ion channel candidate Nanchung-inactive in auditory transduction in an insect ear', *Journal of Neuroscience,* 38(15), pp. 3741-3752.

Wei, E. T. and Seid, D. A. (1983) 'AG-3-5 - a chemical producing sensation of cold', *Journal of Pharmacy and Pharmacology,* 35(2), pp. 110-112.

Wharton, K. A., Johansen, K. M., Xu, T. and Artavanistsakonas, S. (1985) 'Nucleotide-sequence from the neurogenic locus Notch implies a gene-product that shares homology with proteins containing EGF-like repeats', *Cell,* 43(3), pp. 567-581.

Wu, Z. Z., Grillet, N., Zhao, B., Cunningham, C., Harkins-Perry, S., Coste, B., Ranade, S., Zebarjadi, N., Beurg, M., Fettiplace, R., Patapoutian, A. and Muller, U. (2017) 'Mechanosensory hair cells express two molecularly distinct mechanotransduction channels', *Nature Neuroscience,* 20(1), pp. 24-33.

Xiong, W., Grillet, N., Elledge, H. M., Wagner, T. F. J., Zhao, B., Johnson, K. R., Kazmierczak, P. and Muller, U. (2012) 'TMHS is an integral component of the mechanotransduction machinery of cochlear hair cells', *Cell,* 151(6), pp. 1283-1295.

Yan, Z., Zhang, W., He, Y., Gorczyca, D., Xiang, Y., Cheng, L. E., Meltzer, S., Jan, L. Y. and Jan, Y. N. (2013) '*Drosophila* NOMPC is a mechanotransduction channel subunit for gentle-touch sensation', *Nature,* 493(7431), pp. 221-225.

Yorozu, S., Wong, A., Fischer, B. J., Dankert, H., Kernan, M. J., Kamikouchi, A., Ito, K. and Anderson, D. J. (2009) 'Distinct sensory representations of wind and near-field sound in the *Drosophila* brain', *Nature,* 458(7235), pp. 201-U4.

Zhang, W., Cheng, L. E., Kittelmann, M., Li, J. F., Petkovic, M., Cheng, T., Jin, P., Guo, Z. H., Gopfert, M. C., Jan, L. Y. and Jan, Y. N. (2015) 'Ankyrin repeats convey force to gate the NOMPC mechanotransduction channel', *Cell,* 162(6), pp. 1391-1403.

Zhang, W., Yan, Z. Q., Jan, L. Y. and Jan, Y. N. (2013) 'Sound response mediated by the TRP channels NOMPC, Nanchung, and inactive in chordotonal organs of *Drosophila* larvae', *Proceedings of the National Academy of Sciences of the United States of America,* 110(33), pp. 13612-13617.

Zhao, B., Wu, Z. Z., Grillet, N., Yan, L. X., Xiong, W., Harkins-Perry, S. and Muller, U. (2014) 'TMIE is an essential component of the mechanotransduction machinery of cochlear hair cells', *Neuron,* 84(5), pp. 954-967.

zur Lage, P. and Jarman, A. P. (1999) 'Antagonism of EGFR and Notch signalling in the reiterative recruitment of *Drosophila* adult chordotonal sense organ precursors', *Development,* 126(14), pp. 3149-3157.

zur Lage, P., Newton, F. G. and Jarman, A. P. (2019) 'Survey of the ciliary motility machinery of *Drosophila* sperm and ciliated mechanosensory neurons reveals unexpected cell-type specific variations: a model for motile ciliopathies', *Frontiers in Genetics,* 10.

zur Lage, P., Stefanopoulou, P., Styczynska-Soczka, K., Quinn, N., Mali, G., von Kreigsheim, A., Mill, P. and Jarman, A. (2018) 'Ciliary dynein motor preassembly is regulated by *Wdr92* in association with HSP90 co-chapherone, RT2P', *Journal of Cell Biology*.